TARGETING THE MEVALONATE PATHWAY FOR PHARMACOLOGICAL INTERVENTION



Maria Tsoumpra

Nuffield Department of Orthopaedics, Rheumatology and Musculoskeletal Sciences

Green - Templeton College

D.Phil. Thesis

Trinity Term 2011

ABSTRACT

Farnesyl pyrophosphate synthase (FPPS) is a key branch point enzyme in the mevalonate pathway and the main molecular target of nitrogen-containing bisphosphonates (N-BPs), potent inhibitors of osteoclastic activity and the leading drug of choice for conditions characterized by excessive bone resorption. The main aim of this thesis is to investigate the interaction of N-BPs with FPPS in order to gain further insights into the mechanism of drug inhibition. Kinetic and crystallographic studies following site-directed mutagenesis of FPPS reveal key residues involved in stabilization of carbocation intermediate, substrate binding and formation of a tight enzyme-inhibitor complex. The aromatic ring of Tyr204 is involved in N-BP binding but not in the catalytic mechanism, where the hydroxyl moiety plays an important role. Lys200 is implicated in regulation of substrate binding, product specificity and enzyme isomerization which leads to a tight binding inhibition. Phe239 is considered important for the FPPS C-terminal switch which stabilizes substrate binding and promotes the inhibitor induced isomerized state. The highly conserved Arg112, Asp103 and Asp107 are pivotal for catalysis. Successful purification of the full length of Rab geranylgeranyl transferase (RGGT) complex downstream of the FPPS in the mevalonate pathway was achieved and may lead to co-crystallization with BP analogues and identification of the putative site of drug binding. Investigation of the *in vitro* effect of N-BPs on osteoclastogenesis suggest a correlation with FPPS inhibition kinetics for the most potent N-BPs but indicate an alternative mechanism of the disruption of bone resorption by alendronate. Together these results highlight the importance of the multiple interactions of N-BPs with side-chain residues of FPPS which dictate their strength of binding and advance the understanding of their pharmacophore effect.

ACKNOWLEDGEMENTS

My greatest thanks go to Professor Graham Russell, who has appointed me to work on this DPhil project and he was a constant source of moral support and career inspiration. Great thanks to my lab supervisor, Dr James Dunford, for his guidance to my kinetic experiments and his invaluable advice throughout my DPhil. I am also grateful to Professor Udo Oppermann for his supervision throughout this project and his connection to Structural Genomic Consortium, which proved to be a fully equipped and excellent environment to conduct my research.

In am indebted to Dr Bobby Barnett and Dr Joao Muniz, who have patiently guided me through the world of crystallography and they showed full committment to the building of FPPS crystal structures; without them I would never have been able to submit this work. I am deeply grateful to our collaborator Dr Guillaume Mabillau, who thoroughly taught me all tissue culture skills and guided my osteoclastogenesis work. Great thanks to Dr Grazyna Kochan, Dr Aaron Kwaasi and Dr Panagis Filippakopoulos for sharing their invaluable knowledge and taught me how to master new techniques. My special thanks to Dr Richard Walters and Gina Ranieri that kindly processed my crystals to the synchrotron.

I am grateful to Dr Afsie Sabokbar, who has consistently supported and advised me since my arrival at Botnar Research Centre and has never doubted my ability to complete the presented work. Special thanks to Dr Hal Ebetino and Procter and Gamble Pharmaceutics that funded my work.

Finally I would like to thank my parents and sister for their continuous support and faith in me throughout this challenging period.

LIST OF ABBREVIATIONS

Ala, Ala	Alanine
Arg, R	Arginine
Acetyl-CoA	Acetyl-Coenzyme alpha
ADP	Adenosine diphosphate
Ale	Alendronate
APS	Ammonium persulfate
ATP	Adenosine Triphosphate
Asp, D	Aspartic acid
BCA	Bicinchoninic acid
BSA	Bovine serum albumin
BPs	Bisphosphonates
CBR	C-terminal-binding region
cDNA	complementary DNA
CNBr	Cyanogen bromide
DTT	Dithiothreitol
dNTP	Deoxynucleotide triphosphate
CFU	colony-forming unit
CFU-GM	granulocyte macrophage colony-forming unit
CFU-S	colony-forming unit-stem
CHM	Choroideremia (Rab Escort Protein 1)
CHML	Choroideremia like (Rab Escort Protein 2)
CIM	CBR interacting motif
CNBr	Cyanogen bromide
CRB	C-terminal-binding region
CV	Column volume
D	Aspartic Acid
DAPI	4'-6-Diamidino-2-phenylindole
dd	Double distilled
DMAPP	Dimethylallyl pyrophosphate
DMASPP	Dimethylallyl-thiolo-diphosphate
DMSO	Dimethylsulfoxide
dNTP	Deoxynucleotide triphosphate
DTT	Dithiothreitol
ECL	Enchanced Chemiluminescence
EDTA	Ethylenedinitrilotetraacetic acid
ER	Endoplasmic reticulum
ESI-TOF MS	Electrospray ionization time-of-flight mass spectrometry
FBS	Fetal bovine serum

FPP	Farnesyl pyrophosphate
FPPS	Farnesyl pyrophosphate synthase
FTase	Farnesyl transferase
GG	Geranylgeranyl
GGPP	Geranylgeranyl pyrophosphate
GGPPS	Geranylgeranyl pyrophosphate synthase
GGTase-I	Geranylgeranyltransferase type I
Gln, Q	Glutamine
Glu, E	Glutamic acid
Gly, G	Glycine
HEPES	N-2-Hydroxyethylpiperazine-N′-2-ethanesulfonic acid
HMGS	Hydroxymethylglutaryl synthase
HMG-CoA	Hydroxymethylglutaryl-coenzyme alpha
hr	hour
HRP	Horseradish peroxidase
Iba	Ibandronate
ICMT	Isoprenylcysteine carboxyl methyltransferase
Ig-like	Immunoglobulin like domain
IL	Interleukine
Ile, I	Isoleucine
IMAC	Immobilized metal ion affinity chromatography
IPP	Isopentenyl pyrophosphate
IPTG	Isopropyl-1-thio-D-galactopyranoside
ITC	Isothermal titration calorimetry
K, Lys	Lysine
Kb	binding constant
k_{cat}	Catalytic constant
Kd	Dissociation constant
kDa	kilo Dalton
Ki*	Final Inhibition constant
Ki	Initial inhibition constant
K_{isom}	Isomerization constant
K_m	Michaelis Menten constant
LB	Luria Bertani broth
LDL	Low density lipoproteins
Leu, L	Leucine
LRR	leucine-rich repeat domain
LIC	Ligation independent cloning
Lys, K	Lysine
Met	Methionine, M
MES	2-(N-morpholino)ethanesulfonic acid

Mg	Magnesium
M-CSF	Macrophage-colony stimulating factor
min	minutes
MOPS	3-N(Morpholino) propane sulfonic acid
MVA	Mevalonate
NADPH	Nicotinamide adenine dinucleotide phosphate
N-BPs	Nitrogen-containing bisphosphonates
ng	Nanograms
Ni-NTA	Nickel-nitrilotriacetic acid
OC	Osteoclast
O.D.	Optical density
o/n	Overnight
ONJ	Osteonecrosis of the jaw
OPG	Osteoprotegerin
OSCAR	Osteoclast-associated receptor
Pam	Pamidronate
PBMCs	Peripheral Blood Mononuclear Cells
PC	Phosphonocarboxylate
PBS	Phosphate buffer saline
PBS-T	Phosphate buffer saline –Tween20
PCR	Polymerase chain reaction
PEG	Polyethylene Glycol
Phe, F	Phenylalanine
PMSF	Phenylmethyl sulfonyl fluoride
PPi	Inorganic pyrophosphate
PVDF	Polyvinylidene fluoride
RGGT	Rab geranylgeranyl transferase complex
RabGDIs	Rab GDP dissociation inhibitors
RABGGT	Rab geranylgeranyl transferase (alpha & beta subunit)
RABGGTA	Rab geranylgeranyl transferase alpha subunit
RABGGTB	Rab geranylgeranyl transferase beta subunit
RANK	Receptor activator of nuclear factor–kB
RANKL	Receptor activator of nuclear factor–Kb ligand
RBP	Rab binding platform
RCEI	Ras converting enzyme endoprotease
REP	Rab escort protein
Ris	Risedronate
R.T.	Room temperature
SBP	Streptavidin binding peptide
SDS-PAGE	Sodium dodecyl sulfate polyacrylamide gel electrophoresis
sec	second

SET	Solubility enhancement tag
Ser, S	Ser
Sf	*Spodoptera frugiperda*
S.O.C.	Super optimal broth with catabolite repression
TAE	Tris acetate electrophoresis
TB	Terrific broth
TCA	Trichloroacetic acid
TCEP	Tris (2-carboxyethulphosphine)
TE	Tris-EDTA buffer
TEV	Tobacco Etch Virus
TEMED	N,N,N'N'-tetramethylethylenediamine
Thr, T	Threonine
TFB1	Transformation buffer 1
TFB2	Transformation buffer 2
TEV	Tobacco etch virus
TNF	Tumour necrosis factor
TNF-α	Tumour necrosis factor alpha
TRAcP	Tartrate-resistant acidic phosphatase
Trp	Tryptophan
Trx	Thioredoxin
Tyr, Y	Tyrosine
V_{max}	Maximal velocity
Vo	Initial velocity
WT	Wild type
Zol	Zoledronate
Zn	Zinc
µl	microlitre
α-MEM	alpha-minimum essential medium
ΔG	Difference in Gibbs energy
ΔH	Difference in enthalpy
ΔTS	Difference in entropy

LIST OF CONTENTS

ABSTRACT II

ACKNOWLEDGEMENTS III

LIST OF ABBREVIATIONS IV

LIST OF CONTENTS 1

LIST OF FIGURES 12

LIST OF TABLES 19

1. GENERAL INTRODUCTION 21

1.1 THE MEVALONATE PATHWAY 21

1.1.1 Generation of mevalonate; an overview 21

1.1.2 Regulation of mevalonate synthesis 23

1.1.3 Generation of isoprenoid intermediates from mevalonate 24

1.2 FARNESYL PYROPHOSPHATE SYNTHASE (FPPS) 30

1.2.1 Insights into the catalytic mechanism of FPPS 30

1.2.2 The crystal structure of human FPPS reveals enzyme transition between three distinct conformations 38

1.2.3 The products of FPPS catalysis 40

1.3 PROTEIN PRENYLATION, AN OVERVIEW 40

1.4 PRENYLATION BY FARNESYL TRANSFERASE (FTase) & GERANYLGERANYLTRANSFERASE TYPE-I (GGTase-I) 42

1.5. PRENYLATION BY RAB GERANYLGERANYL TRANSFERASE (RGGT) 44

1.5.1 Substrate recognition by RGGT 44

1.5.2 Rab Escort Protein as a chaperone in RGGT catalysis 45

1.5.3 Proposed mechanisms of RGGT catalysis 46
1.5.4 The crystal structure of RGGT in complex with REP1 and Rab..... 49
1.6 POST-PRENYLATION PROCESSING OF RAB 53
1.7 BISPHOSPHONATES AS INHIBITORS OF PRENYLATION.. 54
1.7.1 Bisphosphonates as anti-resorptive agents 54
1.7.3 Molecular mechanisms of bisphosphonate action 57
1.7.3.1 Induction of cell apoptosis by the non-nitrogen BPs 58
1.7.3.2 Inhibition of protein prenylation by N-BPs.....60
1.7.4 Effects of IPP accumulation due to N-BP treatment 63
1.7.5 Clinical applications of bisphosphonates 64
1.8 OSTEOCLASTS AS TARGETS OF BISPHOSPHONATES 67
1.8.1 Osteoclast generation, morphology and function..... 67
1.8.2 Osteoclast targeting by BPs 73
1.9 BISPHOSPHONATE ANALOGUES AS ANTI-TUMOUR AGENTS 74
1.10 AIMS OF THE PROJECT..... 76
2. GENERAL MATERIALS AND METHODS 81
2.1 MATERIALS AND CHEMICALS..... 81
2.2 POLYMERASE CHAIN REACTION (PCR)..... 82
2.2.1 Target gene amplification by PCR..... 82
2.2.2 Colony PCR..... 84
2.2.3 Mutagenesis PCR 85
2.3 LIGATION INDEPENDENT CLONING (LIC) 86
2.3.1 Generation of LIC sites in insert/ vector 86
2.3.2 DpnI treatment 86
2.3.3 T4 DNA polymerase treatment..... 87

2.3.4 Annealing, transformation and mini-prep 88
2.4 RESTRICTION ENZYME CLONING 89
2.4.1 Generation of overhangs in insert/vector 89
2.4.2 Restriction digest 89
2.4.3 Ligation 90
2.5 DNA PURIFICATIONS 90
2.6 ESTIMATION OF NUCLEIC ACID CONCENTRATION 91
2.7 TRANSFORMATION 91
2.8 PREPARATION OF COMPETENT CELLS 92
2.9 AGAROSE GEL ELECTROPHORESIS 95
2.10 SMALL-SCALE PLASMID PREPARATION (Mini-prep) 96
2.11 LARGE-SCALE PLASMID PREPARATION (MaxiPrep) 97
2.12 DNA SEQUENCE ANALYSIS 97
2.13 SEQUENCE ALIGNMENT 98
2.14 GENERATION OF FPPS MUTANTS 98
2.15 PROTEIN EXPRESSION 100
2.15.1 Transformation in T7 RNA polymerase based strain 101
2.15.2 Overnight pre-culture 101
2.15.3 Culture in Terrific Broth (TB) and protein induction via IPTG addition 101
2.15.4 Cell harvesting 102
2.15.5 Cell lysis 102
2.16 PREPARATION OF GLYCEROL STOCKS FROM TRANSFORMED HOSTS 103
2.17 PROTEIN PURIFICATION TECHNIQUES 103

2.17.1 Manual elution from Ni-NTA column 104
2.17.2 Protein purification from streptavidin/aragose resin 105
2.17.3 Immobilized Metal Ion Affinity chromatography (IMAC)..... 105
2.17.4 Gel filtration 106
2.17.5 Tobacco Etch Virus (TEV) protease and thrombin cleavage of tag 106
2.17.6 Anion exchange chromatography 107
2.17.7 Buffer exchange 107
2.18 PROTEIN CONCENTRATION 107
2.19 PROTEIN CHARACTERIZATION AND PURITY 108
2.19.1 Sodium dodecyl sulfate polyacrylamide gel electrophoresis (SDS-PAGE) 108
2.19.1.1 Gel preparation 108
2.19.1.2 Sample preparation 109
2.19.1.3 Electrophoresis 109
2.19.2 Western Blotting Analysis 110
2.19.2.1 Preparation of lysate from cell culture 110
2.19.2.2 Electrophoretic transfer 111
2.19.2.3 Immunoblotting 112
2.19.3 Electrospray ionization time-of-flight mass spectrometry (ESI-TOF MS)..... 113
2.20 GENERATION OF STREPTAVIDIN-AGAROSE RESIN.....114
2.20.1 Expression and purification of recombinant streptavidin 114
2.20.2 Activation of Sepharose resin by cyanogen bromide 115
2.20.3 Coupling of Sepharose resin to streptavidin..... 115
2.21 GENERATION OF TOBACCO ETCH VIRUS PROTEASE ..116
2.22 HIS-TRAP COLUMN REGENERATION.....117

2.23 PROTEIN ASSAY 117

2.24 FPPS ACTIVITY ASSAY 118

2.24.1 Determination of K_m and V_{max} values 119

2.24.2 Bisphosphonate inhibition assay 119

2.25 FPPS KINETIC DATA ANALYSIS 120

2.26 RGGT ASSAY 121

2.27 CRYSTALLIZATION & DATA COLLECTION.....122

2.28 MODEL BUILDING.....124

2.29 ISOTHERMAL TITRATION CALORIMETRY (ITC) 125

2.30 OSTEOCLASTOGENESIS CULTURES 125

2.30.1 Isolation of Peripheral Blood Mononuclear Cells (PBMCs) from blood 125

2.30.2 Isolation of Osteoclasts from PBMCs 126

2.30.3 Tartrate-resistant acid phosphatase (TRAcP) and DAPI staining 127

2.30.4 Cell viability test using Trypan blue 128

2.30.5 Cell viability testing in PBMC cell cultures..... 128

2.31 BACULOVIRAL PROTEIN EXPRESSION.....129

2.31.1 Preparation of bacmid constructs 130

2.31.2 Transfection in Sf9 cell lines 131

2.31.3 Generation of baculoviral stocks..... 132

3. INVESTIGATION OF THE INTERACTION OF FPPS & 135

N-BPs.....135

3.1 INHIBITION OF FPPS BY N-BPs IS A MULTI-STEP PROCESS

.....135

3.2 VERIFICATION OF POINT MUTATIONS OF FPPS 138

3.2.1 Cloning and mutagenesis of FPPS..... 138

3.2.2 Expression and purification of FPPS constructs..... 139

3.3 TIME DEPENDENT INHIBITION CURVES AS A RESULT OF N-BPs TIGHT BINDING 143

3.4 FPPS CRYSTALS SHOW TETRAGONAL SYMMETRY AND HELP TO CHARACTERIZE SUBSTRATE-INHIBITOR BINDING 148

4. THE EFFECTS OF TYR204 FPPS MUTATIONS ON CATALYTIC ACTIVITY, CRYSTAL STRUCTURE AND N- BP BINDING.....155

4.1 INTRODUCTION 155

4.2 KINETIC CHARACTERIZATION OF TYR204 MUTANTS....157

4.3 CRYSTAL STRUCTURES OF TYR204 FPPS MUTANTS SUPPORT ALTERATIONS IN IPP BINDING 164

4.4 ALTERATION OF THE pH PROFILE IN FPPS MUTANTS SUPPORTS FORMATION OF A TYROSINATE ANION 169

4.5 INVESTIGATION OF THE INHIBITION MODE OF WT AND TYR204 FPPS MUTANTS BY N-BPs.....173

4.5.1 Reduction of final inhibition by Ris in tyrosine FPPS mutants reveals the importance of the aromatic ring 176

4.5.2 Inhibition by Zol suggests allosteric regulation of Tyr204 FPPS mutants 179

4.5.3 Inhibition by the amino-alkyl N-BPs reveals the importance of the Tyr204 ring for maintenance of enzyme: inhibitor isomerisation status 188

4.6 CONCLUSIONS 194

5. THE EFFECTS OF Lys200 FPPS MUTATIONS ON CATALYTIC ACTIVITY, CRYSTAL STRUCTURE AND N- BP BINDING 197

5.1 INTRODUCTION 197

5.2 KINETIC CHARACTERIZATION OF LYS200 MUTANTS 205

5.3 CRYSTAL STRUCTURES OF K200G AND K200L FPPS MUTANTS SUPPORT THE KINETIC FINDINGS REGARDING SUBSTRATE SATURATION 211

5.4 INVESTIGATION OF THE INHIBITION MODE OF LYS200 FPPS MUTANTS BY N-BPs 215

5.4.1 Inhibition by heterocyclic N-BPs does not support the importance of the hydrogen bond between N:BP-Lys200 for inhibition 218

5.4.2 Inhibition by the amino-alkyl bisphosphonates reveals the importance of Lys200 for enzyme isomerization 224

5.5 CONCLUSIONS 228

6. FPPS MUTATIONS IN HIGHLY CONSERVED RESIDUES THAT SEVERELY COMPROMISE THE CATALYTIC ACTIVITY AND N-BP BINDING 231

6.1 INTRODUCTION 231

6.2 KINETIC CHARACTERIZATION OF F239A, R112L AND DADA MUTANTS 237

6.3 CRYSTAL STRUCTURES OF F239A AND R112L CONFIRM KINETIC DATA 241

6.3.1 The crystal structures of F239A FPPS reveals a shift in the C-terminal tail 242

6.3.2 The crystal structure of R112L reveals disruption of the catalytic base for proton abstraction from the carbocation intermediate 244

6.4 INVESTIGATION OF THE INHIBITION MODE OF F239A FPPS MUTANT BY N-BPs 246

6.4.1 Inhibition by heterocyclic N-BPs reveals the importance of the hydrophobic C-terminal tail switch for the stabilization of the enzyme: inhibitor isomerization state 248

6.4.2 Inhibition by the amino-alkyl bisphosphonates is strongly suppressed in the F239A mutant 250

6.5 CONCLUSIONS 253

7. INSIGHTS INTO THE ASSEMBLY AND STRUCTURE OF RGGT CATALYTIC COMPONENTS 257

7.1 INTRODUCTION 257

7.2 EXPRESSION AND PURIFICATION STRATEGIES OF RGGT IN E. COLI 261

7.2.1 Single expression of RABGGTA and RABGGTB 262

7.2.2 Co-expression strategies for RABGGTA and RABGGTB 270

7.2.2.1 Cloning both subunits in different multiple cloning sites (MCS) of the same plasmid 270

7.2.2.2 Subcloning of either alpha or beta subunit previously cloned in a high copy plasmid to a bicistronic vector 271

7.2.2.3 Cloning of each subunit in individual plasmids and co-expression by a high copy vector 272

7.3 EXPRESSION OF CHML AND CHM IN E.COLI LEADS TO SEVERE PROTEOLYSIS 275

7.4 PURIFICATION OF RAB SUBSTRATES FROM RECOMBINANT E.COLI VECTORS RESULTS IN HIGH YIELD 281

7.4.1 RAB6B is highly expressed in recombinant *E.coli* 281

7.4.2 Purification of RAB7 from *E. coli* is only feasible at low salt concentration 283

7.5 RGGT ASSAYS REVEAL GERANYLGERANYLATION WITH DUAL EXPRESSION CONSTRUCTS 284

7.6 BACULOVIRAL EXPRESSION OF RGGT COMPLEX.....287

7.7 CONCLUSIONS.....291

8. IN VITRO EFFECTS OF N-BPs ON OSTEOCLASTOGENESIS 294

8.1 INTRODUCTION.....294

8.2 MAIN EXPERIMENTAL DESIGN AND LIMITATIONS OF THE CURRENT STUDY 298

8.3 INHIBITION OF OSTEOCLASTOGENESIS BY N-BPs IS MAINLY ATTRIBUTED TO THE DECREASED PRECURSOR AVAILABILITY AND NOT TO A DEFECTIVE COMMITMENT TO THE OSTEOCLASTIC LINEAGE 301

8.4 ALTERATIONS IN MORPHOLOGY OF IBA- AND ALE-TREATED OCs INDICATE INCREASED FUSION OF OC PRECURSORS.....305

8.5 CONCLUSIONS.....310

9. GENERAL DISCUSSION.....312

9.1 THE IMPORTANCE OF KEY FPPS RESIDUES IN CATALYSIS AND N-BP BINDING: PRESENT AND FUTURE STUDIES 312

9.1.1 The impact of FPPS mutations on enzyme catalysis and substrate binding..... 313

9.1.1.1 Catalytic mechanism.....313

9.1.1.2 GPP product formation and liberation 315

9.1.1.3 DMAPP binding 316

9.1.1.4 IPP saturation.....317

9.1.1.5 Impaired FPP synthesis and GPP accumulation.....318

9.1.1.6 C-terminal lid formation and thus E:I complex isomerization 318

9.1.1.7 GPP binding pocket formation.....319

9.1.2 The impact of FPPS mutations on N-BP binding and inhibition; 322

9.1.2.1 Ris 322

9.1.2.2 Zol 323

9.1.2.3 Iba.....325

9.1.2.4 Ale and Pam.....325

9.2 UNRAVELLING THE ASSEMBLY OF RGGT CATALYTIC COMPONENTS: PRESENT AND FUTURE STUDIES 328

9.3 EFFECTS OF MAJOR CLINICAL N-BPs ON OSTEOCLASTOGENESIS: PRESENT AND FUTURE STUDIES 329

9.4 THE RELEVANCE OF THE ENZYMATIC/MODELING STUDIES WITH REGARD TO THE IN VIVO POTENCY OF N-BPs: PRESENT AND FUTURE STUDIES 331

10. LIST OF REFERENCES 335

APPENDIX A: PRIMERS USED IN PCR REACTIONS 376

APPENDIX B: MAIN FEATURES OF USED VECTORS 377

APPENDIX C: PRIMER DESIGN FOR MUTAGENESIS 379

APPENDIX D: X-RAY DATA COLLECTION AND REFINEMENT STATISTICS.....381

LIST OF FIGURES

Figure 1.1: Generation of mevalonate by acetyl-CoA 22
Figure 1.2: Generation of IPP from mevalonate 25
Figure 1.3: Isomerization of IPP to DMAPP is achieved via a protonation- deprotonation mechanism 27
Figure 1.4: The generation of structural isoprenoid building blocks from IPP and DMAPP 28
Figure 1.5: Aspartate-rich domains are highly conserved among prenylsynthases 32
Figure 1.6: The mechanism of FPPS action as described in Scheme 1 (Hosfield *et al.* 2006) 34
Figure 1.7: Stereo-illustration of the formation of FPPS carbocation intermediate by side chain residues in *E. coli* FPPS 35
Figure 1.8: The mechanism of FPPS action as proposed by Sanchez *et al*. (2006) 37
Figure 1.9: Main amino-acid side chains which play a part in stabilization of partially closed (blue) conformation, closed (green) conformation, IPP binding pocket formation (red) and allylic binding (yellow) site in un-liganded human FPPS 39
Figure 1.10: Protein farnesylation (upper panel) and geranylgeranylation (lower panel) by Farnesyl Transferase (FTase) and Geranyl Transferase Type I GGTase-I respectively 43
Figure 1.11: Geranylgeranylation of one the CC motifs of Rab proteins is carried out by RGGT 44
Figure 1.12: Schematic representation of classical (top) and alternative (bottom) pathway of Rab prenylation by RGGT. 47
Figure 1.13: The catalytic mechanism of RGGT: REP complex 48
Figure 1.14: Ribbon representation of the rat RGGT structure 50

Figure 1.15: RGGT residues involved in REP1 binding and conformational change of RABGGTA leading to isoprenoid binding... 52
Figure 1.16: Molecular structure of inorganic pyrophosphate (left) and BP (right)..... 56
Figure 1.17: The structure of major BPs included in the present study . 57
Figure 1.18: A) Formation of aminoacyl adenylate intermediate is catalysed by aminoacyl-tRNA synthetases, with a concomitant release of PPi and B) Reverse aminoacylation occurs in the presence of non-nitrogen BP and leads to formation of toxic AppCp intermediates 59
Figure 1.19: Representation of the FPPS allylic binding pocket occupied by Ris..... 62
Figure 1.20: The ApppI toxic intermediate is generated by condensation of AMP with the accumulated IPP. 64
Figure 1.21: Osteoclast formation from bone marrow precursors 69
Figure 1.22: The role of RANKL, RANK and OPG in OC activation 71
Figure 1.23: Schematic representation of a resorbing OC 72
Figure 1.24: The point of BP and PC inhibition in mevalonate pathway76
Figure 1.25: Major amino-acids that are considered to play a pivotal role in the interaction of FPPS with Ris 78
Figure 1.26: FPPS inhibition by N-BPs is a multi-step process subjected to successful interaction of side-chain residues with the BP 78
Figure 1.27: Major amino-acids (in blue) that are considered to play pivotal role in the individual steps of FPPS catalytic mechanism. 79
Figure 3.1: Verification of successful FPPS cloning and mutagenesis.. 139
Figure 3.2: Successful purification of Y204A FPPS from p11 vector..... 141
Figure 3.3: LS-MSD TOF data obtained from purified F239A FPPS construct 142

Figure 3.4: Typical inhibition curves obtained from 10 min pre-incubation (p rate) assays and competitive initial rate (i rate) assays of WT with Ris (red) and Ale (blue)..... 146
Figure 3.5: Typical crystal patterns observed in Y204A FPPS mutant using LFS4-A8 screen 150
Figure 3.6: A) X-ray diffraction pattern of human Y204A FPPS showing resolution limit at 2.1 Å B) Predicted diffraction spots for the same crystal (in yellow) calculated in iMosflm 151
Figure 3.7: Detailed Ramachandran plot of the final crystal model of human Y204A FPPS 152
Figure 3.8: 2Fo-Fc electron density maps of F239A FPPS contoured at 1 sigma, showing the position of mutated amino-acid relatively to Ris and IPP 153
Figure 4.1: The proposed hydrogen bond of Tyr204 with the N atom of Pam is disrupted in Y204F and Y204A FPPS mutants..... 156
Figure 4.2: Sequence alignment of FPPS orthologs reveals that Tyr204 is conserved among diverse species..... 157
Figure 4.3: Sequence alignment of human FPPS with GGPPS reveals substitution of Tyr in position 204 with Leu (in red)..... 161
Figure 4.4: Superposition of WT and Y204F FPPS mutant crystal structures reveals changes in the IPP binding pocket 166
Figure 4.5: Superposition of WT and Y204A FPPS mutant crystal structures reveals changes in the IPP binding pocket 167
Figure 4.6: DMASPP position in the binding pocket is stabilized by the conserved aspartate motifs Asp103, Asp107, Asp244 and hydrophobic interactions with Arg192, Gln171, Lys200 and Thr201..... 168
Figure 4.7: Optimal catalytic activities of Tyr204 FPPS mutants are observed in acidic environment..... 170

Figure 4.8: Superposition of WT FPPS (pdb:1ZW5) and Y204A FPPS structures reveals that position of Ris is unaltered in tyrosine mutants. 178
Figure 4.9: The weakening of the hydrogen bond between Lys200 and Thr201 with the imidazole nitrogen of Zol contributes to the increased inhibition in Y204A FPPS mutant 183
Figure 4.10: Thermodynamics of Zol binding to human Y204A FPPS in the presence of 2 mM MgCl2, measured by isothermal titration calorimetry 184
Figure 4.11: A potential model of allosteric regulation caused by Zol binding to Y204A FPPS 187
Figure 4.12: Changes in potency of Iba in Y204F FPPS over time reveal its time dependent inhibition 189
Figure 4.13: Orientation of Lys200 and Thr201 in Y204A FPPS mutant favours formation of hydrogen bonds with gamma carbonyl oxygen and nitrogen of Ale respectively, reinforcing Ale inhibition..... 191
Figure 4.14: Formation of van der Waals interactions between the amino-group of Pam and mutated Tyr204 residue is not favoured in Y204A FPPS mutant, increasing the strength of inhibition..... 193
Figure 5.1: Sequence alignment of FPPS and GGPPS orthologs reveals that Lys200 and Thr201 are conserved among diverse species..... 198
Figure 5.2: The hydrogen bond between the side chain of Lys202 in *E.coli* and O_7 atom of DMAPP contributes to the correct orientation of DMAPP substrate for catalysis..... 200
Figure 5.3: Formation of a hydrogen bond between the Lys207 (Lys200 in human) and the phosphonate oxygen of Ale in *T. cruzi* FPPS assists the N-BP binding to the allylic pocket 202

Figure 5.4: The proposed salt-bridge interactions of Lys200 with the phosphonate groups of N-BPs (in purple) are responsible for the strength of N-BP binding 204
Figure 5.5: Possible effects of Lys200 substitution in substrate binding and product release from FPPS 207
Figure 5.6: Alteration of C-terminal basic tail positioning in K200G FPPS reveals destabilization of the fully closed conformation 213
Figure 5.7: Destabilization of the closed but not partially closed conformations in K200G FPPS 214
Figure 5.8: Orientation of heterocyclic ring of Ris and its positioning in the allylic binding pocket is unaffected in K200G (A) and K200L (B) mutants 222
Figure 5.9: Maintenance of Lys200: FPPS hydrogen bond in T201A mutant is sufficient to properly position the imidazole ring of Zol in the allylic binding pocket 223
Figure 6.1: Proposed mutation effects on highly conserved prenyltransferase residues that alter the strength of N-BP binding 236
Figure 6.2: Superposition of WT FPPS and F239A mutant crystal structures in complex with Zol and IPP or Ris and IPP respectively reveals changes in the positions of the C-terminal tail 243
Figure 6.3: The superposition of WT: IPP: Zol and F239A: IPP: Pam crystal structures reveals changes in the C-terminal tail 244
Figure 6.4: Superposition of WT: IPP: Zol and R112L: IPP crystal structures reveals inability of the enzyme to form the catalytic base for IPP proton abstraction by the carbocation intermediate 245
Figure 6.5: Crystal structure of F239A FPPS: Ris reveals disruption of electrostatic interactions in the allylic binding pocket that contribute to the decreased Ris binding 250

Figure 6.6: Shifting in amino-acid positions in F239A FPPS in complex with Pam destabilizes the closed conformation and the enzyme: inhibitor isomerization step 252
Figure 7.1: Recombinant RABGGTA accumulates in inclusion bodies in *E.coli* cells 264
Figure 7.2: Elution profiles of RABGGTA 265
Figure 7.3: Successful purification of RABGGTB is detected by SDS-PAGE analysis 266
Figure 7.4: Successful isolation of RABGGTA and RABGGTB is detected by Western blotting analysis 267
Figure 7.5: Confirmation of RABGGTA and RABGGTB complex identity by gel filtration on a pre-calibrated Superdex 200 GF column 269
Figure 7.6: Co-expression strategies of RABGGT lead to successful production of both subunits, albeit with low yield 275
Figure 7.7: Analytical gel filtration on a Superdex 200 column shows that CHML fails to recognize and bind RAB6B substrate 279
Figure 7.8: Successful purification RAB6B from *E.coli* 282
Figure 7.9: RAB7 was successfully purified by IMAC and gel filtration from *E.coli* 284
Figure 7.10: Time-course of RAB7 geranylgeranylation catalyzed by the dual expressed RABGGT. 286
Figure 7.11: Photomicrograph of insect cells transduced with a bacmid virus as described in 2.31 288
Figure 7.12: Presence of a 40 kDa band in RABGGTB but not in RABGGTA and CHML lysate obtained from P0 viral stock indicates successful expression of Beta subunit 289

Figure 7.13: The presence of a 70 kDa band in RABGGTA but not in RABGGTB indicates successful elution of alpha subunit. B) Presence of a 80 kDa band in CHM and C) CHML sample indicates possible expression of REP..... 290
Figure 8.1: Stages of OC development from BPMCs in tissue culture. 297
Figure 8.2: Effect on N-BP treatment of OC cells for day 0- 7 303
Figure 8.3: Comparison of the effects of A)Ris B)Zol C)Iba and D)Ale on distinct stages of osteoclastogenesis..... 305
Figure 8.4: An augmentation in the area of Ale- and Iba- treated OCs for day 7-14 is observed at drug concentrations of 10 nM and 100 nM 307
Figure 8.5: Increased size of OC area following treatment between day 7-14 with 10 and 100 nM Iba or Ale..... 308
Figure 8.6: Ris and Zol treatment does not modify the size of OC..... 309
Figure 9.1: Major amino-acids that play pivotal role in FPPS catalytic mechanism as identified in the current study. This scheme comprises an update of the existing mechanism as denoted in Figure 1.26. The present study either confirms (in green), rejects (in black) or introduces (in red) the involvement of FPPS side-chain residues in catalytic mechanism. In blue: role not examined..... 321
Figure 9.2: Updated schematic representation of the mode of inhibition of FPPS by N-BPs. The major amino-acids that are confirmed (in green), or identified (in red) to play a pivotal role in the binding and successful FPPS inhibition by the N-BPs in accordance to the findings of the present research..... 326

LIST OF TABLES

Table 1.1: Isoprenoids and their precursors 29
Table 2.2: PCR cycle conditions for Platinum Taq Polymerase 83
Table 2.3 PCR cycle conditions for Herculase Hot start Polymerase 84
Table 2.5: PCR cycle conditions for Pfu Turbo Polymerase 85
Table 2.6: T4 vector treatment 87
Table 2.7: T4 insert treatment 88
Table 2.8: Antibiotic stocks used in preparation of LB-agar plates 92
Table 2.9: Bacterial strains, antibiotics and company of purchase 93
Table 2.10: Solutions used in preparation of competent cells 94
Table 2.11: Solutions used in Western blotting 111
Table 2.12: Primary antibodies used in Western blotting 113
Table 2.13: Secondary antibodies used in Western blotting 113
Table 2.14: Crystallization screens used 123
Table 2.15: Solutions used for TRAcP staining 128
Table 3.1: Designed FPPS amino-acid mutations and their proposed roles in FPPS catalysis and inhibition by N-BPs 137
Table 3.2 Expected protein mass of FPPS constructs and protein yield142
Table 3.3: Main crystallographic characteristics of solved FPPS structures 154
Table 4.1: Kinetic parameters for FPPS WT, Y204F and Y204A FPPS .. 158
Table 4.2: Estimation of Ki, Ki* and Kisom of Tyr204 mutants derived from inhibition assays with N-BPs 175
Table 4.3: Comparison between WT and Tyr204 mutants Ki, Kint and Ki* inhibition rates by Ris 177
Table 4.4: Statistical analyses of initial and intermediate Ki by Zol 180
Table 4.5: IC_{50} values of mutant enzymes for final inhibition of Zol, compared to the WT inhibition data 181

Table 4.6: Thermodynamic data for Zol binding determined by ITC .. 185
Table 4.7: Statistical analyses of initial and intermediate Ki by aminoalkyl BPs 190
Table 5.1: Kinetic parameters for FPPS WT, K200G, K200L and K200E206
Table 5.2 Estimation of Ki, Ki* and Kisom of WT and Lys200 mutants derived from inhibition assays with N-BPs 217
Table 5.3: Comparison between WT and Lys200 mutants Ki and Ki* rates produced by Ris and Zol 221
Table 5.4: Comparison between WT and Lys200 mutants Ki and Ki* rates by Iba, Ale and Pam 225
Table 6.1: Kinetic parameters for FPPS WT, F239A and R112L mutants237
Table 6.2: Estimation of Ki, Ki* and Kisom of WT and F239A FPPS mutant derived from inhibition assays with N-BPs 247
Table 7.1 Results from 50 ml test expressions of RABGGTA and RABGGTB 263
Table 7.2: Co-expression strategies in *E.coli* led to successful co-purification of RABGGTA/RABGGTB subunits..... 274
Table 7.3: Purification trials of CHML expressed in *E.coli* and their outcome 276
Table 7.4: Purification trials of CHM constructs and their outcome 280
Table 9.1: Summary of suggested role of individual FPPS mutations . 319
Table 9.2: Observed effects of the studied FPPS mutations in N-BP binding..... 327
Table 9.3: Current studies on the interaction of individual point mutations with the major clinical N-BPs 327

1. GENERAL INTRODUCTION

1.1 THE MEVALONATE PATHWAY

1.1.1 Generation of mevalonate; an overview

The mevalonate pathway is the exclusive route of production of all isoprenoids in animals and plays a key role in the biosynthesis of products and intermediates involved in multiple cellular functions such as cholesterol synthesis, intracellular messaging and growth control (Buhaescu and Izzedine, 2007, Goldstein and Brown, 1990, Lynen, 1967, McTaggart, 2006). Systematic studies of cholesterol biosynthesis via administration of isotopic tracers led to the demonstration that acetic acid significantly contributed to the synthesis of the aliphatic side chain of cholesterol (Bloch, 1965, Bloch and Rittenberg, 1942, Wuersch *et al.*, 1952). The isolation of mevalonic acid as an acetate replacing factor for *Lactobacillus acidophilus* (Cresson *et al.*, 1956) combined with the observation of its structural resemblance to hydroxymethylglutarate, a well known derivative of acetate in plants, helped to identify mevalonate as an active intermediate in sterol biosynthesis (Tavormina *et al.*, 1956). Soon afterwards the full pathway of mevalonate generation from acetyl-CoA was elucidated (Lynen, 1967, Lynen *et al.*, 1958, Rudney, 1957).

Mevalonate is synthesized in the cytosol in three individual steps (Figure 1.1).

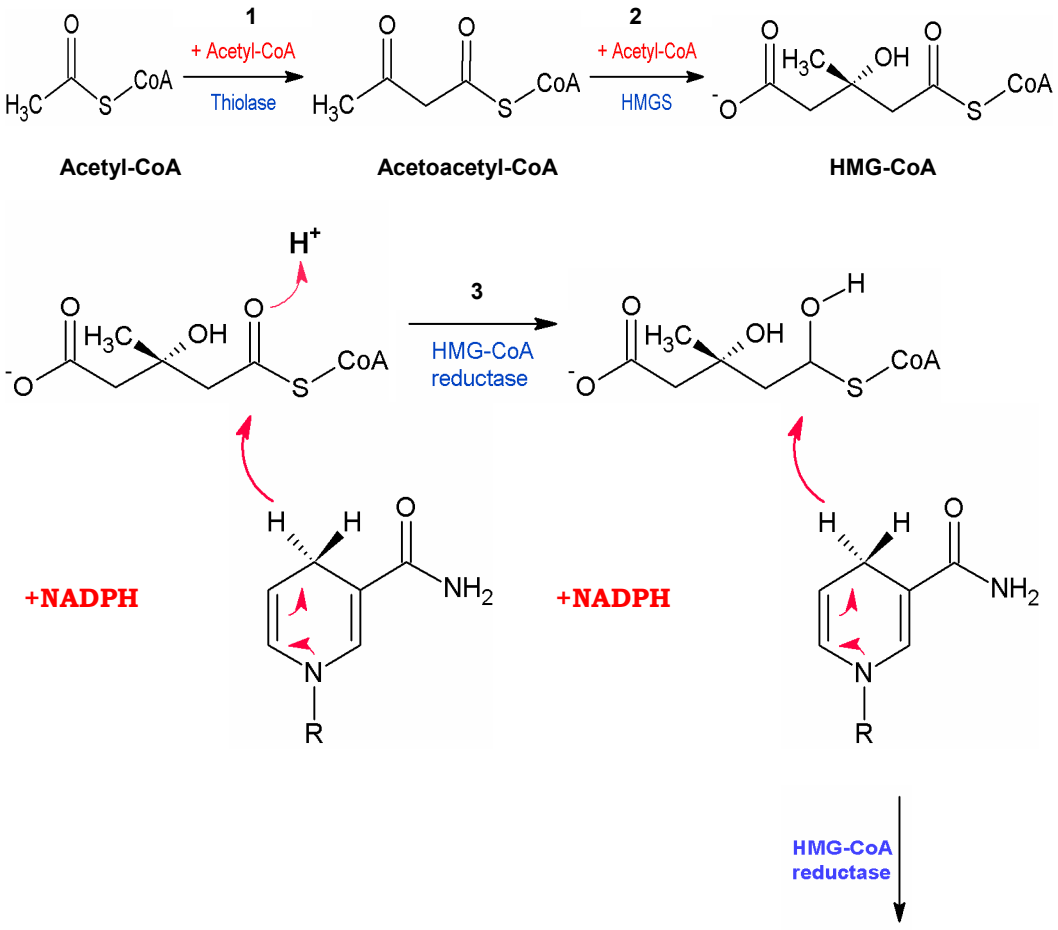
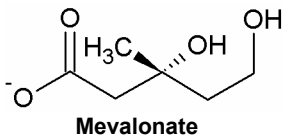


Figure 1.1: Generation of mevalonate by acetyl-CoA

1) Thiolase catalyzes the condensation of two molecules of Acetyl-CoA to yield acetoacetyl-CoA

2) Hydroxymethylglutaryl-CoA synthase (HMGS) catalyzes the condensation acetyl-CoA with acetoacetyl-CoA to yield HMG-CoA

3) Hydroxymethylglutaryl-CoA reductase catalyzes the two final steps of mevalonate formation



First, condensation of two molecules of acetyl-CoA, catalyzed by thiolase, yields the intermediate acetoacetyl-CoA. A subsequent condensation of a third molecule of acetyl-CoA with the derived acetoacetyl-CoA is catalyzed by cytosolic hydroxymethylglutaryl-CoA synthase (HMGS) and results in formation of hydroxymethylglutaryl-coenzyme alpha (HMG-CoA). Finally, the thioester HMG-CoA is converted to the primary alcohol mevalonate by two successive NADPH-dependent reductions, both catalyzed by the endoplasmic reticulum (ER) enzyme hydroxymethylglutaryl-CoA reductase.

1.1.2 Regulation of mevalonate synthesis

Long-term and short-term regulation of mevalonate synthesis in the cell is essential for maintenance of both sterol and non-sterol pathway derivatives in physiological amounts. The bulk end product of mevalonate synthesis is cholesterol but it can also be incorporated into mammalian cells from dietary sources via the bloodstream by receptor-mediated endocytosis of plasma low density lipoproteins (LDL) (Brown and Goldstein, 1979b, Goldstein and Brown, 1990). LDL particles are engulfed by LDL receptors located on the plasma membrane and delivered to lysosomes where they are degraded releasing free cholesterol (Brown and Goldstein,

1985). The balance of endogenous and exogenous cholesterol is achieved through a feedback regulation of both HMG-CoA synthase and reductase, however the rate determining step of the pathway is strictly dependent on the long-term feedback regulation of HMG-CoA reductase (Brown and Goldstein, 1985, Goldstein and Brown, 1990). When LDL is not available, the activities of both enzymes increase, resulting in abundant mevalonate synthesis for production of sterol and non-sterol derivatives (Goldstein *et al.*, 1980). In the presence of LDL, HMG-CoA synthase and reductase activities fall by more than 90%, to a level adequate to maintain synthesis of all the non-sterol products (Brown and Goldstein, 1980). When LDL-cholesterol or exogenous mevalonate supplies are high, the HMG-CoA reductase activity is turned off and mevalonate synthesis is abolished (Brown and Goldstein, 1985). Finally, in case of high intracellular accumulation of cholesterol, the LDL receptor gene is repressed, suppressing LDL receptor synthesis and further delivery of LDL to cells (Goldstein and Brown, 1984).

1.1.3 Generation of isoprenoid intermediates from mevalonate

During cholesterol biosynthesis, formation of phosphorylated intermediates of mevalonate is facilitated by the intermediate

cofactor ATP (Popjak *et al.*, 1958) leading to the generation of the basic isoprene building block, isopentenyl pyrophosphate (IPP) (Bloch, 1965)(Figure 1.2).

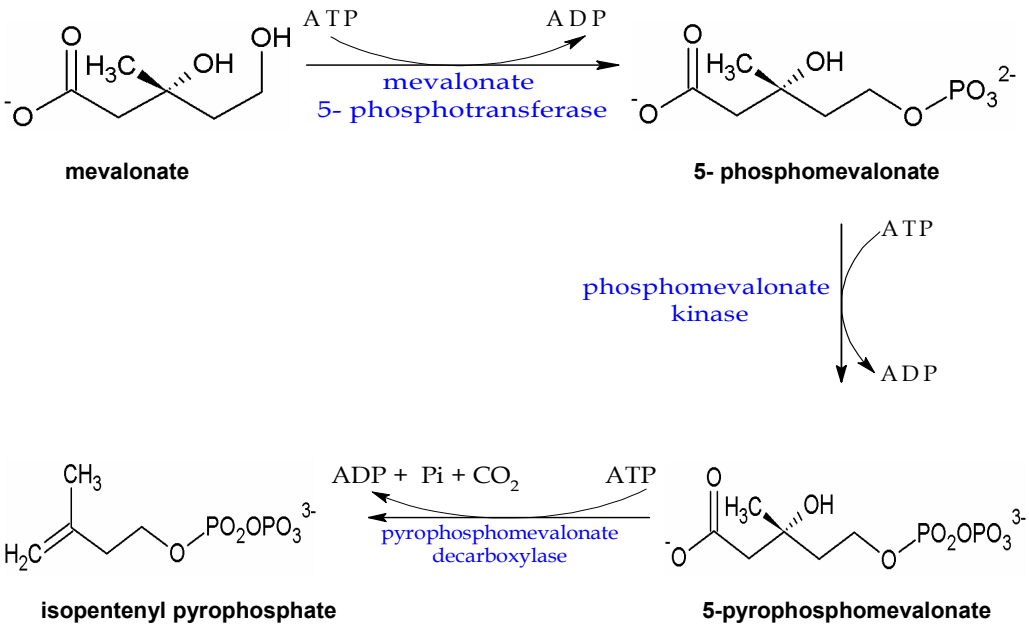


Figure 1.2: Generation of IPP from mevalonate is a result of three ATP-dependent reactions: two phosphorylations catalysed by mevalonate 5-phosphotransferase, phosphomevalonate kinase and a decarboxylation catalysed by pyrophosphomevalonate decarboxylase.

Firstly, the mevalonate 5-phosphotransferase phosphorylates the hydroxyl group of mevalonate, yielding phosphomevalonate (Tchen and Bloch, 1957a, b). Subsequently, phosphomevalonate kinase converts the resulting phosphate group to pyrophosphate (Henning *et al.*, 1959). This step is subject to post-translational regulation via competitive inhibition at the ATP-binding site by

isoprenoid intermediates situated further along the pathway (Dorsey and Porter, 1968, Hinson *et al.*, 1997). Finally, IPP is generated by an ATP-dependent dehydration-decarboxylation reaction (Lehninger, 1982, Lindberg *et al.*, 1962, McTaggart, 2006) where phosphorylation of the tertiary hydroxyl group of 5-pyrophosphomevalonate by ATP promotes subsequent elimination of the carboxylic acid residue as carbon dioxide (De Waard *et al.*, 1959).

Conversion of mevalonate to the activated isoprene intermediates isopentenyl pyrophosphate (IPP) and dimethylallyl pyrophosphate (DMAPP) is essential for subsequent generation of all isoprenoids (Deneris *et al.*, 1984, Goodman and Popjak, 1960). The equilibration between IPP and DMAPP is catalyzed by isopentenyl pyrophosphate isomerase via a protonation-deprotonation mechanism, coordinated by Mg^{2+} ions (Cornforth *et al.*, 1958, Cornforth *et al.*, 1966, Leyes *et al.*, 1999, Street and Poulter, 1990, Voet and Voet, 1995). The Glu116 carboxylic group of the enzyme protonates the C_3-C_4 double bond of IPP, forming a carbocation, whereas abstraction of a proton from the C_2 carbon of IPP is performed by the thiol group of Cys67, leading to DMAPP formation (Wouters *et al.*, 2003)(Figure 1.3).

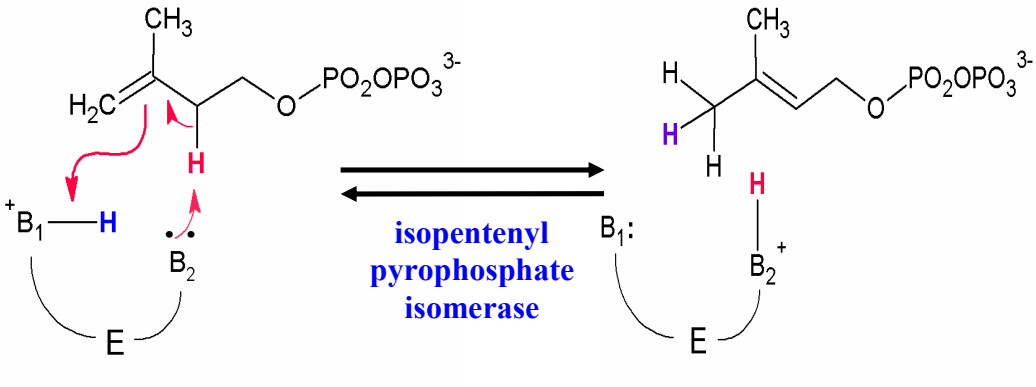


Figure 1.3: Isomerization of IPP to DMAPP is achieved via a protonation-deprotonation mechanism. IPP isomerase catalyzes an antarafacial transposition of hydrogen by a proton addition–elimination mechanism. B_1: thiol group of Cys67 as a proton acceptor B_2: carboxylate group of Glu116 as a proton donor.

Addition of an allylic moiety to the double bond of DMAPP is catalysed by farnesyl pyrophosphate synthase (FPPS) and yields geranyl pyrophosphate (GPP), the next higher member of the isoprenoids. A second round of catalysis by FPPS aids condensation of GPP with IPP to yield the C_{15} farnesyl pyrophosphate (FPP) (Cornforth *et al.*, 1966, Donninger and Popjak, 1966, Popjak and Cornforth, 1966). Finally, addition of IPP to the generated FPP is catalyzed by geranylgeranyl pyrophosphate synthase (GGPPS), and yields the C_{20} geranylgeranyl pyrophosphate (GGPP) (Kavanagh *et al.*, 2006a)(Figure 1.4).

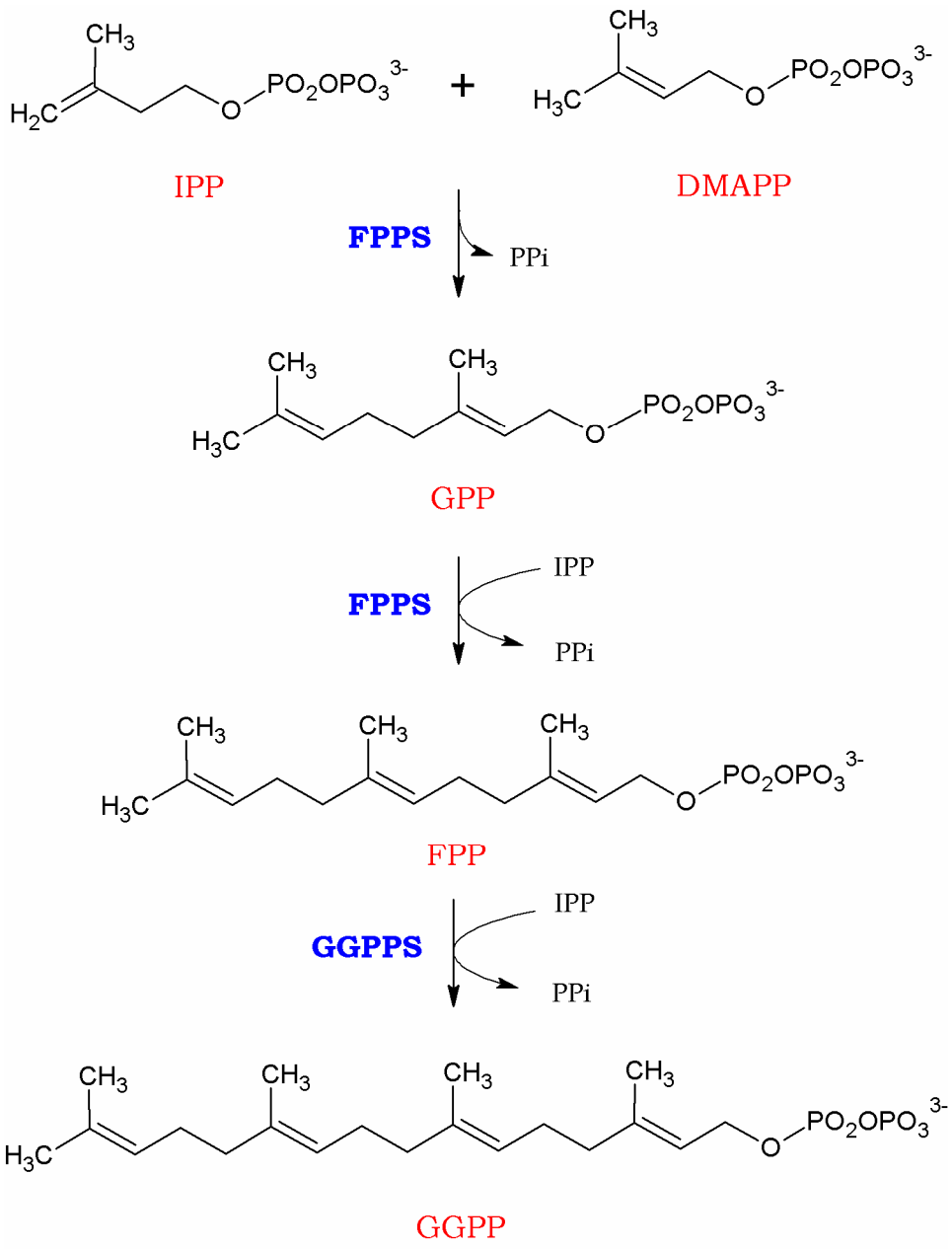


Figure 1.4: The generation of structural isoprenoid building blocks from IPP and DMAPP. FPPS catalyzes a head to tail condensation of the 5-carbon allylic substrate DMAPP with IPP to yield geranylpyrophosphate (GPP) and subsequently a second head to tail condensation of GPP and IPP to yield farnesyl pyrophosphate (FPP). Addition of IPP to FPP is catalyzed by geranylgeranyl pyrophosphate synthase (GGPPS), yielding geranylgeranyl pyrophosphate (GGPP). PPi denotes liberated inorganic pyrophosphate.

This is the branchpoint of the mevalonate pathway which generates all the acyclic structural isoprenoid building blocks (GPP, FPP and GGPP), (Bloch, 1965, Kellogg and Poulter, 1997, Lynen, 1967) whereas additional modifications such as oxidation, reduction and isomerization are required to yield the diverse terpenoid compounds (Table 1.1) (Cane *et al.*, 1991, Roberts, 2007, Ruzicka, 1959).

Table 1.1: Isoprenoids and their precursors

No of C	Name	Precursor
5	Isoterpenes	IPP, DMAPP
10	Monoterpenes	GPP
15	Sesquiterpenes	FPP
20	Diterpenes	GGPP
30	Triterpenes	condensation of 2 FPP molecules
40	Tetraterpenes	condensation of 2 GGPP molecules
>40	Polyterpenes	condensation of terpene intermediates

The main precursor of sterol compounds, squalene, derives from a head-to-head condensation of two FPP units catalyzed by squalene synthase (Popjak *et al.*, 1961, Zhang *et al.*, 1993). Formation of cholesterol precursor lanosterol occurs via squalene oxidation and subsequent cyclization of the reaction product (Bloch, 1965, Woodward and Bloch, 1953). Demethylation and reduction of lanosterol to cholesterol is a 19-step reaction process,

catalyzed by enzymes associated with the ER membranes (Gaylor, 2002, Risley, 2002, Voet and Voet, 1995).

1.2 FARNESYL PYROPHOSPHATE SYNTHASE (FPPS)

1.2.1 Insights into the catalytic mechanism of FPPS

Farnesyl pyrophosphate synthase (FPPS) is a 78-80 kDa homodimeric enzyme (Barnard and Popjak, 1981) that catalyzes the head-to-tail condensation of the 5-carbon allylic substrate DMAPP with IPP to yield the C_{10} geranylpyrophosphate (GPP) and subsequently a second head-to-tail condensation of GPP and IPP to yield the C_{15} farnesyl pyrophosphate (FPP) (Porter and Spurgeon, 1981, Voet and Voet, 1995). FPPS catalysis is specific for IPP (Poulter and Rilling, 1976), however either DMAPP (Glickman and Schmid, 2007) or GPP (Lewis *et al.*, 2008, Mekkriengkrai *et al.*, 2004) can be used as substrates to synthesize GPP or FPP, respectively. In the absence of DMAPP, binding of two IPP molecules can occur at the FPPS active site but without formation of GPP (Reed and Rilling, 1976). In the absence of IPP, FPPS can also catalyze the hydrolysis of GPP to geraniol, however at a greatly reduced rate (Poulter and Rilling, 1976).

The presence of distinct allylic (DMAPP/GPP) and homoallylic (IPP) binding sites in FPPS and the dependence of allylic substrate

binding on divalent metal ions has been established (Reed and Rilling, 1976). The FPPS reaction mechanism seems to be highly ordered, with the allylic substrates first occupying the relevant binding site (Laskovics and Poulter, 1981, Rondeau *et al.*, 2006). However discrimination between the structurally similar DMAPP and IPP by the allylic binding site is not always possible, leading to inhibition of catalysis in presence of elevated concentrations of IPP (Reed and Rilling, 1976). Early biochemical studies indicated the dependence of FPPS reaction on divalent metal ions such as Mg^{2+} and Mn^{2+} and simultaneous release of allylic product and pyrophosphate (Poulter *et al.*, 1978). Surprisingly enough the high energy liberated from inorganic pyrophosphate does not appear to facilitate catalysis, nor does it favour the reaction thermodynamically. It is the complexing of the diphosphate moieties with the metal ions that aid chelation and proper orientation of the substrates for catalysis (Gotoh *et al.*, 1992). Identification of the dependence of catalysis on aspartate moieties in highly conserved motifs in several prenylsynthases from a range of unrelated species (Ashby and Edwards, 1990, Joly and Edwards, 1993)(Figure 1.5) led to hypothesis that binding of diphosphate moieties of allylic substrates through Mg- bridges is crucial for catalysis (Joly and Edwards, 1993).

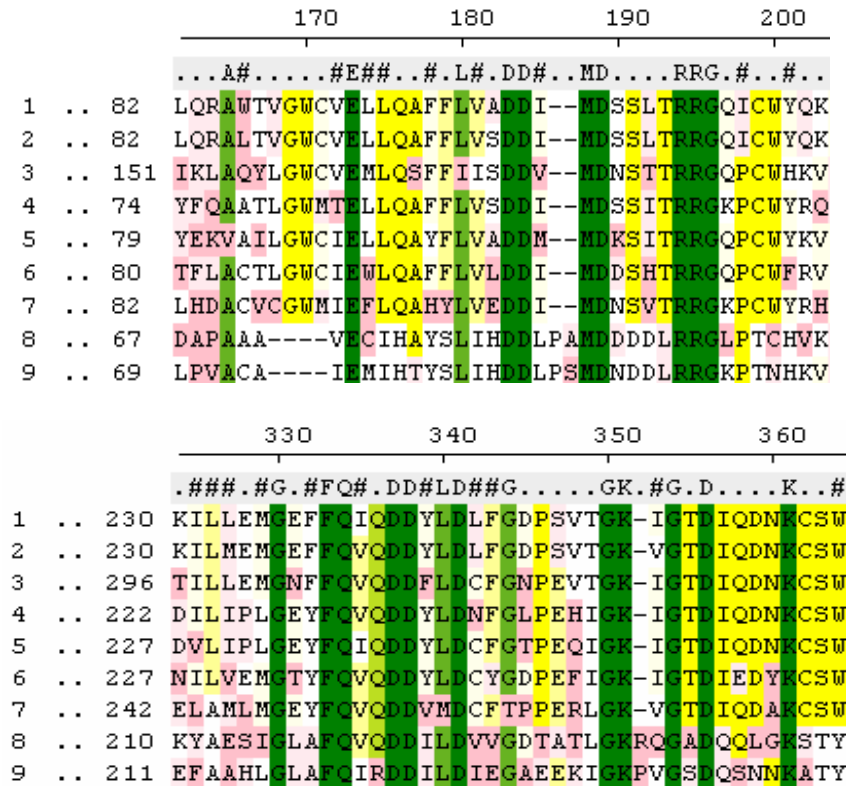


Figure 1.5: Aspartate-rich domains are highly conserved among prenylsynthases. Sequence alignment of FPPS from: 1: human (*Homo sapiens*) 2: murine (*Mus musculus*), 3: insect (*Drosophila melanogaster*), 4: fungi (*Neurospora crassa*), 5: yeast (*Saccharomyces cerevisiae*), 6: plant (*Zea mays*), bacteria (7*: Bacillus stearothermophilus*, 8: *Escherichia coli*), 9: parasite (*Trypanosoma brucei*) reveal the presence of the highly conserved aspartate-rich domains (dark green) among unrelated species.

Confirmation of the above theories came from studies on avian FPPS that revealed the strict dependence of aspartate-rich sequences on metal ion binding for catalysis (Tarshis *et al.*, 1994). The currently accepted mechanism is of utmost interest as it is one

of the few known that proceeds via the elimination of pyrophosphate and the subsequent formation of a carbocation intermediate (Cornforth and Popjak, 1959, Poulter *et al.*, 1978, Poulter and Rilling, 1976, Rilling and Bloch, 1959). A study of the crystal structure of the *E. coli* and *S. aureus* FPPS in complex with IPP and the non-cleavable DMAPP analogue dimethylallyl S-thiolodiphosphate (DMASPP) (Phan and Poulter, 2000) supported the theory of a three step ionization-condensation-elimination mechanism (Hosfield *et al.*, 2004) and favoured the hypothesis of allylic carbocation formation originally suggested by Poulter and Rilling (1976). This observation agrees with studies performed with *Trypanosoma cruzi* FPPS where the aspartate-rich regions located in the central cavity of the catalytic site are mediating the binding of prenyl pyrophosphates to the protein via formation of salt bridge interactions with three Mg^{2+} ions (Gabelli *et al.*, 2006). On the basis of crystallographic and kinetic data, two distinct schemes of FPPS catalysis have been proposed:

Scheme 1: Ionization of DMAPP is facilitated by the trinuclear Mg cluster of the enzyme where all three Mg^{2+} ions form linkages with the un-esterified oxygen of the pyrophosphate, enhancing the juxtaposition of the hydrophobic C_5 isoprenoid tail of the IPP in the right conformation for subsequent catalysis (Gabelli *et al.*, 2006, Garzoni *et al.*, 2004, Hosfield *et al.*, 2004)(Figure 1.6).

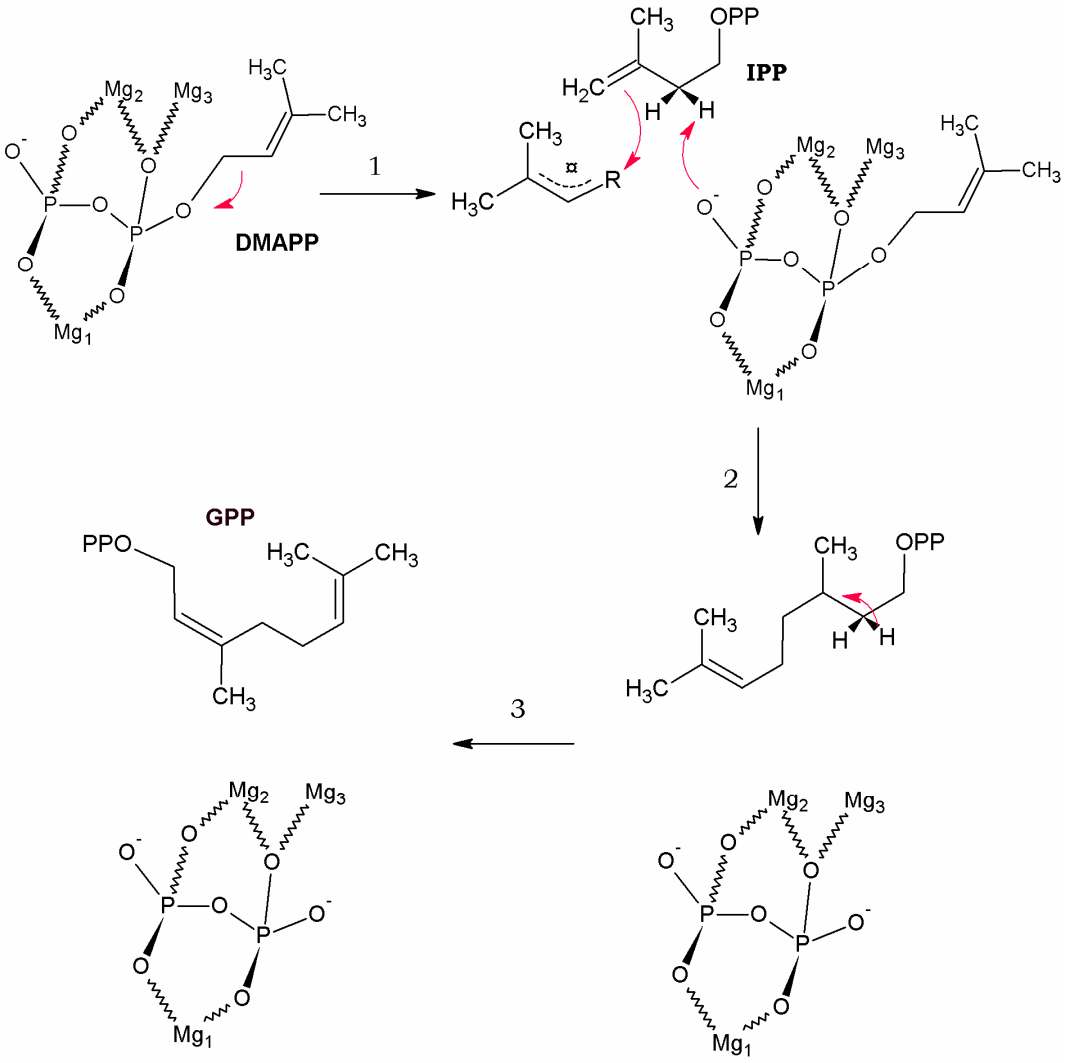


Figure 1.6: The mechanism of FPPS action as described in Scheme 1 (Hosfield *et al.* 2006). DMAPP ionization facilitated by the tri-nuclear Mg cluster generates the carbocation intermediate (1) which in turn alkylates the C_5 bond of IPP (2). Elimination of final product GPP is facilitated by proton abstraction of the condensed intermediate facilitated by DMAPP pyrophosphate oxygen.

The carbocation binding site is supposedly formed by the interaction of the negative carbonyl oxygen of Lys202 and the side-

chain oxygen of Thr203 and Gln241 with the positively charged C_1, C_2 and C_3 atoms of DMAPP (Hosfield *et al.*, 2004), (Figure 1.7).

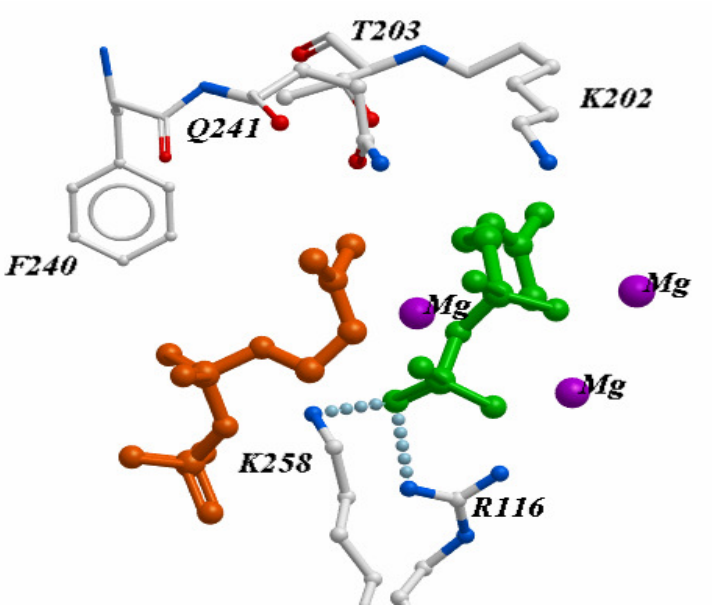


Figure 1.7: Stereo-illustration of the formation of FPPS carbocation intermediate by side chain residues in *E. coli* FPPS. Interaction of the positively charged C_1 C_2 and C_3 atoms of DMSAPP with the side chain oxygens of Thr203 and Gln241 and the carbonyl oxygen of Lys202 result in formation of carbocation intermediate. The negative charged of the generated pyrophosphate is stabilized by the tri-nuclear Mg cluster (purple spheres). The free pyrophosphate oxygen of DMASPP (green) forms the catalytic base for the removal of proR hydrogen of IPP (orange) and subsequent formation of C_3-C_5 double bond. Adapted from pdb:1RQI, Hosfield *et al.* (2004).

The tri-nuclear Mg cluster stabilizes the developing negative charge of the liberated pyrophosphate which in turn aids stabilization of the developed positive allylic charge. The cation formed condenses with the nucleophilic C_3- C_5 double bond of IPP. Finally elimination of the isoprenoid reaction product GPP is

achieved by de-protonation of the condensed intermediate by the free pyrophosphate oxygen (Hosfield *et al.*, 2004).

Scheme 2: Ionization of allylic substrate DMAPP occurs as described in scheme 1, generating a transition state with a carbocationic character (Figure 1.8).

Formation of the C_1-C_4 bond between IPP and DMAPP, rupture of the C_1-oxygen bond between DMAPP- carbocation intermediate and hydrogen transfer from IPP to the pyrophosphate moiety of DMAPP occur simultaneously rather than in three individual steps (Sanchez *et al.*, 2006). Condensation and elimination steps are similar to Scheme 1 (Rilling and Bloch, 1959, Sanchez *et al.*, 2006). It has however to be stated that Scheme 2 is exclusively based on computer simulation using quantum and molecular mechanics modeling methods whereas Scheme 1 is backed up by hard evidence.

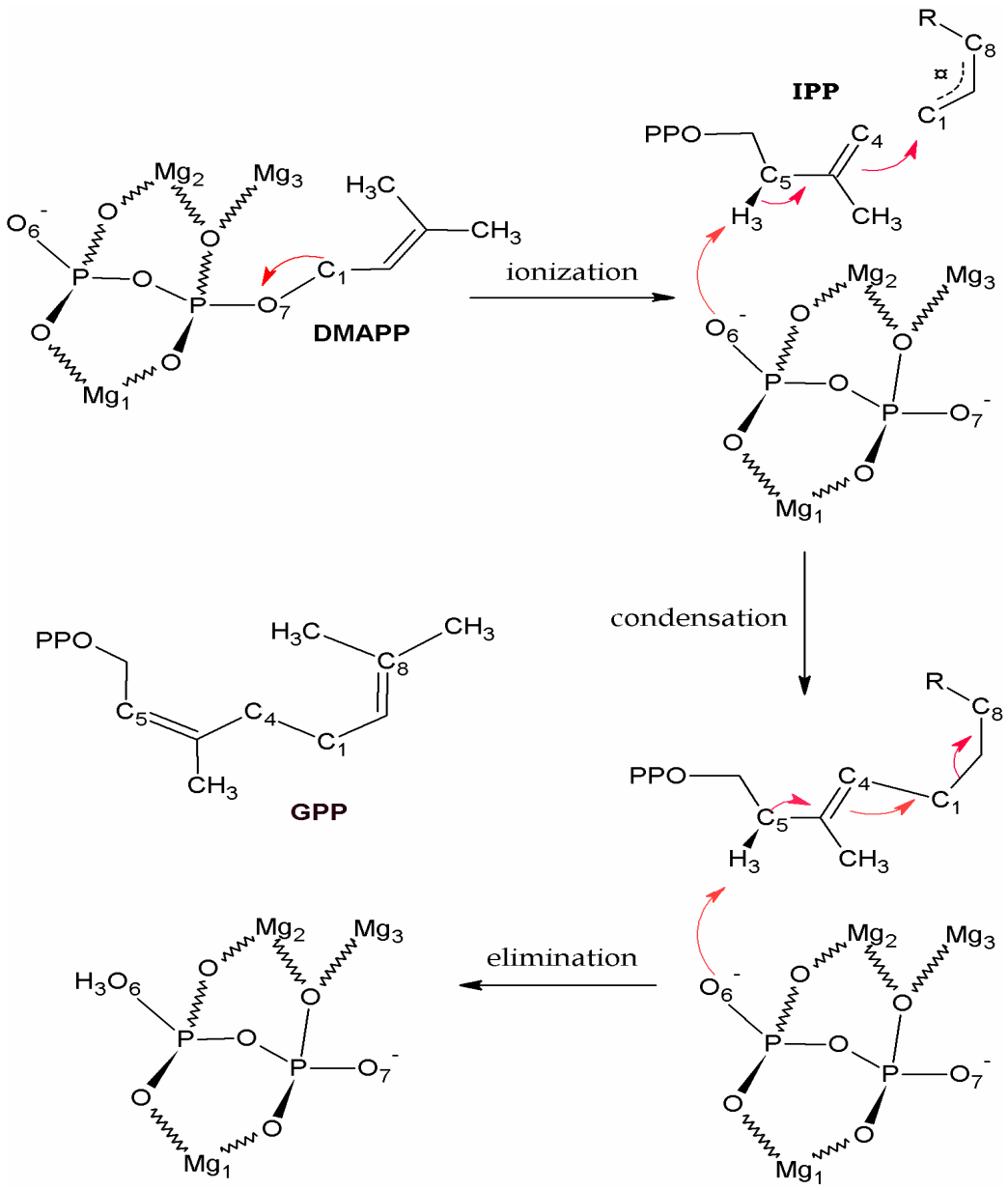


Figure 1.8: The mechanism of FPPS action as proposed by Sanchez *et al.* (2006). Ionization of DMAPP is facilitated by the tri-nuclear Mg centre and generates the carbocation intermediate At this stage formation of C_1-C_4 bond and H_3 transfer to the negative pyrophosphate O_6 occur simultaneously. Condensation of the nucleophilic C_3-C_5 double bond of IPP follows. Elimination of GPP is achieved by proton abstraction from the condensed intermediate

1.2.2 The crystal structure of human FPPS reveals enzyme transition between three distinct conformations

Studies on un-liganded human FPPS highlighted the important side chain residues for catalysis and revealed the enzyme transition between three distinct conformations, depending on the status of ligand binding (Rondeau *et al.*, 2006). Each subunit of the FPPS dimer is composed of thirteen alpha helices, with the conserved aspartate-rich regions localized in the α4 and α8 helix. The catalytic ligand-binding site is located in a large partly hydrophobic central cavity mainly formed by Lys200, Thr201, Arg113, Asp243 and Asp247, well shielded from the bulk solvent (Figure 1.9) (Kavanagh *et al.*, 2006b). Upon occupation of the allylic binding site, FPPS adopts a partially closed conformation which allows restriction of further GPP binding and prompts formation of the IPP binding site. This conformation is stabilized by electrostatic interactions between the aspartate motifs, the three Mg^{2+} ions and the pyrophosphate unit of the allylic substrate. Upon IPP binding, Lys57, Arg60 and Arg113 side chains (Figure 1.9) directly interact with the pyrophosphate group of IPP, prompting rearrangement of the highly basic C-terminus tail of the enzyme (Lys350, Arg351, Arg352, Lys353), which seals the newly formed IPP binding pocket thus stabilizing the fully closed

conformation (Kavanagh *et al.*, 2006b, Rondeau *et al.*, 2006)(Figure 1.9).

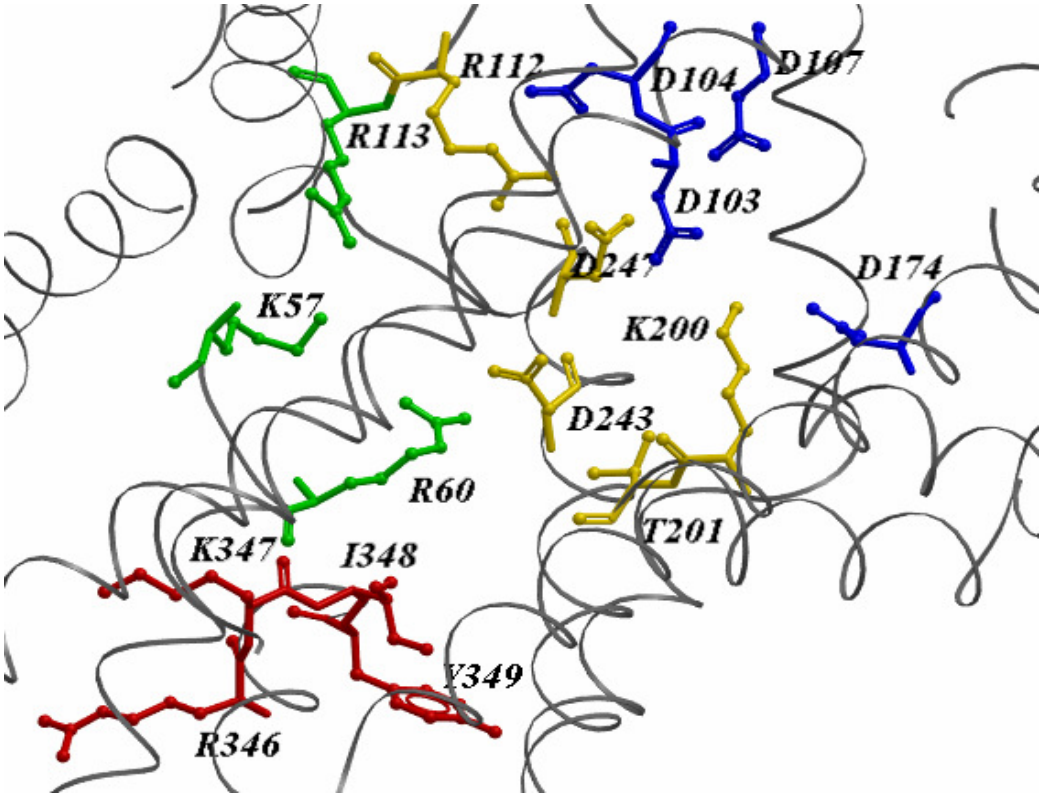


Figure 1.9: Main amino-acid side chains which play a part in stabilization of partially closed (blue) conformation, closed (green) conformation, IPP binding pocket formation (red) and allylic binding (yellow) site in un-liganded human FPPS. Adapted from Rondeau *et al.* 2006 (pdb: 2F7M).

Finally, upon termination of catalysis and release of pyrophosphate from the allylic substrate, interactions between aspartate-rich motifs and Mg^{2+} ions weaken, destabilizing the closed conformation. This transition to an open conformation is

essential for product release and translocation of GPP to the allylic site for a subsequent round of catalysis (Rondeau *et al.*, 2006).

1.2.3 The products of FPPS catalysis

Apart from the indisputable role of FPPS in the biosynthesis of sterols (Brown and Goldstein, 1979a, Zhang *et al.*, 1993) the enzyme is required for production of ubiquinones (Ashby and Edwards, 1990), dolichols (Matsuoka *et al.*, 1991) and heme (Weinstein *et al.*, 1986). The products of FPPS and GGPPS, FPP and GGPP, are also substrates for prenyltransferases, leading to generation of farnesylated (Clarke, 1992) or geranylgeranylated proteins respectively (Coxon *et al.*, 2000).

1.3 PROTEIN PRENYLATION, AN OVERVIEW

Protein prenylation is the post-translational attachment of either the 15-carbon farnesyl (FPP) or the 20-carbon geranylgeranyl isoprenoid (GPP) group to cysteine residues near the C-terminus of intracellular proteins via thioether linkages (McTaggart, 2006). The attached lipid is essential for proper function of the modified protein because it promotes protein anchorage to internal cell membranes which results in initiation or modulation of critical cellular functions such as pivotal signaling

pathways, protein-protein interactions, apoptosis and intracellular vesicular trafficking (Casey, 1995, Casey and Seabra, 1996, Seabra, 1998, Sinensky, 2000). Prenylated proteins include the small GTP binding proteins or GTPases (Ras, Rho, Rac, Rab) (Hancock *et al.*, 1989, Marshall, 1993, Schafer and Rine, 1992, Seabra, 1998), heretotrimeric G proteins (Hamm and Gilchrist, 1996), phosphodiesterases (Anant *et al.*, 1992) and nuclear lamins (Farnsworth *et al.*, 1989, Zhang and Casey, 1996). GTPases comprise the largest group of prenylated proteins and can play a role in regulation of cell proliferation and apoptosis (Lacal, 1997), in cytoskeletal organization (Dunford *et al.*, 2001, Ridley and Hall, 1992, Ridley *et al.*, 1992, Zhang *et al.*, 1995) and in vesicular trafficking (Ridley, 2006, Symons and Rusk, 2003, Zerial and Stenmark, 1993).

Prenylation is mainly catalyzed by three enzymes: farnesyl transferase (FTase), geranylgeranyltransferase type I (GGTase-I) and geranylgeranyltransferase type II or Rab geranylgeranyl transferase (GGTase-II or RGGT) (Liang *et al.*, 2002, Maurer-Stroh *et al.*, 2003). All three known protein prenyltransferases are evolutionarily conserved, ubiquitously expressed heterodimeric enzymes and are composed of distinct alpha and beta subunits with the zinc-containing active site in the latter subunit (Desnoyers and Seabra, 1998, Seabra *et al.*, 1991).

1.4 PRENYLATION BY FARNESYL TRANSFERASE (FTase) & GERANYLGERANYLTRANSFERASE TYPE-I (GGTase-I)

The closely related FTase and GGTase-I share a common 48 kDa alpha subunit but have distinct beta subunits, which determine their substrate specificity (Casey and Seabra, 1996). They catalyze transfer of a 15 carbon isoprenoid lipid from FPP or a 20 carbon lipid from GGPP to their target proteins (Reid *et al.*, 2004)(Figure 1.10). FTase and GGTase-I are also termed CAAX prenyltransferases because they recognize a conserved motif at the C termini of their substrate termed the CAAX box (Lane and Beese, 2006, Moores *et al.*, 1991, Reiss *et al.*, 1990). The cysteine residue C is the site of prenylation, A is always an aliphatic amino acid whereas the X denotes the carboxyl terminal residue of the motif and determines the nature of the isoprenoid to be added (Reiss *et al.*, 1990). When "X" is a serine, methionine, or glutamine, the protein becomes a target of FTase whereas if it is a leucine, it is subjected to modification by GGTase-I (Casey and Seabra, 1996, Desnoyers and Seabra, 1998, Seabra *et al.*, 1991). However certain substrates can be processed by both enzymes, although the substrate range of GGTase-I seems to be more restricted (Roskoski and Ritchie, 1998). Following prenylation, proteins are targeted to the ER, where the AAX residues are cleaved by a Ras converting enzyme endoprotease (RCEI) and the carboxyl group of the

terminal cysteine is linked as a methylester by the isoprenylcysteine carboxyl methyltransferase (ICMT) (Clarke *et al.*, 1988, Konstantinopoulos *et al.*, 2007, Otto *et al.*, 1999). Proteins are subsequently targeted to the plasma membrane where they attach via their isoprenoid lipid anchor. Further description of FTase and GGTase–I is beyond the scope of this thesis.

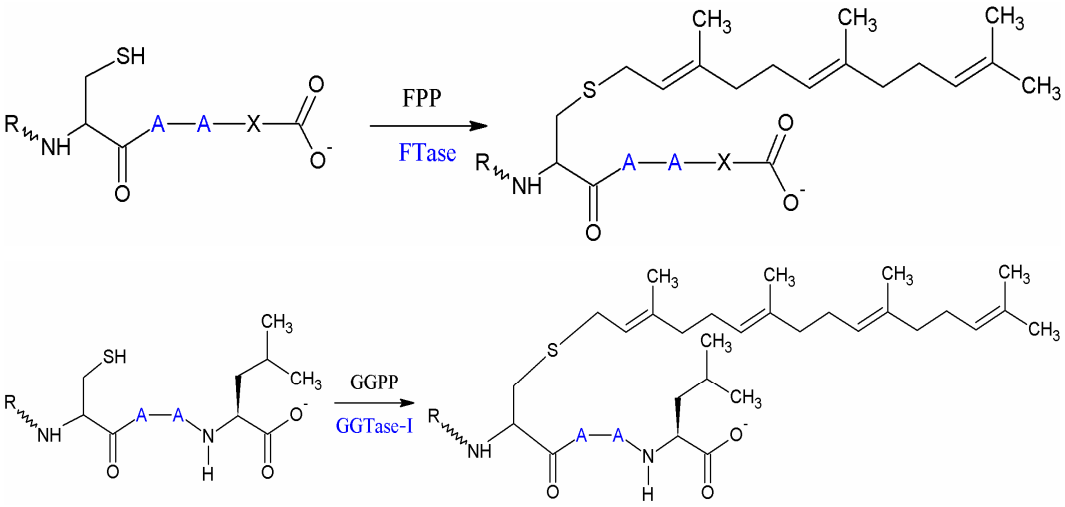


Figure 1.10: Protein farnesylation (upper panel) and geranylgeranylation (lower panel) by Farnesyl Transferase (FTase) and Geranyl Transferase Type I GGTase-I respectively. FPP: Farnesyl pyrophosphate, GGPP: geranylgeranylpyrophosphate, A: aliphatic amino-acid , X: serine, methionine, or glutamine.

1.5. PRENYLATION BY RAB GERANYLGERANYL TRANSFERASE (RGGT)

1.5.1 Substrate recognition by RGGT

Rab geranylgeranyl transferase (RGGT) catalyses the covalent attachment of geranylgeranyl (GG) units to two C-terminal cysteine residues of target proteins (Alexandrov *et al.*, 1999, Zhang, 2003) (Figure 1.11).

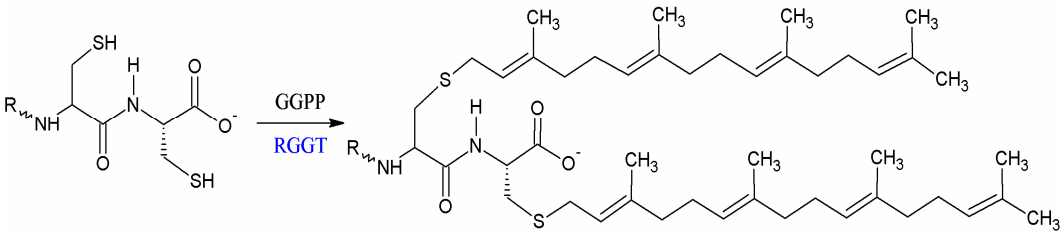


Figure 1.11: Geranylgeranylation of one the CC motifs of Rab proteins is carried out by RGGT. GGPP: Geranylgeranylpyrophosphate, RGGT: Rab Geranyl Geranyl Transferase

RGGT exclusively prenylates Rab proteins, which are members of a distinct family of the Ras-related GTPases and are key regulators of vesicular transport in secretory and exocytic/endocytic pathways (Goody *et al.*, 2005). RGGT can recognize Rabs that contain two cysteine residues near or at the C terminus in different motifs such as CC, CXC, CCX, CCXX, or CCXXX (Calero *et al.*, 2003, Desnoyers and Seabra, 1998) whereas

Rab proteins possessing the CAAX motif can be a target of either GGTase-I or RGGT (Leung *et al.*, 2007, Wilson *et al.*, 1998).

1.5.2 Rab Escort Protein as a chaperone in RGGT catalysis

RGGT is unique among other prenyltransferases because it is unable to directly recognize its substrate and can only exert its function when associated with a chaperone protein called Rab Escort Protein (REP)(Seabra *et al.*, 1992b, Shen and Seabra, 1996). There are two known mammalian REP proteins, REP1 and REP2 (Pereira-Leal *et al.*, 2003, Takai *et al.*, 2001) which share 76 % homology in humans and therefore they are able to substitute for each other in a substrate-specific manner in all tissues except the retina (Alory and Balch, 2001). Deletions of the chromosomal locus encoding REP1 results in an X-linked retinal degeneration called choroideremia, possibly triggered by defective prenylation of certain Rabs (Cremers *et al.*, 1994, Rak *et al.*, 2004, Seabra *et al.*, 1995).

REPs are closely related to Rab GDP Dissociation Inhibitors (RabGDIs), cytosolic factors responsible for delivery and removal of Rab proteins to and from their target membrane (Pfeffer *et al.*, 1995). Both REP and RabGDIs can recognize and bind Rabs, however RabGDIs preferentially bind prenylated Rabs, whereas

REP1 and REP2 only recognize unprenylated Rabs (Leung *et al.*, 2006). Due to their inability to bind RGGT, RabGDIs role seems to be restricted to facilitating Rab recycling in and out of membrane compartments, whereas REP exclusively presents Rabs to RGGT for prenylation and subsequently delivers them to the target membrane (Alexandrov *et al.*, 1994, Pfeffer *et al.*, 1995).

1.5.3 Proposed mechanisms of RGGT catalysis

Based on kinetic studies (Anant *et al.*, 1998, Thoma *et al.*, 2001a, Thoma *et al.*, 2001b, Thoma *et al.*, 2000, Thoma *et al.*, 2001c) there are two proposed routes describing the mode of Rab protein prenylation by RGGT (Leung *et al.*, 2006)(Figure 1.12). The most prevalent model of RGGT function is the so-called classical pathway and states that the un-prenylated Rab must form a tight complex with REP prior to its recognition by RGGT (Andres *et al.*, 1993).

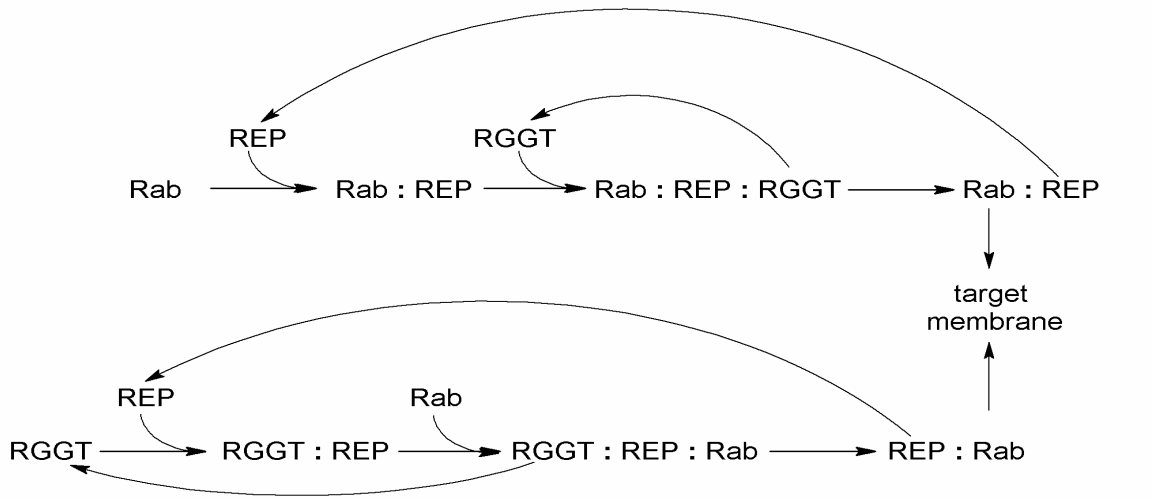


Figure 1.12: Schematic representation of classical (top) and alternative (bottom) pathway of Rab prenylation by RGGT.

REP binds Rab via the Rab-binding platform (RBP) and the C-terminal-binding region (CBR). The RBP is important for the recognition of substrate by RGGT and the assembly of the ternary RGGT:REP:Rab complex, whereas binding of the C-terminal Rab hydrophobic residues (CBR interacting motif, CIM) to CBR increases complex affinity (Rak *et al.*, 2004, Thoma *et al.*, 2001c). Dislocation of the first formed bound isoprenoid from RGGT occurs when a second GGPP molecule binds to the active site (Guo *et al.*, 2008a) (Figure 1.13).

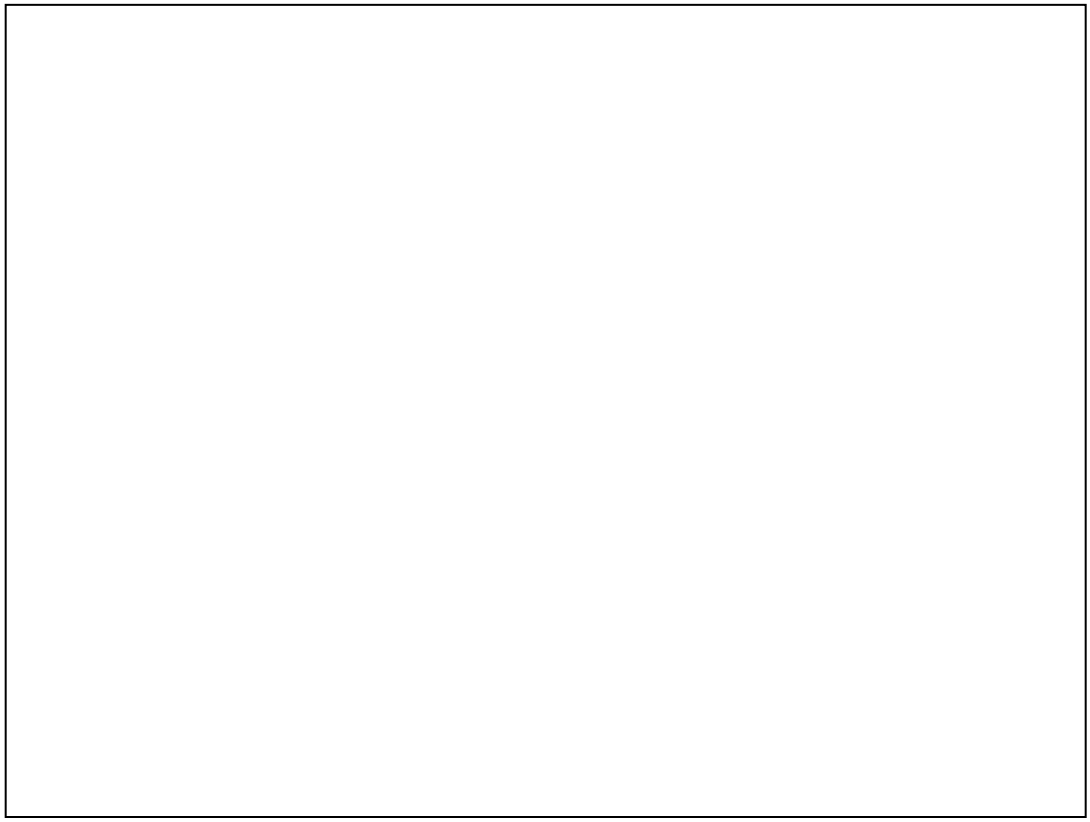


Figure 1.13: The catalytic mechanism of RGGT: REP complex. Figure from Guo *et al.* 2008a. **Figure has been removed due to Copyright restrictions**

Prenylation of the second cysteine moiety is a much slower step, as a result of a steric hindrance imposed by the conjugated lipid (Thoma *et al.*, 2001c). Following geranylgeranylation, REP remains associated with RGGT, masking the prenyl groups from the solvent and therefore increasing their solubility (Olkkonen and Ikonen, 2000). After delivery of prenylated Rab to the target

membrane, REP is released into the cytosol where it can participate in a new cycle of prenylation.

The alternative proposal states that REP must first associate with RGGT in presence of GGPP and then the complex binds to unprenylated Rab, but at a much slower rate (Thoma *et al.*, 2001c). The choice of pathway is dependent on the concentration of components of the ternary complex and GGPP; at high concentrations the alternative pathway is favoured whereas at low concentrations the classical pathway prevails (Leung *et al.*, 2006).

1.5.4 The crystal structure of RGGT in complex with REP1 and Rab

Mammalian RGGT is a heterodimer composed of a tightly associated 60 kDa alpha subunit and a 38 kDa beta subunit (Armstrong *et al.*, 1993, Seabra *et al.*, 1992a). The crystal structure of rat RGGT revealed that alpha subunit is composed of a helical domain, an immunoglobulin like (Ig-like) domain and a leucine-rich repeat (LRR) domain (Zhang *et al.*, 2000)(Figure 1.14).

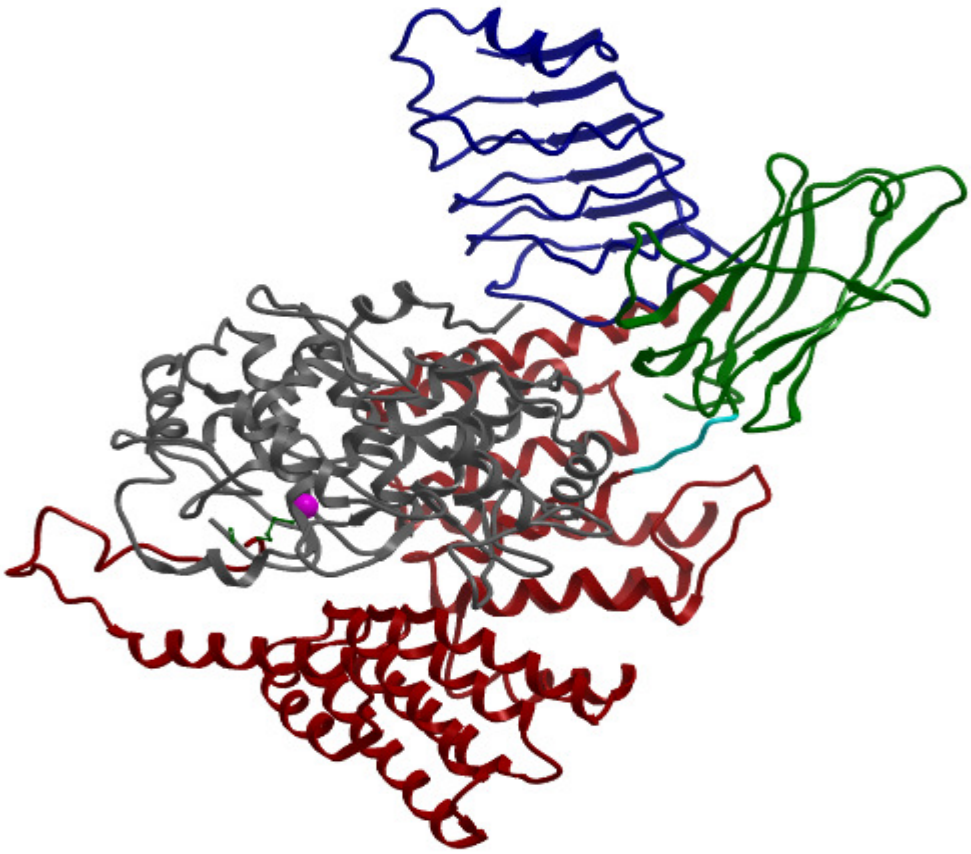


Figure 1.14: Ribbon representation of the rat RGGT structure. Adapted from Zhang *et al.*, 2000 (pdb 1DCE). In red: helical domain of the alpha subunit; in blue: LRR domain; in green, Ig-like domain; in grey, beta subunit, light purple: zinc ligand

The alpha domain is structurally similar to FTase whereas Ig-like and LRR domains are inserted between helices 11 and 12 at the C terminus and are unique among prenyltransferases. The helical domain is thought to play a role in recognition and binding of Rab substrate (Rasteiro and Pereira-Leal, 2007). The Ig-like and LRR domains do not participate in the formation of the catalytic ternary complex with REP1 (Pylypenko *et al.*, 2003) but may serve

as regulators of intracellular membrane function or protein binding and have possibly been introduced in mammals throughout evolution to perform additional functions (Dursina *et al.*, 2002, Rasteiro and Pereira-Leal, 2007). The beta subunit is formed by 12 alpha helices forming a hydrophobic cavity that accommodates the GGPP substrate (Guo *et al.*, 2008b, Zhang *et al.*, 2000), (Figure 1.14). The zinc ion is coordinated by Asp288, Cys240 and His290 of beta subunit whereas the fourth ligand is residue His2 on alpha subunit.

REP1 consists of two domains: domain I is the largest, composed of four beta sheets and six alpha helices, whereas domain II is composed of five alpha helices. The interface of RGGT:REP1 complex is formed by interaction of domain II of REP1, with the helical domain of the alpha subunit of RGGT (Figure 1.15). Amino acids of the helix E of REP1 (Arg290, Lys294, Met286, Met291) establish hydrogen bonds and hydrophobic interactions with amino acids located in helix 10 (Asn217, Ala218, Phe220, Thr221) and 12 (Leu377, Glu378) of RGGT alpha subunit. Residues located in helix D of REP1 (Phe279) form hydrophobic interactions with amino acids of helix 8 (Ile171, Thr172) and 10 (Leu214, Ala218) of RGGT (Pylypenko *et al.*, 2003). The apolar residues of CBR domain of REP1 form a hydrophobic cavity which accommodates the C-terminus of the Rab substrate (Rak *et al.*,

2004). The restrictive size of the hydrophobic channel does not permit accommodation of two isoprenoid moieties, leaving the second lipid loosely associated with the surface of REP, readily available for membrane interaction (Rak *et al.*, 2003).

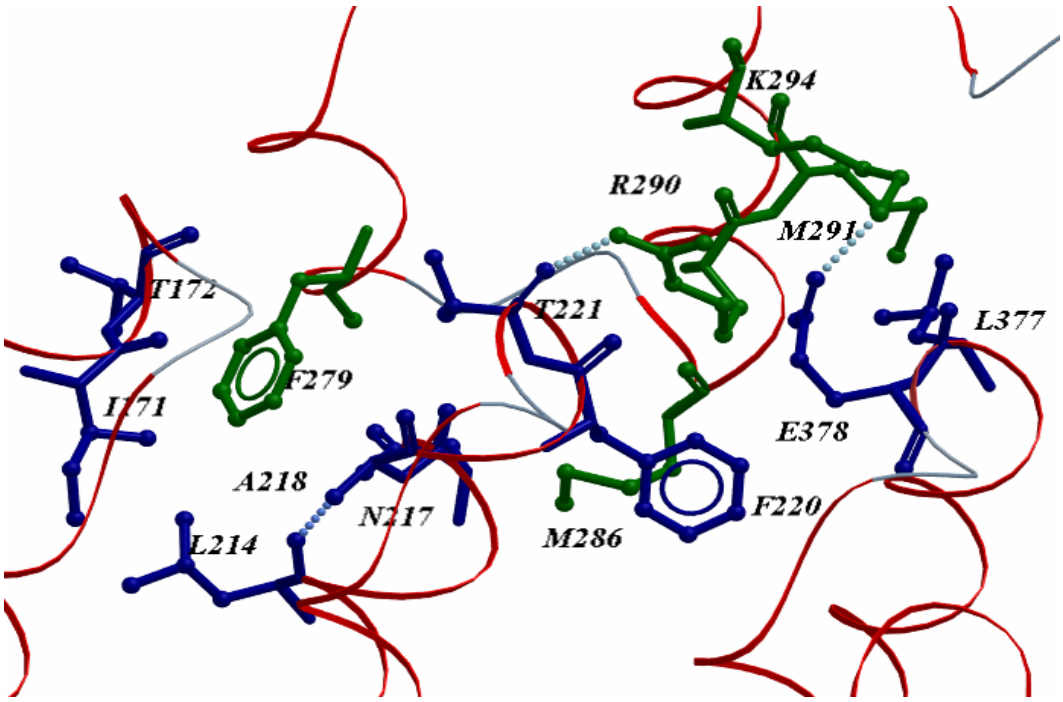


Figure 1.15: RGGT residues involved in REP1 binding and conformational change of RABGGTA leading to isoprenoid binding. Amino-acids of domain II of REP1 (in green) interact with the helical domain of the RABGGTA (in blue). Figure adapted from pdb: 1LTX Pylypenko *et al*. 2003.

Upon binding of REP1 to RGGT the disordered N-terminus and helices of alpha subunit re-orientate to face REP1 whereas the Tyr241, Trp244 and His190 residues of beta subunit are also subjected to conformational changes in order to allow binding of the isoprenoid substrate (Pylypenko *et al.*, 2003). Following

geranylgeranylation of both cysteine targets, the C-terminus of Rab is released from the active site of RGGT and associates with the lipid binding site of REP. The conformational change induced in domain II of REP triggers the dissociation of the ternary complex (Guo *et al.*, 2008b).

1.6 POST-PRENYLATION PROCESSING OF RAB

Post-prenylation processing of Rab proteins varies according to the position of their cysteine residues. Rab proteins possessing the CAAX motif are delivered to the ER by REP, where they first undergo proteolysis of AAX tripeptide catalysed by RCEI and are then methylated by ICMT on their C-terminal prenylcysteine prior to targeting to the plasma membrane (Section 1.4) (Leung *et al.*, 2007). Proteins containing the CXC motif are directly subjected to carboxymethylation by ICMT, bypassing the RCEI modification step (Farnsworth *et al.*, 1994). Carboxymethylation enhances protein hydrophobicity and increases affinity for the membranes by a factor of 10-100 fold (Silvius and l'Heureux, 1994, Smeland *et al.*, 1994), however the importance of this post-translational modification in Rab function is still a subject of investigation, as its absence does not seem to interfere with correct membrane targeting (Bergo *et al.*, 2001, Leung *et al.*, 2007, Leung *et al.*, 2006,

Michaelson *et al.*, 2005). Rabs possessing adjacent cysteines do not require post-prenylation processing and can be directly targeted to specific organelles (Leung *et al.*, 2007).

1.7 BISPHOSPHONATES AS INHIBITORS OF PRENYLATION

1.7.1 Bisphosphonates as anti-resorptive agents

The demonstration that inorganic pyrophosphate (PPi), a well known intermediate of several biosynthetic pathways, was able to prevent dissolution of hydroxyapatite crystals led to the hypothesis that it plays an important role as a regulator of *in vivo* calcification (Fleisch *et al.*, 1966). However, the *in vivo* efficacy of PPi is limited, as it is prone to hydrolysis by alkaline phosphatases. Therefore PPi was only able to inhibit calcification of soft tissues when administered intravenously, bypassing the gastrointestinal tract (Schibler *et al.*, 1968). The screening for PPi analogues resistant to the action of phosphatases led to discovery of bisphosphonates (BPs) as potent inhibitors of calcium phosphate crystallization *in vitro* and bone resorption and ectopic calcification *in vivo* (Fleisch *et al.*, 1969, Francis *et al.*, 1969), even when administered orally (Fleisch *et al.*, 1970). Currently, BPs are the drugs of choice for bone diseases characterized by excessive osteoclastic bone resorption such as osteoporosis (Pazianas *et al.*, 2010, Watts and

Diab, 2010), PAGET's disease (Langston *et al.*, 2010, Ralston *et al.*, 2008), cancer of the bone (Neville-Webbe *et al.*, 2010) and malignant hypercalcaemia (Ralston *et al.*, 1989, Saunders *et al.*, 2004).

1.7.2 General structure of bisphosphonates

Bisphosphonates are structural analogues of inorganic pyrophosphate (Figure 1.16) (Russell *et al.*, 2007). Their stability is attributed to the carbon atom that replaces the oxygen atom between phosphates, rendering them resistant to chemical and enzymatic hydrolysis. The presence of phosphonate groups allows strong attachment of BP to bone surface, due to cooperative binding of the negatively charged oxygen atoms to the abundant Ca^{2+} ions. Most BPs contain a hydroxyl group at R^1, which allows high affinity for calcium crystals and bone mineral. Variations in the BP structure are the result of substitutions in R^1 and R^2 side-chains attached to the carbon atom of the P-C-P backbone (Russell *et al.*, 2008). The R^1 regulates affinity for calcium binding and attachment to bone minerals whereas R^2 group mainly determines the anti-resorptive potency of BPs (van Beek *et al.*, 1998). The mechanism of inhibition of bone remodeling of BPs is strictly dependent on the nature of the R^2 group but both R^1 and R^2 are

required for bone binding (Rogers *et al.*, 1995, Russell, 2006).

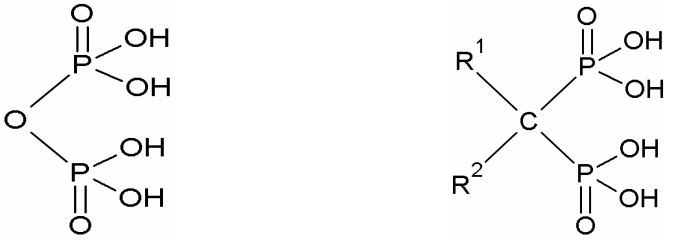


Figure 1.16: Molecular structure of inorganic pyrophosphate (left) and BP (right)

The presence of a hydroxyl group in R^1 strongly increases the *in vivo* anti-resorptive potency of nitrogen-containing bisphosphonates (N-BPs) and their affinity for hydroxyapatite crystals. The presence of a primary amine in the R^2 alkyl side-chain in alendronate (Ale), pamidronate (Pam) and ibandronate (Iba) increases the anti-resorptive potency by 100-5000 fold when compared to the first generation BP etidronate (Crepin *et al.*, 2010). When the amino group is localized in the heterocyclic ring of R^2 in risedronate (Ris) and zoledronate (Zol), the potency increases up to 10,000 fold (Russell *et al.*, 2007) (Figure 1.17). Removal of the nitrogen atom from the heterocyclic ring of Ris results in formation of the phenyl analogue NE58022, with a complete loss of slow binding kinetics of FPPS and reduced competitive inhibition rate (Dunford *et. al.*, 2008).

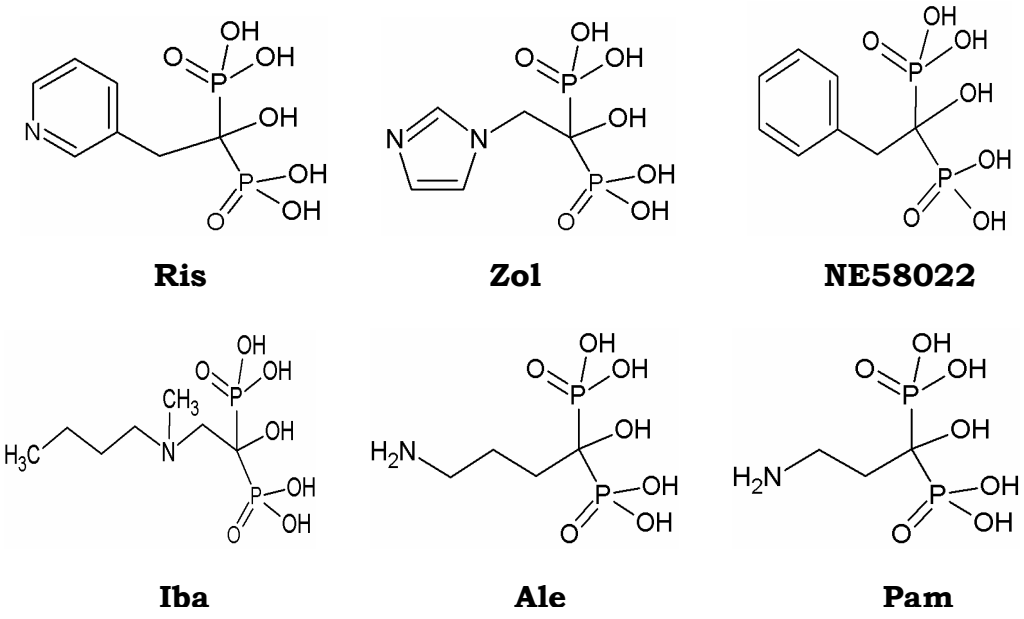


Figure 1.17: The structure of major BPs included in the present study. Upper panel: heterocyclic BPs Risedronate (Ris), Zoledronate (Zol) and Ris analogue NE58022. Lower panel: aminoalkyl N-BPs Ibandronate (Iba), Alendronate (Ale) and Pamidronate (Pam). All are clinically used except NE58022.

1.7.3 Molecular mechanisms of bisphosphonate action

The mechanism of bisphosphonate action is dependent on the presence of a nitrogen atom in the R^2 side chain. The first generation non-nitrogen BPs contain short R^1 and R^2 chains and are intracellularly metabolized to toxic ATP analogues which can induce cell apoptosis (Frith *et al.*, 1997). The N-BPs are considerably more potent inhibitors of bone resorption and mainly

exert their function by inhibition of FPPS resulting in the lack of post-translational modification of key regulatory proteins e.g. GTPases, leading to osteoclast dysfunction (Luckman *et al.*, 1998a, Luckman *et al.*, 1998b, Russell, 2006).

1.7.3.1 Induction of cell apoptosis by the non-nitrogen BPs

The simple BPs are metabolized to non-hydrolysable ATP analogues by reversal of the aminoacylation reactions catalyzed by aminoacyl-tRNA synthetases (Frith *et al.*, 1997, Rogers *et al.*, 1996) (Figure 1.18).

Formation of the non-hydrolysable AppCp-type metabolite is a result of substitution of the β,γ – phosphate groups of ATP with the P-C-P moiety of BP (Benford *et al.*, 1999, Frith *et al.*, 1997, Rogers *et al.*, 1992). Intracellular accumulation of the AppCp-type ATP analogue results in competitive inhibition of mitochondrial adenine nucleotide translocase (ANT), which is involved in the regulation of the permeability transition pore in mitochondria thus leading to apoptosis (Lehenkari *et al.*, 2002).

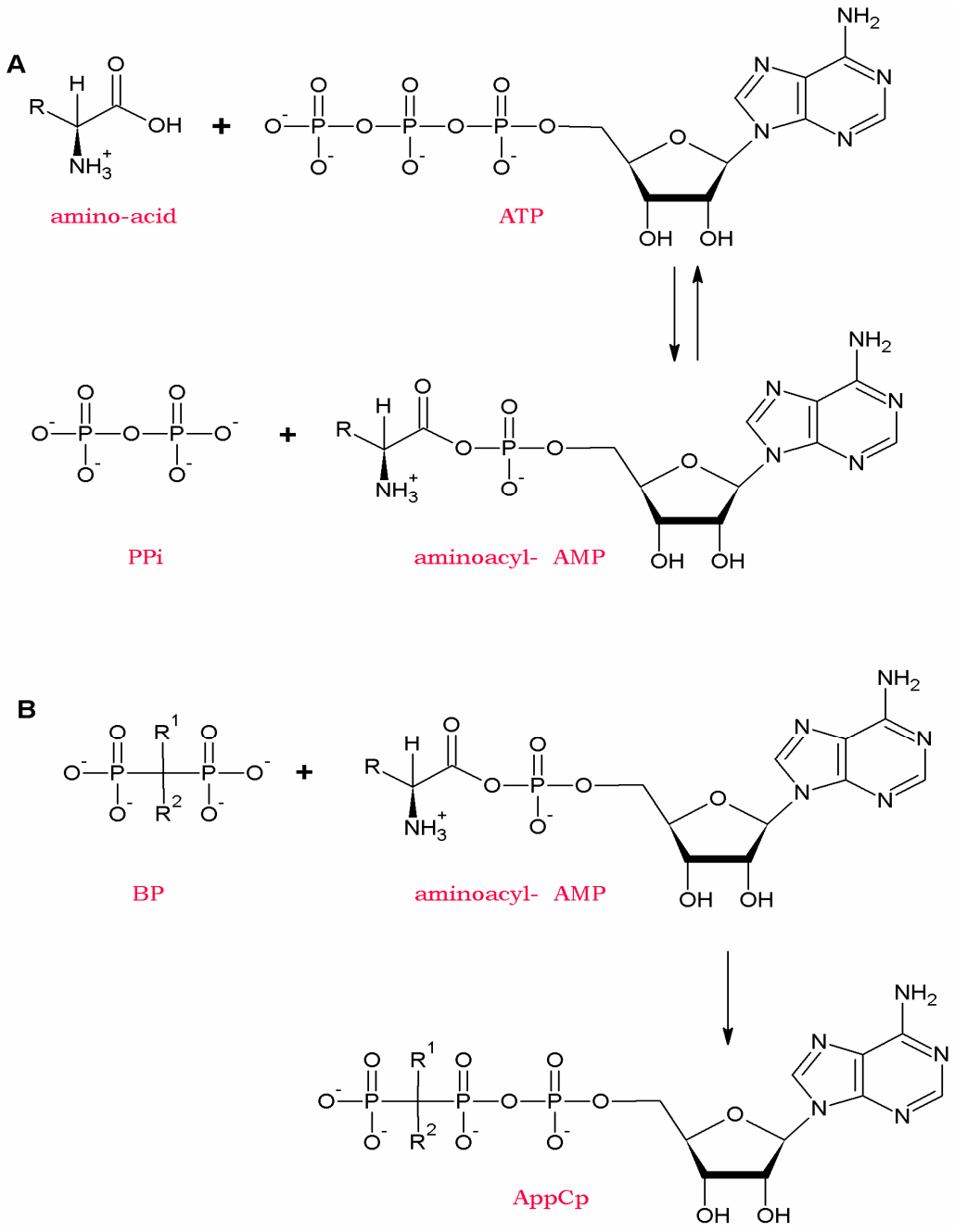


Figure 1.18: A) Formation of aminoacyl adenylate intermediate is catalysed by aminoacyl-tRNA synthetases, with a concomitant release of PPi and B) Reverse aminoacylation occurs in the presence of non-nitrogen BP and leads to formation of toxic AppCp intermediates.

1.7.3.2 Inhibition of protein prenylation by N-BPs

The first indication that enzymes of the mevalonate pathway are targets of N-BPs came from macrophage studies where ibandronate was found to inhibit squalene synthase and thus cholesterol biosynthesis (Amin *et al.*, 1992). Further studies demonstrated that N-BPs inhibits protein prenylation mainly by blocking the action of FPPS (Luckman *et al.*, 1998a, Luckman *et al.*, 1998b, van Beek *et al.*, 1999a, b) and causing accumulation of un-prenylated Rac, Cdc42 and Rho GTPases in osteoclast and macrophage cells (Dunford *et al.*, 2006).

The molecular mechanism of FPPS inhibition by N-BPs is highly complex and has been a subject of thorough investigation. Early experimental work suggested that N-BPs achieve FPPS inhibition by mimicking the isoprenoid substrates DMAPP and GPP and finally occupying the allylic binding site (Martin *et al.*, 1999). Kinetic studies have helped to characterize the mechanism of FPPS inhibition by BPs as a slow- tight binding, taking place in at least two individual steps (Kavanagh *et al.*, 2006b). The initial, rapid-stage is a competitive, reversible inhibition of DMAPP/GPP substrate by BP that leads to a formation of an enzyme- inhibitor complex. Full inhibition is attained after ten minutes where an enzyme isomerization step facilitates binding of the second substrate, isopentenyl pyrophosphate (IPP), and reduces

dissociation of the N-BP inhibitor. This inhibition is slow, irreversible and is best characterized as uncompetitive-mixed.

The crystal structure of human FPPS with heterocyclic BPs Ris (Kavanagh *et al.*, 2006b) and Zol (Rondeau *et al.*, 2006) demonstrated that N-BPs compete for and successfully bind to the allylic substrate binding pocket of FPPS, in strict agreement with the proposed kinetic model. Crystallographic data with the aminoalkyl BPs Ale, Iba and Pam confirmed binding to the allylic substrate site which leads to stabilization of the closed conformation of FPPS by interaction with both aspartate-rich motifs via the tri-nuclear Mg cluster (Rondeau *et al.*, 2006). The octahedral coordination of the individual metal site is based on the spatial arrangement of the BP oxygen atoms, the side chain carboxylate groups of Asp103, Asp107 and Asp243 and water molecules (Figure 1.19). Increased inhibition by N-BPs is achieved by the positioning of the nitrogen atom in the proposed carbocation-binding site resulting in competitive inhibition with the allylic substrate (Kavanagh *et al.*, 2006b). In case of the most potent Ris and Zol, the BP binding is strengthened by hydrogen bond interactions of the protonated heterocyclic nitrogen atom with the conserved Lys200 and Thr201 residues, facilitating imitation of carbocation intermediate (Rondeau *et al.*, 2006).

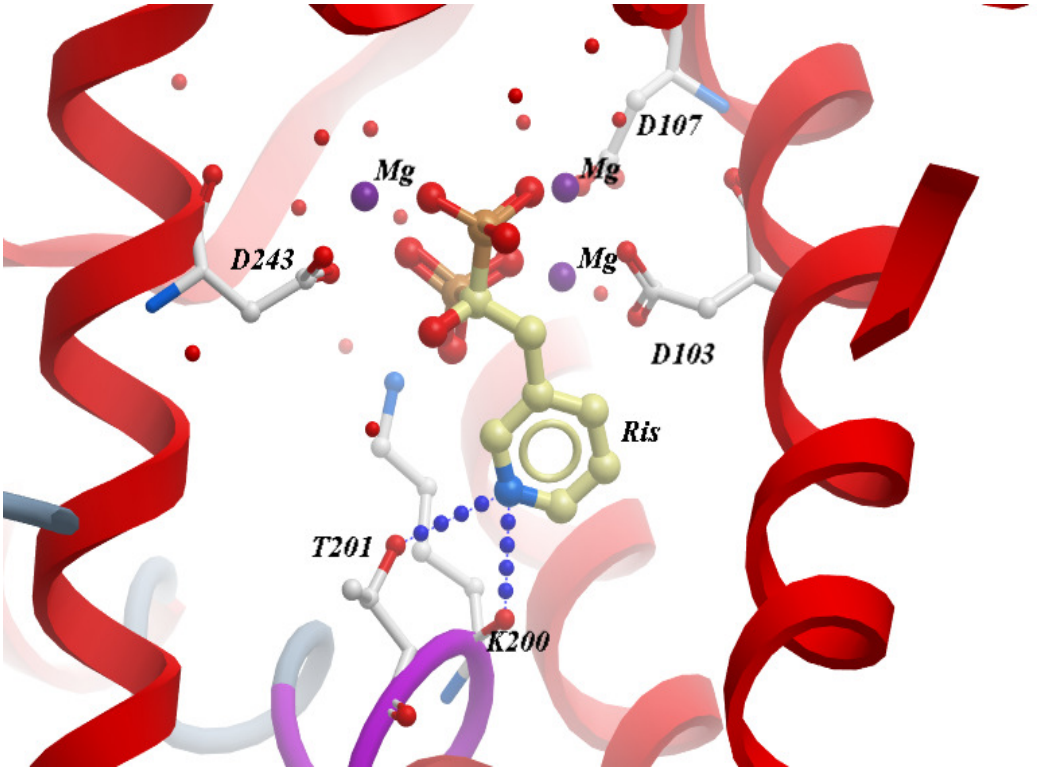


Figure 1.19: Representation of the FPPS allylic binding pocket occupied by Ris. Coordination of Ris is achieved by: Mg^{2+} ions (purple spheres), carboxylate groups of Asp103, Asp107 and Asp243, hydrogen bonds with Lys200 and Thr201 (blue spheres), and water molecules (orange spheres). Adapted from Kavanagh *et al*. 2008, pdb 1YV5.

Direct salt-bridge interactions of Arg112 and Lys257 with the BP moiety contribute to its proper orientation. Further stabilization of the N-BP: FPPS complex occurs upon IPP binding, with subsequent induction of enzyme isomerization, coupled to structural alterations. The most important structural rearrangement occurring at this step comprises a shifting of the highly basic hydrophobic tail (Lys350, Arg351, Arg352, Lys353)

which leads to reduction of the active site volume. This conformational alteration strengthens the ternary complex formation and significantly increases BP inhibition (Kavanagh *et al.*, 2006b, Rondeau *et al.*, 2006).

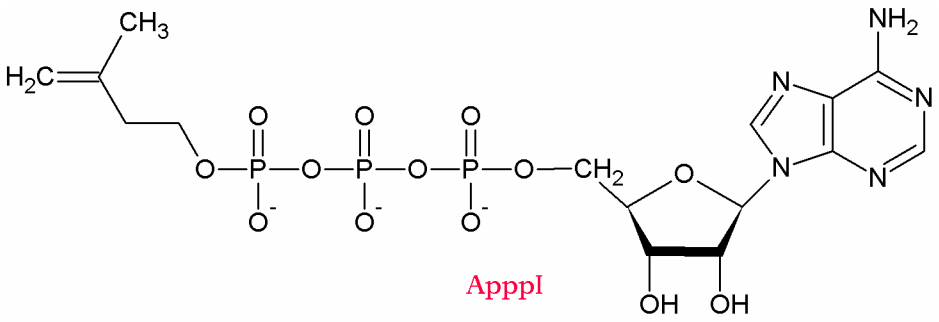
1.7.4 Effects of IPP accumulation due to N-BP treatment

Inhibition of FPPS by N-BPs causes intracellular accumulation of IPP, the upstream metabolite in the mevalonate pathway which results in the following effects:

i) Acute-phase reaction due to activation of γ,δ-T cells by the presence of IPP. This is a common side-effect of intravenous N-BP administration, caused by activation and proliferation of a subset of γ,δ-T cells after recognition and binding of IPP via the T-cell receptor (Benford *et al.*, 1999, Gober *et al.*, 2003, Roelofs *et al.*, 2009, Thompson *et al.*, 2006b). The symptoms of the pro-inflammatory acute response caused by production of tumor necrosis factor and interleukins 6 (Hewitt *et al.*, 2005, Thiebaud *et al.*, 1997) resemble those of common flu (Adami *et al.*, 1987) and are predominant upon first administration of N-BP (Russell *et al.*, 2008).

ii) Generation of ApppI toxic metabolite (Figure 1.20) by condensation of adenosine monophosphate with IPP (Monkkonen

et al., 2006, Raikkonen *et al.*, 2009) with toxic effects similar to AppCp-type analogues (Section 1.7.7.2).


CH3
H2C
O
P
O
O
O

and hip fractures in post-menopausal osteoporotic women (Papapoulos, 2010, Silverman, 2009) and suppress excessive bone turnover in Paget disease patients (Ralston *et al.*, 2008).

Bisphosphonates have also been proposed to be potential antiparasitic agents as they selectively inhibit the ATP-dependent hexokinase of *Trypanosoma cruzi,* the causative agent of Chagas disease (Hudock *et al.*, 2006, Sanz-Rodriguez *et al.*, 2007). Successful *in vitro* growth inhibition of *Trypanosoma brucei* (Martin *et al.*, 2002), *Toxoplasma gondii* (Ling *et al.*, 2005), *Cryptosporidium parvum* (Artz *et al.*, 2008), *Plasmodium vivax* (Artz *et al.*, 2010) and *Plasmodium falciparum* by BPs has also been reported (Ghosh *et al.*, 2004, Martin *et al.*, 2001) whereas intravenous administration of Pam radically cured cutaneous leishmaniasis (Rodriguez *et al.*, 2002, Yardley *et al.*, 2002).

Clinical trials and *in vitro* data showed that BPs were effective in reduction of skeletal-related complications in the bone treatment associated with malignancies such as metastatic prostate cancer (Saad *et al.*, 2004), pancreatic cancer (Green, 2005), breast cancer (Body *et al.*, 2004, Fournier *et al.*, 2008, Fournier *et al.*, 2010, Hortobagyi *et al.*, 1996), ovarian carcinoma (Clezardin *et al.*, 2005), neuroblastoma (Sohara *et al.*, 2005), lung cancer (Rosen *et al.*, 2003, Yano *et al.*, 2003) and osteolytic metastasis (Berenson *et al.*, 2001). BPs are also proposed to have

anti-tumour effects *per se* which may be exerted via inhibition of angiogenesis (Santini *et al.*, 2002, Stresing *et al.*, 2010), tumor cell invasion (Boissier *et al.*, 2000), or adhesion to extracellular matrices (Boissier *et al.*, 1997, van der Pluijm *et al.*, 1996), activation of gamma-delta T-cells (Kunzmann *et al.*, 2000, Roelofs *et al.*, 2009), modulation of growth factor production such as cytokines (Ferretti *et al.*, 2005), collagenases (Derenne *et al.*, 1999) or simply by increasing apoptosis of tumor cells (Shipman *et al.*, 1997, Tassone *et al.*, 2003). The most notable effect is in reduction of bone myeloma (Morgan *et al.*, 2010) via increased apoptosis of tumour cells *in vivo* (Shipman *et al.*, 1997). A combination of BP administration together with established anti-cancer agents can result in a synergistic growth inhibition of cancer cell lines (Green, 2003, Tassone *et al.*, 2000).

Suppression of bone remodeling by the most potent clinical BPs is associated to a potential therapeutic complication called osteonecrosis of the jaw (ONJ), characterized by persistence of non-healing exposed bone in maxillofacial region and lytic or sclerotic lesions expanding in the soft tissue area (Khosla *et al.*, 2007, Marx, 2003). ONJ was mainly observed in patients who received N-BPs by intravenous administration, usually as a treatment for malignancies with a calculated incidence of 1-2 % or after radical dental treatment (Henry *et al.*, 2011, Morag *et al.*,

2009). However, the underlying pathophysiology of ONJ is unclear and a suppressed alveolar remodelling in the jaw, a site of high bone turnover, was proposed to cause osteocytic death and consequently matrix necrosis (Allen, 2009). The rarity of this condition and the lack of a control group of subjects not exposed to BP makes the determination of a valid statistical incident risk in BP exposed patients difficult and inaccurate (Abrahamsen, 2010).

1.8 OSTEOCLASTS AS TARGETS OF BISPHOSPHONATES

1.8.1 Osteoclast generation, morphology and function

Osteoclasts (OC) are giant, multinucleated cells and along with osteoblasts and osteocytes compose the basic multicellular units (BMU) responsible for the bone remodelling process and maintenance of bone homeostasis (Suda *et al.*, 1992). The nature of OC precursor was long debated (Nijweide *et al.*, 1986) as they reside in bone marrow and could therefore belong to haematopoietic or stromal cell lineage (Burger *et al.*, 1982, Ko and Bernard, 1981). The most prevalent theory states that OC originally derive from haematopoietic stem cells (colony-forming unit-stem, CFU-S)(Ash *et al.*, 1980), scarce in circulation (Molendijk *et al.*, 1986) but abundant in bone marrow, the main site of haematopoiesis (Kondo *et al.*, 2003, Scheven *et al.*, 1987).

The earliest identified OC progenitor is the granulocyte macrophage colony-forming unit (CFU-GM), the precursor of monocytes, macrophages and granulocytes (Kurihara *et al.*, 1990, Menaa *et al.*, 2000, Miyamoto *et al.*, 2001). At this stage, cells express the receptor activator of nuclear factor–kB (RANK) whose interaction with RANK ligand (RANKL), present on pre-osteoblast and stromal cells, is indispensable for induction of the terminal phases of differentiation and commitment to the OC line(Boyce and Xing, 2007, Khosla, 2001). CFU-GM cells are highly proliferative and under the influence of macrophage-colony stimulating factor (M-CSF) and RANKL form the mononuclear OCs that can tightly adhere to bone, express tartrate-resistant acid phosphatase (TRA_CP) and are capable of bone resorption (Miyamoto and Suda, 2003). Fusion of mononuclear OC precursors results in the formation of polykaryon (multinucleate) immature OCs which, under the influence of RANKL and in combination with other osteoclastogenic cytokines such as tumor necrosis factor-alpha (TNF-α) (Zou *et al.*, 2001) and interleukin-1 (Wei *et al.*, 2005), yields the mature OCs (Pfeilschifter *et al.*, 1989, Roodman, 2006, Udagawa, 2002) (Figure 1.21).

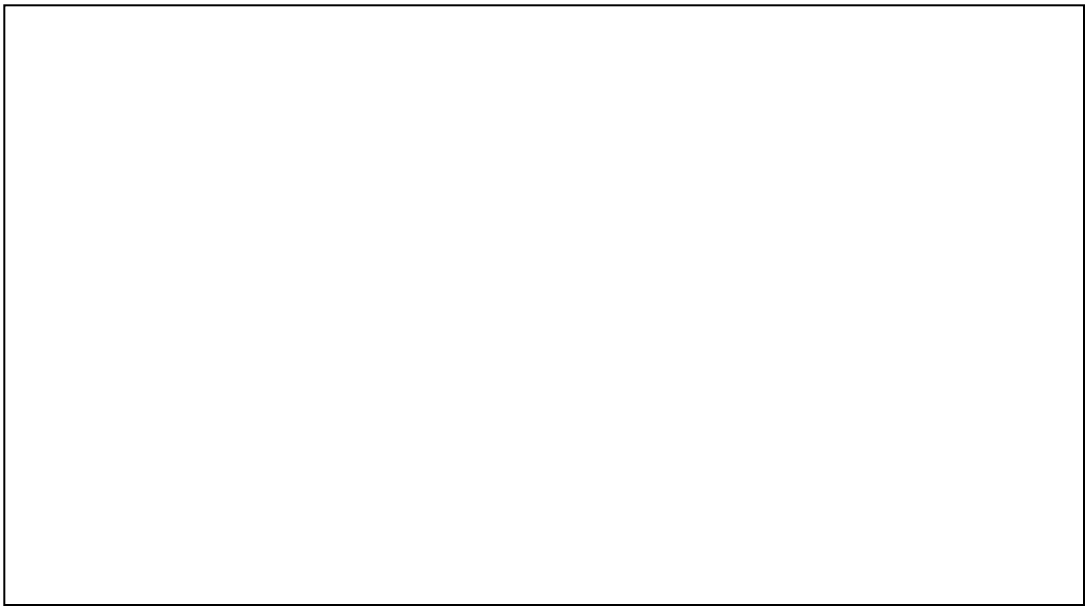


Figure 1.21: Osteoclast formation from bone marrow precursors. Adapted from Boyle *et al*. (2003). **Figure has been removed due to Copyright restrictions**

Regulation of OC formation is mainly mediated via the two osteoclastogenetic cytokines M-CSF (Hattersley *et al.*, 1991, Yoshida *et al.*, 1990) and RANKL (Hofbauer *et al.*, 1999, Lacey *et al.*, 1998, Wong *et al.*, 1997). Both M-CSF and RANKL are indispensable for the induction of genes encoding characteristic proteins of the mature OC such as cathepsin K (Bossard *et al.*, 1996, Drake *et al.*, 1996), TRAcP (Clark *et al.*, 1989) osteoclast-associated receptor (OSCAR) (Kim *et al.*, 2002) and calcitonin receptor (Nicholson *et al.*, 1986). However, only RANKL mediates the formation of resorption pits and the osteolytic action of the OC

(Burgess *et al.*, 1999, Udagawa *et al.*, 1999) whereas M-CSF sustains the proliferation and survival of OC progenitors (Kodama *et al.*, 1991, Tanaka *et al.*, 1993) and the motility of mature OCs (Arai *et al.*, 1999, Teitelbaum and Ross, 2003).

RANKL is a member of membrane-bound TNF family proteins, expressed by osteoblast-stromal cells and their progenitors and is an indispensable regulator of OC differentiation, activity and survival (Lacey *et al.*, 1998, Nakagawa *et al.*, 1998). RANKL is expressed either in a membrane-bound or soluble form with the latter speculated to play a more important role in osteoclastogenesis (Khosla, 2001, Nakashima *et al.*, 2000, Wada *et al.*, 2006). OC precursors can recognize and bind RANKL through their receptor RANK, when in contact with osteoblast-stromal cells. This interaction enables transduction of signals that lead to OC differentiation in the presence of M-CSF, the activation of resorption by mature OCs, and their survival and participation in new cycles of bone resorption (Boyle *et al.*, 2003).

The negative regulator of osteoclastogenesis, osteoprotegerin (OPG), is a cytokine secreted by osteoblasts in response to anabolic agents (Holen and Shipman, 2006, Lacey *et al.*, 1998). When OPG binds RANKL limits the latter's availability to OC precursors and results in decreased osteoclastogenesis, OC survival and bone resorption (Boyle *et al.*, 2003, Tsuda *et al.*, 1997). When OPG

binds to osteoprotegerin ligand, activation of isolated mature OCs is inhibited (Lacey *et al.*, 1998, Simonet *et al.*, 1997) (Figure 1.22). There are several genes responsible for the regulation of osteoclastogenesis, but the relative ratio of RANKL to OPG is the main determinant factor (Roodman, 2006).

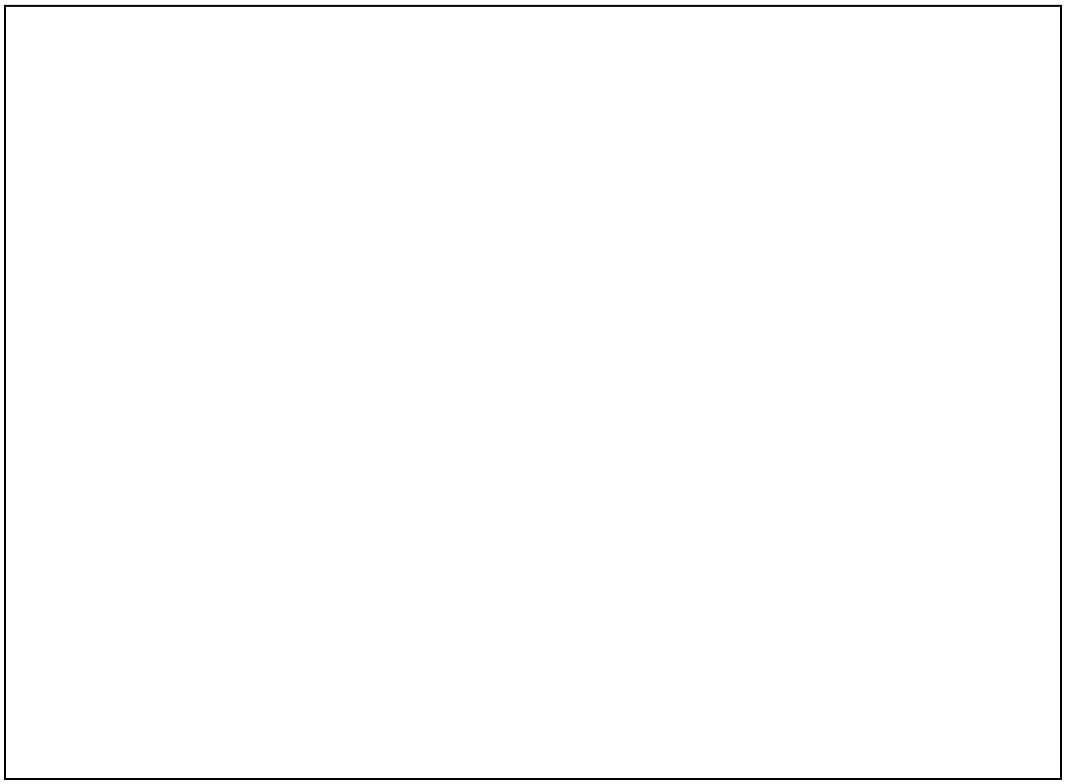


Figure 1.22: The role of RANKL, RANK and OPG in OC activation. Figure from Holen and Shipman, 2008. **Figure has been removed due to Copyright restrictions**

The most characteristic feature of a mature OC which differentiates it from other polynucleate cells is the existence of a clear zone and a ruffled border (Figure 1.23). The clear zone is

devoid of cellular organelles and is in tight contact with the bone surface, isolating and thus defining the resorption site (Suda *et al.*, 1992). The ruffled border is an area with deep invaginations, rich in coated vesicles, phagosomes and residual bodies and represents the active site of bone resorption.

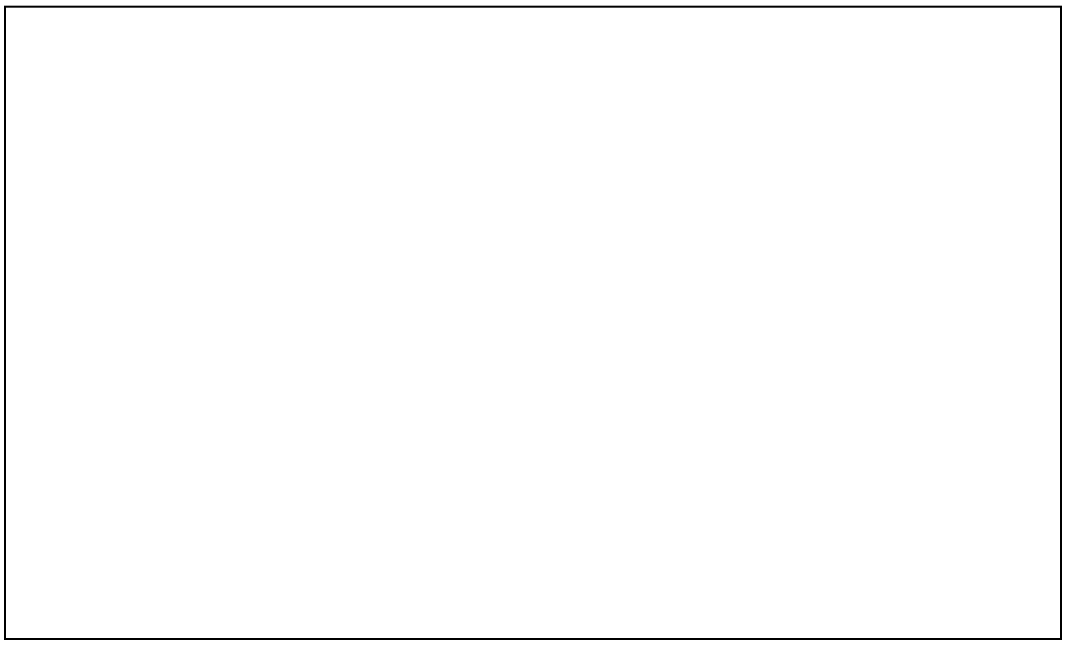


Figure 1.23: Schematic representation of a resorbing OC. Adapted from http://www.pharmaceutical-int.com/article/tracp-5b-assays-tartrate-resistant-acid-phosphatase-5b.html. **Figure has been removed due to Copyright restrictions**

Formation of the ruffled border occurs as a result of cytoskeletal polarization which occurs in a resorbing OC (Teitelbaum, 2000) and it is the site of active secretion of lysosomal proteases and transport of H^+ which acidifies the underlying bone matrix called resorption lacunae and thus activates the proteases

(Blair *et al.*, 1989). Dissolvation of hydroxyapatite crystals is followed by digestion of protein and mineral components facilitated by the released lysosomal enzyme cathepsin K (Zou and Teitelbaum, 2010). The products of matrix degradation are transported via transcytotic vesicles through the OC and released through a functional secretory domain in basolateral membrane (Figure 1.23).

1.8.2 Osteoclast targeting by BPs

The highly endocytic OCs can internalize BPs bound to bone mineral surfaces by fluid-phase endocytosis. The membrane bound-vesicles containing BP are subsequently acidified by the OC proton pump, reducing the negative charge of the phosphonate groups and thus allowing diffusion of BP across the membrane. Disruption of the OC cytoskeleton and ruffle border occurs, leading to cell apoptosis (Thompson *et al.*, 2006a).

Both nitrogen and non-nitrogen BPs induce caspase activation in OCs eventually leading to their apoptosis (Hughes *et al.*, 1995, Neville-Webbe *et al.*, 2010, Reszka *et al.*, 1999) In the case of non-nitrogen BPs, reverse aminoacylation leads to formation of cytotoxic metabolites (Section 1.7.2.1) and also causes OC apoptosis (Rogers *et al.*, 2000) as a result of hyperpolarization and

breakdown of the mitochondrial membrane (Frith *et al.*, 2001, Frith *et al.*, 1997, Selander *et al.*, 1996). Upon ultrastructural examination, OCs obtained from animals treated with BPs exhibited shrinkage of the ruffle border, nuclear aberrations and abnormal lysosomes and were therefore characterized as "frustrated osteoclasts" (Morton and Howell, 1988, Plasmans *et al.*, 1980). Treatment of OC with N-BPs results in lack of protein prenylation of small GTPases leading to alteration and disruption of key OC processes and functions described in Section 1.3 (Flanagan and Chambers, 1991). Inactivation of Rho and Rac GTPases is considered responsible for defective OC adhesion, migration and bone resorption (Faccio *et al.*, 2003) and also leads to apoptosis (Fukuda *et al.*, 2005).

1.9 BISPHOSPHONATE ANALOGUES AS ANTI-TUMOUR AGENTS

Bisphosphonates have proved to be excellent drugs of choice for bone-associated diseases but their anti-tumour properties, despite being well characterized *in vitro*, are still debated due to the controversial results of clinical trials (Neville-Webbe *et al.*, 2010, Shipman *et al.*, 2000). Their high selectivity for hydroxyapatite, due to the presence of two phosphonate groups (Rogers *et al.*, 2000), does not permit significant amounts of drug to reach the

plasma or soft tissues, limiting the deficiency of protein prenylation to bone tissue and restricting their potential anti-cancerous or anti-parasitic action. Therefore current research is focused on the identification of BP analogues which selectively inhibit prenylation by targeting enzymes downstream of FPPS in the mevalonate pathway and thus to successfully target other tissues rather than bone. A specific block of protein prenylation via direct inhibition of FTase, GGTaseI or RGGT may accentuate the beneficial effects of BP while avoiding the acute-phase reaction provoked by IPP accumulation (Section 1.7.3).

BP analogues where one phosphonate group is replaced by a carboxylate (called phosphonocarboxylates, PCs) were shown to selectively inhibit RGGT and thus geranylgeranylation of small Rab GTPases without altering the activity of FPPS (Baron *et al.*, 2009, Coxon *et al.*, 2001) (Figure 1.24). PCs have lower affinity than BPs for bone mineral due to the lack of one phosphonate group and are therefore less likely to anchor to bone or re-attach after release and suppress OC resorption (van Beek *et al.*, 1998). Consequently, they have increased availability to other cells in the bone marrow microenvironment compared to high affinity BPs (Nancollas *et al.*, 2006). Indeed PCs have proved to reduce skeletal tumour growth without disrupting bone remodeling (Fournier *et al.*, 2008) and also effectively inhibited tumour cell invasion *in vitro* albeit in a less

effective manner than BPs (Boissier *et al.*, 2000). Although minor modifications in the side chain of PCs were shown to alter the strength of RGGT inhibition and their biological activity (Baron *et al.*, 2009, Marma *et al.*, 2007, McKenna *et al.*, 2010) their mode of interaction with RGGT requires further clarification. Thus PCs might prove effective anti-tumour agents and combat Rab-associated diseases.

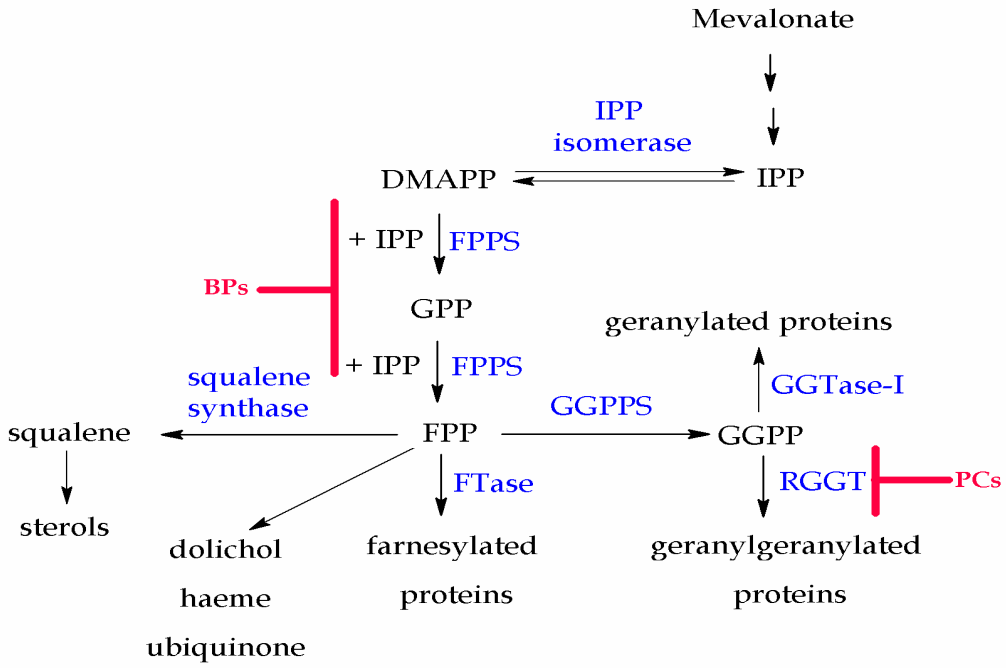


Figure 1.24: The point of BP and PC inhibition in mevalonate pathway. BPs inhibit the action of FPPS whereas PCs directly prevent geranylgeranylation by RGGT.

1.10 AIMS OF THE PROJECT

This thesis aims to clarify the pharmacophore properties of the major clinical BPs in combination with their mode of action by: i) identification of the biochemical and structural alterations of

FPPS upon drug binding ii) elucidation of the mechanism of selective inhibition of RGGT by phosphonocarboxylate analogues of N-BPs and iii) investigation the *in vitro* effects of BPs on OC formation, differentiation and survival.

It was hypothesized that the time- dependent inhibition of FPPS by N-BPs is a result of isomerization of an enzyme –inhibitor complex that prevents dissociation of substrate (Kavanagh *et al.*, 2006b), however important details of the postulated mechanism are still unresolved. In order to test the proposed inhibition model, point mutations to residues considered critical for N-BP interactions (Figure 1.25) inhibition mechanism (Figure 1.26) or substrate binding (Figure 1.27), were designed and introduced into human FPPS. Expression, purification and characterization of the resulting constructs via kinetic studies and crystallography aimed to aid identification of important catalytic residues, allow detailed investigation of the enzyme isomerization effects and give further insights into the BP inhibition mechanism.

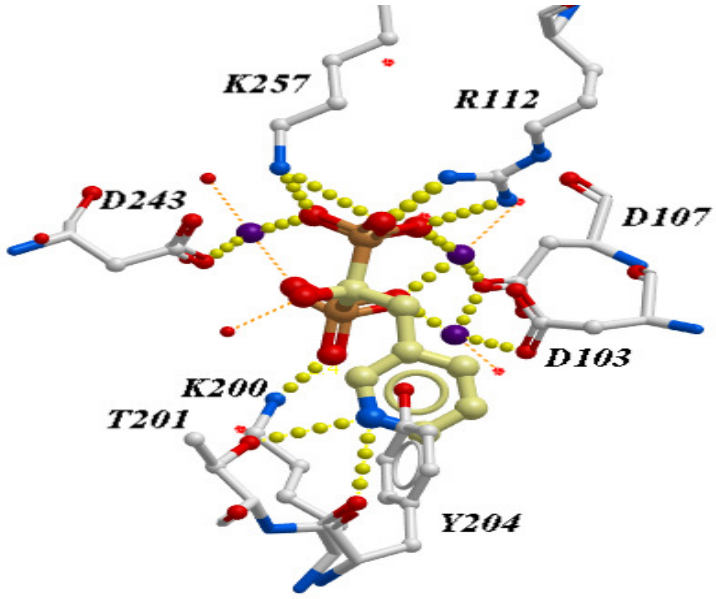


Figure 1.25: Major amino-acids that are considered to play a pivotal role in the interaction of FPPS with Ris. Representations: Mg^{2+} ions as purple spheres, water molecules as red spheres, hydrogen bonds/ electrostatic interactions as yellow spheres, metal –water interactions as orange dots. Figure adapted from pdb 1YW5.

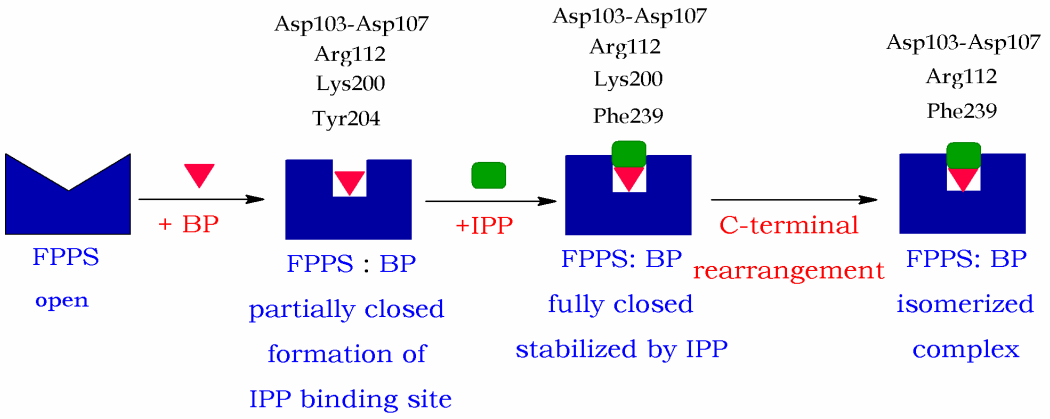


Figure 1.26: FPPS inhibition by N-BPs is a multi-step process subjected to successful interaction of side-chain residues with the BP. Key amino-acids that are considered important for the *in vitro* efficacy of N-BPs and their point of interaction in the inhibition mechanism are denoted.

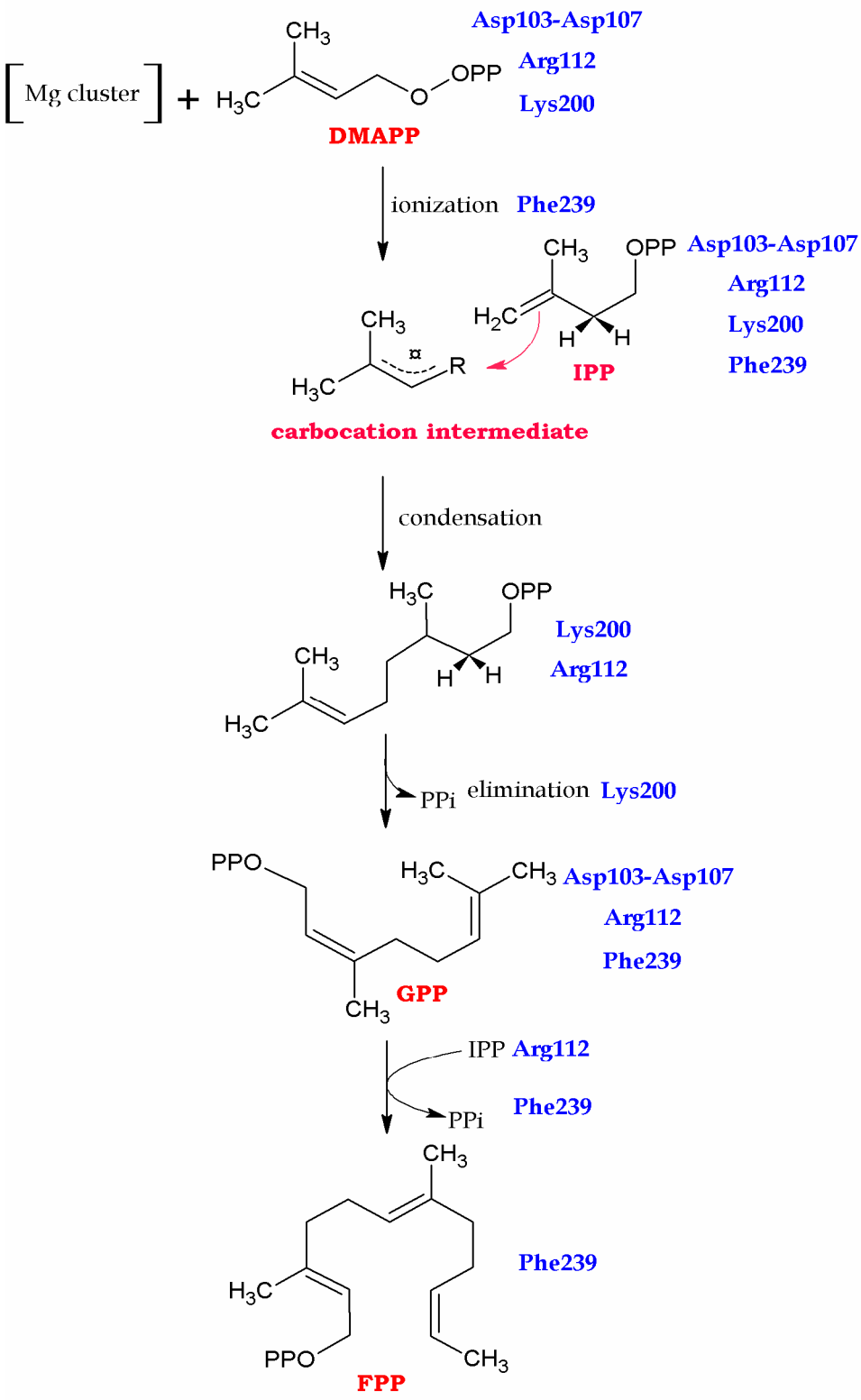


Figure 1.27: Major amino-acids (in blue) that are considered to play pivotal role in the individual steps of FPPS catalytic mechanism.

It is speculated that PC inhibitors allow substrate binding to RGGT but prevent the second round of GG addition by binding adjacent to the active site (Baron *et al.*, 2009). However a high resolution crystal structure of human RGGT with PC is essential to confirm the putative binding site of PCs and its absence limits our understanding of the molecular mechanism of inhibition. In this project an attempt was made to express and purify the components of the ternary RGGT:REP:Rab complex and to investigate their mode of interaction. Kinetic studies and screening with novel PCs should reveal the mechanism of drug inhibition whereas the crystal structure of the complex with different peptide substrates can help identification of the PC binding site and thus facilitate the design of more potent and selective RGGT inhibitors.

The final part of the thesis examines the *in vitro* effects of BP in human osteoclastogenesis from peripheral blood monuclear cells (PBMCs). Alterations in OC precursor fusion, OC morphology and apoptosis may reflect the mode of action of drug upon administration on distinct stages of osteoclastogenesis and accounts for the mechanism of defective resorption observed with clinical BPs *in vivo.*

2. GENERAL MATERIALS AND METHODS

2.1 MATERIALS AND CHEMICALS

The wild type ("native") versions of the genes used in this study were obtained from the IMAGE/Mammalian Gene Collection (Geneservise Ltd, Cambridge, UK), (Table 2.1). CHM entry clone was a kind gift from Professor Miguel Seabra, Imperial College, London. Rab6B clone was obtained from Dr Hee-Won Park, SGC, Toronto.

Table 2.1: Genes and proteins employed in the present study

Code	Gene name	Protein encoding
CHM	Choroideremia (Rab escort protein 1)	Rab Escort Protein 1 (REP1)
CHML	Choroideremia Like (Rab escort protein 2)	Rab Escort Protein 1 (REP2)
FPPS	Farnesyl Pyrophosphate Synthase	Farnesyl Pyrophosphate Synthase
RABGGTA	Rab Geranyl Geranyl Transferase Alpha subunit	Rab Geranyl Geranyl Transferase (RGGT)
RABGGTB	Rab Geranyl Geranyl Transferase Beta subunit	Rab Geranyl Geranyl Transferase (RGGT)
Rab6B	Rab 6B isoform	RAB6B
Rab7	Rab 7	RAB7

Oligonucleotides were purchased from Eurofins MWG (Invitrogen, Paisley, UK). Modified standard Expression LIC vectors were all based on pET-28a (Novagen, Madison, USA) and were provided by Structural Genomics Consortium, Oxford, UK. All restriction digest enzymes were purchased from New England Biolabs (Hitchin, UK). Unlabelled geranyl pyrophosphate (GPP) and isopentenyl pyrophosphate (IPP) were purchased from Echelon, (Amersfoort, Netherlands). Isopentenyl Pyrophosphate (1-^{14}C) triammonium salt (Catalog no: ARC 0541) was purchased from American Radiolabeled Chemicals Inc (Cardiff, UK). All bisphosphonates were a kind gift from Procter and Gamble Pharmaceuticals (Cincinnati, OH, USA), except for pamidronate and alendronate which were from Sigma – Aldrich (Dorset, UK).

All chemicals were of the highest quality available and were purchased from Sigma-Aldrich or Fisher Scientific (Leicestershire, UK) unless otherwise stated.

2.2 POLYMERASE CHAIN REACTION (PCR)

2.2.1 Target gene amplification by PCR

Polymerase chain reaction (PCR) was used to amplify the oligonucleotides against RABGGTA, RABGGTB, CHM and CHML genes by incorporating the specific flanking overhangs to the ends

of cDNAs of interest prior to cloning into the desired vector. The PCR mixture for CHM and CHML contained 100 ng template DNA, 5 µl/reaction of 10 x PCR buffer, 0.2 µM deoxynucleotide triphosphate (dNTP) mix, 1.5 mM $MgSO_4$, 0.2 µM of forward and reverse primer, 1 Unit/reaction Platinum@ *Taq* DNA Polymerase (Invitrogen). Nuclease-free water was added to bring the volume to 50 µl. PCR thermocycler conditions were as shown in Table 2.2.

Table 2.2: PCR cycle conditions for Platinum Taq Polymerase

Cycles	Degrees °C	Time	
Preheating lid	95	5 min	
Denaturation	95	50 sec	
Annealing	54	50 sec	X30 cycles
Elongation	68	2.5 min	
	68	5 min	
Hold	15	pause	

The PCR mixture for RABGGTA and RABGGTB contained 100 ng of template DNA, 5 µl/reaction of 10 x Herculase Buffer, 0.8 µM dNTP mix, 0.25 µM of forward and reverse primer, 2% of dimethylsulfoxide (DMSO), 2.5 U/reaction Herculase Hotstart DNA Polymerase (Agilent, California, USA). Nuclease free water was added to bring the volume to 50 µl. PCR conditions were as shown in Table 2.3.

Table 2.3 PCR cycle conditions for Herculase Hot start Polymerase

Cycles	Degrees °C	Time	
Preheating lid	95	5 min	
Denaturation	95	50 sec	
Annealing	54	50 sec	x 30 cycles
Elongation	72	2.5 min	
	72	5 min	
Hold	15	pause	

2.2.2 Colony PCR

Confirmation of successful incorporation of ligated sample into the desired vector was achieved by colony PCR. The PCR mixture contained the following: a template colony, 2 µl/reaction of 10 x NH_4 Buffer [160 mM $(NH_4)_2SO_4$, 670 mM Tris-HCl pH 8.8, 0.1 % stabilizer], 1.5 µM $MgCl_2$ solution, 1 µM dNTP mix, 3 % DMSO, 0.2 µM of forward and reverse primer and 1.5 Unit/ reaction of BIOTAQ Red (Bioline, Starstedt, Germany). Nuclease free water was added to bring the volume of up to 20 µl. PCR thermocycle conditions are shown in Table 2.4:

Table 2.4: PCR cycle conditions for BIOTAQ Red Polymerase

Cycles	Degrees °C	Time	
Preheating	95	5 min	
Denaturation	95	50 sec	
Annealing	54	50 sec	x 30 cycles
Elongation	68	2.5 min	
	68	5 min	
Hold	15	pause	

2.2.3 Mutagenesis PCR

Denaturation of parental FPPS DNA, annealing of mutagenesis primers and mutant strand synthesis was carried out with *Pfu* polymerase (Agilent, UK). The PCR mixture contained the following: 5 µl of 10 x QuikChange Multi reaction buffer, 100 ng of template DNA, 40 pmol of forward and reverse mutagenesis primers, 2 µl of 25 mM dNTP mix and 1 Unit/Reaction of *PfuTurbo* polymerase. Nuclease free water was added to a volume of 50 µl. PCR cycles shown in Table 2.5:

Table 2.5: PCR cycle conditions for Pfu Turbo Polymerase

Cycles	Degrees °C	Time	
Preheating lid	95	5 min	
Denaturation	95	50 sec	
Annealing	60	50 sec	x 18 cycles
Elongation	68	10 min	
	68	5 min	
Hold	15	pause	

All PCRs were performed using a Gene Amp® PCR System 9700 (Applied Biosystems) and products were analysed on 1% agarose gel (Section 2.9). Primers were designed using vector NTI software (Invitrogen, Paisley, UK) (Appendix A).

2.3 LIGATION INDEPENDENT CLONING (LIC)

Most of the target genes required for construct production were cloned into the desired vector with the method of Ligation Independent Cloning (LIC) that allows directional cloning of the specific PCR products and is independent of restriction enzyme digestion or ligation reactions (Aslanidis and de Jong, 1990).

2.3.1 Generation of LIC sites in insert/ vector

LIC sites compatible with the LIC vector, were incorporated into the gene-specific primer sequences encoding an in-frame ATG codon and a termination codon. LIC expression vector was also treated with the appropriate restriction enzyme in order to create a linearized product for subsequent exonuclease treatment. All LIC enabled vectors encode for *SacB* gene that allows positive selection of the successfully incorporated DNA insert in the presence of sucrose (Bramucci and Nagarajan, 1996, Jager *et al.*, 1995). For a list of vectors and their features please see Appendix B.

2.3.2 DpnI treatment

When template and vector to be cloned had the same antibiotic resistance, PCR products were treated with DpnI restriction endonuclease to eliminate the template's backbone and

thus facilitate subsequent ligation with the vector. Typically 10 units of DpnI were added to a 50 µl PCR reaction mixture and sample was incubated at 37 °C for at least 1 hour (hr).

2.3.3 T4 DNA polymerase treatment

Both insert and vector were purified as described in section 2.5 and treated with T4 DNA polymerase (Novagen) in the presence of the relevant deoxynucleotide for the generation of complementary overhangs. Samples were incubated at 22 °C for 30 min and subsequently at 80 °C for 20 min for enzyme inactivation in a thermocycler. See Tables 2.6 and 2.7 for details of the reaction mixture.

Table 2.6: T4 vector treatment

Vector treatment	**(µl)**
Plasmid digested DNA (equiv 3 mg)	50
Sigma H_2O	23.5
10 X Novagen Polymerase Buffer	10
dNTP (25mM)	10
DTT (1 M)	0.5
BSA (10mg/ml) (NEB)	1
Novagen T4 Polymerase (2.5 U/µl)	5
TOTAL	100

Table 2.7: T4 insert treatment

Insert treatment	**(µl)**
Insert DNA	5
Sigma H_2O	1.5
10 X Novagen Polymerase Buffer	1
dNTP (25 mM)	1
DTT (100 mM)	0.5
BSA (10mg/ml) (NEB)	0.5
Novagen T4 Polymerase (2.5 U/µl)	0.5
TOTAL	10

2.3.4 Annealing, transformation and mini-prep

For annealing, 1µl of treated plasmid was mixed with 3 µl of insert in a PCR tube. Tubes were incubated for 10 min at 22 ^{0}C and were subsequently transferred on ice. Chemically competent Mach-1 or XL10 Gold cells were used for transformation as described in Section 2.8. Transformants were plated Luria Bertani (LB)/agar plates containing 5 % sucrose. Colony PCR for confirmation of insert (Section 2.2.2) and the mini-prep DNA preparation procedure was followed (Section 2.10).

2.4 RESTRICTION ENZYME CLONING

2.4.1 Generation of overhangs in insert/vector

PCR was used to amplify the oligonucleotides against the gene of interest by incorporating the specific flanking restriction enzyme sites to the ends of cDNAs prior to cloning into the appropriate vector. PCR conditions are as described in Section 2.2.1.

2.4.2 Restriction digest

Plasmid DNA (40 µl) or vector DNA (typical concentrations between 200-1200 ng/µl) was subjected to restriction digest with the appropriate restriction enzymes that generated a 5'- overhang prior to ligation. Plasmid or vector DNA was mixed with 1 µl of BSA (10 mg/ml), 5 units of each restriction enzyme and 6 µl of appropriate buffer (NEB). Sterile double distilled water (ddH_2O) was added to make up a total volume of 60 µl. The digest was incubated at the optimal temperature recommended for at least 3 hr. The efficiency of digest reaction was checked by loading 10 % of the reaction product onto an agarose gel for electrophoresis (Section 2.9).

2.4.3 Ligation

Joining of the overhangs of enzyme digested and purified PCR products and vector was executed by T4 DNA ligase (Cat.No. M0202S, NEB), according to the manufacturer's instructions. Briefly, insert and vector were mixed in a 1:4 or 1:8 molar ratio (minimum of 100 ng vector) with 1 µl of T4 DNA ligase (NEB), 3 µl of 10 x DNA ligase buffer containing ATP as catalytic cofactor (Cat. No. B0202S, NEB) and nuclease-free ddH_2O to make up to a final volume of 30 µl. All ligations were allowed to proceed overnight (o/n) at 4 ºC.

2.5 DNA PURIFICATIONS

PCR and restriction digested DNA products were purified by QIAquick PCR Purification Kit according to the manufacturer's instructions (Qiagen, Crawley, UK). Final products were eluted with 50 µl ddH_2O.

DNA vector fragment for ligation were extracted from 1 % agarose gel using the Qiaquick gel extraction kit (Qiagen). The DNA was eluted in 30 µl of ddH_2O according to the manufacturer's instructions (www.qiagen.com).

2.6 ESTIMATION OF NUCLEIC ACID CONCENTRATION

DNA and RNA concentrations and the ratio of absorbance at 260 nm and 280 nm for all experimental analyses were estimated using a Nanodrop.

2.7 TRANSFORMATION

Chemically competent *E. coli* cells of the appropriate strain prepared as described in Section 2.8 were slowly defrosted on ice. 10 µl of ligation reaction mixture was gently mixed with 40 µl of competent *E. coli* and incubated on ice for 20 min. If transformation was carried out with a confirmed DNA sample obtained from a mini prep culture, 1 µl of sample was used. Cells were then heat-shocked at 42 ^{0}C for 45 seconds and placed immediately on ice for 2 min. Subsequently 200 µl of warm 2 x LB medium was added to the cells and the mixture was incubated at 37 ^{0}C for 45 min with vigorous shaking. The cells were centrifuged at 5,000 rpm for 5 min and 140 µl of supernatant was discarded. The pellet was resuspended in a further 50 µl of 2 x LB, plated onto a selective LB agar plates containing the appropriate antibiotic diluted 1/100 from stock (Table 2.8) and incubated at 37 ^{0}C o/n. Only bacteria that have taken up the desired plasmids and

thus contained the antibiotic resistance cassette, could grow on the agar.

Table 2.8: Antibiotic stocks used in preparation of LB-agar plates

Antibiotic	Dilution
Ampicillin	100 mg/ml in water
Cloramphenicol	34 mg/ml in ethanol
Gentamycin	7 mg/ml in water
Kanamycin	50 mg/ml in water
Tetracycline	10 mg/ml in ethanol

2.8 PREPARATION OF COMPETENT CELLS

Competent cells of the relevant *E. coli* strains were prepared according to the $CaCl_2$ method as described below.

Day 1: A loopful of commercial competent bacterial strain was streaked onto a 5.5 cm LB-agar plate containing the appropriate antibiotic (Section 2.7) in a final dilution 1/1000. The plate was incubated at 37 °C o/n. For a list of strains, antibiotic required and the supplier, see Table 2.9.

Day 2: A single colony from bacteria plating was used to inoculate 5 ml of super optimal broth with catabolite repression (S.O.C.) media (Table 2.10). The culture was grown o/n at 37 °C at 180 rpm.

Day 3: The o/n culture (5 ml) was used to inoculate 200 ml of S.O.C. medium. The culture was placed at 37 °C and 200 rpm. The optical density (O.D.) was monitored at 600 nm until it reached 0.5. The cells were then dispersed in pre-chilled 50 ml Falcon tubes and harvested by centrifugation at 4,000 rpm for 10 min at 4 °C. The medium was completely removed and the pellet was carefully resuspended in 0.33 volumes of ice-cold transformation buffer 1 (Table 2.10). The pellet was incubated for 45 min on ice and then centrifuged at 3,500 rpm for 15 min. The buffer was removed and pellets were resuspended thoroughly and gently in 0.08 volume of ice cold transformation buffer 2 (Table 2.10). The cells were incubated on ice for 15 min. Aliquots (0.5 ml) were dispensed into pre-chilled sterile Eppendorf tubes, snap frozen in liquid nitrogen and stored at – 80 °C. Aliquots were not refrozen after thawing, but discarded.

Table 2.9: Bacterial strains, antibiotics and company of purchase

Strain	Antibiotic required	Company
MachI	no antibiotic	Invitrogen
XL1 –Blue	tetracyclin 10 µg/ml	Stratagene
XL-10 Gold	chloramphenicol 34 µg/ml	Stratagene
BL21 (DE3) –R3	no antibiotic	SGC
BL21(DE3)-R3- pRARE	chloramphenicol 34 µg/ml kanamycin 100 µg/ml	Novagen
DH10Bac	kanamycin 100 µg/ml tetracyclin 10 µg/ml	Invitrogen

Table 2.10: Solutions used in preparation of competent cells

S.O.C. medium	2% bacto-tryptone (MERCK), 0.5 % bacto-yeast extract (Fluka), 10 mM NaCl, 2.5 mM KCl. The pH was brought to 7 with 10M NaOH and the solution was autoclaved to sterilize. Sterile glucose (20 mM) was added immediately prior to use.
Transformation Buffer 1	30 mM CH_3CO_2K, 100 mM RbCl (FLUKA), 10 mM $CaCl_2.2H_2O$, 50 mM $MnCl_2.4H_2O$, 15% (v/v) glycerol. The pH was brought to 5.8 with 1M CH_3COOH prior to addition of $MnCl_2.4H_2O$, then the pH was readjusted and the solution was filter sterilized.
Transformation Buffer 2	10 mM MOPS free acid, 10 mM RbCl, 75 mM $CaCl_2.2H_2O$ (VWR), 15% (v/v) glycerol. The pH was brought to 6.8 with KOH, and the solution was filter sterilized.

The transformation efficiency and number of independent clones screened were determined in order to assess the effectiveness of the procedure. Serial dilutions (1/10, 1/100, 1/1000 and 1/10000) of a confirmed high copy plasmid (e.g. pNIC28) were used for transformation in LB-agar plates containing the appropriate antibiotic for selection (kanamycin 50 μg/ml for pNIC28) and left to grow o/n. The following day, the colonies corresponding to each dilution were counted and the colony forming units (CFU) were determined:

$$CFU = \frac{(\text{no. of colonies observed}) x (\text{dilution ratio}) x (\text{original volume})}{\text{plated volume}}$$

The transformation efficiency was equal to the CFU divided by the µg of plasmid DNA used. Typical values indicating high transformation efficiency ranged between 10^5 - 10^6 CFU/µg DNA plasmid.

2.9 AGAROSE GEL ELECTROPHORESIS

The yield and integrity of double-stranded DNA fragments was determined by agarose gel electrophoresis. The gels (1%) were prepared by dissolving 1 g agarose in 100 ml of 1 x Tris Acetate Electrophoresis (TAE) buffer (Fisher) respectively. The suspension was brought to boil in a microwave (full power, 4 min) and subsequently was allowed to cool to approximately 50 °C. SYBR safe stain (Invitrogen) was added to a final concentration of 5% before the gels were poured and left to set in the gel apparatus.

Samples were mixed with 6 x loading dye [10 mM Tris-HCl, pH 7.7, 0.25% (w/v) bromophenol blue (Life Sciences), 30% (v/v) glycerol] in a ratio of 6:1 (v:v) and an aliquot (6 µl) was loaded to the well. A 1kb Plus DNA ladder (NEB) was used as a guide for

determination of the molecular weight of the DNA fragments. Electrophoresis was performed at ~100V for 30 min. DNA bands were visualized by UV exposure and photographed.

2.10 SMALL-SCALE PLASMID PREPARATION (Mini-prep)

LB broth (5 ml) containing the relevant antibiotic was inoculated with a bacterial colony in a sterile 50 ml tube and cultured o/n at 37 ^{0}C with vigorous shaking (200 rpm). Cultures were centrifuged for 20 min at 4000 rpm and plasmid DNA was extracted using the QIAprep Spin Miniprep kit (Qiagen, Crawley, UK) according to manufacturer's instructions (www.qiagen.com). Briefly, bacteria were resuspended in buffer P1 [50 mM Tris-HCl pH 8, 10 mM EDTA, 100 μg/ml RNaseA], lysed under alkaline conditions in solution P2 [200 mM NaOH, 1% SDS] and neutralized with high salt buffer P3 [3 M CH_3CO_2K pH 5.5]. The lysate was centrifuged for 10 min at high speed (13,000 rpm) to remove cell debris. The supernatant obtained was loaded on a QIAPREP silica membrane and centrifuged at high speed to ensure DNA binding to the membrane. Subsequently, the membrane was washed with buffer PB (guanidine hydrochloride and isopropanol based) for the removal of endonucleases and buffer PE (ethanol based) for the elimination of bacterial RNA, protein, salt and other impurities.

Finally, DNA was successfully eluted by addition of TE buffer [10 mM Tris-HCl pH 7.5, 1 mM EDTA] to the membrane and stored at –20 ^{0}C.

2.11 LARGE-SCALE PLASMID PREPARATION (MaxiPrep)

Large scale purification of plasmids from bacterial cultures was required for maintenance of DNA stock for storage/further use. LB broth (5 ml) containing the appropriate antibiotic was inoculated with a single bacterial colony and incubated at 37 ºC, 180 rpm for 6 hr. LB broth with the appropriate antibiotic was inoculated with 3 ml of the starter culture and incubated o/n at 37 ^{0}C with vigorous shaking. Plasmid DNA was extracted using the GenElute™ HP Plasmid Maxiprep Kit (Sigma, Cat. No: NA0310) according to manufacturer's instructions (www.sigmaaldrich.com). DNA was eluted in 500 µl of sterile TE and stored at -20^{0}C.

2.12 DNA SEQUENCE ANALYSIS

All DNA mini prep samples were subject to sequence analysis by LARK technologies, Takeley, UK, to confirm the integrity of insert DNA. Optimal alignment scores of random sequence was carried out with the BLAST program

(http://www.ncbi.nlm.nih.gov) that requires a file of DNA input in FASTA format. Confirmation of point mutations in the p11_FPPS constructs was carried out by pairwise sequence alignment using Vector NTI software (Invitrogen) and visualization of corresponding electropherograms by Finch TV software (Geospiza).

2.13 SEQUENCE ALIGNMENT

The FPPS sequences were extracted from NCBI and were aligned using the program ClustalW (www.ebi.ac.uk/clustalw). Crystal structures were aligned using Internal Coordinate Mechanics (ICM) program (Molsoft, La Jolla, CA).

2.14 GENERATION OF FPPS MUTANTS

A clone encoding human FPPS encompassing residues (derived from clone accession number gi61680822) in p11 vector was obtained from Kunde Guo, SGC, Oxford. The FPPS template for mutagenesis was prepared from a stock of PLysRARE cells using the plasmid purification described under mini-prep in Section 2.10.

Mutagenesis of FPPS Y204F, Y204A and R112L constructs was achieved by the method of overlapping PCRs. More specifically, a first PCR was performed with a forward primer that introduced

the single point mutation in the target codon in combination with the universal pET reverse primer, followed by a second PCR using the universal T7 forward primer and the point mutagenesis reverse primers. Products from both PCRs were mixed in an equimolar ratio and subjected to a third PCR reaction using T7 forward and pET reverse primers that extended the template. Subsequently both p11 vector and PCR inserts were subjected to restriction digest with BamHI and NdeI for the generation of sticky ends. Initial overlapping PCRs and restriction digests were performed by Dr James Dunford, Botnar Research Centre, Oxford.

Ligation was performed by annealing 10 μl of the DNA derived from the third PCR with 1 μl of p11 vector in a typical molar DNA ratio vector: insert 1:4. Transformation with competent MachI cells and subsequent plating in LB-ampicillin selective plates (100 μg/ml) followed. Please see Section 2.7 for further details.

Generation of the remainder of the FPPS mutants was carried out with QuikChange Site-Directed mutagenesis kit (Agilent Technologies, Cheshire, UK), according to the manufacturer's instructions (http://www.stratagene.com) with minor modifications. Native plasmid strand PCR used the p11 vector containing the wild-type FPPS as template and two synthetic oligonucleotide primers containing the desired mutation (Section 2.2.3). The PCR product was digested with DpnI enzyme (typically

1 µl of DpnI (equivalent to 20 units) per 25 µl of PCR reaction product) for successful elimination of methylated and hemimethylated parental DNA. Transformation with XL10 Ultra competent cells (provided with kit) followed. Briefly, 45 µl of competent cells were slowly thawed on ice. Mercaptoethanol (2 µl) was added to each tube and samples were incubated for 10 min on ice, with a gentle swirl every 3 min. PCR product (5 µl) was added to each tube and the samples were incubated on ice for 30 min. The rest of the procedure was carried out as described in Section 2.7.

Mutagenesis primers were designed according to manufacturer's instructions. Further details can be found in Appendix C.

2.15 PROTEIN EXPRESSION

Small scale experiments (50 ml) were initially performed to test for the expression of the constructs. Once protein expression was detected for a particular construct, large scale preparations (1 L) followed.

2.15.1 Transformation in T7 RNA polymerase based strain

Mini prep DNA was transformed in *E. coli* strains BL21(DE3)-R3 or BL21-R3-pRARE2 in LB plates selected for the appropriate antibiotic. Plates were incubated o/n at 37 °C.

2.15.2 Overnight pre-culture

A single colony of *E.coli* BL21 containing the appropriate expression vector was obtained from LB /Agar plate or 10 µl of a partially thawed glycerol stock (Section 2.16) was used to inoculate the appropriate amount of LB media (10 ml of LB per litre of TB for maxi scale protein production or 5 ml of LB per 50 ml of TB for test expression cultures) containing the appropriate antibiotic (1/1000 dilution). Cultures were incubated o/n at 37 °C with shaking at 200 rpm.

2.15.3 Culture in Terrific Broth (TB) and protein induction via IPTG addition

The o/n starter culture (10 ml) was used to inoculate 1 L of Terrific Broth (TB, Merck, KGaA, Darmstadt, Germany) in baffled shake flasks (or 0.5 ml of culture in 50 ml of TB when protein was grown for test expression) and the appropriate antibiotic

concentration. Cultures were grown at 160 rpm, 37 °C. The O.D. was monitored at 600 nm until reached 1.2- 1.5. At this stage, the temperature was reduced to 18 °C and expression of the recombinant gene was induced by addition of 0.2 mM of isopropyl-1-thio-D-galactopyranoside (IPTG) (or 0.01 mM IPTG for the 50 ml cultures) to induce T7 RNA polymerase production and thus enable protein expression. The culture was incubated o/n at 18 ° C with shaking at 160 rpm to allow protein production to occur.

2.15.4 Cell harvesting

Cells were harvested via centrifugation at 5,500 rpm for 15 min at 4°C and resuspended in lysis buffer containing 50 U/ml of benzonase nuclease HC (Novagen), protease inhibitors [1 tablet of Complete EDTA-free (Roche, Hertfordshire, UK) per 50 ml of culture] and 0.5 mM of TCEP. The pellet was either stored at -20 °C until required or rapidly processed in step (2.16.5).

2.15.5 Cell lysis

Cells resuspended in lysis buffer [50 mM HEPES pH 7.5, 500 mM NaCl, 5 mM imidazole, 0.5 mM TCEP, 0.2 µM PMSF, 5% (v/v) glycerol] were slowly defrosted and lysed by sonication for 6 min with 10 sec pulses and 20 sec pauses. In some cases, sonication

time was prolonged until cells were completely lysed. The lysed cells were placed in centrifuge tubes (363647, Beckman Coulter) and cell debris and precipitate DNA was spun down at 22,000 rpm for 45 min in a JA 25.50 rotor in an Avanti J-20 XPI centrifuge (Beckman Coulter). The supernatant was passed through a 0.2 μm filter before used for protein purification as described in Section 2.18.

2.16 PREPARATION OF GLYCEROL STOCKS FROM TRANSFORMED HOSTS

An aliquot (800 μl) of bacterial culture grown o/n as described in Section 2.15.2 was mixed thoroughly with 200 μl of 70% autoclaved glycerol (Fisher Scientific) in sterile cryovials and stored at –80 °C. To inoculate a starter culture, the glycerol stock was taken out and kept on ice until partially thawed. A small number of cells were picked with a sterile loop and immediately placed in 5 ml of culture media. The partially frozen stock was immediately returned to -80 °C.

2.17 PROTEIN PURIFICATION TECHNIQUES

All purifications apart from 2.17.1 and 2.17.2 were performed in Akta Explorer system (GE Healthcare) and 2 ml fractions were

collected in 96 well plate. Protein was routinely monitored by measuring absorbance at 280 nm and peak fractions were analysed for purity by SDS-PAGE (Section 2.19.1) and were subsequently pooled.

2.17.1 Manual elution from Ni-NTA column

A 5 ml Ni-NTA column (Qiagen) was prepared by elution with 30 ml deionized water and then 5 column volumes (CV) of Ni-NTA binding buffer [50 mM HEPES pH 7.5, 500 mM NaCl, 20 mM Imidazole, 0.5 mM TCEP, 5% (v/v) glycerol]. Alternatively, Ni-NTA regenerated resin (1-2 ml bed volume) in 20 % ethanol was applied and the column was equilibrated by the addition of 6 CV deionized water and 6 CV of Ni-NTA binding buffer. The volume of the Ni-NTA resin used was pre-determined by the predicted protein yield from test expression analysis. Protein lysate was applied directly to the column which was washed with 2 CV of binding buffer and subsequently with 2 CV of wash buffer [50 mM HEPES pH 7.5, 500 mM NaCl, 40 mM imidazole, 0.5 mM TCEP, 5% (v/v) glycerol] for the elimination of unspecifically bound proteins. Finally, the protein of interest was eluted by the application of 4 x 5 ml of Ni-NTA elution buffer [50 mM HEPES pH 7.5, 500 mM NaCl, 250 mM imidazole, 0.5 mM TCEP, 5 % (v/v) glycerol].

2.17.2 Protein purification from streptavidin/aragose resin

The procedure was similar to that described in 2.17.1 except for the following modifications: i) 2 ml of streptavidin/agarose resin (Section 2.20) was used instead of Ni-NTA regenerated resin ii) streptavidin column buffer [50 mM HEPES pH 7.5, 250 mM NaCl, 0.5 mM TCEP] was used instead of Ni-NTA binding buffer and iii) elution was achieved with streptavidin elution buffer [50 mM HEPES pH 7.5, 250 mM NaCl, 0.5 mM TCEP, 2 mM biotin in place of Ni-NTA elution buffer.

2.17.3 Immobilized Metal Ion Affinity chromatography (IMAC)

The column (His Trap_FF_crude_1 ml, GE Healthcare) was equilibrated with 20 CV of deionized water followed by 20 CV of binding buffer. The clarified cell lysate was passed through the column at a flow rate of 1 ml/min. The column was washed with 30 CV of Ni-NTA binding buffer (Section 2.17.1) and 10 CV of wash buffer (Section 2.17.1) to eliminate non-specifically bound proteins. Finally, the protein of interest was eluted by the application of 20 CV of Ni-NTA high imidazole elution buffer [50 mM HEPES pH 7.5, 500 mM NaCl, 400 mM imidazole, 0.5 mM TCEP, 5% (v/v) glycerol].

2.17.4 Gel filtration

A Superdex 16/60 200 column (GE Healthcare) was pre-equilibrated with gel filtration (GF) buffer [50 mM HEPES pH 7.5, 500 mM NaCl, 0.5 mM TCEP, 5% (v/v) glycerol] for 1.5 CV at a flow rate of 1 ml/min. Subsequently protein lysate (volume between 0.5 -2 mls) was loaded on the column. The column was then eluted with 1.5 CV (equivalent to 150 ml) of GF buffer and 1.5 ml fractions collected in a 96 deep well plate.

2.17.5 Tobacco Etch Virus (TEV) protease and thrombin cleavage of tag

Removal of hexahistidine, SBP or GST protein tag was executed with TEV protease or thrombin, depending on the cleavage site built into the vector. For TEV cleavage, 25 µl of 6 mg/ml TEV (for preparation see Section 2.21) per 10 mg of protein were added to pooled fractions concentrated in GF buffer (Section 2.17.4). For thrombin cleavage, 250 µl of thrombin (2 mg/ ml) (Roche) per 10 mg of protein was added to fractions concentrated in thrombin cleavage buffer [50 mM Tris-HCl pH 8, 150 mM NaCl, 1 mM TCEP, 2.5 mM $CaCl_2$]. In both cases cleavage was allowed to proceed o/n at 4 ºC. Removal of thrombin from the cleaved protein

sample was carried out with anion exchange chromatography as described in Section 2.17.6.

2.17.6 Anion exchange chromatography

Anion exchange chromatography was performed with a HP-Q-HiTrap 5 ml global column (GE Healthcare). The column was initially equilibrated with 10 CV of buffer A [50 mM Tris-HCl pH 7.5, 1 mM DTT]. Subsequently, protein was eluted with a 10-100% linear gradient of buffer B [50 mM Tris-HCl pH 7.5, 1 M NaCl, 1 mM DTT] for 20 CV.

2.17.7 Buffer exchange

When rapid buffer exchange was required between the various purifications steps, protein was concentrated up to 1 mg/ml (Section 2.18) and passed through a NAP 10 column (GE Healthcare) eluting with the appropriate buffer. The procedure was carried out according to the manufacturer's instruction.

2.18 PROTEIN CONCENTRATION

Purified proteins were concentrated using either 4 ml or 15 ml concentrators with the appropriate molecular weight cut-off

(Amicon Ultra-15 10,000 MWCO or 30,000 MWCO, Millipore) for biophysical studies or crystallographic screening.

2.19 PROTEIN CHARACTERIZATION AND PURITY

2.19.1 Sodium dodecyl sulfate polyacrylamide gel electrophoresis (SDS-PAGE)

The purity and molecular weight of individual protein was assessed by sodium dodecyl sulfate polyacrylamide gel electrophoresis (SDS-PAGE).

2.19.1.1 Gel preparation

Resolving gels typically contained 10 % acrylamide, however the concentration ranged from 7.5 % to 15 % depending on the application. Resolving gels were composed of the relevant percentage of acrylamide/bisacrylamide solution (crosslinker ratio 37.5:1) (Biorad) and resolving buffer [0.375 M Tris-HCl pH 8.8, 0.1 % SDS]. Polymerization was initiated by addition of 10 % ammonium persulphate (APS) and 0.004 % N,N,N'N'-tetramethylethylenediamine (TEMED). Gels were overlaid with 2 ml of butanol and left to stand for at least 45 min, to allow polymerization to occur. Stacking gels contained 4%

Acrylamide/Bisacrylamide solution and separation buffer [0.125 M Tris-HCl pH 6.8, 10 % SDS]. Polymerization initiated by addition of APS (10%) and TEMED (0.004 %). Butanol was carefully decanted and stacking gel was poured on top of resolving gel, the appropriate comb for well formation was inserted and gel was allowed to polymerize for 15 min.

2.19.1.2 Sample preparation

The lysate to be assessed was resuspended in lysis buffer [50 mM HEPES pH 7.5, 500 mM NaCl, 5 mM Imidazole, 0.5 mM TCEP, 0.2 µM PMSF, 5% (v/v) glycerol], sonicated for 1 min with a 50% pulse, mixed with 4 x Laemmli buffer [0.25M Tris-HCl pH 6.8, 20% ß-mercaptoethanol, 40% (v/v) glycerol, 0.02 % bromophenol blue, 8% (w/v) SDS] in a ratio of 4:1 (v/v) and then denatured by heating at 95°C for 5 min. Insoluble material was removed by centrifugation at 13,000 rpm for 5 min. An aliquot of the supernatant (12 µl) or 10-20 µg protein from pre-cleared cell extracts was loaded on gel.

2.19.1.3 Electrophoresis

SDS-PAGE was carried out using a Mini Protean III apparatus (BioRad, Munchen, Germany) according to the manufacturer's instructions. The gel was run with 1x MES (2-N-morpholino)ethanesulfonic acid) buffer (Biorad, Hertfordshire, UK)

or 1x Tris-glycine buffer [250 mM Tris-HCl pH 8.3, 200 mM glycine, 0.5% (w/v) SDS, pH 8.3] at 150V for 55 min. Subsequently, the gel was washed 3 times with deionized water, stained with Instant Blue Coomassie stain (Expedeon, Harston, UK), for 30 min on a shaker, destained with deionized water and scanned. Commercial protein molecular weight standard (5 μl) was used as reference and for sample recognition.

2.19.2 Western Blotting Analysis

Western Blotting was performed to detect the presence of the desired protein in cell lysates.

2.19.2.1 Preparation of lysate from cell culture

Cells were cultured in 25 cm^3 flasks, typically to a concentration of 5 x 10^7 cells/ml. Cells were washed with ice-cold PBS and resuspended in 0.5 ml of ice-cold TNE lysis buffer (Table 2.11). Cells were carefully scraped, sonicated with 10 sec pulses and 20 sec pauses for 1 min and if not used immediately, flash-cooled in liquid nitrogen and stored at -80 °C. When required the sonicated extract was slowly defrosted on ice and left rotating o/n at 4 °C. The following day, the extract was centrifuged at 13000 rpm for 30 min at 4 °C. The level of protein expression in the supernatant was determined with BCA assay (Section 2.23).

Typically 10-20 µg of protein was used to load an SDS-PAGE gel. For preparation of lysate from protein purifications please see Section 2.19.1.

2.19.2.2 Electrophoretic transfer

Cells were homogenized in western blot lysis buffer and cell extract was separated by 10% SDS-PAGE gels as described in 2.19.1 and transferred on to Polyvinylidene fluoride (PVDF) membrane (Millipore), in protein transfer buffer (Table 2.11) at 100 V/300 mA at 4^0 C for 1 hr using a BioRad Mini Trans-Blot Electrophoretic Transfer system.

Table 2.11: Solutions used in Western blotting

TNE Lysis Buffer	50 mM Tris-HCl pH 7.5, 2 mM EDTA, 150 mM NaCl, 5 mM NaF, 100 µM Na_3VO_4, 1% protease inhibitor cocktail (Sigma P8340), 1% NP-40 Sodium vanadate was activated for maximal inhibition of protein tyrosine phosphatases as described by (Gordon, 1991).
Transfer Buffer	25 mM Tris base, 250 mM glycine, 20% (v/v) methanol
10 x PBS	137 mM NaCl, 2.7 mM KCl, 10 mM Na_2HPO_4, 1.76 mM KH_2PO_4. The pH was adjusted to 7.4 with HCl
PBS-T	0.1 % Tween-20 in PBS
Blocking buffer	100 ml PBS, 5 g skimmed milk (Marvel)

2.19.2.3 Immunoblotting

Following transfer, membranes were incubated with blocking buffer at 4^0 C for at least 1 hr to prevent non-specific background binding of the applied antibodies. Membranes were washed three times with 100 ml PBS-Tween (PBS-T) for 5 min with mild shaking and incubated with the selected primary antibody in PBS and 1% BSA for 2 hr. Blots were washed five times with PBS-T for 5 min and were subsequently probed with the horseradish peroxidase (HPR) conjugated antibody in PBS for 1 hr. Membranes were washed three times with 100 ml PBS-T for 5 min. Throughout the whole procedure, membranes were maintained under gentle shaking. Membranes were incubated with Enchanced Chemiluminescence (ECL) reagent (Amersham Biosciences, Little Chalfont, UK) and were visualized with UVP chemidoc system with a Chem500 digital camera using Visionworks software. For a list of all antibodies used see Tables 2.12 and 2.13.

Table 2.12: Primary antibodies used in Western blotting

Antibody	Manufacturer	working dilution
Anti-FLAG Rabbit Monoclonal IgG	Sigma (Cat No F7425)	1/1000
Anti-Cathepsin K Goat IgG	Santa Cruz (sc-6506)	1/1000
Anti-Calcitonin Receptor Goat Polyclonal IgG	Santa Cruz (sc-8858)	1/1000
Anti-OSCAR Goat Polyclonal IgG	Santa Cruz (sc-34235)	1/1000
Anti-Actin-Rabbit Polyclonal IgG	Sigma (A2066-5)	1/1000

Table 2.13: Secondary antibodies used in Western blotting

Antibody	Manufacturer	working dilution
Anti Rabbit IgG HRP	Sigma (Cat No A0545)	1/5000
Anti Goat HRP	Sigma (Cat No A0545)	1/4000

2.19.3 Electrospray ionization time-of-flight mass spectrometry (ESI-TOF MS)

Further assessment of the molecular mass of purified protein was carried out with an Agilent LC/MSD TOF system with reversed-phase HPLC coupled to electrospray ionization and an orthogonal time-of-flight mass analyzer. Protein solution (1 µl, 1 mg/ml) was mixed 49 µl of loading solution [50% (v/v) methanol in 5% (v/v) formic acid] and 3 µl were used for injection. Proteins

were desalted prior to mass spectrometry by rapid elution off a C3 column with a gradient of 5-95% acetonitrile in water with 0.1% formic acid. Measurements and deconvolution of data were performed according to manufacturer's instructions.

2.20 GENERATION OF STREPTAVIDIN-AGAROSE RESIN

Preparation of streptavidin-binding protein coupled to agarose resin was performed for subsequent isolation of biotin tagged constructs, cloned in pBEN1 vector. The plasmid encoding for the 159 residue streptavidin, (strain) was a kind gift of Dr Gallizia, Milan, Italy and was expressed in *E. coli* BL21(DE3) strain.

2.20.1 Expression and purification of recombinant streptavidin

The procedure was performed as described by (Gallizia *et al.*, 1998). Briefly, 8 L of cell culture was harvested, lysed by sonication and purified on a iminobiotin column except that purified protein was eluted with 100 mM acetic acid pH 2.9, fractions were concentrated with Amicon 30000 MWCO and dialyzed o/n against PBS, pH 7.4 , at 4 ºC.

2.20.2 Activation of Sepharose resin by cyanogen bromide

The hydroxyl groups of sepharose polymer can combine with cyanogen bromide (CNBr) to yield a cyclic imido-carbonate, required for coupling of desired ligands under basic conditions (Axen and Vretblad, 1971). For every eight liters of purified streptavidin preps, 40 ml of Sepharose 4B resin in 50% ethanol (Amersham) were used for subsequent coupling. The resin was washed with 2 x 100 ml of deionized water. An aliquot (20 gr) was added 30 ml of 3.3 M sodium phosphate of pH 11.2 and resuspended slowly by mild stirring. CNBr (2 g) was added and allowed to react with the resin for 2 min prior to application of vacuum filtration. The resin was washed with 200 ml of ice-cold 25 mM sodium phosphate pH 6 followed by 500 ml of deionized water. The activated resin was resuspended in coupling buffer [100 mM $NaHCO_3$ pH 8.5, 500 mM NaCl], collected in a 50 ml Falcon tube and placed at 4 ºC. The procedure was repeated until all the resin was activated by CNBr.

2.20.3 Coupling of Sepharose resin to streptavidin

Ten ml rStreptavidin solution (concentrated to 3.5 mg/ml) were added to 1 ml of a solution containing 100 mM $NaHCO_3$, pH 8.5 and 500 mM NaCl and left o/n with gentle mixing at 4 °C. The

absorbance at 280 nm was measured to determine the amount of unbound protein. The suspension was centrifuged at 800 rpm for 5 min and the supernatant (excessive streptavidin) was used in a subsequent Sepharose coupling cycle. The coupled resin was washed with 3 CV of coupling buffer to remove any unbound protein and subsequently blocked with 1 M ethanolamine, pH 8.0 for 2 hr at room temperature (R.T.) on a shaker. The resin was centrifuged for 5 min at 800 rpm, 4 ºC and was conditioned by washing with 2CV of the mildly alkaline coupling buffer followed by 2CV of CH_3COONa pH 4.0, 500 mM NaCl. The washing was repeated four times and finally the coupled resin was mixed with 2CV of 20% ethanol and stored at 4 ºC until required.

2.21 GENERATION OF TOBACCO ETCH VIRUS PROTEASE

Tobacco Etch Virus (TEV) protease, cloned into the p11 vector (Appendix B) as an N-terminally 6His-tagged fusion protein, was expressed as described in 2.16. Bacterial lysate was cleared of insoluble material via high speed centrifugation (22000 rpm for 45 min) and was first applied to a Ni-NTA column (2.17.3). Then, Ni-NTA elution buffer was exchanged with GF (2.17.7) and protein was subjected to gel filtration (2.17.4). Purified samples were pooled and concentrated up to 10 mg/ml, to avoid protein

precipitation. EDTA, glycerol and TCEP were added to give final concentrations of 0.5 mM 20 % and 0.1 mM respectively. The protein was aliquoted in 100 µl PCR strips, snap frozen in liquid nitrogen and stored in -80 ºC.

2.22 HIS-TRAP COLUMN REGENERATION

Ni-NTA resin was regenerated after each protein purification by washing with 1 CV of Milli-Q Water and stripped of Ni^{2+} by the addition of 30 mM EDTA pH 8.0 (1 CV). Any precipitated protein and debris were removed by the addition of 0.2 M NaOH (1 CV) and left for up to 2 hr. The dissolved proteins were washed off with 2 CV of binding buffer and 1CV of Milli-Q Water. The resin was recharged with 1 CV of 100 mM $NiSO_4$, washed with 5 CV of Milli-Q Water, resuspended in 2 volumes of 20% ethanol and stored at 4 ºC.

Regeneration of His-Trap FF-crude 1 ml columns was performed according to the manufacturer's instruction (http://www.apczech.cz/pdf/instructions-histrap-ff-crude-kit.pdf).

2.23 PROTEIN ASSAY

Determination of protein concentration was performed as described in the BCA (bicinchronic acid) Protein Assay Reagent kit

(Fisher) Protein Assay Protocol under the microplate section. BSA concentrations ranging from 0.2-2 mg/ml were used as protein standards. Briefly, protein sample or protein standard (25 µl) were mixed with 200 µl of BCA working reagent in a 96-well microtitre plate. Samples were incubated at 37 ºC for 30 min to allow reduction of Cu^{2+} to Cu^{1+} by protein and subsequent chelation of Cu^{1+} by BCA, detected by colour change (green to purple). Optical densities were measured at 595 nm on a Spectra Maxplus 384 Microplate Reader (Molecular Devices) and data were analysed using accompanying software.

2.24 FPPS ACTIVITY ASSAY

The activity of FPP synthase was measured by the method of Reed and Rilling (Reed and Rilling, 1976) with modifications. For kinetic analysis, FPPS was assayed in a final volume of 100 µl in assay buffer [50 mM Tris-HCl pH 7.7, 2 mM $MgCl_2$, 0.5 mM TCEP, 50 µg/ml BSA]. Reactions were started either by the simultaneous addition of the substrates (10 µM of ^{14C}IPP, 400 KBq/µmol and 10 µM GPP) or the enzyme and allowed to proceed for at least 3 min at 37 ºC. It was checked that the activity measured was the same by either procedure. The reaction was quenched by the addition of 0.2 ml of concentrated HCl: methanol (1/4, v/v) and tubes were left for

a further 10 min at 37 °C. The reaction product was then extracted with 0.4 ml of Scintillant (MicroScint-E, Perkin Elmer) and after thorough mixing and brief centrifugation the amount of radioactivity in the upper phase was determined by direct counting using a Perkin Elmer 1450 LSC Microbeta scintillation Counter.

2.24.1 Determination of K_m and V_{max} values

Determination of K_m^{IPP} and K_m^{GPP} was achieved by varying the concentration of either IPP or GPP ranging from 0.5- 100 µM while keeping the concentration of the second substrate at 10 µM. The 80 µl master mix contained 10 µl of 10 x assay buffer (Section 2.24), 10 µl of ^{C14}IPP or GPP and 50 µl of H_2O. Reaction was always initiated by addition of 20 µl of enzyme diluted with Tris-HCl buffer pH 7.7 to a concentration which gave a linear initial rate of the reaction and less than 20 % of the substrate had been consumed when the reaction was terminated.

2.24.2 Bisphosphonate inhibition assay

Determination of bisphosphonate (BP) inhibition was achieved by assaying the enzyme activity at a variety of BP concentrations. For initial rate assay the master mix contained 10 µl of BP (1 nM-5 mM), 10 µl of 10 x assay buffer, 20 µl substrates [10 µM of ^{C14}IPP

and GPP] and water up to 80 µl. The reaction was started by the addition of enzyme (20 µl).

For BP pre-incubation assay, 20 µl of the enzyme was pre-incubated with 10 µl of 10x conc. BP, 10 µl of 10 x assay buffer and 40 µl of water for 10 min. The reaction was initiated by the addition of 20 µl of substrate [10 µM of ^{C14}IPP and GPP]. Incubation time and enzyme concentration was adapted according to the respective activity of individual mutants, however all data were collected for times where product accumulation was linear with time.

2.25 FPPS KINETIC DATA ANALYSIS

Data were fitted to the appropriate kinetic models by nonlinear regression using PRISM (GraphPad, San Diego). Determination of tight-binding ligand characteristics were analyzed by a method based on the equation developed by Morrison (Morrison, 1969, Morrison and Walsh, 1988):

$$\frac{Vi}{Vo} = 1 - \frac{([E] + [I] + Ki_{app}) - \sqrt{([E] + [I] + Ki_{app})2 - 4[E][I]}}{2[E]}$$

The overall Ki dissociation constant was calculated from Ki_{app} using the model of competitive inhibition (Copeland, 1996, Morrison, 1969):

$$Ki = \frac{Ki_{app}}{1 + \frac{[GPP]}{K_m GPP}}$$

The isomerisation constant of the enzyme inhibitor complex was calculated from the overall (Ki*) and initial inhibition constant (Ki) using the following equation (Copeland, 1996):

$$K_{isom} = \frac{Ki - Ki*}{Ki}$$

2.26 RGGT ASSAY

The activity of Rab Geranyl Geranyl transferase complex was measured by determining the amount of [^{3}H] GGPP transferred to Rab proteins (Baron *et al.*, 2009, Seabra *et al.*, 1992b). The standard reaction mixture contained the following concentrations in a final volume of 20 µl: 40 mM HEPES (pH 7.5), 3 mM $MgCl_2$, 5 µM $ZnCl_2$, 1 µM GDP, 5 mM DTT, 0.3% CHAPS, 100mM NaCl, 5µM [^{3}H] GGPP (specific activity = 800 dpm/pmole), 100 nM RGGT proteins, 5 µM REP1 or REP2, 5 µM Rab. Proteins were all diluted

and stored in a buffer containing 50 mM HEPES (pH 7.5), 1 mM TCEP, 5% glycerol, 0.2 % NP-40. Enzyme reaction started by addition of 5 µl RABGGT (equivalent to 100 nM) and allowed to proceed at 37 °C for 15 min, 30 min, 45 min or 60 min. The reaction was quenched by the addition of 100 µl trichloroacetic acid (TCA) and the reaction mixture was transferred to a Millipore 96 well plate and vacuum filtered. The wells were washed 5 x 100 µl of 10 % TCA followed by 3 X 100 µl of 100% ethanol and vacuum filtered after each addition. Scintillation fluid (80 µl) (Beta Scint) was added to each well and radioactivity in each well was determined using a Perkin Elmer 1450 LSC microbeta scintillation counter. Appropriate control reactions (no REP, no substrate or no enzyme) were also tested for activity.

2.27 CRYSTALLIZATION & DATA COLLECTION

All ligands used for FPPS co-crystallization (N-BPs, IPP and DMASPP) were prepared as 20 mM stock solutions in 100 mM Tris-HCl pH 7.7. $MgCl_2$ was prepared as a 100 mM aqueous stock solution. The ligands were added to the concentrated protein (15 mg/ml) to a final concentration of 2 mM each whereas $MgCl_2$ was added to a final concentration of 4 mM.

The crystallisation plates used were CrystalQuick 3-sitting drop plates (Greiner BioOne) and the crystallisation screens used are shown in Table 2.14. Protein-crystallisation solution drops were generated by a Mosquito automated liquid handler (Labtech TTP). Three different v/v ratios of protein solution: precipitant were used (2:1, 1:1: 1:2) to a final volume of 300 nl. The reservoirs and the protein drops in the plates were sealed using a 'Seal-It' instrument (Abgene) and placed at 20 °C in Minstrel incubators (Rigaku Corp.) for imaging.

Table 2.14: Crystallization screens used

Screen name	Screen condition
JCSG-C11	2 M $(NH_4)SO_4$, 0.1 M acetate pH 4.5
LFS4-A8	0.2 M NH_4Cl, 20.0% (v/v) PEG, 10 % (v/v) EtGly
LFS-4 090109-02-A10	0.10M MgCl2; 20.0% (v/v) PEG 6K; 10.0% EtGly
LFS-4 090109-02-A12	0.01M ZnCl2; 20.0% (v/v) PEG 6K; 10.0% EtGly
LFS-4 090109-02-A08	0.20M NH4Cl; 20.0% (v/v) PEG 6K; 10.0% EtGly
LFS-4 090109-02-A07	0.20M NaCl; 20.0% (v/v) PEG 6K; 10.0% EtGly
LFS-4 090109-02-A11	0.05M CaCl2; 20.0% (v/v) PEG 6K; 10.0% EtGly

Crystals were visible in plates generally after three days of incubation and were mounted in nylon loops using standard

CrystalCaps (Hampton Research Corp.). A single crystal was transferred to a cryo-protectant prepared with 20% glycerol, 80% screen solution and flash-frozen in liquid nitrogen. Data were collected at a resolution between 1.6- 2.7 Å at the Diamond Synchrotron, Beamline I02, by Richard Walter, Shamrock Structures LTD, Chicago.

2.28 MODEL BUILDING

Indexing and integration of collected data was performed using MOSFLM (Powell, 1999) and symmetry-related reflections were scaled by SCALA (Evans, 2006) and converted into amplitudes by TRUNCATE. Initial phases were calculated by molecular replacement with PHASER (McCoy *et al.*, 2007) using WT FPPS in complex with Zol (PDB code: 1ZW5) as a starting model. Models were completed manually with COOT (Emsley and Cowtan, 2004) and refined with REFMAC5 (McCoy *et al.*, 2005) package. In all cases, thermal motions were analyzed using TLSMD (Painter and Merritt, 2006) and hydrogen atoms were included in late refinement.

The structures of the Thr201 to Ala FPPS mutant in complex with Zol and of Tyr204 to Ala FPPS mutant in complex with Ris: IPP were solved by myself. Building of other crystal models

presented in this thesis was performed in collaboration with Joao Muniz (SGC, Xray Crystallography group) and Bobby Barnett (Procter & Gamble, Cincinnati, OH).

2.29 ISOTHERMAL TITRATION CALORIMETRY (ITC)

Calorimetric measurements were carried out at 10 ºC using a VP-ITC titration calorimeter (MicroCal Inc., Northampton, MA). FPPS protein (40 μM) was dialyzed extensively against 10 mM HEPES pH 7.7, 100 mM NaCl and 0.5 mM TCEP and the identical buffer was used to dissolve the Zol (300 μM). Titration experiment consisted of a 2 μl first injection of Zol followed by 8 μl injections into the 1.5 ml cell containing the protein. The change in heating power was recorded throughout reaction time, until equilibrium was achieved. Data were analyzed by using multiple-binding site model implemented in the ORIGIN software package (OriginLab, Northampton, UK).

2.30 OSTEOCLASTOGENESIS CULTURES

2.30.1 Isolation of Peripheral Blood Mononuclear Cells (PBMCs) from blood

Peripheral blood mononuclear cells (PBMC) were isolated from blood (NHS Blood and Transplant, Bristol, UK) obtained from

healthy donors. Blood was diluted 1:1 (v/v) in alpha-minimum essential medium (α-MEM) (Lonza, Cheltenham, UK), layered over filtered Histopaque-1077 solution and centrifuged for 25 min at 2300 rpm, 4 ºC. The PBMC layer was collected, diluted 1:10 (v/v) in α-MEM and centrifuged for 15 minutes at 1500 rpm, 4 ºC. The cells were resuspended in α-MEM 1:20 (w/v) and centrifuged at 1400 rpm for 15 min, 4 ºC. Cells were carefully dispersed in α-MEM supplemented with 10% Fetal bovine serum (FBS) (Gibco), L-glutamine (2 mM), penicillin (50 µg/ml) and streptomycin (50 µg/ml) (Invitrogen, Paisley, UK), counted with haemocytometer and approximately 2 x 10^6 cells were dispersed in each well of 24 well plate.

2.30.2 Isolation of Osteoclasts from PBMCs

All cultures were maintained for up to 16 days in α-MEM supplemented with 10% FBS, L-glutamine (2 mM), penicillin (50 IU/ml) and streptomycin (50 µg/ml) under normoxic conditions (37 ˚C, 5% CO_2 in air) in a humidified atmosphere. PBMCs were cultured in presence of 25ng/ml huM-CSF (R&D Systems Europe, UK) and 100 ng/mL soluble huRANKL (PeproTech, London, UK) and the relevant concentrations of BPs (Ris, Zol, Iba, Ale). Culture medium, BPs and growth factors were replenished every 3–4 days.

Negative control cultures were maintained in MEM/FBS with M-CSF alone in presence or absence of RANKL.

2.30.3 Tartrate-resistant acid phosphatase (TRAcP) and DAPI staining

The extent of osteoclast formation was assessed by counting the number of multinucleated tartrate-resistant acid phosphatase (TRAcP) positive cells (Minkin, 1982). At the end of culture, cells were washed twice with PBS, fixed with 3.7% p-formaldehyde in PBS for 10 min, and washed three times with PBS. TRAcP was visualized using naphthol AS-BI phosphate as a substrate, with reaction of the product with Fast Violet B salt (Burstone, 1958, Tsuchiya *et al.*, 1995). This was achieved by addition of 1 ml of mixed staining solution A: solution B in 1:1 ratio per well and incubation at 37 °C in the dark for 2.5- 3 hr or until a blue colour was developed (Table 2.15). Cells were washed three times with PBS and covered with 100 M NaF for 30 min to inhibit the reversibility of TRAcP reaction. Wells were washed twice with PBS and once with MilliQ water. Cells were incubated with 4'-6'-diamidine-2-phenylindole dihydrochloride (DAPI, Roche, Mannheim, Germany) (1 µg/ml in PBS), for 30 min in the dark. Cells were washed twice with PBS and once with MilliQ water and plates were kept in the dark before imaging with Olympus

fluorescent microscope. TRAcP-positive multi-nucleated cells (>3 nuclei) were counted and assigned as osteoclasts whereas DAPI staining was used to quantify the osteoclast nuclei.

Table 2.15: Solutions used for TRAcP staining

Acetate-tartrate buffer	29.6 mM CH_3COOH, 70.4 mM CH_3COONa, 10 mM sodium tartrate pH 5 was adjusted to 5 with 1 M NaOH
Solution A	10 mg of Naphthol AS-BI Phosphate, 0.5 ml of DMSO, 15 ml of acetate-tartrate buffer pH 5
Solution B	20 mg of Fast Violet B, 0.5 ml of DMSO, 15 ml of acetate-tartrate buffer pH 5

2.30.4 Cell viability test using Trypan blue

Increased plasma membrane permeability as a result of apoptosis was visualised by addition of trypan blue (0.05%), a dye that is impermeable to living cells with intact cell membranes but is incorporated into dead/apoptotic cells. To determine the number of viable cells, single cell suspensions were diluted in trypan blue and counted using a haemocytometer.

2.30.5 Cell viability testing in PBMC cell cultures

After 48 hr of PBMC culture, the cell suspension medium containing floating cells was collected in Eppendorf tubes and

centrifuged at 3000 rpm for 10 min. The supernatant was decanted and each plate well containing the adherent cells was washed with 1 ml cold PBS and then incubated with 250 µl of pre-warmed trypsin (37 ˚C) for 10 min at R.T. to detach adherent cells. The mixture containing the detached adherent cells was collected and pooled in the Eppendorf tubes containing the floating cells. Cells were spun at 3000 rpm for 10 min, the supernatant was carefully removed and cells were resuspended in 25 µl trypan blue 0.04%. An aliquot (10 µl) was transferred to a haemocytometer and the percentage viability of cells was determined by counting the cells under a light microscope.

2.31 BACULOVIRAL PROTEIN EXPRESSION

Insertion of the gene of interest into the baculovirus genome is based on site-specific transposition of an expression cassette into a baculovirus shuttle vector (bacmid) propagated in *E. coli*. Recombinant bacmids are constructed by transposing a mini-Tn7 element from the donor plasmid pFastBac which contains the gene of interest, to the mini-*att*Tn7 attachment site on the bacmid. Transposition is facilitated by a helper plasmid that confers resistance to tetracycline and encodes the transposase gene.

2.31.1 Preparation of bacmid constructs

Cloning of all genes of interest in the selected pFB-CTHF vector (Appendix B) was carried out as previously described (Section 2.3). The recombinant plasmid DNA was transformed into DH10Bac competent cells (Invitrogen) as described in Section 2.7 except that incubation time at 37 °C was prolonged to 4 hr. Cells were serially diluted to 1:10, 1:100 and 1:1000 using fresh S.O.C. medium and grown at 37 °C for 48 hr on agar plates containing tetracycline (10 µg/ml), kanamycin (50 µg/ml), gentamycin (7 µg/ml), IPTG (40 µg/ml) and X-gal (100 µg/ml). Presence of the recombinant bacmid results in disruption of the lacZ peptide due to the insertion of the mini-Tn7 into the mini*att*Tn7attachment site which gives white bacterial colonies, whereas blue colonies harbour the unaltered bacmid. To exclude the possibility of incorrect selection of a white colony, four white colonies per construct were selected and re-streaked on fresh LB agar plates containing 50 µg/ml kanamycin, 7 µg/ml gentamycin, 10 µg/ml tetracycline, 100 µg/ml Bluo-gal, and 40 µg/ml IPTG. Plates were incubated o/n at 37°C.

A single colony confirmed to have a white phenotype on re-streaked plates containing Bluo-gal and IPTG was selected with a sterile toothpick and inoculated into 2 ml LB medium supplemented with 50 µg/ml kanamycin, 7 µg/ml gentamycin and

10 μg/ml tetracycline. The o/n culture was collected and centrifuged at 4000 rpm for 15 min. The supernatant was carefully decanted and the pellet was resuspended in buffer P1 (0.3 ml) by gentle pipetting. Buffer P2 (0.3 ml) was added and sample was incubated at R.T. for 5 min to allow lysis. Addition of neutralization buffer P3 (0.6 ml) occurred dropwise, gently mixing throughout the procedure. A thick white precipitate was formed. The sample was placed on ice for 10 min and was subsequently centrifuged for 10 min at 14,000 x g. The supernatant was transferred to a new tube containing 0.8 ml absolute isopropanol, mixed gently and incubated on ice for 10 min. The sample was centrifuged for 15 min at 14,000 rpm at R.T. The formed supernatant was removed and addition of 0.5 ml of 70% ethanol was added. The pellet was washed by gently inverting the tube a few times and centrifuged for 5 min at 14,000 g. An extra wash with isopropanol was performed and supernatant was carefully aspirated. The pellet was air dried briefly and the DNA was dissolved in 40 μl of TE buffer and stored at 4 ºC until required.

2.31.2 Transfection in Sf9 cell lines

1 ml of *Spodoptera frugiperda* 9 (Sf9) cells (density 7 x 10^5 cells/ml) were dispersed into each well of 6-well plate in insect

express medium (with penicillin/streptomycin). The plate was incubated o/n at 27 ºC to allow the cells to settle to a monolayer. For each well to be transfected, 5 µl of DNA was used (at least 2 µg of DNA was required per transfection). DNA was mixed with 100 µl of Grace's medium (Gibco) (serum free) without antibiotics. 10 µl of insect GeneJuice transfection reagent (Novagen) was mixed with 100 µl of Grace's medium (pre-warmed). The diluted DNA was added dropwise to the diluted GeneJuice reagent. The mixture was incubated at R.T. for 15 min. After the 15 min incubation, 0.8 ml of Grace's medium was added to each vial. The medium from the cells was aspirated carefully and the transfection mixture was added to each well. The cover was carefully placed on the plate which was sealed with parafilm and incubated at 28 ºC. After 5 hr, Grace's medium was replaced with insect expression medium (with antibiotics) and incubated at 28 ºC for 48 hr. Cells were then examined under the microscope, where successful infection of all samples was observed. Control wells had confluent cells whereas areas of clearing were visible in all infected wells.

2.31.3 Generation of baculoviral stocks

Supernatant of all infected wells was harvested and kept at 4 ºC as P0 viral stock.

2.31.3.1 Generation of P1 viral stock

3ml of Sf9 cells (2 x 10^6 cells/ml) were dispersed into each well of a sterile 24-deep-well block and were infected with 120 µl of P0 viral stocks. The block was covered with porous seal and incubated at 28 ºC at 450 rpm for 72 hr in a Glas-Col incubator. The remaining P0 stock was centrifuged at 1,500 g (2,500rpm) for 20 min at R.T. The supernatant was collected in a falcon tube. The P0 viral stock was stored at 4 ºC, protected from light.

2.31.3.2 Generation of P2 viral stock

The supernatant of Sf9 P1 culture was collected via centrifugation (2500rpm, 20 min). Cells were examined under microscope for signs of infection and 3 ml of Sf9 cells (2 x 10^6 cells/ml) were dispersed into each well of a sterile 24-deep-well block. Cells were infected with 120 µl of P1 virus stocks. The block was covered with porous seal and incubated at 29 ºC at 450 rpm for 72 hr in a Glas-Col incubator. The remaining P1 stock was centrifuged at 1,500g (2,500rpm) for 20 min at R.T. and stored at 4 ºC.

2.31.3.3. Generation of P3 viral stock

The supernatant of Sf9 culture (P2) was collected via centrifugation (2500rpm, 20 min) and examined under microscope for signs of infection. 100 ml of Sf9 cells (2 x 10^6 cells/ml) were dispersed into each well of a sterile 24-deep-well block. Cells were infected with all the P2 viral stock. The block was covered with porous seal and incubated at 29 ºC at 450 rpm for 72 hr in a Glas-Col incubator.

3. INVESTIGATION OF THE INTERACTION OF FPPS & N-BPs

3.1 INHIBITION OF FPPS BY N-BPs IS A MULTI-STEP PROCESS

Previous experimental work has characterized the mechanism of FPPS inhibition by BPs as a slow- tight binding, taking place in at least three individual steps (Kavanagh *et al.*, 2006b, Rondeau *et al.*, 2006). The initial, rapid stage is a classical 'competitive inhibition' where GPP/DMAPP and BP compete for the allylic binding site on the FPPS that leads to a formation of an enzyme-inhibitor complex. With the WT enzyme, full inhibition is only obtained after 10 min when, upon BP-induced enzyme isomerization the volume of the active site is reduced, resulting in a tight complex formation that significantly increases inhibition. Finally the second substrate, IPP, binds to the complex and a second isomerization event induces further structural rearrangements of the amino acids forming the C-terminal tail of FPPS that prompt closure of the IPP binding pocket, shielding the active site (Kavanagh *et al.*, 2006b, Laskovics and Poulter, 1981, Rondeau *et al.*, 2006, Song and Poulter, 1994).

Despite the recent advances in the interpretation of the FPPS inhibition mechanism, many details regards the structural

rearrangement of FPPS upon substrate and inhibitor binding, as well as the mode of interaction between BP and FPPS leading to formation of the FPPS:BP complex and stronger inhibition, are still unknown. In order to further investigate these phenomena, we designed point mutations in individual amino acids that were thought to either: i) play a pivotal role in the catalytic mechanism ii) are positioned in the GPP and IPP binding site or in the C-terminal lid or iii) interact or form contacts with N-BPs and thus are involved in inhibition or iv) are involved in the mechanism that drives the isomerization of the enzyme: inhibitor complex (Table 3.1). The kinetic parameters of the expressed protein mutants and crystallographic studies with clinically important BPs were investigated with the aim of assessing the putative roles of specific amino acid residues in catalysis, enzyme inhibition and mode of drug binding.

Table 3.1: Designed FPPS amino-acid mutations and their proposed roles in FPPS catalysis and inhibition by N-BPs

Original amino-acid	Mutation	Proposed role of the residue	Possible mutation effects
Thr201	Ala	Stabilisation of carbocation intermediate	Disruption of H-Bond network with side-chain nitrogen of the N-BP
Tyr204	Phe	Interaction with N-BP side-chain and/or hydrophobic interactions with substrate	Disruption of H-Bond network with side-chain nitrogen of the N-BP
Tyr204	Ala	Interaction with N-BP side-chain and/or hydrophobic interactions with substrate	Disruption of H-Bond network with side-chain nitrogen of the N-BP
Phe 239	Ala	Involvement in catalysis & allylic substrate binding	Reduced k_{cat} & K_m^{GPP}
Lys200	Glv	Phosphonate-enzyme interaction	Disruption of phosphonate-enzyme interaction
Lys200	Leu	Phosphonate-enzyme interaction	Disruption of phosphonate-enzyme interaction while preserving hydrophobic interactions
Lys200	Glu	Phosphonate-enzyme interaction	Disruption of N-BP inhibition & catalysis
Arg112	Leu	Phosphonate-enzyme interaction	Disruption of phosphonate-enzyme interaction
Asp103	Ala	Phosphonate-enzyme interaction involved in catalysis	Disruption of catalysis
Asp103/Asp 107	Ala	Phosphonate-enzyme interaction involved in catalysis	Disruption of catalysis

3.2 VERIFICATION OF POINT MUTATIONS OF FPPS

3.2.1 Cloning and mutagenesis of FPPS

Human FPPS (residues 1–353 (P14324)) was cloned into the p11 vector (Appendix B) as an N-terminally 6His-tagged fusion protein with a TEV protease cleavage site. Insertion of point mutations in the FPPS plasmid was achieved by site-directed mutagenesis. The result of a typical cloning procedure of FPPS mutants are shown below (Figure 3.1). Initially the double stranded DNA of p11_FPPS construct is replicated by *PfuTurbo* DNA polymerase in a PCR reaction (Section 2.2.3) which extends the pair of synthetic oligonucleotide primers containing the desired mutation and anneals them to the denatured plasmid. Elimination of the parental, non-mutated template is achieved by treatment with DpnI endonuclease, which selectively digests methylated DNA, only present in the original plasmid propagated in the *E. coli* host strain (Section 2.3.2). Transformation of the double-stranded DNA plasmid with XL-10 Ultracompetent cells (Section 2.14) and plating onto agar-LB plates (Section 2.7) followed. Selection of colonies positive for the insert was achieved by colony PCR (Section 2.2.2), and the expected 1140 bp product band was visualized by agarose gel electrophoresis (Section 2.9), (Figure 3.1.A). An aliquot of the DNA produced from mini-prep by overnight cultures of the

positive colonies (Section 2.10) was sequenced (Section 2.12), to confirm the desired point mutations (Figure 3.1.B).

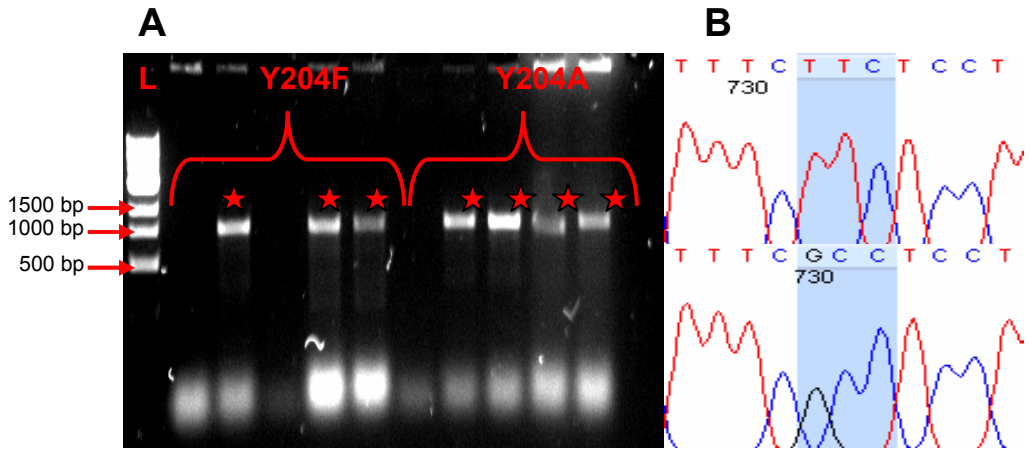


Figure 3.1: Verification of successful FPPS cloning and mutagenesis A) An aliquot (5 µl) of colony PCR product was run on 1% agarose gel to confirm integrity of FPPS DNA samples isolated from individual colonies (Section 2.2.2). Only samples demonstrating a band around 1140 bp (denoted by asterisk) were selected for sequencing. L: Invitrogen 1kbp ladder B) Verification of mutated codon in Y204F and Y204A FPPS construct by sequencing. The corresponding electropherogram (visualized by Finch TV software) indicates the position of mutated amino-acid TTC or GCC (highlighted in blue) encoding either Phe or Ala in position 204, respectively.

3.2.2 Expression and purification of FPPS constructs

Protein expression from FPPS constructs was performed as described in Section 2.15. All FPPS mutants showed a high level of expression and solubility, producing a clear extract after the final high speed centrifugation (Section 2.15.5). The first step of the purification was Ni-NTA IMAC (Section 2.17.3), (Figure 3.2 A,C).

After IMAC, Ni-NTA elution buffer was exchanged with GF (2.17.7). When the purified protein was destined to be used for crystallization trials, the 6His-tag was removed by incubation with TEV protease (Section 2.17.5) and complete digestion was confirmed by electrospray ionization mass spectrometry (Section 2.19.3). The cleaved 6His-tag was successfully separated from the protein by passing the digest through Ni-NTA resin and collecting the unbound fraction (Section 2.17.4). The TEV-cleaved protein was further purified by gel filtration chromatography using a Superdex 200 column on AKTA purifier system (Section 2.17.4). Typical column elution profiles and SDS-PAGE electrophoretograms are shown in Figure 3.2 B,D and illustrate the successful expression and purification of the desired protein. Similar data were obtained for all of FPPS mutants studied. The yield of FPPS mutants averaged approximately 14 mg/L of culture, but varied between different mutants and was generally lower than WT (Table 3.2). The mutant proteins were stable during the purification procedure with little apparent degradation. Protein mass was confirmed by LS-MSD TOF (Figure 3.3), where all protein constructs showed the predicted mass +/- 2 Daltons error, in agreement with the instrument specification.

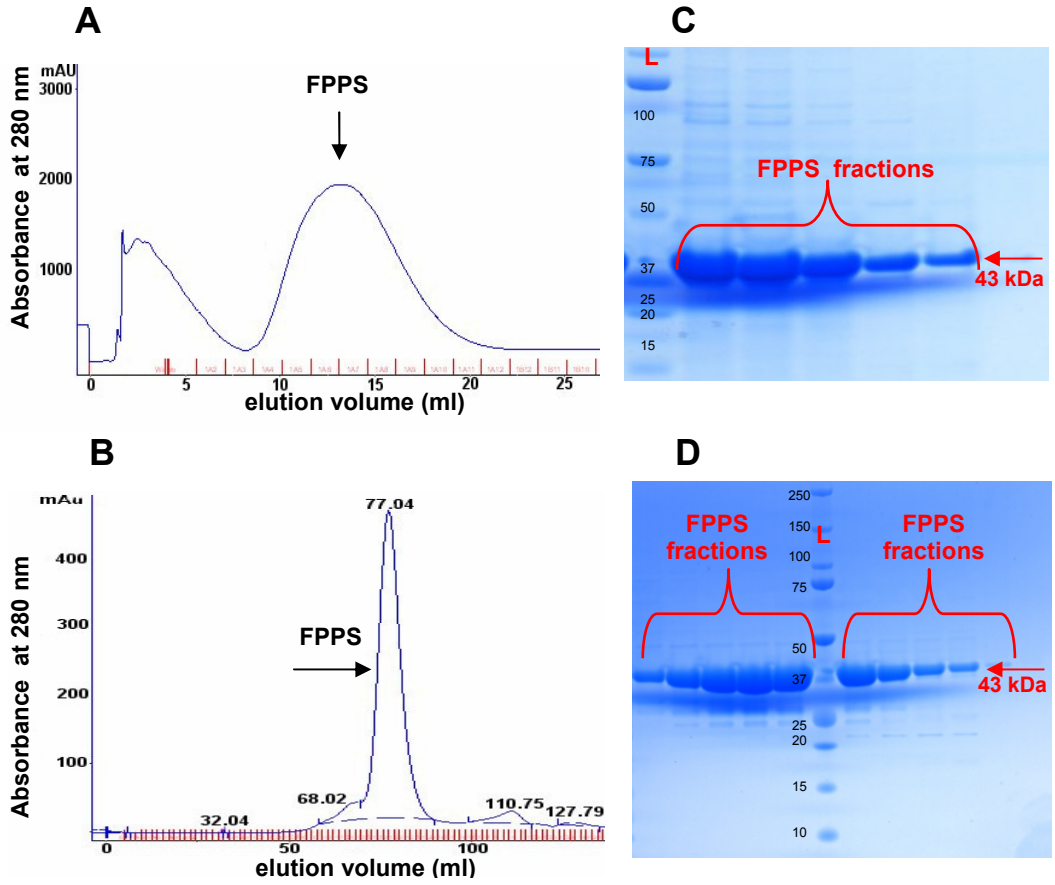


Figure 3.2: Successful purification of Y204A FPPS from p11 vector. Elution profiles of Y204A FPPS obtained from A) IMAC and B) GF stages performed on Akta Express system and the corresponding SDS-PAGE analysis of representative purified fractions peaks (C & D). Successfully eluted protein (tagged) was approximately 43 kDa. L: Precision Plus Protein Standard all blue ladder (Biorad).

Table 3.2 Expected protein mass of FPPS constructs and protein yield

FPPS Construct	Estimated Mass (tagged)	Estimated Mass (cleaved)	Yield (mg/L)
WT	43094.2	40726.7	45
T201A	43064.2	40696.7	25
Y204F	43078.9	40710.7	11.3
Y204A	43002.1	40634.6	10.4
R112L	43051.2	40683.7	17
F239A	43018.2	40650.6	34.2
K200G	43023.1	40655.6	21.5
K200L	43079.2	40711.5	12.4
K200E	43095.1	40727.7	30
D103A	43050.2	40682.5	13
D103D107A	43006.2	40638.5	12

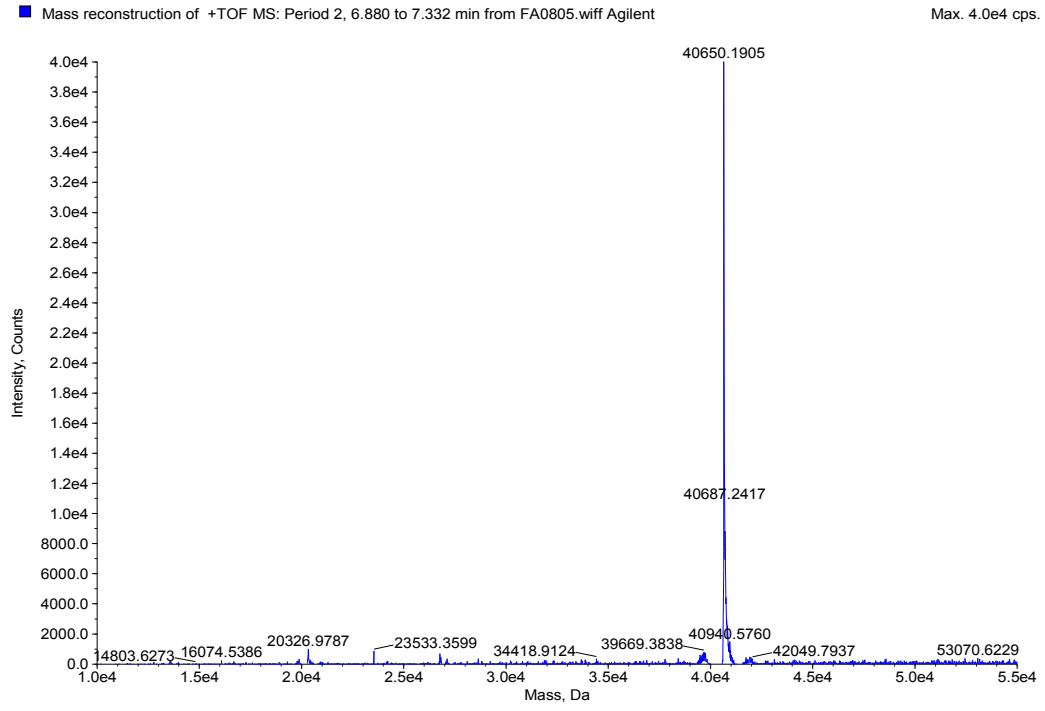


Figure 3.3: LS-MSD TOF data obtained from purified F239A FPPS construct. Purification of Y204A FPPS construct resulted to a 40650 kDa protein, in perfect agreement with the theoretical predicted mass for the particular mutation.

3.3 TIME DEPENDENT INHIBITION CURVES AS A RESULT OF N-BPs TIGHT BINDING

Characterization of the kinetic properties of each individual mutant was achieved by estimating K_m^{IPP} and K_m^{GPP} as described in Section 2.24.1. The assay time and the enzyme concentration were carefully selected after performing time-course assays for individual mutants to avoid a significant change in substrate concentration during the course of the reaction and thus eliminate the possibility of underestimation of enzyme activity at low substrate concentrations. Once the affinities of the mutant enzyme for individual substrates were determined, inhibition studies with BPs were performed.

The mechanism of inhibition of BPs has been characterized as tight slow binding (Dunford *et al.*, 2008, Kavanagh *et al.*, 2006b) and can be described using the following model (Morrison and Walsh, 1988):

$$E + I \underset{K_4}{\overset{K_3}{\rightleftharpoons}} EI \underset{K_6}{\overset{K_5}{\rightleftharpoons}} EI^*$$

where:

Ki = K_3/K_4 is the initial dissociation constant for E·I and thus an estimate of the competitive inhibition of GPP by N-BPs

Ki* = (Ki x K_6)/ (K_5+K_6) is the final dissociation constant resulting upon enzyme isomerization and

K_{isom} = K_5/ K_6 is the rate constant for conversion of isomerized FPPS: BP complex back to FPPS: BP.

Consistently, all N-BPs studied produced a time-dependent increased inhibition of WT and mutant FPPS, as demonstrated by the Ki, Ki* and K_{isom} values, calculated as described in Section 2.25. The overall inhibition constant (Ki*) values were calculated from the initial inhibited rate data, where the experiment was initiated by the addition of enzyme, and the pre-incubated rate data, where the enzyme was pre-incubated with BP and the reaction started by the addition of substrate. The constants were then corrected for the allylic (GPP) and IPP substrate affinity of the enzyme (K_m^{GPP} and K_m^{IPP}) and also GPP and IPP concentration. All data were fitted to Morrison's model of tight binding inhibition that predicts an inhibitor: enzyme binding ratio equal to 1 (Morrison and Walsh, 1988). An alternative estimate of the extent of BP inhibition was the IC_{50} values defined as the BP concentration that gives 50% inhibition for the tested compounds, both in initial rate and pre-incubation rate experiments. The IC_{50} values determined were in strict agreement with the inhibition pattern described from Morrison and Walsh. However, the IC_{50} value is not a good indicator of BP binding as it is strongly dependent on the relevant

enzyme concentration and cannot be correctly used to study differences between FPPS constructs, because the enzyme concentration in the assay varies. But the IC_{50} values were used to assess significance of inhibition data and compare differences in BP potencies across mutants in cases where the experimental data would not fit to the Morrison's tight site titration model due to a shifting from the permissible enzyme: inhibitor 1:1 binding ratio. Increased inhibition was consistently observed after a pre-incubation time period of 10 min, and indeed maximal inhibition for WT and FPPS mutants was attained after 8 min and not significantly increased when tested after prolonged pre-incubation time periods (12, 15 or 20 min). In most of the cases the potency of BP increased upon pre-incubation compared to initial rates, producing typical inhibition curves as shown in Figure 3.4. However a shift in drug potency from initial competitive to final mixed inhibition was not observed with all mutants tested and in these cases the reduced K_{isom} indicated reversibility of the inhibition.

K_i, K_{isom} and IC_{50s} were analyzed for significance using one way ANOVAs with a Tukey's *post hoc* test and also with unpaired *t*-test. As a general rule, the standard error for the determination of these kinetic parameters was less than 10 % and the R^2 value above 0.9. However in cases of slow-rate mutants the existing

model could not satisfy the experimental data but the resulting low root square values or higher standard errors did not arise from inconsistence in repetition of experiments. Figure 3.4 shows typical inhibition curves obtained from pre-incubation and initial rate assays. Calculated data for WT enzyme were used as control point in all assays performed and were in perfect agreement with Dunford *et al.* (2008).

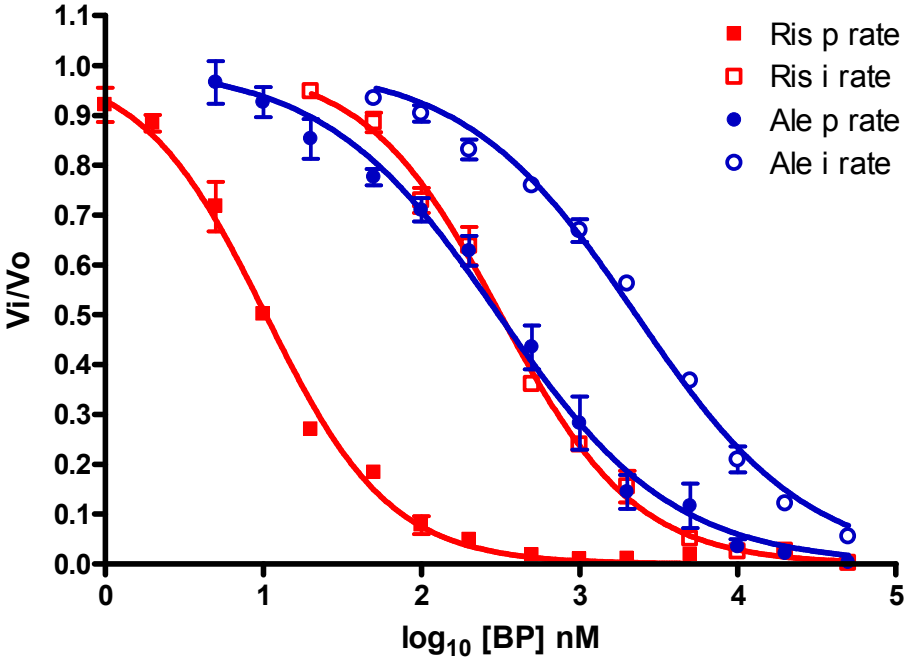


Figure 3.4: Typical inhibition curves obtained from 10 min pre-incubation (p rate) assays and competitive initial rate (i rate) assays of WT with Ris (red) and Ale (blue). Data are average of five independent experiments, $R^2 > 0.98$, error bars represent SEM.

There are certain limitations to the Morrison's and Walsh kinetic model used here to interpret the experimental data

resulting from FPPS inhibition assays with the clinical N-BPs, as the [IPP] and [GPP] used were always kept at 10 μM. This concentration is adequate for the WT FPPS, as saturation of both substrates is achieved at 10 μM of either substrate; however the calculated K_m^{IPP} was significantly raised in all mutant constructs examined, which would require higher [IPP] in the assay in order to saturate the enzyme. In an ideal situation, [IPP] should be raised to correspond to four times the K_m^{IPP} value, as most kinetic models are based on the fact that saturation of the substrate should be attained to obtain valid kinetic data. However the reasons why [IPP] was kept constant at 10 μM were the following: i) if [IPP] was altered according to the mutation there would be no valid point of comparison between WT and mutants, as they would be assayed differently, ii) a raised [IPP] does not correspond to the physiological levels of substrate available in the natural environment and would therefore produce artifactual results, iii) preliminary experiments using a high [IPP] indicated competition with the GPP for occupation of the allylic binding pocket (data not shown) and iv) the [IPP] and [GPP] are taken into account and subtracted when calculating the K_{app} and finally the Ki values (Section 2.25).

Similarly all experiments were performed at pH 7.7 to allow direct comparison between WT and mutant inhibition rate, despite

of the fact that this was not the optimal pH condition for all mutants.

3.4 FPPS CRYSTALS SHOW TETRAGONAL SYMMETRY AND HELP TO CHARACTERIZE SUBSTRATE-INHIBITOR BINDING

Initial crystallization trials of FPPS mutants were set using the known optimal conditions for WT (Kavanagh *et al.*, 2006b). However when crystallization with the standard conditions failed to yield crystals or crystalline precipitates, systematic screening using different salts, precipitants or pH was performed in order to identify new conditions subjected to optimization. The crystals obtained were of different shapes, mostly dependent of the nature on the ligand and the screen used and rather independent of the position of the mutation (Figure 3.5). The most common pattern was cross-shaped crystals, mainly found as aggregates that required splitting prior to mounting (Figure 3.5 F).

Crystals were mounted at 20 °C using 20% glycerol or 100% ethylene glycol as cryoprotectant, depending on the screen content. Crystallization trials at 4 ºC were also attempted, with the aim of slowing down the rate of crystal formation (3-5 days when at 20º C) and to avoid aggregation in blocks however the resulting crystals, although single and well shaped, gave poor diffraction patterns and

were difficult to cryo-protect. It was also observed that addition of cryoprotectant during mounting was necessary even it was when included in precipitant solution and its absence led to uneven freezing and the generation of internal ice rings that disrupted the crystal integrity.

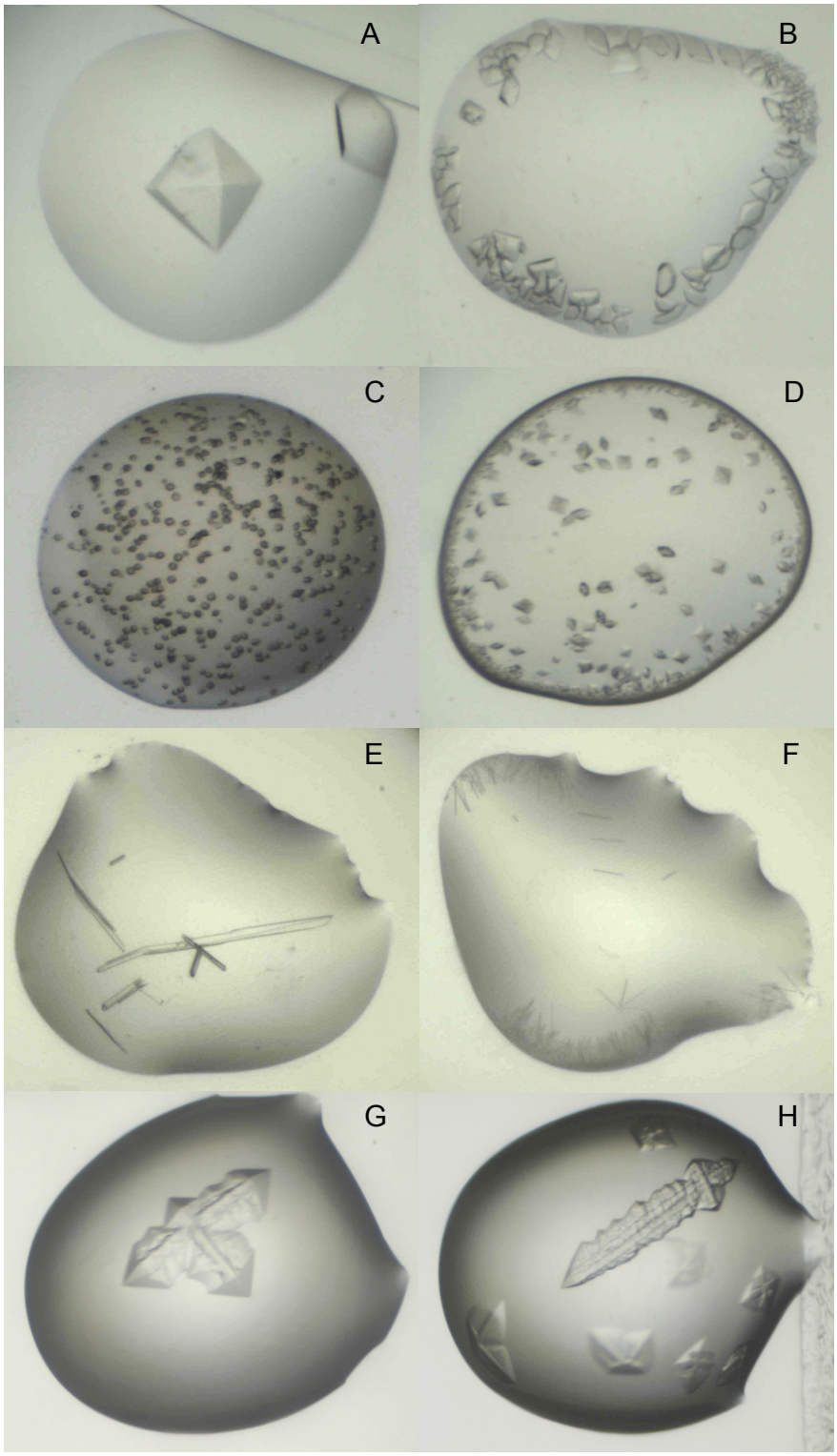


Figure 3.5: Typical crystal patterns observed in Y204A FPPS mutant using LFS4-A8 screen A) large single B) plates C) spherical microcrystals D) small octahedral single crystals D) plates E) rods F) needles G) cross shape and H) pyramids

All the FPPS crystals studied diffracted between 1.6 and 2.3 Å and for those exhibiting poorer resolution optimization trials were set up. The results of a typical diffraction pattern in iMosfilm (Figure 3.6) indicated P4 (tetragonal) as the correct space group however, after determination of Laue group and calculation of Matthew's co-efficient by POINTLESS, the symmetry group was restricted to $P42_12_12$ by running Reindex (in CCP4 package) on all processed symmetry-related reflections by SCALA.

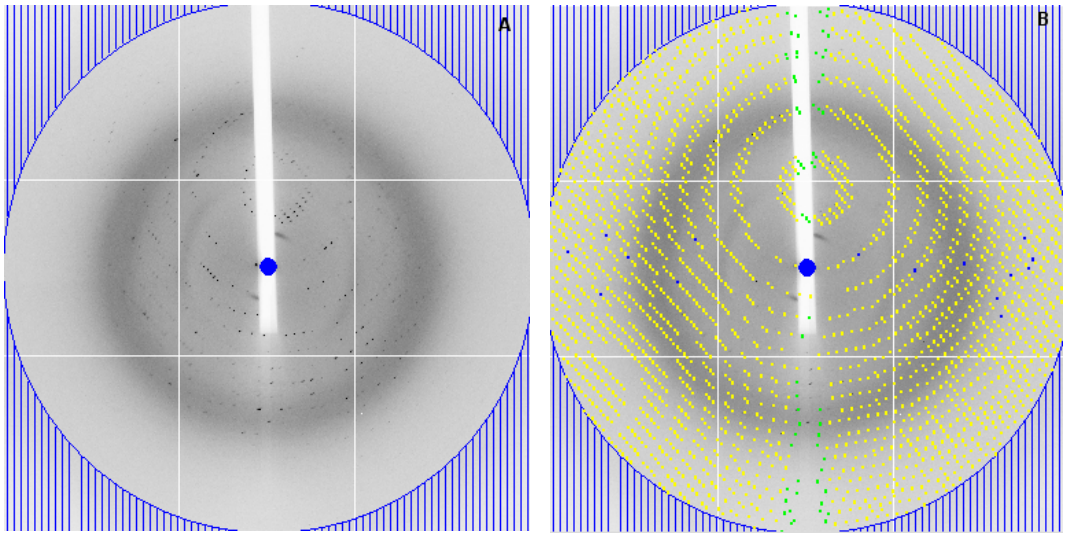


Figure 3.6: A) X-ray diffraction pattern of human Y204A FPPS showing resolution limit at 2.1 Å B) Predicted diffraction spots for the same crystal (in yellow) calculated in iMosflm. Data collected at Diamond Light Source.

Structure building was carried out as described in Section 2.28. Iterative rounds of refinement using COOT allowed

continuous monitoring of R_{free} and R_{factor} values whereas the R_{ms} Bond angles and R_{ms} bond length values were kept as close to 1.5 and 0.015 Å respectively. The stereochemistry for all side-chains was also monitored using a Ramachandran plot. For example, in Y204A FPPS in complex with Ris, 99.1 % of all residues were in preferred regions, 0.9 % in allowed regions and none in outline regions (Figure 3.7).

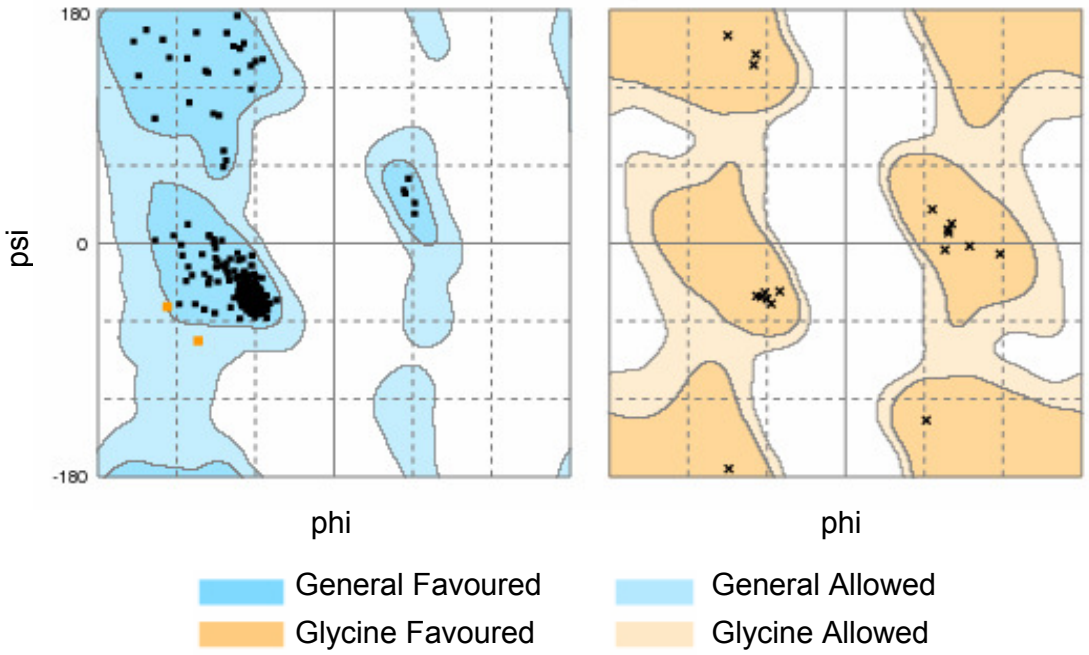


Figure 3.7: Detailed Ramachandran plot of the final crystal model of human Y204A FPPS. The final model was validated through the distribution and combination of dihedric tortion angles (phi and psi). The result indicates that 99.1 % of residues are positioned in favoured regions (dark blue), 0.9 % in allowed regions (light blue) and none in outline regions (white). Diagram generated by Rampage software (Lovell *et al.*, 2003).

The generated Fourrier electrodensity maps ($2F_o$-F_c) contoured at 1 sigma indicated the favourable state of individual amino-acid

conformations (Figure 3.8). A table containing all X-ray data collection and refinement statistics can be found in Appendix D whereas all FPPS solved crystal structure and resolutions are listed in Table 3.3.

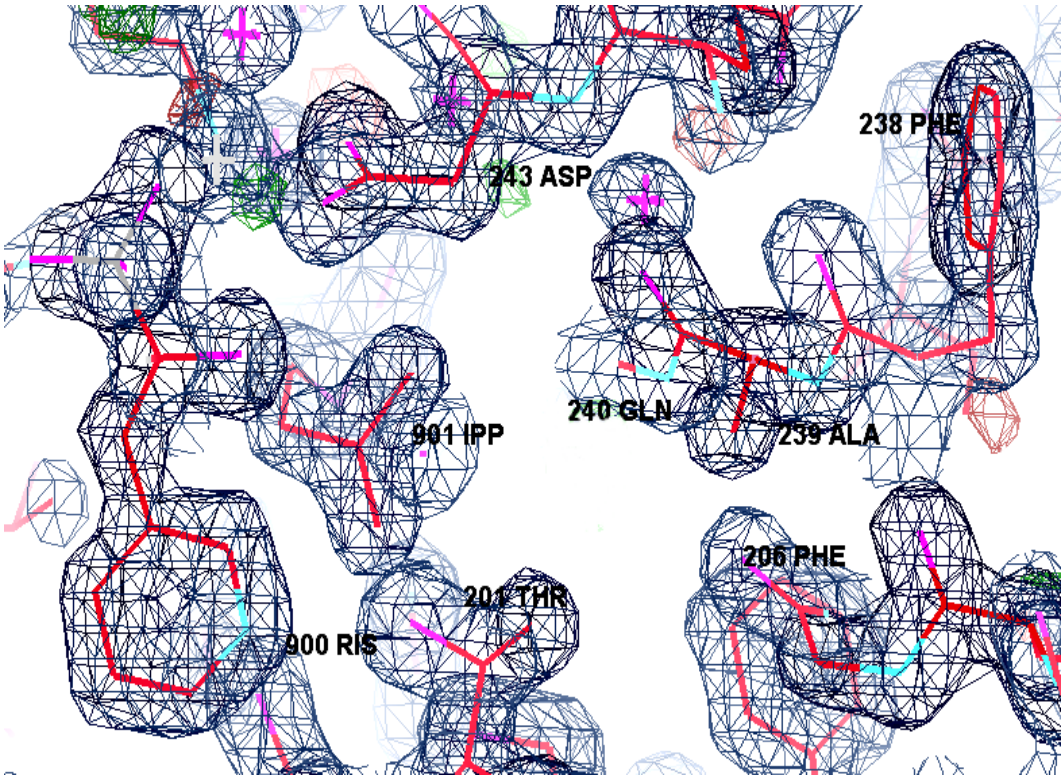


Figure 3.8: 2Fo-Fc electron density maps of F239A FPPS contoured at 1 sigma, showing the position of mutated amino-acid relatively to Ris and IPP.

Table 3.3: Main crystallographic characteristics of solved FPPS structures

FPPS Construct	Comp. 1	Comp. 2	Screen	Res Å
T201A	Zol		LFS4-A8	1.98
Y204F	Ris	IPP	LFS4-A8	1.96
Y204A	Ris		LFS4-A8	2.03
Y204A	Ris	IPP	LFS4-A8	1.92
Y204A	Zol		LFS-4 090109-02-A10	2.4
Y204A	Ale		JCSG-C11	1.8
Y204A	Pam		LFS4-A8	1.95
Y204A	Pam	IPP	LFS4-A8	2.18
Y204A	DMASPP	IPP	JCSG-C11	2.96
K200G	Ris		LFS4-A8	2.11
K200L	Ris	IPP	LFS-4 090109-02-A12	2.35
F239A	Ris		LFS4-A8	1.43
F239A	Ris	IPP	LFS4-A8	1.46
F239A	Pam		LFS4-A8	2
F239A	Pam	IPP	LFS4-A8	2.1
R112L		IPP	LFS4-A8	1.7

4. THE EFFECTS OF TYR204 FPPS MUTATIONS ON CATALYTIC ACTIVITY, CRYSTAL STRUCTURE AND N-BP BINDING

4.1 INTRODUCTION

Previous experimental work in our laboratory indicated that Tyr204 in human FPPS is possibly involved in stabilization of Ris side chain via hydrophobic interactions (Kavanagh *et al.*, 2006b). Formation of a tight enzyme-inhibition complex would further be strengthened due the enthalpy-driven binding mode of Ris that forces water exclusion from the active site (Yin *et al.*, 2006). Furthermore, the position of the hydroxyl of the tyrosine residue at a short distance from the amino-group of Pam (3 Å) as shown by Rondeau et al. (2006), favours formation of a hydrogen bond with the inhibitor and partly accounts for the strong inhibitory effect of the aminoalkyl BPs (Figure 4.1). Although an active role for Tyr204 in the FPPS conformational switch has not previously been proposed, its position in close proximity with IPP does not exclude a possible involvement in the isomerisation of the enzyme, the orientation of the IPP substrate towards the carbocation site or in the stabilization of the carbocation itself during catalysis.

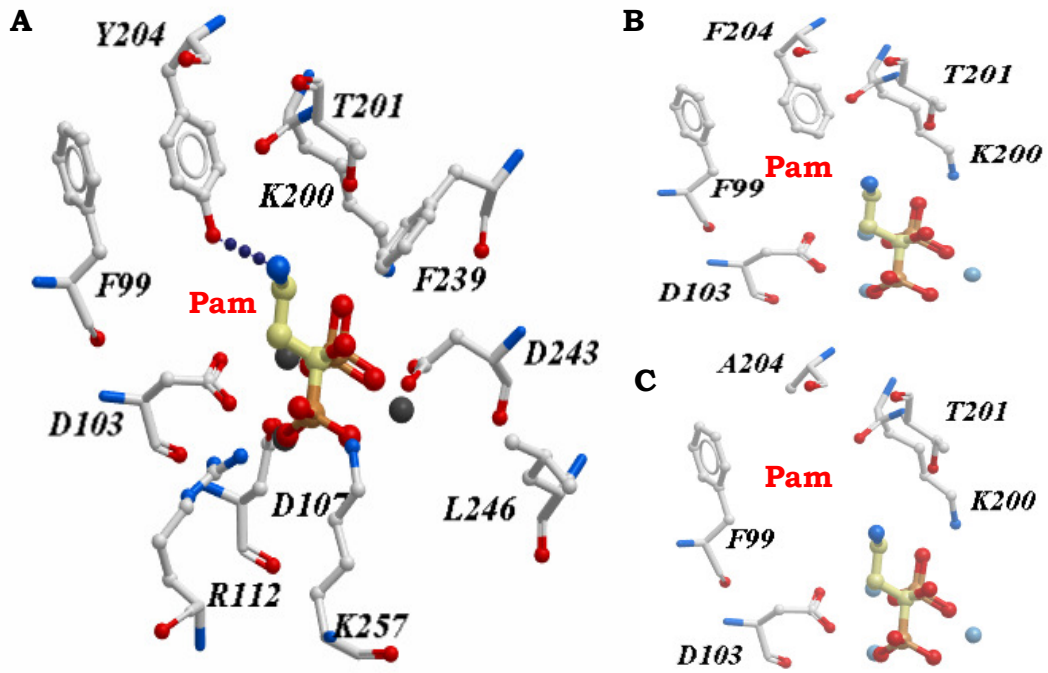


Figure 4.1: The proposed hydrogen bond of Tyr204 with the N atom of Pam is disrupted in Y204F and Y204A FPPS mutants. A) The proximity of OH group in Y204 with the N atom of Pam favours formation of a hydrogen bond, increasing the strength of inhibition. Removal of the OH moiety by replacement of Y204 with F204 (B) or A204 (C) abolishes formation of hydrogen bond and increases the distance between atoms. Figure adapted from pdb 2F89 (Rondeau *et al*. 2006).

Comparison of the amino acid sequences of FPPS revealed that Tyr204 is conserved between species (Figure 4.2). However Tyr204 does not fall in the category of the seven highly conserved residues among prenyltransferases (Koyama *et al.*, 1996) which are pivotal for catalysis and substrate binding.

The role of Tyr204 in FPPS catalytic mechanism and BP inhibition was investigated via generation of i) a tyrosine to

phenylalanine (Y204F) mutant that would allow maintenance of the phenyl ring and thus should not disrupt the proposed hydrophobic interactions and ii) a tyrosine to alanine (Y204A) mutant that would remove the bulk of phenyl ring and thus abolish such interactions.

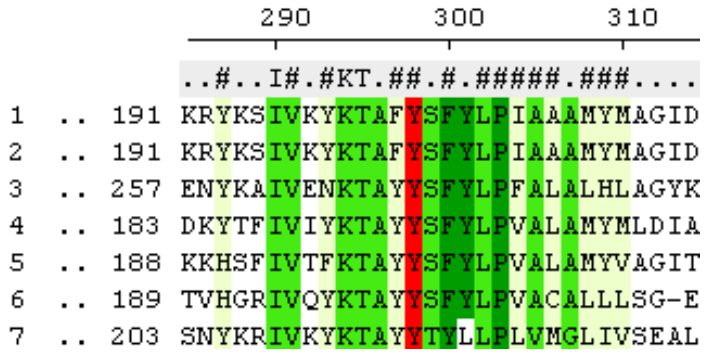


Figure 4.2: Sequence alignment of FPPS orthologs reveals that Tyr204 is conserved among diverse species. Sequences of FPPS from 1: human (*Homo sapiens*) 2: murine (*Mus musculus*), 3: insect (*Drosophila melanogaster*), 4: fungi (*Neurospora crassa*) 5: yeast (*Saccharomyces cerevisiae*), 6: plant (*Zea mays*) and 7: bacteria (*Bacillus Stearophilus*) were aligned with ICM pro, revealing the conserved Tyr204 residue (in red).

4.2 KINETIC CHARACTERIZATION OF TYR204 MUTANTS

Determination of kinetic parameters was carried out for both Y204F and Y204A FPPS mutants (Table 4.1).

Table 4.1: Kinetic parameters for FPPS WT, Y204F and Y204A FPPS. Mutation of Tyr204 residue increases the Km^{IPP} and reduces the catalytic activity of the enzyme for both IPP and GPP substrates whereas Km^{GPP} is almost unaffected. Results for Km and kcat are expressed as means +/- SEM, $n \geq 6$, $R^2 \geq 0.9$

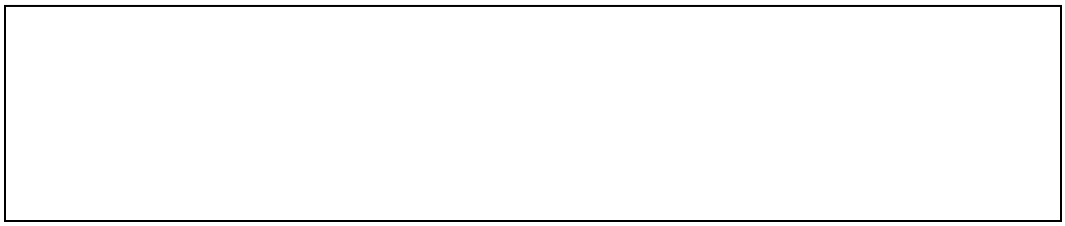
	WT	**Y204F**	**Y204A**
$\mathbf{K_m^{GPP}}$ **(μM^{-1})**	2.07 ± 0.2	1.8 ± 0.65	2.12 ± 0.4
$\mathbf{K_m^{IPP}}$ **(μM^{-1})**	1.8 ± 0.3	33.53 ± 4.9	44.14 ± 5
$\mathbf{k_{cat}}$ **(s^{-1})**	0.385 ± 0.015	0.085 ± 0.006	0.052 ± 0.0027
$\mathbf{k_{cat}/K_m^{IPP}}$ ($\mu M^{-1}/s^{-1}$)	0.6	0.0024	0.0011

If we consider the following scheme:

$$E \underset{K_{-1}}{\overset{K_1[S_1]}{\rightleftharpoons}} E\text{-}S_1 \underset{K_{-2}}{\overset{K_2[S_2]}{\rightleftharpoons}} E\text{-}S \underset{K_{-3}}{\overset{K_3}{\rightleftharpoons}} E\text{-}S^* \underset{K_{-4}}{\overset{K_4}{\rightleftharpoons}} E\text{-}P \underset{K_{-5}}{\overset{K_5}{\rightleftharpoons}} E$$

Scheme 1: Representation of a common enzyme-substrate catalytic reaction, leading to product formation and release of free enzyme for a new round of catalysis. E: FPPS enzyme, S_1: first substrate, S_2: second substrate, ES: Enzyme substrate complex, ES*: transition state of the reaction, E-P: enzyme-product formation and E: enzyme liberation.

In this case, substitution for the two substrates GPP and FPP will result in scheme 2 (omitting the transition state for simplicity):



Scheme 2: Representation of a typical FPPS catalytic reaction, leading to product (FPP) liberation. (Song and Poulter, 1994). **Scheme has been removed due to Copyright restrictions**

The kinetic study of the mutants revealed K_m values for the allylic GPP substrate comparable to that of the WT while the K_m for IPP was significantly increased for both mutants ($p<0.001$ in each case). Taking into account that K_m is an indicator of the strength of dissociation of IPP from the E-GPP-IPP complex, an increased K_m for IPP may be interpreted as a reduction of IPP binding affinity to the complex, resulting in an inability to achieve saturation even at high IPP concentrations (100 μM instead of the standard 10 μM). Consequently, the catalytic activity of the mutants (k_{cat}), in relation to the second substrate IPP, was also decreased to approximately 22 % for Y204F and 13.5 % for Y204A mutant when compared to the WT enzyme. A reduced k_{cat} is an indication of structural modifications occurring after substrate binding. As the K_m^{GPP} is unaffected, it is most likely that perturbations in the catalytic mechanism occur following IPP binding. The most logical side-effect of the mutations would be the slower utilization of IPP due to

slower catalytic turnover, which would also influence the FPP formation rate. Such a product accumulation is not detectable in the catalytic reaction, since IPP and GPP values still fit to a proper saturation curve, albeit with a steeper slope. The situation might be different if DMAPP is used as substrate, as the reduced K_{cat} might then possibly reflect in accumulation of GPP rather than FPP, as equilibrium favours the left hand-side of K_2[IPP]. Furthermore the reduced k_{cat} indicates an increased probability of reversibility of the reaction and thus dissociation of enzyme-product complex and higher probability of the enzyme to return to the transition state.

Such an alteration for the homoallylic substrate affinity was not expected, as there was no evidence of involvement of this residue in substrate binding or catalysis so far. Tyrosine is replaced by leucine in most of the GGPP synthases which remain biologically active, possibly due to maintenance of a similar pK_a (Figure 4.3). The presence of tyrosine in FPPS might therefore be a result of protein evolution in mevalonate pathway that would enable FPPS to carry out its function as a high throughput enzyme, in agreement with its pivotal role and place at a major branch of mevalonate pathway.

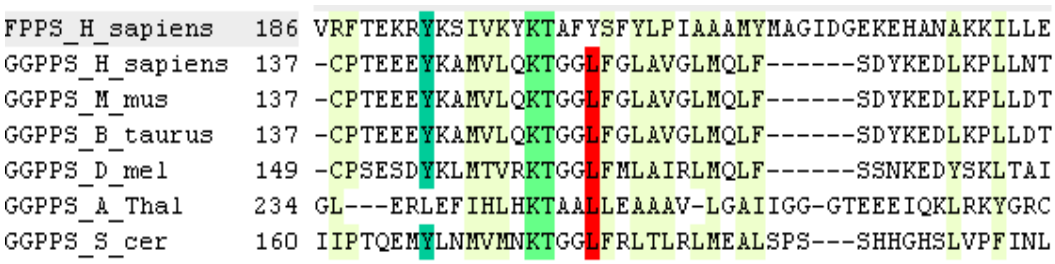


Figure 4.3: Sequence alignment of human FPPS with GGPPS reveals substitution of Tyr in position 204 with Leu (in red). Sequences of GGPPS from human (*Homo sapiens*), murine (*Mus musculus*), bovine (*Bos taurus*), insect (*Drosophila melanogaster*), plant (*Arabidopsis thaliana*), and yeast (*Saccharomyces cerevisiae*) were aligned with *Homo sapiens* FPPS (highlighted) using Molsoft ICM pro.

Such consistent behaviour of both tyrosine mutants demonstrates that the lack of catalytic activity cannot be attributed to the absence of the bulky aromatic ring, still preserved in Y204F FPPS. Therefore the initial hypothesis that catalysis and proper IPP substrate positioning is mainly facilitated by tyrosine ring interactions with the carbocation intermediate is not supported by the present data. At this stage it can be hypothesized that the presence of the hydroxyl moiety is far more important for enzyme activity than the presence of the phenyl ring. Also, catalytic rate is significantly decreased but not completely abolished and therefore the current studies suggest the possible involvement of Tyr204 in catalysis but exclude a key role of this residue in FPPS function.

An alternative hypothesis might be a disrupted interaction of the pi electrons located on the aromatic ring which would account for the loss of stabilization of the carbocation intermediate. However in both cases substitution of Tyr cannot explain the similar reduction in catalytic efficiency observed in either mutant, as maintenance of the bulky tyrosine residue in Y204F should preserve the catalytic activity of the enzyme, rather than resulting in a K_{cat} comparable to that obtained upon removal of the phenyl ring in Y204A mutant.

The position of Tyr204 favours van der Waals interactions with the terminal carbon of FPPS substrate which could account for disruption of the IPP binding site and thus increased K_m in both mutants. This is despite of the fact that direct interaction with the pyrophosphate groups of IPP is observed with residues located on the active site of enzyme (Lys57, Arg60, Arg113) and not with the KRRK C-terminal tail of FPPS (Kavanagh *et al.*, 2006b).

To further investigate the importance of the hydroxyl moiety in the mutated tyrosine, the k_{cat}/K_m^{IPP} ratio for all constructs was determined (Table 4.1). k_{cat}/K_m is generally a better indicator of the catalytic efficiency of a particular enzyme and preferred to k_{cat} when dealing with comparative enzymatic strength as it takes into account the substrate specificity and does not solely depend on ground state binding interactions (Fersht, 1998). The k_{cat}/K_m^{IPP}

was proved to be decreased in Y204F and Y204A compared to WT as a result of both a decreased k_{cat} and increased K_m^{IPP}. Therefore the thermodynamic parameters governing the transition state of each mutant are worthy of further examination. Because WT and mutants use the same IPP substrate and were assayed under the same enzymatic conditions, the transition state energies at constant temperature can be determined using the following equation (Copeland, 1996).

$$\Delta\Delta G_{ES}* = -RT \ln \frac{(k_{cat} / K_m)_{WT}}{(k_{cat} / K_m)_{MUTANT}}$$

Scheme 3: The difference in Gibbs energy between WT and Tyr204 mutants can be estimated from the k_{cat}/Km^{IPP} ratio : $\Delta\Delta G_{ES}$: the difference in the free energy of activation (Gibbs energy) of the transition state complex enzyme substrate (ES), R= gas constant 8.312 J (mol K)$^{-1}$ and T: temperature in Kelvin.

Determination of the $\Delta\Delta G_{ES}$ value for WT/Y204F reveals difference in transition state of approximately 14 kcal/mol and for WT/Y204A of 16.2 kcal/mol. The initial hypothesis, that the tyrosine residue plays a significant role in catalysis, probably during the transition state, is therefore sustainable. This role could be formation of a tyrosinate anion during catalysis or the formation

of hydrogen bond with the substrate and these possibilities are examined below.

4.3 CRYSTAL STRUCTURES OF TYR204 FPPS MUTANTS SUPPORT ALTERATIONS IN IPP BINDING

It is not clear whether the increased K_m^{IPP} of the mutants can be attributed to a defective or altered binding pocket site, the inability of the enzyme to accommodate the IPP substrate or a disruption of crucial molecular interactions between Tyr204 and IPP. Crystallographic studies were employed to elucidate the role of Tyr204 in N-BP and IPP binding.

The present model indicates that the binding of IPP results in conformational changes in the active site. Three amino-acids, Lys57, Arg60, and Arg113, directly interact with the pyrophosphate group of IPP and upon a conformational switch of FPPS the C-terminus seals the newly formed IPP binding pocket (Kavanagh *et al.*, 2006b, Rondeau *et al.*, 2006). In WT FPPS, Tyr204 is found in close proximity with IPP, therefore it is possible that it plays an active part in properly orienting the IPP substrate towards the carbocation site or in stabilizing the IPP molecule in the correct position during catalysis. This can be via a tyrosinate ion derived from the interaction of the OH group of Tyr with a basic

Arg residue (such as Arg112/Arg60) in the vicinity. If such an electronegatively charged oxygen is generated it may be capable of repelling the terminal double bond of IPP and position IPP into the right place in the binding pocket.

Superposition of the WT and Y204F (Figure 4.4) or WT and Y204A (Figure 4.5) models obtained from interaction of enzyme with IPP and Ris reveals a shift in the IPP position by 0.8 Å and 0.6 Å respectively. The decreased Phe204/Ala204-IPP distance may possibly reflect an inability of the mutant to switch conformation following IPP binding or to the inability for IPP to be correctly positioned in the binding pocket. Indeed, a loss of the OH moiety would explain such different behaviour and could reflect the inability of the enzyme to push IPP towards the binding site. A similar pattern was observed in the crystal structure of Y204A: IPP with Pam, indicating that the shifting of IPP was not a unique phenomenon associated with Ris (data not shown). However, indications for a protonation/deprotonation mechanisms remain to be proven.

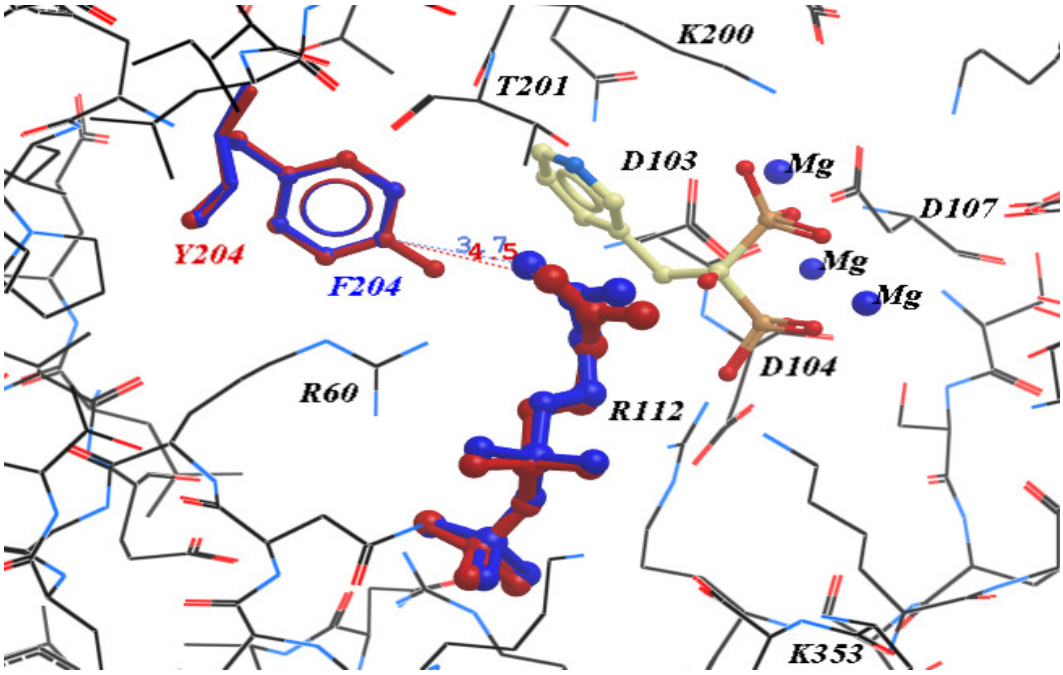


Figure 4.4: Superposition of WT and Y204F FPPS mutant crystal structures reveals changes in the IPP binding pocket. Upon binding of the allylic substrate conformational changes mainly affecting Asp103 and Asp107 residues take place, resulting in closure of the allylic binding site. Upon binding of IPP, a further isomerisation event occurs where the C-terminal amino-acid tail of the enzyme forms a lid over the IPP binding site. Among other amino acids, the Tyr204 position is also affected by IPP binding, which is positioned 3.3 Å away from IPP in WT. However the observed distance between the Phe204 and IPP molecule is 3.7 Å instead of 4.5 Å. This shifting reflects changes in IPP binding pocket, resulting in alteration of an isomerization effect and the inability of FPPS to switch to a fully closed conformation. WT IPP is shown in red, Y204F IPP in blue and Y204A IPP in green. WT structure adapted from pdb: 1ZW5 (Rondeau *et al*. 2006).

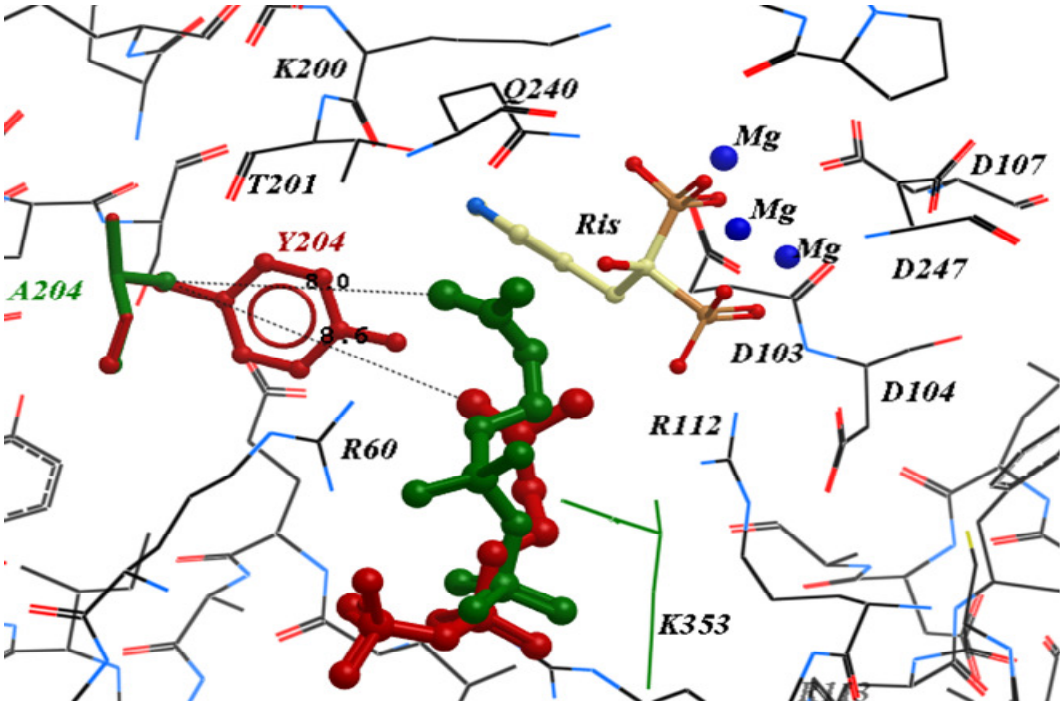


Figure 4.5: Superposition of WT and Y204A FPPS mutant crystal structures reveals changes in the IPP binding pocket. A similar profile of IPP shifting observed in Figure 4.4 is observed in crystal structure of Y204F with Ris and IPP where the distance between the A204 and IPP molecule is 8.6 Å instead of 8.0 Å. WT IPP in shown in red, Y204F IPP in blue and Y204A IPP in green. WT structure adapted from pdb: 1ZW5 (Rondeau *et al*. 2006).

In contrast, the position of DMAPP binding is not affected by the Tyr204 mutation as revealed by the crystal structure of Y204A FPPS with the non-cleavable analogue of DMAPP, DMASPP and IPP at 2.9 Å (Figure 4.6).

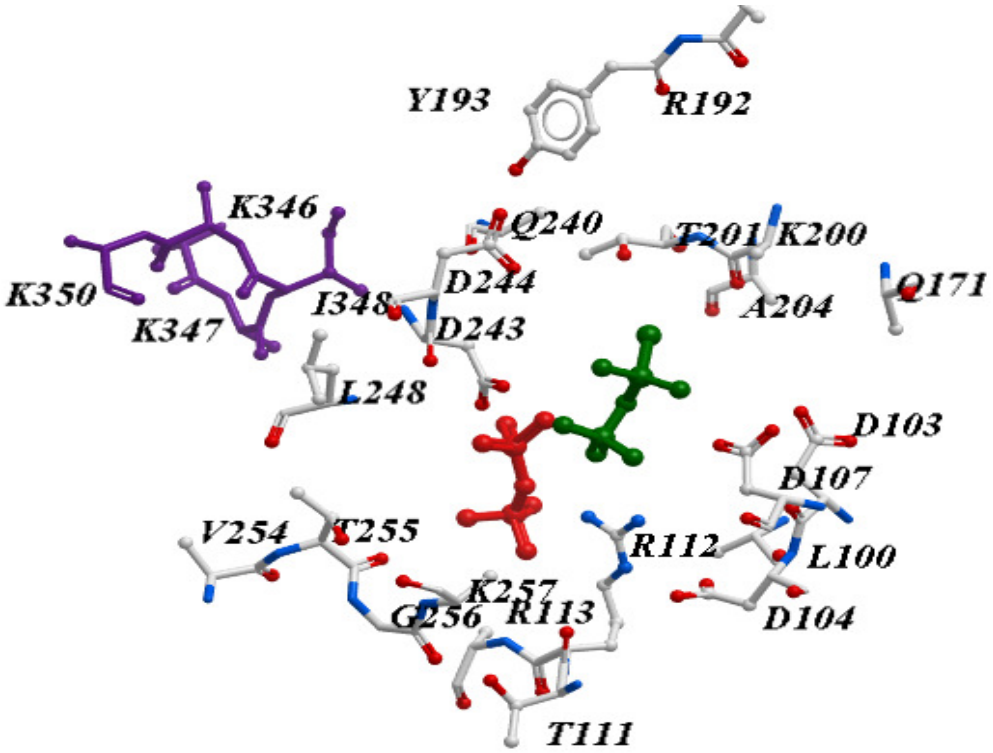


Figure 4.6: DMASPP position in the binding pocket is stabilized by the conserved aspartate motifs Asp103, Asp107, Asp244 and hydrophobic interactions with Arg192, Gln171, Lys200 and Thr201. IPP substrate is kept in a reactive conformation due to electrostatic or hydrophobic interactions with key residues of FPPS such as Arg112, Arg113, Lys257. In green: DMASPP, in red: IPP, in purple: C terminal tail.

The hydrocarbon tail of the DMASPP is located into the isoprenoid lipid pocket and its position is stabilized by hydrophobic interactions with Gln71 and Arg192 on one subunit, and Phe99, Leu100, and Thr201 on the other, keeping it in proximity to C_1-C_4 IPP atoms in strict agreement with the *E.coli* model proposed by Hosfield *et al.* 2006. The octahedral coordination of the Mg^{2+} ions by protein, pyrophosphate, water

oxygens and side chain of aspartates Asp104, Asp107 and Asp244 persists. However as this is the only existing crystal structure of human FPPS with both allylic and homoallylic substrates, it is not possible to check for minor alterations of DMASPP position and only a relative comparison with the published *E. coli* structure can be attempted.

4.4 ALTERATION OF THE pH PROFILE IN FPPS MUTANTS SUPPORTS FORMATION OF A TYROSINATE ANION

To further investigate the role of Tyr204 in catalysis and the impact of pH on the maximal activity of the enzyme, pH dependence studies were performed for WT and mutated enzyme. It has been already established that for WT FPPS the optimal catalytic activity is obtained at pH 7.7 (Dunford, unpublished data) however this assumption might not be valid in Tyr204 mutants, due to alteration of the amino acid side-chain that might have drastically affected the enzyme properties and the ability of FPPS to fully participate in the catalytic mechanism. The enzyme activity for WT and Tyr204 mutated FPPS constructs was evaluated at nine different pH conditions. Taking into account the facts that IPP saturation is not achieved under the standard enzyme reaction conditions used here (where the concentration of IPP and GPP is

10 μM) and that the K_m for both IPP and GPP may be altered at different pH, a proper estimation of K_{cat} and pKa values cannot be obtained and only informed speculations can be made at this stage. Assuming the K_m value remains constant at each pH point, an estimation of the pKa values was attempted for WT and mutants and gave the following profiles (Figure 4.7).

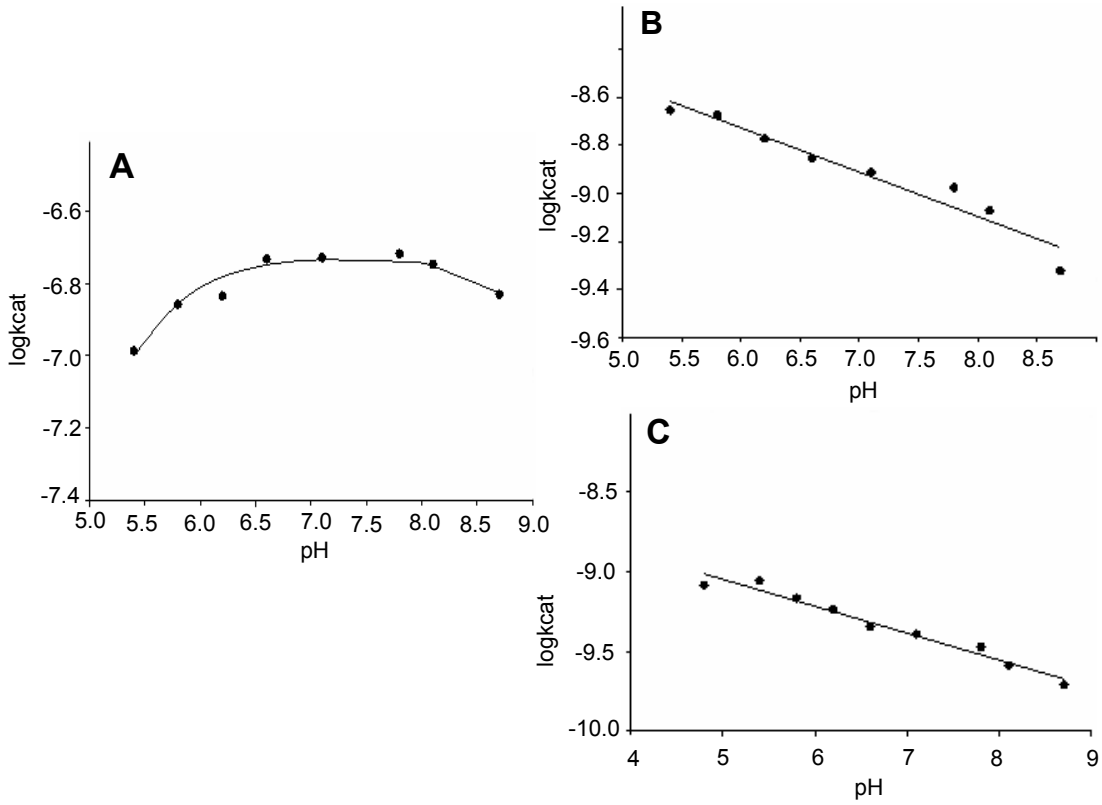


Figure 4.7: Optimal catalytic activities of Tyr204 FPPS mutants are observed in acidic environment. pH dependence studies were conducted for (A) WT, B) Y204F and C) Y204A FPPS catalyzed reactions. The activity assay was performed as described in section 2.24 but using Tris-Maleate buffer to facilitate assay of the enzyme under standard conditions at all pH values. Graph represents means obtained from four individual experiments performed in duplicate and error bars represent SEM (error bars smaller than the symbols used), concentration of IPP and GPP were 10 μM.

The pH profile obtained for WT is a typical bell shape curve, where catalytic activity is optimal at pH values between 6 to 8 and is reduced at either high or low pH (Figure 4.7.A). This comes in striking contrast with both mutants which display their highest catalytic turnover in an acidic environment whereas the activity seems to drop gradually with the increase in pH, altering the typical bell shape pH profile to data best fitting a linear regression (Figure 4.7B and 4.7C).

It is generally accepted that a bell-shape curve spread over two pH units is an indicator of two ionizing groups taking part in catalysis (Brocklehurst, 1994), expressed by two different pKa values calculated as 5.3 and 9.3 for the WT. Both Tyr204 mutations appear to cause abolition of the acidic pKa value and thus suppression of a possible ionization mechanism. Furthermore, taking into consideration that the pKa value of the Tyr groups is approximately 10.4 (Bohren *et al.*, 1994), the reduced value found in the WT might correspond to a reaction of the tyrosine residue with an adjacent basic residue such as Arg60 or Arg112. These results strongly support the role of the hydroxyl group of Tyr204 as a proton donor where its removal alters the pH profile of the enzyme. If the ionization step in FPPS catalysis progresses via removal of a negative charge from the allylic

pyrophosphate (Poulter and Rilling, 1976), a proton donation from Tyr204 could accelerate the reaction. Therefore, a possible abolition of one out of two pKa tyrosine values, as suggested from the altered pH profile in both mutants, might indicate suppression of the ionization mechanism. However the observed increased activity at low pH is inconsistent with the proposal that a tyrosinate ion acts to force IPP into a catalytically competent position. In addition, it is not always possible to attribute a pKa value to a single group, as the ionization state observed might be an outcome of multiple ionizing groups taking part in catalysis, therefore the observed results might be misleading (Zographos *et al.*, 1995). In addition, stabilization of PPi was proposed to be facilitated by the tri nuclear Mg cluster and such a theory excludes any possible involvement of tyrosine in ionization process (Hosfield et al., 2004). Perhaps the hydroxyl of the tyrosine aids in the stabilisation of an unknown reaction intermediate that is generated as the condensation step occurs.

Chemical rescue of a mutated tyrosine ring involved in catalysis has been successfully conducted with ketosteroid isomerase, where addition of low molecular weight phenols to the reaction mixture accounted for the loss of the pKa of a titratable group and restored catalytic activity, efficiently proving the importance of tyrosine hydroxyl in the catalytic reaction (Brooks

and Benisek, 1992, Brooks *et al.*, 1998). In this case phenol would act as a nucleophile in place of the proposed tyrosine proton transfer donor (Cole *et al.*, 2003). Similar attempts to rescue the catalytic activity of FPPS mutants by addition of phenol (pKa 9.95), 2-fluorophenol (pKa 8.8) or 2,6-difluorophenol (pKa 7.5) (concentration ranging from 0.01 nM to 100 mM) to the reaction mixture gave negative results (data not shown) and thus failed to support a role of Tyr in FPPS catalysis. However the failure of chemical rescue might be attributed to inability of the phenols to properly fit the catalytic active site due to distance alterations between the IPP and the mutated residue or might simply reflect steric conflicts regarding the formation of enzyme-product complex (Pival *et al.*, 2008). Further kinetic studies and the generation of other constructs are essential to confirm the role of Tyr204 in catalysis.

4.5 INVESTIGATION OF THE INHIBITION MODE OF WT AND TYR204 FPPS MUTANTS BY N-BPs

All N-BPs examined produced a time-dependent increased inhibition of FPPS, as demonstrated by the Ki and Ki* values (Table 4.4). The mode of inhibition of Tyr204 mutants was assessed at three different time points and compared to the relevant WT

values: i) at 3 min, which was the minimal incubation time where activity of the enzyme was measurable and thus accounts for the competitive inhibition rate (Ki) of GPP towards N-BP binding, ii) after 10 min pre-incubation of enzyme with the inhibitor, which accounts for the maximal inhibition (Ki*) achieved with N-BP after isomerization takes place and iii) after 5 min incubation of enzyme with the N-BP, to obtain an intermediate rate (Kint) between initial and final inhibition and thus assess the overall behaviour of the enzyme. The shift in potency from the competitive, initial stage to the final isomerized state was assessed with the K_{isom}, which was corrected for K_m^{GPP}, as the affinity for the allylic substrate remained unaltered in both WT and mutants and thus was chosen as a fair point of comparison.

Different patterns of inhibition were observed with the five clinical N-BPs and some are examined in more detail in the individual sections below.

Table 4.2: Estimation of Ki, Ki* and Kisom of Tyr204 mutants derived from inhibition assays with N-BPs. Initial (Ki) and intermediate (Kint) inhibition constant values were obtained when inhibition assays were initiated by the addition of enzyme and 3 min or 5 min incubation respectively whereas final Ki (Ki*) was calculated when enzyme was pre-incubated with BP for 10 min and the reaction started by the addition of substrate. The constants obtained were then corrected for the affinity for GPP substrates (Km^{GPP}) as described in Section 2.25. K_{isom} was calculated from Ki and Ki* as described in section 2.25. ND: not determined. Results are expressed as means +/- SEM, $R^2 > 0.95$ and $n \geq 6$.

BP	Construct	Ki (nM) 3 min	Kint (nM) 5 min	Ki* (nM) 10 min	K_{isom}^{IPP}
Ris	WT	56.6 ± 3.1	31.02 ± 1.5	0.8 ± 0.06	69.3
	Y204F	58.32 ± 4.5	157.12 ± 10.7	2.3 ± 0.4	24
	Y204A	17.7 ± 1.3	112 ± 8.9	3.2 ± 0.8	4.6
Zol	WT	62.9 ± 5.1	48.62 ± 2.4	0.06 ± 0.03	1276.9
	Y204F	54.2 ± 4.4	48.83 ± 3.7	ND	ND
	Y204A	29.8 ± 3.1	35.54 ± 3.5	ND	ND
Iba	WT	207.7 ± 13.4	101.36 ± 4.5	4.6 ± 0.4	44.1
	Y204F	233.1 ± 10.5	60.45 ± 4.3	2.9 ± 0.6	78.3
	Y204A	142.2 ± 6	64.3 ± 4.8	4.3 ± 0.8	32.4
Ale	WT	388.3 ± 31.3	166.46 ± 9.5	56.5 ± 4.9	5.9
	Y204F	431.2 ± 37.3	231.56 ± 11.4	7.25 ± 1	58.5
	Y204A	253.9 ± 14.4	187.16 ± 11.1	26.9 ± 2.5	8.5
Pam	WT	181.5 ± 6	142.98 ± 7.9	51.9 ± 3.3	2.5
	Y204F	199.9 ± 10.35	107.44 ± 5.4	21.7 ± 1.8	8.2
	Y204A	195.6 ± 9.8	127.27 ± 9.2	73.6 ± 7.7	1.7
NE58022	WT	365.9 ± 15.9	ND	301 ± 17.6	0.2
	Y204F	30.2 ± 2.7	ND	23.1 ± 2.4	0.3
	Y204A	23.8 ± 2.4	ND	10.4 ± 2	1.1

4.5.1 Reduction of final inhibition by Ris in tyrosine FPPS mutants reveals the importance of the aromatic ring

Statistical analysis for Ki, Kint and Ki* values obtained from enzyme assays experiments after 3, 5 and 10 min incubation with Ris with the mutants gave the following results summarized in Table 4.3.

It is worth noticing that competitive (3 min) inhibition is virtually unaffected by the Y204F substitution, yielding a Ki comparable to that of WT, but it is suppressed in Y204A mutant. This result confirms the role of the phenyl ring in Ris binding, whereas the hydroxyl moiety does not favour Ris over GPP nor is it responsible for initial Ris binding to the pocket. Contrary to expectations, inhibition rate after 5 min incubation with the N-BP was reduced compared to the initial rate in both Y204F and Y204A mutants, indicating that the enzyme loses the ability to maintain the isomerized state. This observation is supported by comparisons of the Ki* between WT and mutants, as it is significantly reduced in Y204A FPPS but not in Y204F FPPS, revealing that presence of the aromatic ring plays a role, but is not essential to maintain inhibition. A possible explanation for maintenance of Ris inhibition in Y204F FPPS might be a large entropic change deriving from a typical aromatic interaction between the phenyl rings of Tyr204 and Ris (Burley and Petsko, 1986), where pi stacking bonds would

force water displacement from the active site and thus strengthen inhibition (Kavanagh *et al.*, 2006b). Participation of the Tyr204 in edge to face contacts with the aromatic ring of Ris would be favoured in Y204F but not in Y204A mutation, accounting for the increased Ki (Couture *et al.*, 2005).

Table 4.3: Comparison between WT and Tyr204 mutants Ki, Kint and Ki* inhibition rates by Ris. Data were analysed for significance with one way ANOVA and Tukey post –hoc test as grouped below whereas in case of two values unpaired tailed t-test was used for comparison. ND : Not determined.

Groups of comparison	Construct 1	Construct 2	1 vs 2 Ris	1 vs 2 NE58022
Y204F	Y204F Ki	Y204F Kint	< (p <0.001)	ND
Ki, Kint	Y204F Ki	Y204F Ki*	> (p <0.01)	No difference
and Ki*	Y204F Kint	Y204F Ki*	> (p <0.001)	ND
Y204A	Y204A Ki	Y204A Kint	< (p <0.001)	ND
Ki*, Kint	Y204A Ki	Y204A Ki*	No difference	No difference
and Ki	Y204A Kint	Y204A Ki*	> (p <0.001)	ND
All	Y204F Ki	WT Ki	No difference	< (p <0.001)
constructs	Y204A Ki	WT Ki	> (p <0.001)	< (p <0.001)
Ki	Y204F Ki	Y204A Ki	< (p <0.001)	No difference
All	Y204F Kint	WT Kint	> (p <0.001)	ND
constructs	Y204A Kint	WT Kint	> (p <0.001)	ND
Kint	Y204F Kint	Y204A Kint	> (p <0.01)	ND
All	Y204F Ki*	WT Ki*	No difference	< (p <0.001)
constructs	Y204A Ki*	WT Ki*	> (p <0.05)	< (p <0.001
Ki*	Y204F Ki*	Y204A Ki*	No difference	No difference

The common parameter in both mutants is the removal of the hydroxyl group which might account for a misplacement of the reactive groups and a concomitant decrease in FPPS reaction rate as observed in Section 4.3. This would be in agreement with the pH study (Figure 4.7) that supports an active role of the OH moiety as proton donor. Alterations on IPP binding site do not affect the position of Ris in binding pocket in either mutant (Figure 4.8), however they might account for changes in electrostatic interactions between Ris and the mutated residue and thus for the decreased final inhibition and eventually the reversibility of inhibition, as shown by the elevated K_{isom}.

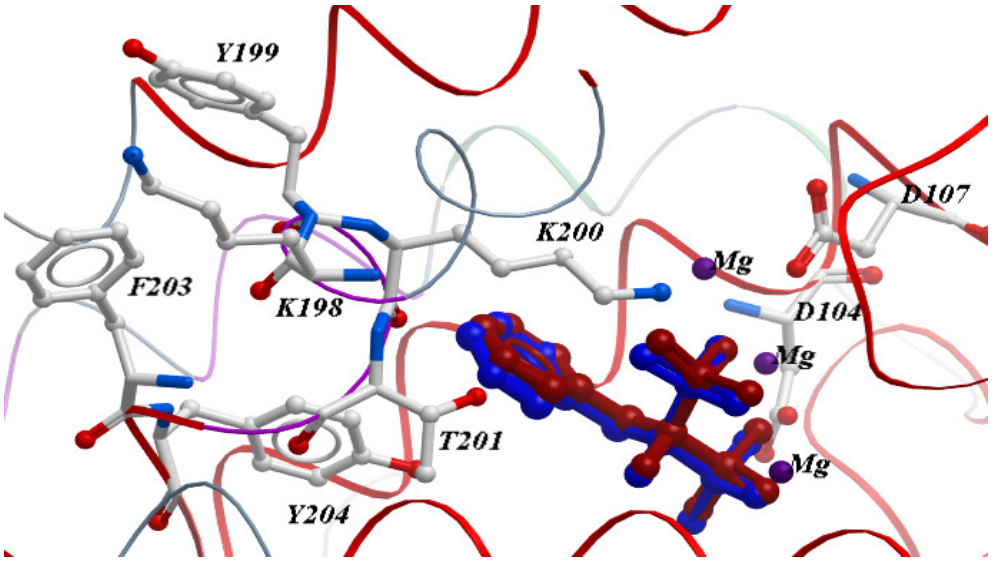


Figure 4.8: Superposition of WT FPPS (pdb:1ZW5) and Y204A FPPS structures reveals that position of Ris is unaltered in tyrosine mutants.

Kinetic studies with the Ris analogue NE58022, which lacks the nitrogen atom, were performed to assess the importance of nitrogen atom in Ris positioning in the binding pocket. The lack of nitrogen atom should render the NE58022 analogue a weak inhibitor, however Ki and Ki* values obtained for both Tyr mutants were comparable to those obtained for Ris. Given the proven importance of the ring nitrogen atom in time dependent inhibition as the hydrogen bond formation with Lys200 and Thr201 should properly orient the heterocyclic ring of Ris for FPPS binding (Dunford *et al.*, 2008), the increased potency of Y204F and Y204A FPPS mutants is difficult to explain. It appears that selection of the protonated form of Ris by FPPS does not play such an important role in the inhibition by Tyr204 mutants, as NE58022 does not carry a positive charge and thus lacks the ability to form a protonated form, yet it remains a potent inhibitor, compared to Ris.

4.5.2 Inhibition by Zol suggests allosteric regulation of Tyr204 FPPS mutants

Given the similar nature of the heterocyclic ring of Ris and Zol, the mode of initial inhibition by Zol of the Tyr204 mutants was expected to be as described in Section 4.5.1. It was however

observed that Ki was unaltered for Y204F FPPS, while it was increased for Y204A FPPS, with similar patterns observed for the intermediate 5 min inhibition (Table 4.4).

Table 4.4: Statistical analyses of initial and intermediate Ki by Zol. Data were analysed for significance with one way ANOVA and Tukey post –hoc test as grouped below whereas in case of two values unpaired tailed t-test was used for comparison.

Group of comparison	Construct 1	Construct 2	Ki 1 vs 2
Y204F Ki & Kint	Y204F Ki	Y204F Kint	No difference
All constructs Ki	Y204F Ki	WT Ki	No difference
	Y204A Ki	WT Ki	< (p <0.001)
	Y204F Ki	Y204A Ki	> (p <0.01)
Y204A Ki* & Kint	Y204A Ki	Y204A Kint	No difference
All Constructs Kint	Y204F Kint	WT Kint	No difference
	Y204A Kint	WT Kint	< (p <0.05)
	Y204F Kint	Y204A Kint	> (p <0.05)

Assessment of Ki* for Zol inhibition rate in Tyr204 mutants was problematic as the general assumption of 1:1 enzyme: inhibitor binding ratio was not valid in this case. The estimation of inhibitor concentration required for 50% inhibition (IC_{50}) corresponded to a value lower than half of the enzyme concentration, making impossible the determination of Ki* and

$K_{isom.}$ The IC_{50} was the only available way of determining the strength of Zol inhibition (Table 4.5).

Table 4.5: IC_{50} values of mutant enzymes for final inhibition of Zol, compared to the WT inhibition data.

Enzyme	[Enzyme] nM	Theoretical max IC_{50} (nM) Zol	Experimental IC_{50} Zol (nM)
Y204F	134	67	34 ± 2.2
Y204A	292	146	92.9 ± 5.3
WT	8	4	3.8 ± 0.16

The increased final inhibition of Tyr204 mutants with Zol was initially attributed to the absence of the bulky tyrosine phenyl ring which allows proximity of Zol to the mutated Tyr204 and the development of novel electrostatic- hydrophobic interactions that increase the strength of inhibition. Furthermore, the bifurcated hydrogen bond of the protonated nitrogen of Zol with Lys200 and Thr201 should still be preserved in Tyr204 mutants, as the position and orientation of both residues is unaltered in crystal structures with Ris, keeping the imidazole ring of Zol well-ordered in the allylic binding pocket (Rondeau *et al.*, 2006). Additional van der Waals contacts formed due to Tyr204 mutation may contribute to the rigidity of the imidazole ring and thus the increased inhibition.

The crystal structure of Y204A in complex with Zol was obtained after several trials with precipitant screens and was used to re-evaluate the proposed model and detected alterations on the electrostatic interactions and of position of the residues which play pivotal role in the formation of the allylic binding pocket. The most obvious change observed is lengthening of the Lys200 (from 3 to 3.2 Å) and Thr201 (from 2.9 to 3.4 Å) bifurcated hydrogen bond with the nitrogen atom of the imidazole ring, that causes Zol disorientation in the allylic binding pocket (Figure 4.9). Due to the weakening of this bifurcated hydrogen bond, the imidazole ring cannot be fixed in the proper position for inhibition of catalysis, but instead moves deeper into the allylic binding pocket, increasing the strength of final inhibition. In addition, the mutated Ala204 residue is now positioned at the far end of the binding pocket (Figure 4.9B) whereas the Tyr204 was previously in close proximity to the imidazole ring (Figure 4.9A).

The presence of the bulky aromatic ring of Tyr204 delimits the size and volume of the binding pocket, creating a hydrophobic environment for the accommodation of the isoprenoid substrate. The Tyr ring possibly contributes to the imidazole fixation by creating a hydrophobic environment suitable for substrate accommodation in the binding pocket. It is therefore expected that maintenance of the aromatic ring in Y204F FPPS can still preserve

the hydrophobicity of the binding pocket without affecting the orientation of Zol and thus modifying the pattern of competitive inhibition. All this led to the proposal that the disruption of bifurcated hydrogen bond shifts the position of imidazole ring in the binding pocket and accounts for the increased strength of inhibition by Zol.

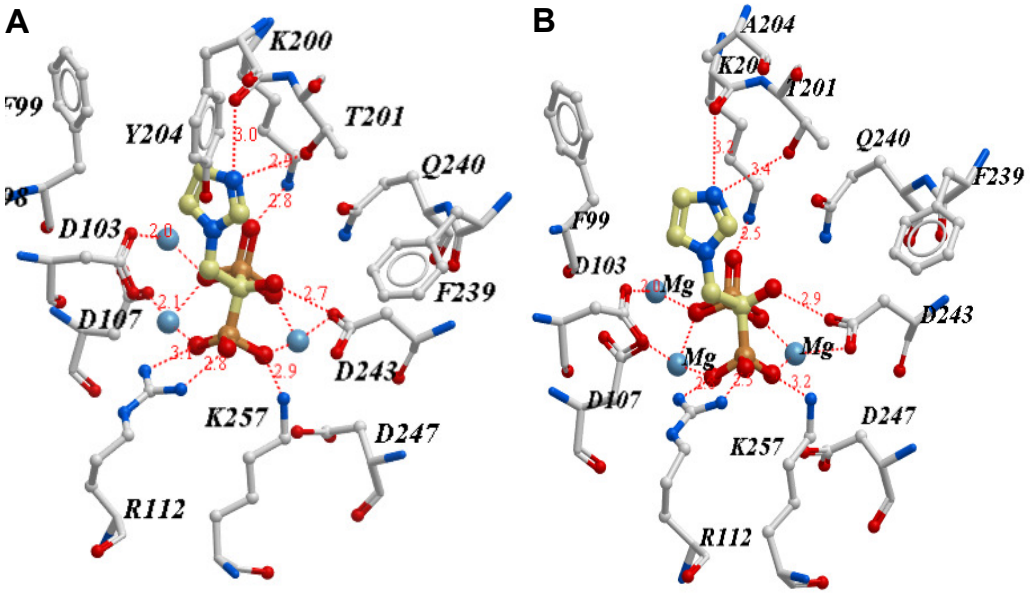


Figure 4.9: The weakening of the hydrogen bond between Lys200 and Thr201 with the imidazole nitrogen of Zol contributes to the increased inhibition in Y204A FPPS mutant. A) In WT FPPS the imidazole ring of Zol is well oriented due to the bifurcated hydrogen bond between Lys200 and Thr201 and the nitrogen atom of Zol, fixing Zol in the allylic binding pocket. B) In Y204A FPPS the increased distance between nitrogen of Zol and oxygen atom of Thr201 (from 2.9 to 3.4 Å) and between Lys200 and imidazole ring (from 3.0 to 3.2 Å) weakens both hydrogen bonds. Ala204 is too far to limit the size of the allylic binding pocket. The interactions between Mg ions and pyrophosphate moieties persist but are unable to fix Zol in the binding pocket. WT structure adapted from pdb: 1ZW5 (Rondeau *et al*. 2006).

The unexpected altered enzyme: inhibitor ratio prompted further investigation of the thermodynamic parameters governing Zol binding to Y204A FPPS by ITC. Titration of Zol against FPPS in the presence of Mg^{2+} at pH 7.7 (Figure 4.10) resulted in a strongly exothermic reaction, comparable to that observed in WT FPPS (Kavanagh *et al.*, 2006b, Yin *et al.*, 2006).

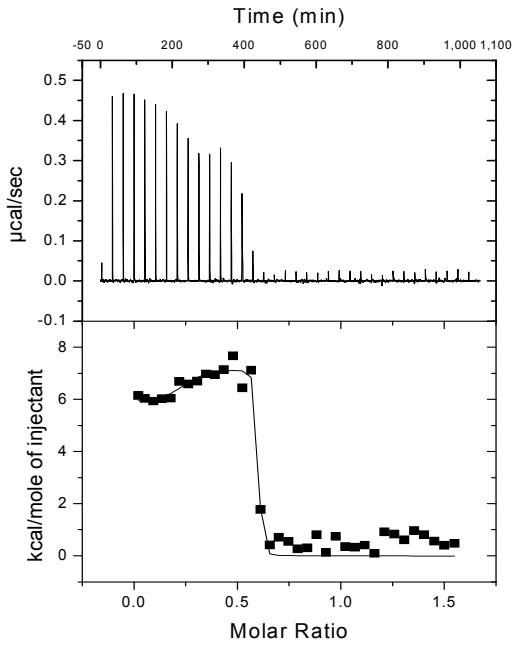


Figure 4.10: Thermodynamics of Zol binding to human Y204A FPPS in the presence of 2 mM $MgCl_2$, measured by isothermal titration calorimetry. Upper panel: Raw ITC data for Zol binding to Y204A FPPS. Lower panel: Representative fitting curve. Method as described in section 2.29.

The calculated Kds (<10^{-9} M) indicate a tight association of FPPS with the ligand, as expected from the kinetic analyses (Table 4.6). Zol binding to Y204A FPPS is a slow, tight binding process, entropy-driven, due to the presence of the bulky side chain resulting in strong ion-dipole interactions and thus to high enthalpy when desolvating the ligand (Yin *et al.*, 2006). In addition, taking into account that the pH value is 7.7 and that the imidazole side chain has a pKa of approximately 6.7, the non-protonated form of the side chain of Zol should prevail over the protonated form in solution.

Table 4.6: Thermodynamic data for Zol binding determined by ITC. WT data from Kavanagh *et al*. (2008). Kb: binding constant, Kd: dissociation constant, ΔH: Difference in enthalpy, ΔTS, difference in entropy, ΔG: Difference in Gibbs free energy, N:binding sites.

Sample	Model	Kb x 10^6 (M^{-1})	Kd (μM)	ΔH (kcal/mol)	ΔTS (kcal/mol)	ΔG (kcal/mol)	N
WT FPPS Zol/Mg^{2+}	Single site binding	64 ± 2.0	0.015	2.1 ± 0.03	12.1	-10	0.93
Y204A FPPS Zol/Mg^{2+}	double site binding: 1st site	7820 ± 4100	0.0013	5.9 ± 0.6	18.7	-12.8	0.23
Y204A FPPS Zol/Mg^{2+}	double site binding: 2nd site	323 ± 1030	0.003	7.2 ± 0.5	18.2	-11	0.35

In contrast with the ITC data for WT FPPS:Zol that fit to a one binding site model, the Y204A FPPS:Zol data fit well the two-site binding model, indicating that when one molecule of Zol binds to the mutant, it somehow affects the conformation of active site of the second FPPS molecule in the dimer, thus changing the mode of binding of the second Zol to it. This change may explain the fact that the kinetic data cannot not fit the Morrison's equation of tight binding that predicts that the inhibitor: ligand ratio should be 1:1. This is the basic assumption valid for WT FPPS (Figure 4.11), where inhibition of the dimer occurs when two molecules of Zol binds to the individual subunits. The picture is different for Y204A FPPS, where binding of one molecule of Zol is sufficient to inactivate the enzyme, possibly by rendering the monomer rigid and thus preventing flexing of the second monomer, which would otherwise be catalytically active. This model of allosteric regulation takes into account the fact that no cooperative binding for BPs to FPPS has been observed until recently; therefore the binding site for a BP in the second subunit of the dimer was thought to be capable of binding Zol with the same affinity as the first one. However it is not clear whether the ITC data support a theory of new interactions of Zol with the Y204A FPPS mutant. The observed alteration in ΔG is in complete agreement with the determination of $\Delta\Delta G$ from the kinetic parameters in 4.2 and supports an alteration

in the mechanism of enzyme catalysis and consequently in mode of inhibition.

The recent discovery of an allosteric binding site in FPPS (Jahnke *et al.*, 2010) demonstrates that the enzyme is capable of being allosterically regulated. As FPPS is a dimer, it is possible that Zol binding to one subunit of the Tyr mutants causes some allosteric regulation, causing inhibition of both subunits but this theory remains to be tested.

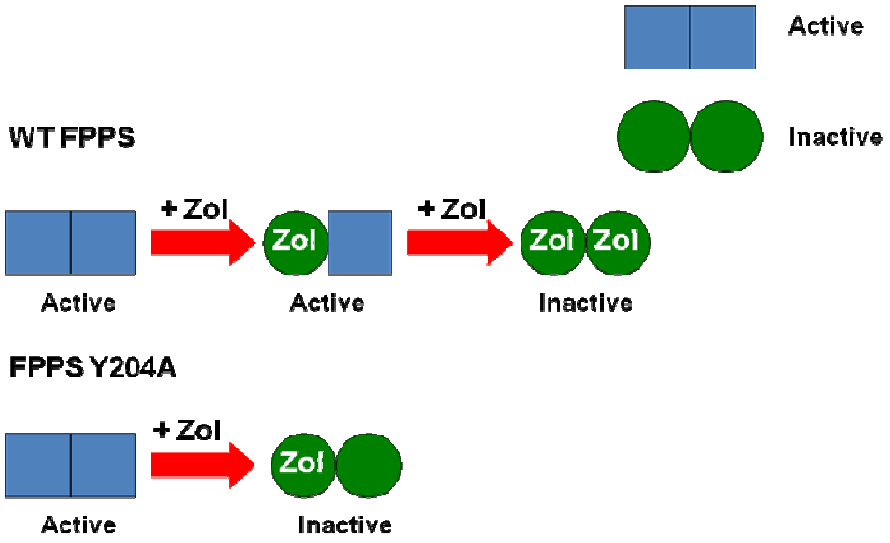


Figure 4.11: A potential model of allosteric regulation caused by Zol binding to Y204A FPPS. The WT FPPS dimer is active even after binding of one molecule of Zol. Only after the binding of a second molecule of Zol to the second free subunit, FPPS is inactivated (upper panel). On the contrary, binding of one molecule of Zol is capable of rendering the Y204A FPPS enzyme inactive (lower panel).

4.5.3 Inhibition by the amino-alkyl N-BPs reveals the importance of the Tyr204 ring for maintenance of enzyme: inhibitor isomerisation status

The creation of Tyr204 mutants was mainly aimed at elucidating the potential involvement of this residue in FPPS inhibition by aminoalkyl BPs. It was hypothesized that inhibition by Pam is strengthened by the formation of a hydrogen bond with the hydroxyl of the Tyr204 (Rondeau *et al.*, 2006) despite of the ill defined position of its nitrogen atom in electrodensity maps. On the contrary, the nitrogen atom of Ale is oriented towards Thr201 and forms a hydrogen bond with the gamma oxygen atom of Thr201 but not with Tyr204. Similarly, the tertiary amino group of Iba and the long side chain do not favour such a hydrogen bond formation in neither of the two known conformations adopted when binding to FPPS. If the above observations are correct, then removal of hydroxyl moiety in both tyrosine mutants should result in decreased Pam inhibition, leaving Iba and Ale inhibition unaffected.

All aminoalkyl N-BPs produced a time-dependent inhibition for WT and Tyr204 mutants, which gradually increased with the incubation time (Figure 4.12 and Table 4.7). As expected, overall inhibition by Iba is virtually unaffected in tyrosine mutants whereas competitive and intermediate inhibition is increased for both mutants, with Y204A producing the lowest Ki and Kint (Table

4.11). The results confirm that the hydrophobic interactions of the Iba pentyl side chain are far more important in FPPS inhibition than any possible hydrogen bond formation and that absence of the bulky phenyl ring in Y204A allows accommodation of the long hydrocarbon chain to the binding pocket and reinforces hydrogen bonds/ electrostatic interactions with other amino-acids (Figure 4.14), increasing the competitive inhibition rate. However inhibition is weakening with incubation time, possibly due to high IPP saturation rate and the low K_{isom} indicates reversibility of inhibition and prevalence of transition to isomerisation FPPS state.

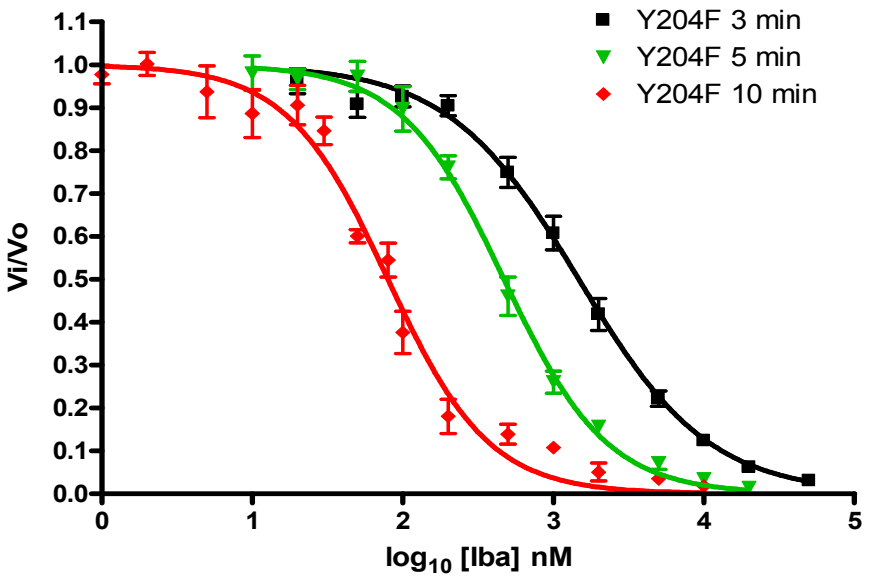


Figure 4.12: Changes in potency of Iba in Y204F FPPS over time reveal its time dependent inhibition. Shifting in Iba potency with incubation time demonstrates that the inhibitor is capable of producing a time-dependent, irreversible inhibition. Similar patterns were observed with Ale and Pam in both tyrosine mutants.

As predicted, similar patterns were observed for competitive inhibition by Ale, with Ki statistically decreased for Y204A but not for Y204F FPPS mutant (Table 4.7).

Table 4.7: Statistical analyses of initial and intermediate Ki by aminoalkyl BPs. Data from table 4.3 were analyzed for significance with one way ANOVA and Tukey post – hoc test.

Group of comparison	Construct No 1	Construct No 2	1 vs 2 Iba	1 vs 2 Ale	1 vs 2 Pam
Y204F Ki, Kint and Ki*	Y204F Ki	Y204F Kint	> (p <0.001)	> (p <0.001)	> (p <0.001)
	Y204F Ki	Y204F Ki*	> (p <0.001)	> (p <0.001)	> (p <0.001)
	Y204F Kint	Y204F Ki*	> (p <0.001)	> (p <0.001)	> (p <0.001)
Y204A Ki, Kint and Ki*	Y204A Ki	Y204A Kint	> (p <0.001)	> (p <0.001)	> (p <0.01)
	Y204A Ki	Y204A Ki*	> (p <0.001)	> (p <0.001)	> (p <0.001)
	Y204A Kint	Y204A Ki*	> (p <0.001)	> (p <0.001)	> (p <0.01)
All constructs Ki	Y204F Ki	WT Ki	No difference	No difference	No difference
	Y204A Ki	WT Ki	< (p <0.01)	< (p <0.05)	No difference
	Y204F Ki	Y204A Ki	> (p <0.001)	> (p <0.05)	No difference
All constructs Kint	Y204F Kint	WT Kint	< (p <0.001)	> (p <0.01)	< (p <0.05)
	Y204A Kint	WT Kint	< (p <0.001)	No difference	No difference
	Y204F Kint	Y204A Kint	No difference	> (p <0.05)	No difference
All constructs Ki*	Y204F Ki*	WT Ki*	No difference	< (p <0.001)	< (p <0.01)
	Y204A Ki*	WT Ki*	No difference	< (p <0.001)	> (p <0.05)
	Y204F Ki*	Y204A Ki*	No difference	< (p <0.01)	< (p <0.001)

The crystal structure of Y204A FPPS with Ale confirms that the orientation of the nitrogen atom of Ale as well as the increased A204: Ale distance does not permit their interaction (Figure 4.13).

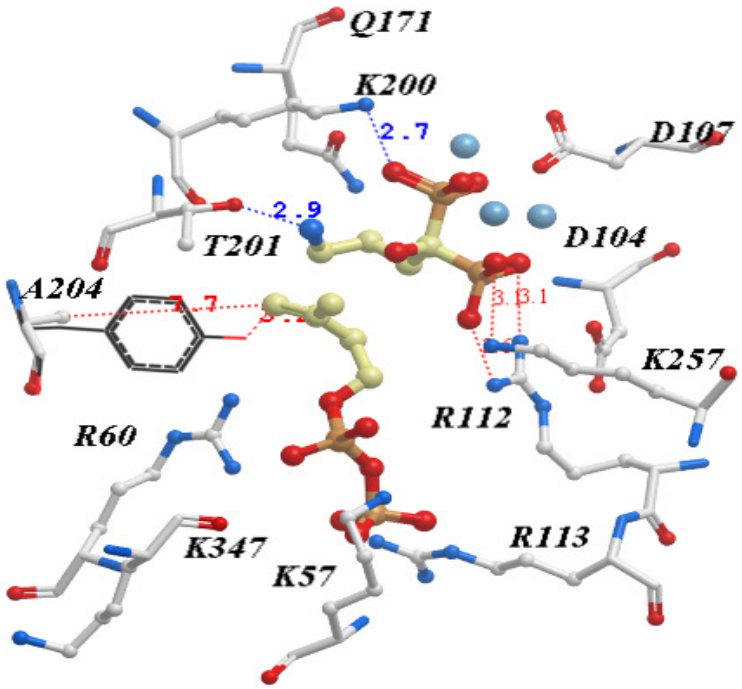


Figure 4.13: Orientation of Lys200 and Thr201 in Y204A FPPS mutant favours formation of hydrogen bonds with gamma carbonyl oxygen and nitrogen of Ale respectively, reinforcing Ale inhibition. The mutated Ala204 is positioned too far away (7.7 Å instead of 3.2 Å) to repel the double bond of IPP and push it deeper to the homoallylic binding pocket, but favours accommodation of the flexible Ale chain and fixation by Lys200/Thr201 electrostatic interactions (in dashed blue lines).

However absence of electrostatic repulsion between the bound IPP and the mutated A204 shortens the distance between Ale and Lys200/Thr201 and thus reinforces the strength of electrostatic

interactions, previously observed in WT FPPS accounting for the increased competitive inhibition. The situation slowly reverses over the time course, with Kint of WT equivalent to the Y204A one and Y204F FPPS appearing the least inhibited. Finally, comparison of Ki* indicates that Y204F FPPS is by far the most strongly inhibited, with Y204A showing an intermediate rate between WT and Y204F.

Contrary to expectations, the Ki values obtained for both Tyr204 mutants for Pam, were identical to the WT, indicating that, even after possible rupture of the hydrogen bond between Pam and tyrosine residue, the BP is still capable of competing with the GPP substrate and occupy the allylic binding site. However Kint indicated that Y204F was inhibited strongest, whereas Y204A and WT demonstrated a similar, less inhibited pattern. Finally, overall inhibition was significantly increased for both Y204F but was almost unaltered in Y204A FPPS mutant. A possible explanation for the increased inhibition for both Ale and Pam in Y204F but not in Y204A mutant might be the formation of novel van de Waals interactions between the positively charged amino group of Ale or Pam and the pi electron cloud of the Phe204 phenyl ring (Burley and Petsko, 1986) previously inhibited due to interference by the hydroxyl group (Figure 4.14). This theory would also explain the bigger decrease in Ki* for Ale, due to the difference in the length of the carbon chain, with the amino group of Pam being further

removed from the phenyl ring. Removal of the phenyl ring in the Y204A mutant results in abolition of these interactions and an increased Ki* for both Ale and Pam, almost restoring the latter back to that in the WT enzyme. The crystal structure of Pam with Y204A reveals the relevant position of the mutated residue regarding the nitrogen moiety of Pam and supports this hypothesis (Figure 4.14).

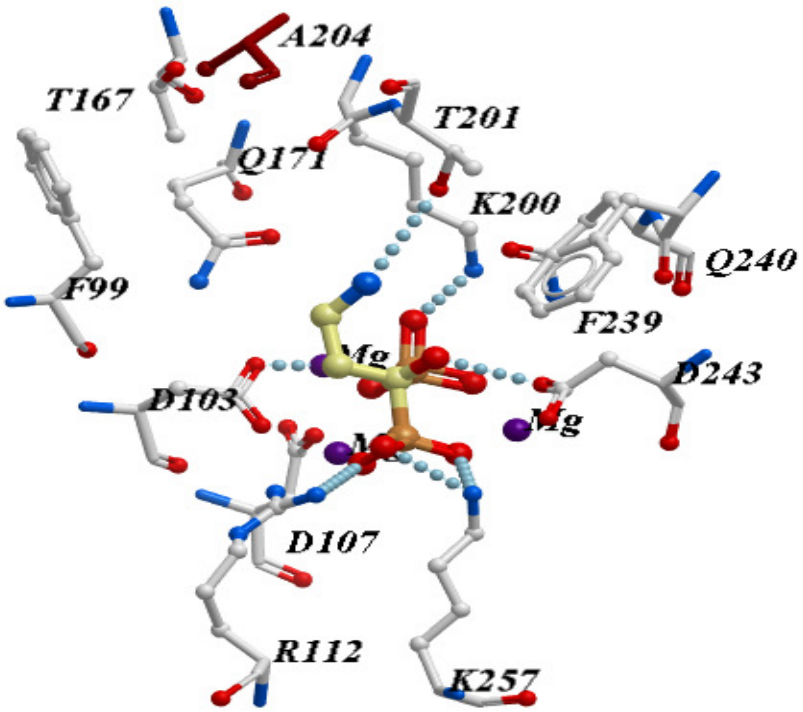


Figure 4.14: Formation of van der Waals interactions between the amino-group of Pam and mutated Tyr204 residue is not favoured in Y204A FPPS mutant, increasing the strength of inhibition. The position of Ala204 away from any functional group of N-BP does not allow any interactions that would increase the strength of inhibition.

Finally, in Y204F mutant all aminoalkyl N-BPs lose the ability to keep the enzyme in the closed conformation, as indicated by the decreased K_{isom}, but this is not the case in Y204A FPPS, where K_{isom} is comparable of that of WT (Table 4.4). It seems that the phenyl ring plays an active role in FPPS isomerisation effect and formation of the IPP binding site but not in N-BP binding.

4.6 CONCLUSIONS

All experiments described in this chapter aimed to elucidate the role of Tyr204 in FPPS catalysis and N-BP inhibition and led to some surprising results regarding the importance of tyrosine in FPPS catalysis. Tyr204 substitutions resulted in a K_m^{GPP} value comparable to that of the WT while they drastically increased the K_m^{IPP} and significantly decreased the k_{cat}. The inability of Tyr204 mutated FPPS constructs to achieve IPP saturation was attributed to improper formation of the IPP binding pocket and thus switch to a fully closed conformation upon substrate binding. The absence of hydroxyl moiety was considered responsible for the lost ability of FPPS to further push the IPP into the binding pocket and thus accounts for similar patterns of behaviour in both conservative and non-conservative mutations, demonstrating that the maintenance

of phenyl ring cannot preserve catalytic activity. This explanation also was supported by the pH studies, where activity of enzyme in both mutants was higher at low pH values, compensating for the lost protonation of the hydroxyl moiety. Furthermore, if abolition of a pKa point in Tyr204 mutants is attributed to the absence of tyrosine, this may explain the suppression of an ionization mechanism. Phenol rescue experiments failed to raise the catalytic activity by restoring the lost basic pka point, confirming the prevalent role of hydroxyl moiety over the phenyl ring in catalysis.

Investigation of the inhibition mode by clinical N-BPs resulted in several inhibition patterns which revealed the complexity of FPPS inhibition. Ris became a weaker competitive and tight binding inhibitor in Y204A FPPS but not in Y204F FPPS, indicating possible hydrophobic interactions of the phenyl ring with Ris that reinforces the strength of inhibition. However preservation of the phenyl ring failed to also preserve the K_{isom}, indicating reversibility of inhibition by Ris in Tyr204 mutants. Zol became a stronger inhibitor possibly due to alterations in the strength of the bifurcated hydrogen bond between Lys200: Thr201 and imidazole ring that allowed migration of the inhibitor deeper in the binding pocket. Some evidence of a possible allosteric regulation of FPPS by Zol that alters the binding ratio in FPPS mutants is also given from the investigation of the thermodynamic parameters governing its

mode of inhibition. The increased final inhibition of Ale and Pam in Y204F FPPS was also a result of the development of van der Waals/ electrostatic interactions between phenyl ring and nitrogen atom of N-BP, not present in the Ala mutant. A similar pattern of competitive inhibition was observed for Iba, whereas Ki* values were virtually unaffected, as predicted from the crystal structures.

In conclusion, the investigation proved the importance of the aromatic ring of Tyr204 in N-BP binding but not in catalysis, where the hydroxyl moiety seems to play an important role.

5. THE EFFECTS OF Lys200 FPPS MUTATIONS ON CATALYTIC ACTIVITY, CRYSTAL STRUCTURE AND N-BP BINDING

5.1 INTRODUCTION

Structural alignment of prenyltransferases among diverse species reveals that Lys200, along with Thr201 belongs to one of the seven highly conserved domains among species, named region V (Koyama *et al.*, 1993) (Figure 5.1). This region was shown to be involved in binding the allylic FPPS substrate in the chicken enzyme (Brems *et al.*, 1981) and therefore it was proposed that the putative role of Lys200 would be the fixation of the pyrophosphate moiety of GPP (Blanchard and Karst, 1993). The position of the Lys200 amino group in avian prenyltransferase suggests that it may participate in catalysis by activation of the diphosphate leaving group, and therefore subsequent stabilization of the carbocation intermediate and proton abstraction of C_2 of IPP (Tarshis *et al.*, 1996, Tarshis *et al.*, 1994).

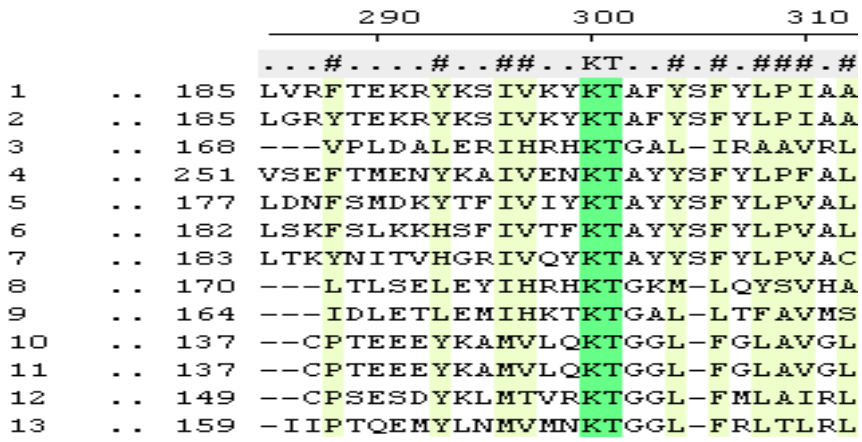


Figure 5.1: Sequence alignment of FPPS and GGPPS orthologs reveals that Lys200 and Thr201 are conserved among diverse species. Sequences of FPPS from 1: *Homo sapiens 2: Mus musculus* 3: *Escherischia coli*, 4: *Drosophila melanogaster*, 5: *Neurospora crassa,* 6: *Saccharomyces cerevisiae*, 7: *Zea mays* 8: *Trypanosoma brucei*, 9: *Staphylococcus aureus* and GGPPS orthologs 10: *H. sapiens* 11: *M. musculus* 12: *D. melanogaster* and 13: *S. cereviciae* were aligned with ICM pro, revealing the conserved Lys200 and Thr201 residues (in green).

The first indication for an active role for Lys200 in catalysis came from studies on *B. stearothermophilus*, where substitution of Lys200 with alanine significantly increased the K_m^{IPP} and strongly suppressed the K_{cat} confirming the Lys200 involvement in IPP binding and thus stabilization of the resulting carbocation intermediate (Koyama *et al.*, 1996). Hydrophobic interactions between the side-chain of Lys200 and the diphosphate moiety of DMASPP substrate analogue position its hydrocarbon tail in close proximity to IPP, facilitating generation of the carbocation in *E.coli* and *S. aureus* FPPS (Hosfield *et al.*, 2004). Studies with *H. sapiens*

FPPS demonstrated that although Lys200 does not appear to play an important role in the transition between the open, partially closed and closed FPPS conformations, it contributes to the octahedral coordination of tri-nuclear metal cluster, along with conserved aspartate side-chain groups and water molecules (Rondeau *et al.*, 2006). The carbonyl of Lys200 faces the central cavity and along with the conserved aspartate-rich motifs in helix 4 and 8, contributes to the formation of the hydrophobic ligand binding site. In the FPPS reaction mechanism proposed by Sanchez *et al.* (2006) the side chain of Lys200 forms a hydrogen bond with the O_7 atom of DMAPP and it is possibly involved in DMAPP fixation and correct orientation during catalysis (Figure 5.2). Heterolytic cleavage of C_1-O_7 DMAPP bond and polarization of the O_7 oxygen increases the basicity of the DMAPP and favours production of the carbocation intermediate and subsequent hydrogen abstraction from C_4 of IPP (Figure 1.8). In the scheme proposed by Kavanagh *et al.* (2006) (Figure 1.6), the carbocation intermediate generated upon DMAPP-IPP binding is stabilized through hydrophobic interactions with the carbonyl group of Lys200 and electrostatic interactions with the Mg:PPi moiety (Kavanagh *et al.*, 2006b, Rondeau *et al.*, 2006). In both schemes, the putative role of Lys200 is to stabilize the carbocation intermediate formed during the condensation of the two substrates

by assisting binding of IPP with the DMAPP: FPPS intermediate and not by promoting GPP fixation (Dunford *et al.*, 2008, Poulter and Rilling, 1976). An active participation of the positively charged Lys200 as a proton donor to the DMAPP or charge acceptor from the pyrophosphate moieties has been suggested (Koyama *et al.*, 1996), but more recent studies failed to confirm the active involvement of Lys200 in the catalytic mechanism (Sanchez *et al.*, 2006).

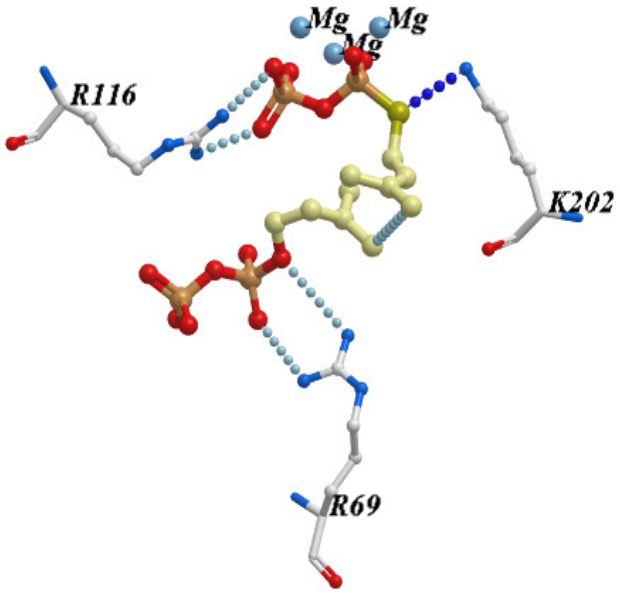


Figure 5.2: The hydrogen bond between the side chain of Lys202 in *E.coli* and O_7 atom of DMAPP contributes to the correct orientation of DMAPP substrate for catalysis. A) Upon heterolytic cleavage of C_1-O_7 DMAPP bond (shown here with S atom of the non-hydrolysable analogue DMASPP), the generated carbocation intermediate forms a C_1-C_4 bond with the IPP whereas Arg116 (in human Arg112), Arg69 (in human Arg67) form salt bridge interactions with the pyrophosphate moities of DMASPP and IPP respectively. The three Mg ions and water molecules (omitted here for simplicity) assist in substrate orientation. Figure adapted from pbd: 1RQI (Hosfield *et al.* 2006).

Studies with clinical BPs indicated that the carbonyl oxygen of Lys200, along with the hydroxyl residue of Thr201 aid in properly positioning the nitrogen atom of the N-BP in the allylic binding pocket (Kavanagh *et al.*, 2006b). Firm evidence about the role of Lys200 in N-BP binding comes from studies on *T. cruzi* FPPS crystal structure in complex with Ale, where the positively charged Lys200 forms a hydrogen bond with the third oxygen of one phosphonate, while the other two oxygen atoms form direct contacts with the Mg^{2+} ions (Figure 5.3)(Gabelli *et al.*, 2006). In turn, Mg^{2+} ions mainly interact with the FPPS protein through the conserved aspartate-rich motifs Asp104, Asp107 and Asp243, normally employed to interact with the allylic DMAPP/GPP substrate (Dunford *et al.*, 2008, Martin *et al.*, 1999). In all crystal structures of human FPPS with the five clinical N-BPs, Lys200, along with the conserved Arg112 and Lys257 form direct salt-bridge interactions with the N-BP moiety (Kavanagh *et al.*, 2006b, Rondeau *et al.*, 2006). The strength of Zol inhibition is strongly dependent on the successful formation of a bifurcated hydrogen bond between its protonated heterocyclic imidazole ring and the oxygen atoms of Lys200 and Thr201 (Rondeau *et al.*, 2006). The nitrogen atom of the heterocyclic ring of Ris is in close proximity (< 3 Å) to Lys200 and Thr201 and is therefore still capable of forming

hydrogen bonds with their carbonyl oxygens (Figure 5.4 A)(Kavanagh *et al.*, 2006b). The hydrogen bonding with Lys200 is absent in human FPPS complexes with Ale or Pam, but the hydrophobic interactions with the N-BP phosphonate groups persist. Finally, the N-methyl substituent of Iba is capable of van der Waals interactions with both Thr201 and Lys200 that reinforce the strength of inhibition (Rondeau *et al.*, 2006).

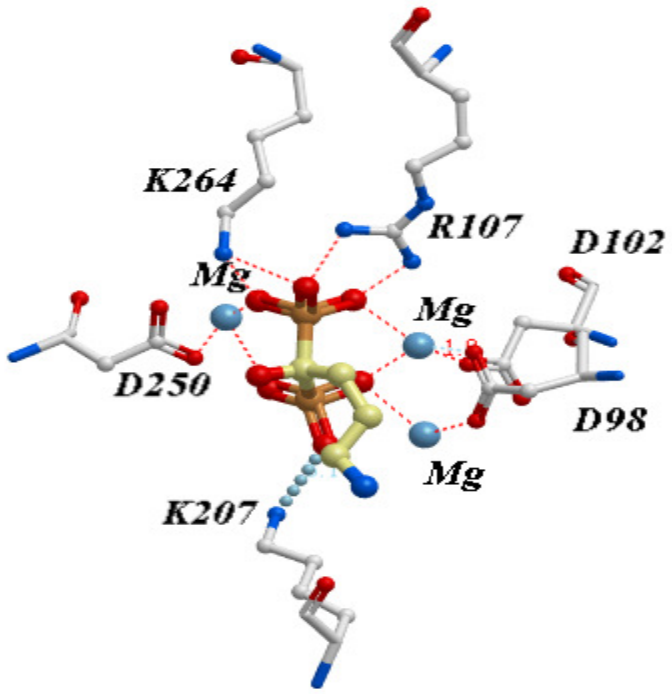


Figure 5.3: Formation of a hydrogen bond between the Lys207 (Lys200 in human) and the phosphonate oxygen of Ale in *T. cruzi* FPPS assists the N-BP binding to the allylic pocket. Specific polar interactions between Mg and phosphonate groups of Ale are denoted in orange lines. Water molecules are omitted for simplicity. Figure adapted from pdb:1YHM Gabelli *et al.* (2006).

The role of Lys200 in the FPPS catalytic mechanism and BP inhibition was investigated via generation of i) a lysine to leucine (K200L) mutant that should disrupt the phosphonate-enzyme interaction whilst preserving existing hydrophobic interactions (Figure 5.4 B) , ii) a lysine to glycine (K200G) mutant that would be unable to preserve hydrophobicity and disrupt phosphonate-enzyme interactions (Figure 5.4C) and iii) a lysine to glutamic acid (K200E) mutant that would reverse the polarity of the side-chain and should disrupt catalysis and abolish N-BP binding at this position (Figure 5.4D).

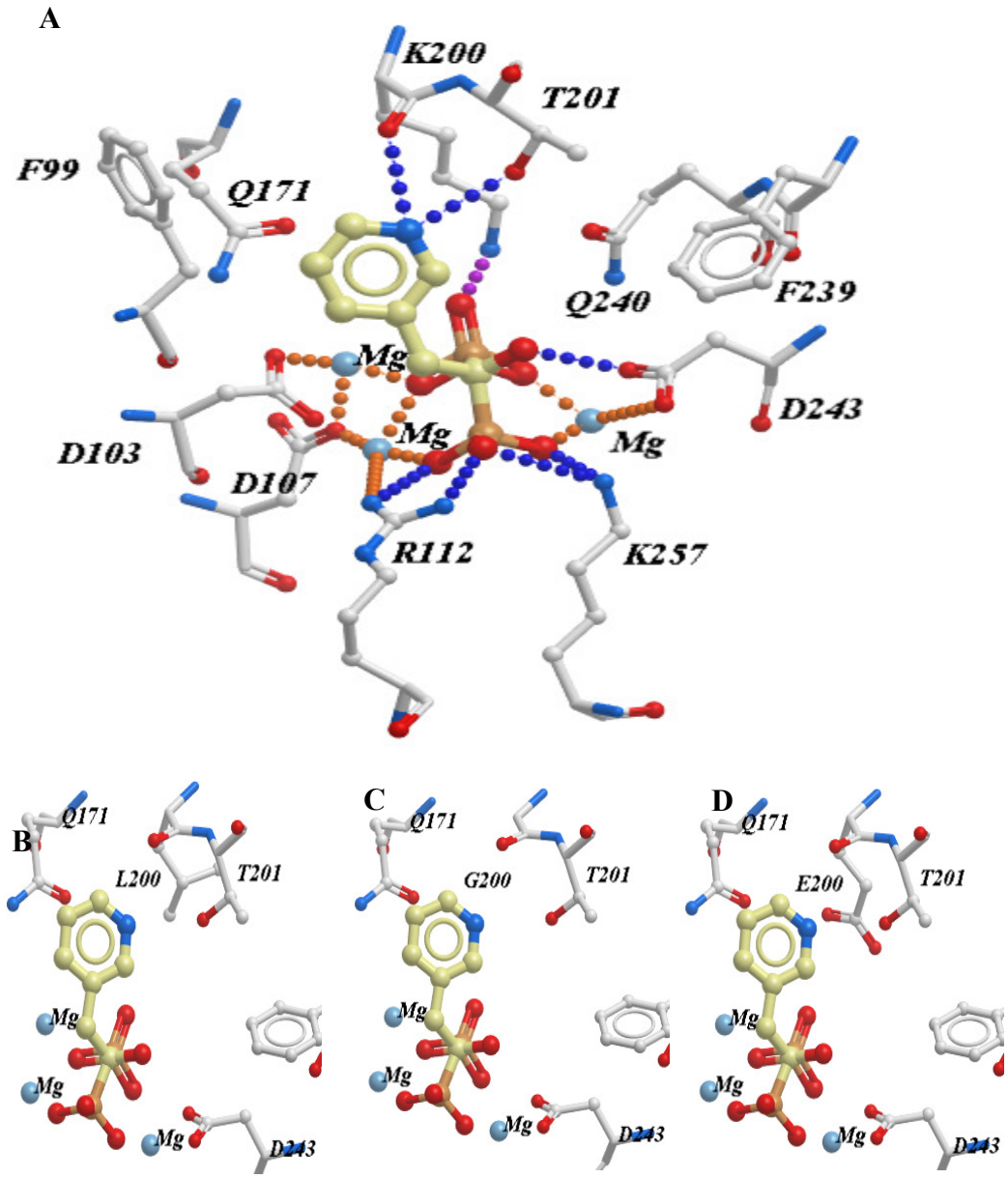


Figure 5.4: The proposed salt-bridge interactions of Lys200 with the phosphonate groups of N-BPs (in purple) are responsible for the strength of N-BP binding. A) Octahedral coordination of the three Mg ions is achieved via the conserved Asp103, Asp107 and Asp243, phosphonate oxygens and water molecules (omitted here for simplicity). Lys200, R112 and K257 form salt bridge interactions with the phosphonate moiety. Hydrophobicity of leucine side chain in K200L (B) should help maintain hydrophobic interactions whereas the apolar glycine in K200G (C) and negatively charged glutamic acid in K200E (D) substitutions should abolish them. Hydrogen bonds shown as blue spheres, phosphonate:Lys200 salt-bridge interaction as purple spheres and metal ion interactions as orange spheres. Figure adapted from pdb 2F89.

5.2 KINETIC CHARACTERIZATION OF LYS200 MUTANTS

Determination of kinetic parameters was carried out for the three purified Lys200 FPPS mutants (Table 5.1). K200G and K200L show saturation kinetics for the allylic substrate GPP comparable to that of the WT (Tukey post-hoc, $p>0.5$) whereas the K_m^{GPP} for K200E was significantly increased ($p<0.001$). The maintenance of K_m^{GPP} at physiological levels was predictable from all previous structural studies, illustrating the role of Lys200 in allylic substrate binding (Kavanagh *et al.*, 2006b, Sanchez *et al.*, 2006). All mutants show a similar alteration profile regarding IPP saturation, as the K_m^{IPP} was significantly increased ($p<0.001$), with the K200E FPPS construct presenting the most dramatic alteration; almost a 40-fold increase. The increase in K_m^{IPP} is in accordance with results of kinetic studies performed with *B. stearothermophilus* FPPS, where the highest K_m^{IPP} was observed with Lys57 and Lys200 substitutions while the K_m^{GPP} remained virtually unaltered (Koyama *et al.*, 1996).

Table 5.1: Kinetic parameters for FPPS WT, K200G, K200L and K200E. Results for K_m and k_{cat} are expressed as means +/- SEM, $n \geq 6$, $R^2 \geq 0.9$

	WT	**K200G**	**K200L**	**K200E**
K_m^{GPP} (μM^{-1})	2.07 ± 0.2	5.02 ± 0.6	1.94 ± 0.4	11.01 ± 1.6
K_m^{IPP} (μM^{-1})	1.8 ± 0.3	10.64 ± 1.7	42.19 ± 6.8	85.26 ± 14.3
k_{cat} (s^{-1})	0.385 ± 0.015	0.0033 ± 0.0002	0.0072 ± 0.0007	0.009 ± 0.001
k_{cat}/K_m^{IPP} ($\mu M^{-1}/s^{-1}$)	0.6	0.000313	0.000171	0.00011

Such alterations in the kinetic profile were predictable for the K200G mutant, as substitution of Lys with an apolar aminoacid such as glycine should not result in a substantial alteration of GPP saturation kinetics, as already shown when K200 was replaced with an the neutral Ala in *B. stearothermophilus* by Koyama *et al.* (1996). However the K200G point mutation, similarly to K200A substitution, caused a 5-fold increase in K_m^{IPP}, confirming the proposed role of Lys200 in assisting binding of the diphosphate moieties of IPP (Koyama *et al.*, 1996). In this case GPP generation and subsequent FPP formation is not compromised (Figure 5.5.C).

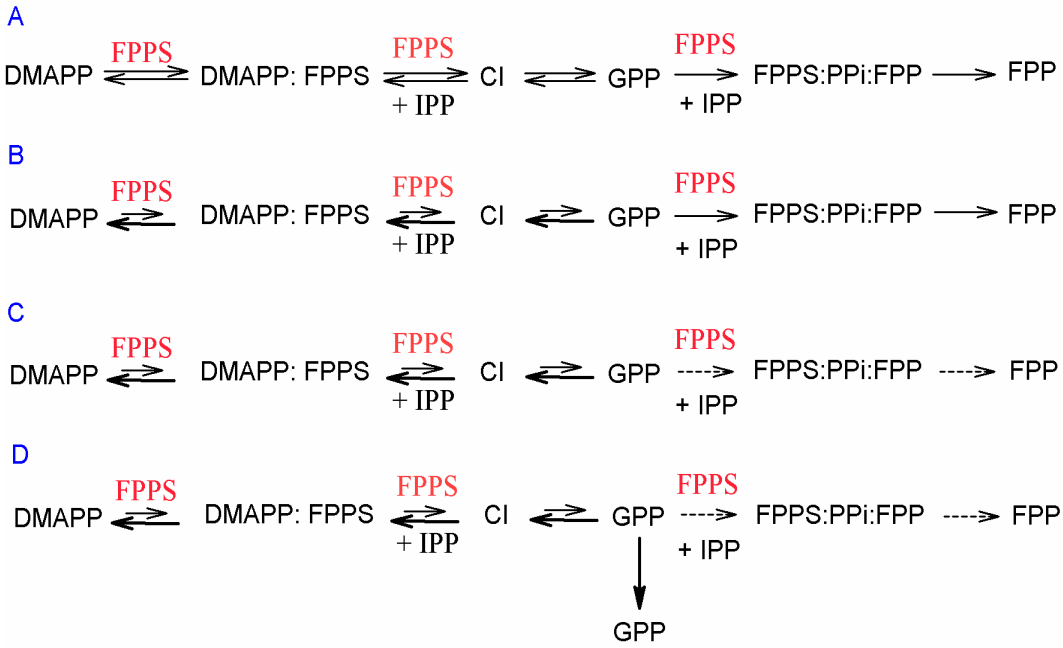


Figure 5.5: Possible effects of Lys200 substitution in substrate binding and product release from FPPS. A) Heterolytic cleavage of C_1-O_7 DMAPP bond by WT FPPS generates a carbocation intermediate (CI) which condenses with the IPP and liberates GPP. A second condensation of GPP with IPP generates the final product FPP. B) In K200G FPPS, loss of electrostatic attraction between the mutated Lys and O_7 oxygen of DMAPP results in misalignment of DMAPP substrate and decreased affinity for the first IPP binding, shifting the equilibrium to the left hand site and thus decreasing catalysis without affecting FPP product formation. C) In K200L FPPS, reduced ability of the enzyme to bind the homoallylic substrate results in slower catalytic rate and impaired FPP synthesis, without compromising GPP liberation. D) In K200E FPPS, decreased affinity for both IPP and GPP substrates shifts the equilibrium of the reaction to the left hand site, with a possible accumulation of GPP product that might lead to inability to condense with GPP and form FPP altering the end product of reaction.

Similarly, substitution of Lys with the hydrophobic Leu helps to maintain the side chain of Leu residue in the hydrophobic allylic binding pocket and thus does not alter GPP binding. The raised

K_m^{IPP} value indicates reduced ability of FPPS to recognize and bind the homoallylic substrate, compromising FPP product synthesis (Figure 5.5 D). This effect might be attributed to impaired ability of enzyme to bind DMAPP due to abolition of the Lys positive charge that results in loss of electrostatic attraction between DMAPP and FPPS enzyme. Subsequent proton abstraction from the C_2 atom of IPP and IPP binding to the carbocation intermediate is obstructed, without any impairment in GPP formation and liberation.

Finally substitution of the positively charged Lys with the negatively charged Glu dramatically alters the affinity for both allylic and homoallylic substrates possibly by disruption of the C_1-O_7 hydrogen bond between FPPS and DMAPP as proposed by Sanchez *et al.* (2006). The resulting dislocation of the DMAPP due to the repulsion generated by the negatively charged Glu, prevents subsequent IPP binding and therefore results in decreased catalysis and impaired GPP production. In addition, failure of the formed carbocation intermediate to properly attack the C_4 carbon of IPP might also inhibit the hydrogen transfer from the formed GPP to the leaving pyrophosphate group, blocking liberation of GPP or its subsequent condensation with IPP. Furthermore, the remarkable decrease in IPP affinity of the K200E mutant might be a cause of GPP accumulation (Koyama *et al.*, 1996), with a concomitant selective suppression of the isoprenoid C_5-C_{10}

elongation step (Blanchard and Karst, 1993). Similarly, the decrease in GPP affinity observed in K200E FPPS, might result in accelerated release of GPP from the enzyme, simultaneously compromising FPP synthesis. If both effects are combined the major end product of the reaction would be GPP rather than FPP (Figure 5.5 D). However, accumulation of GPP should only occur if the Lys200 residue is directly implicated in GPP product release and does not necessarily derive from an inability to saturate the FPPS with either IPP or GPP substrate. A characteristic example is substitution of K200E in yeast FPPS where accumulation of GPP does not occur and thus product specificity is unaltered (Plochocka *et al.*, 2000). Chromatographic analysis of the reaction products by HPLC/mass spectrometry should be employed to investigate the issue further but is beyond the scope of the present study.

Mutagenesis significantly suppressed the catalytic activity of all Lys200 constructs and it was hence necessary to increase both enzyme concentration and incubation time in the FPPS assay in order to accurately calculate the reaction rates. Replacement of the highly conserved positively charged Lys with a non-charged residue, should drastically reduce the catalytic activity of the enzyme. This was indeed the case in the K200G substitution, where K_{cat} was suppressed by almost 100- fold. Since Gly occupies a smaller volume than Lys, it permits accommodation of either

GPP or IPP in the binding pocket, negatively influencing the FPPS selection for substrate specificity. Alteration of the size of the binding pocket in the active site may allow binding of two molecules of IPP, altering the isoprenoid product length (Plochocka *et al.*, 2000, Tarshis *et al.*, 1996, Tarshis *et al.*, 1994). Suppression of K_{cat} was less dramatic in the K200L and K200E mutants with 50-fold and 40-fold decrease in K_{cat} respectively when compared to the WT.

The K_{cat} value is calculated based on the V_{max} observed in relationship to the IPP turnover and does not take into account changes in substrate saturation. Since Lys200 mutations raise the K_m^{IPP} and at the same time lower the K_{cat} but with a different fold, change, the K_{cat}/K_m^{IPP} ratio is useful to collectively assess the effect of the specific mutation (Koshland, 2002). When all K_{cat}/K_m^{IPP} ratios were compared, catalysis by the K200E FPPS construct appears to be the most compromised; with K200L showing a similar decrease and K200G showing 2 to 3- fold higher activity compared to both K200E and K200L. As Glu has a negative charge, it is positioned at the far end of the allylic binding pocket and therefore unable to interact with DMAPP or IPP, hence the catalytic activity is lowered. A similar effect on catalysis is observed with the K200L substitution, as Leu lacks the ε-amino group of Lys which is considered responsible for stabilization of the carbocation

intermediate and facilitation of C_2 deprotonation of IPP (Plochocka *et al.*, 2000, Tarshis *et al.*, 1996). Finally substitution with Gly does not allow maintenance of residue hydrophobicity or electrostatic interactions and catalysis is also suppressed. However in all Lys substitutions catalysis still occurs albeit at a rate substantially slower than that observed in Tyr204 substitutions (Table 4.1). This scenario seems to be a fairer representation of the catalytic effect of Lys200 mutations, as there is no specific indication for a pivotal role of this residue in catalysis and the observed suppression arises from the impaired IPP binding, leading to GPP liberation and decreased FPP synthesis, rather than a deficiency in the catalytic mechanism.

5.3 CRYSTAL STRUCTURES OF K200G AND K200L FPPS MUTANTS SUPPORT THE KINETIC FINDINGS REGARDING SUBSTRATE SATURATION

A statistically increased K_m^{IPP} was calculated for all Lys200 FPPS mutants and was attributed to disruptions of different stages of the catalytic mechanism. The mildly elevated K_m^{IPP} in K200G possibly arose from misalignment of DMAPP substrate and the inability of the enzyme to recognize and bind the first IPP molecule,

without possible disruptions of the homoallylic binding site that would affect the second IPP binding event and thus FPP formation. However, enlargement of the allylic binding site due to the presence of the small sized Gly could decrease the enzyme binding specificity for GPP, permitting accommodation of IPP instead. In the K200L mutant a possible disruption in the formation of the homoallylic binding pocket should obstruct GPP formation and subsequent binding of the second IPP molecule. On the contrary, maintenance of hydrophobicity due to the presence of Leu should not alter the size of the allylic pocket or the specificity for GPP binding. Structural studies were employed to spot any alterations in FPPS conformation that would support any of the proposed theories.

The crystal structure of K200G in complex with Ris reveals a shifting of the normally well orientated C-terminal lid, with a calculated minimum RMSD of 0.59 Å of ^{347}KIY^{349}, indicating an inability of the enzyme to switch to the closed conformation and thus stabilize the bound IPP to the homoallylic pocket (Figure 5.6). This is accompanied by a shifting in position of the main amino-acids taking part in stabilization of the fully closed conformation: Lys57 and Arg60 but not the amino-acids that contribute to the stabilization of the partially closed conformation such as Asp104, Asp107, Asp174 and Lys266 (Figure 5.7). Unfortunately, the

failure to co-crystalize K200G FPPS with IPP limits our understanding regarding the IPP orientation to the pocket which may also account for the increased K_m^{IPP}. However, prediction of possible binding pockets with the ICM software revealed no alteration in IPP binding, confirming that the absence of the positively charged Lys200 does not affect IPP orientation to the homoallylic pocket (data not shown).

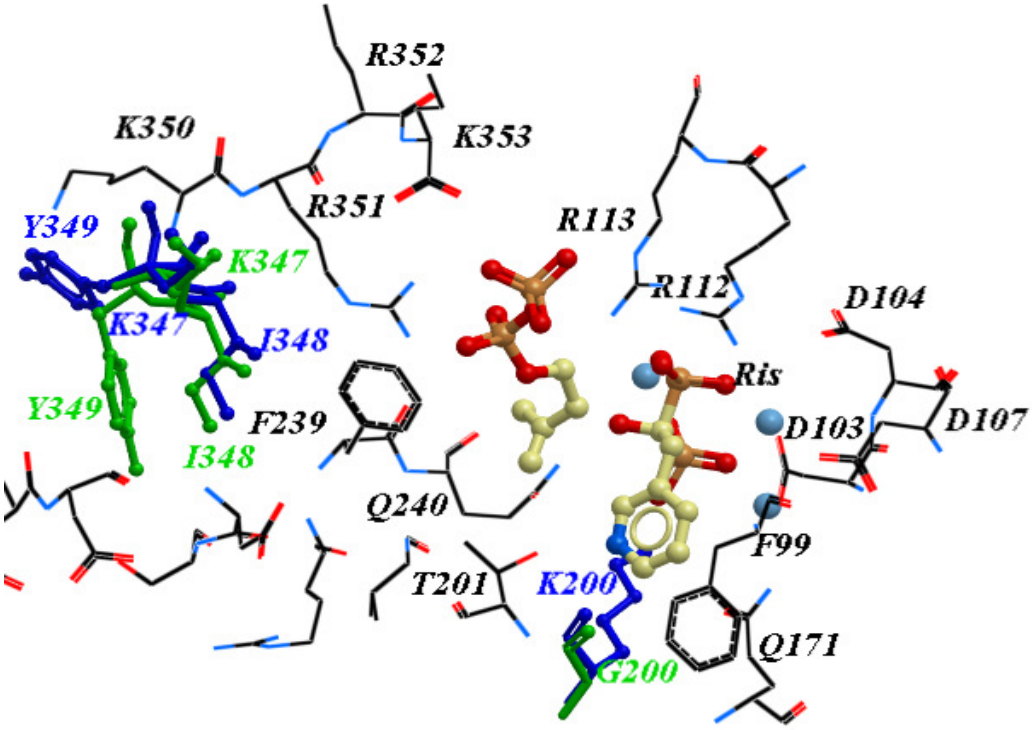


Figure 5.6: Alteration of C-terminal basic tail positioning in K200G FPPS reveals destabilization of the fully closed conformation. The ^{347}KIY^{349} section of hydrophobic tail is shifted away from the IPP binding site by 0.59 Å whereas the positions of IPP and Ris remain unaffected by the mutation. In WT FPPS, IPP and affected residues are labeled in blue, in F239A FPPS IPP and residues are labeled in green, Mg in light blue spheres. WT adapted from pdb: 1ZW5 (Rondeau *et al*. 2006)

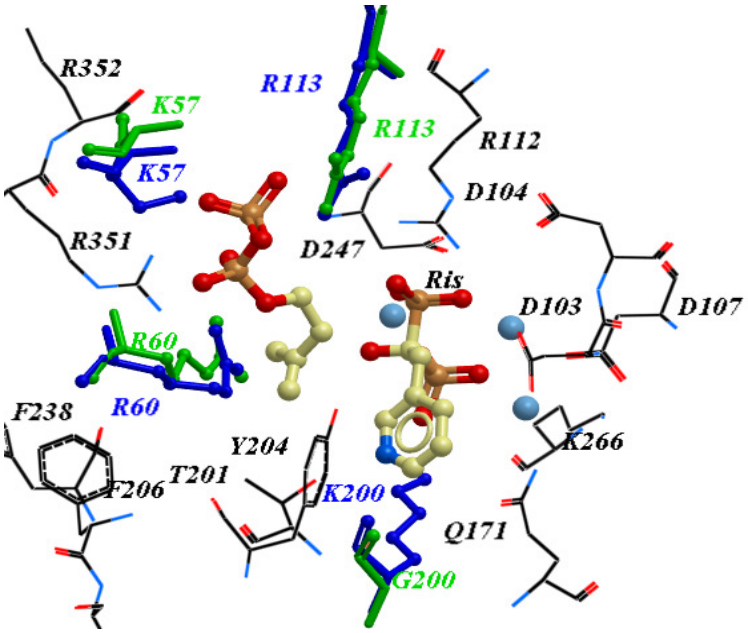


Figure 5.7: Destabilization of the closed but not partially closed conformations in K200G FPPS. Shifting of Lys57, Arg60 and Arg113, along with the amino-acids of the C-terminal tail destabilized the closed conformation in K200G FPPS. However the position of Asp103, Asp104, Asp107 and Lys266 that stabilize the partially closed conformation is unaffected. In WT FPPS, IPP and residues are labeled in blue, in K200G FPPS IPP and residues are labeled in green, Mg in light blue spheres. WT adapted from pdb: 1ZW5 (Rondeau *et al.* 2006).

The most important finding from the K200G mutation is the dramatic alteration observed in the allylic binding pocket size, calculated by ICM software to be approximately 528 Å^3 for the WT but increased to 722 Å^3 for the K200G FPPS mutant. This predictable increase in size can strongly compromise the ability of the mutated enzyme to distinguish between allylic and homoallylic substrate that may lead to the binding of longer isoprenoid

residues to the DMAPP/GPP pocket, concomitantly decreasing the IPP or GPP/DMAPP affinity for their respective sites.

On the contrary, the size of the allylic binding pocket and the position of amino-acids that play part in GPP binding or stabilization of the partially closed and closed conformation remained unaltered in the K200L crystal structure in complex with Ris and IPP. Similarly the IPP position and orientation regarding the Ris was comparable to that of the WT. The only predicted alteration in K200L FPPS structure would be the orientation of DMAPP, however lack of X-ray data with the DMAPP and IPP makes it impossible to draw any conclusions regarding the rupture of the proposed hydrogen bond.

5.4 INVESTIGATION OF THE INHIBITION MODE OF LYS200 FPPS MUTANTS BY N-BPs

The mode of Lys200 FPPS inhibition by N-BPs was assessed at different time points, chosen on the basis of their individual kinetic behaviour (Table 5.2). For K200G, Ki was calculated from data obtained at 3 min incubation, which was the minimal time where activity of the enzyme was measurable and thus should account for the competitive inhibition of GPP binding by N-BP. However,

the data was subject to increased variability due to the low activity of the enzyme. Initial activity was also calculated after 5 and 7 min incubation and since these rates did not change substantially from the 3 min values, K_{isom} was calculated from data obtained after a 7 min incubation period which gave the most accurate time-points without significantly altering the result. As K200L and K200E showed similar inhibition profile, initial rate data were calculated after 5 min incubation, as 3 min incubation yielded statistically inaccurate values due to low incorporation of radioactivity into the product. All statistical comparisons of initial activities between WT and Lys200 mutants were performed using the 3 min WT data and not the corresponding 5 min or 7 min time points, as these would represent intermediate inhibition rate data for the WT enzyme. Finally for all mutants, Ki* was calculated after the standard 10 min pre-incubation of enzyme with the inhibitor, which accounts for the maximal inhibition achieved with N-BP after isomerization takes place and did not alter significantly after that period of time (data not shown).

Table 5.2 Estimation of Ki, Ki* and Kisom of WT and Lys200 mutants derived from inhibition assays with N-BPs. Initial inhibition constant (Ki) values were obtained when inhibition assays were initiated by the addition of enzyme and 3 min, 5 min or 7 min incubation whereas final Ki (Ki*) was calculated when enzyme was pre-incubated with BP for 10 minutes and the reaction started by the addition of substrate. The constants obtained were then corrected for the affinity for GPP as described in section 2.25. K_{isom} was calculated from Ki and Ki* as described in section 2.25. ND: not determined. Results are expressed as means $^{+/-}$SEM, $R^2 > 0.95$ and $n \geq 6$. Negative values are denoted in red.

BP	Construct	Ki (nM)	Ki* (nM)	K_{isom} (GPP)	K_{isom} (IPP)
Ris	WT	56.6 ± 3.1	0.8 ± 0.06	69.3	82
	K200G	99.9 ± 17.8	62.8 ± 16.3	0.6	2.3
	K200L	47.9 ± 6.3	74.3 ± 10.4	-0.4	2.4
	K200E	393.2 ± 52.3	621.5 ± 66.4	-0.4	5
Zol	WT	62.9 ± 5.1	0.06 ± 0.03	1076.9	1271
	K200G	36.6 ± 24.4	ND	ND	ND
	K200L	42.6 ± 5.4	34.2 ± 5.2	0.2	5.5
	K200E	63.8 ± 14.5	54.2 ± 12.7	0.2	10.2
Iba	WT	207.7 ± 13.4	4.6 ± 0.4	44.1	52.3
	K200G	22.7 ± 6.2	20.7 ± 7.6	0.1	1.3
	K200L	116.5 ± 10.6	142.1 ± 14.6	-0.2	3.3
	K200E	132.7 ± 17.1	91.5 ± 30.8	0.5	12.8
Ale	WT	388.3 ± 31.3	56.5 ± 4.9	5.9	7.1
	K200G	276.4 ± 31.6	82.3 ± 12.2	2.4	5.9
	K200L	173.3 ± 14.6	235 ± 17	-0.3	2.8
	K200E	1101.5 ± 105.2	1440.1 ± 142.3	-0.2	6.3
Pam	WT	181.5 ± 6	51.9 ± 3.3	2.5	3.1
	K200G	460.4 ± 38.8	72.6 ± 12.6	5.3	12.1
	K200L	8552.4 ± 906.7	3717.4 ± 505.5	1.3	11
	K200E	15223.3 ± 1339	38452.7 ± 3776	-0.6	2.8

The shift in potency from the competitive, initial stage to the final isomerized state was assessed using the K_{isom}, which was corrected for K_m^{GPP}, as the affinity for the allylic substrate remained unaltered in WT and Lys200 mutants whereas K_m^{IPP} was significantly increased. In some cases where negative values were generated due to a decrease in inhibition with time, K_m^{IPP} was also provided as a second point of comparison. Different patterns of inhibition were observed with each of the five clinical N-BPs and some are examined in more detail in the individual sections below.

5.4.1 Inhibition by heterocyclic N-BPs does not support the importance of the hydrogen bond between N:BP-Lys200 for inhibition

The heterocyclic ring structures of Ris and Zol are positioned in a hydrophobic environment mainly generated by surrounding side-chains of residues Phe99, Leu100, Thr167, Lys200 and Tyr204 and their nitrogen atom is found within hydrogen-bonding distance of the Thr201 oxygen and the carbonyl oxygen of Lys200 (< 3.0 Å)(Kavanagh *et al.*, 2006b). Furthermore, direct electrostatic interactions between the side-chain amino-group of Lys200 and the phosphonate group of Ris or Zol possibly assist in N-BP binding (Rondeau *et al.*, 2006). It was therefore suggested that any alteration of the highly conserved Lys200 should disrupt the

phosphonate- Lys200 interaction but not the nitrogen- Lys200 hydrogen bonding and thus decrease the inhibition. Different patterns were observed for Ris and Zol inhibition, possibly arising from the diverse nature of the heterocyclic ring and not from disruption of the electrostatic interactions-hydrogen bonding.

As expected, final inhibition by Ris was strongly suppressed in all Lys200 mutants, whereas initial inhibition was only altered for K200E FPPS (Table 5.3). Such an alteration of inhibition pattern by Ris is easy to explain. In the case of K200L mutant, hydrophobicity of the allylic binding pocket is maintained, favouring binding of the heterocyclic ring of Ris in the DMAPP/GPP site. In the K200G mutant, the neutral glycine does not promote hydrophobicity nor is capable of changing the nature of the hydrophobic binding pocket. Consequently, binding of Ris is less favoured in K200G than K200L, but still occurs. In both cases, orientation of the heterocyclic ring of Ris is maintained, possibly due to the presence of Thr201 hydrogen bonding, despite of the weakening of Lys200-Ris hydrogen bonding (from 3 Å in 3.2 Å in K200G and 3.5 Å in K200L FPPS) (Figure 5.8) and competitive inhibition remains virtually unaffected. A similar situation occurs in T201A mutation, where disruption of Thr201 hydrogen bond does not alter Ris inhibition pattern (Dunford, Tsoumpra *et al.*, unpublished data).

Finally, the Ki and Ki* produced by Ris were both significantly increased in the K200E mutant (Table 5.3), as predicted from the alteration of the hydrophobic environment due to replacement of the positively charged lysine that does not support accommodation of the heterocyclic ring of Ris. If the increase of both K_m^{GPP} and K_m^{IPP} leads to GPP accumulation, then GPP could have higher affinity for the DMAPP/GPP hydrophobic pocket, whereas Ris would be unable to compete with the excess GPP for the allylic binding site, thus markedly increasing the Ki. Even in the case of GPP displacement by Ris and subsequent Ris binding to the allylic site, the reduced affinity for IPP would disrupt proper shifting of the C-terminal hydrophobic tail and thus the EI* isomerization status would not be favoured (Section 3.3). This is the case in K200E FPPS mutant, as K_{isom} is strongly suppressed, indicating reversibility of inhibition. The increased K_m^{IPP} value in K200E and K200E mutants, mainly generated as the result of the inability of the enzyme to bind the second IPP molecule, might be another factor that affects Ki* and $K_{isom,}$ as the isomerization step that can only occur upon proper IPP binding, which enhances fixation of ligands and sequesters the site from bulk solvent (Kavanagh *et al.*, 2006b).

Table 5.3: Comparison between WT and Lys200 mutants Ki and Ki* rates produced by Ris and Zol. Data were analyzed for significance with one way ANOVA and Tukey post –hoc test as grouped below.

Group of comparison	Construct 1	Construct 2	1 vs 2 Ris	1 vs 2 Zol
K200G Ki & ki*	K200G Ki	K200G Ki*	No difference	>>(p <0.001)
K200L Ki & Ki*	K200L Ki	K200L Ki*	No difference	No difference
K200E Ki & Ki*	K200E Ki	K200E Ki*	< (p <0.05)	No difference
All constructs Ki	K200G Ki	WT Ki	No difference	No difference
	K200G Ki	K200L Ki	No difference	No difference
	K200G Ki	K200E Ki	< (p <0.001)	No difference
	K200L Ki	WT Ki	No difference	No difference
	K200L Ki	K200E Ki	< (p <0.001)	< (p <0.05)
	K200E Ki	WT Ki	> (p <0.001)	No difference
All constructs Ki*	K200G Ki*	WT Ki*	> (p<0.001)	<<(p <0.001)
	K200G Ki*	K200L Ki*	No difference	<<(p <0.001)
	K200G Ki*	K200E Ki*	< (p <0.001)	<<(p <0.001)
	K200L Ki*	WT Ki*	> (p <0.001)	> (p <0.01)
	K200L Ki*	K200E Ki*	< (p <0.001)	No difference
	K200E Ki*	WT Ki*	> (p <0.001)	> (p <0.001)

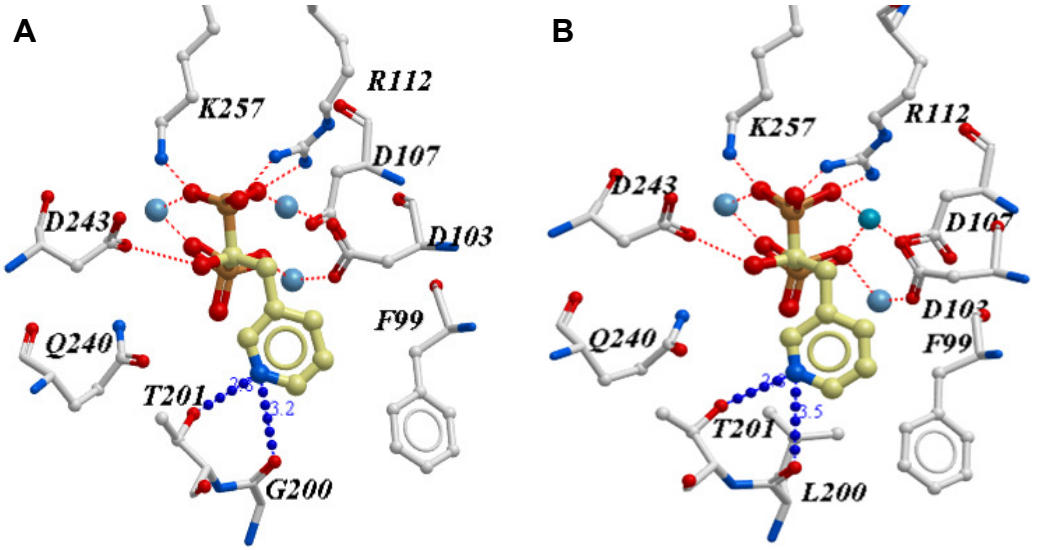


Figure 5.8: Orientation of heterocyclic ring of Ris and its positioning in the allylic binding pocket is unaffected in K200G (A) and K200L (B) mutants. Disruption of the Lys200 salt-bridge interactions with the phosphonate group of Ris and weakening of the Lys200 hydrogen bond with the nitrogen atom of Ris in K200G (A) and K200L (B) but maintenance of the Thr201: Ris hydrogen bond allows correct orientation of the heterocyclic ring of Ris.

Surprisingly, no significant alterations were observed in competitive inhibition of Lys200 mutants by Zol, indicating that possible weakening of the hydrogen bond of Lys200 with the imidazole ring and abolition of electrostatic interaction between Lys200: phosphonate moiety does not affect GPP displacement or drug binding. This result agrees with mutation studies on FPPS Thr201, where mutation of the residue in T201A disrupts the hydrogen bond between Thr201 and Zol, but does not affect competitive inhibition (Dunford, Tsoumpra *et al.* unpublished data). These observations when combined demonstrate that

conservation of one of two hydrogen bonds formed by Lys200 or Thr201 is sufficient to maintain proper orientation of the imidazole ring and thus any possible alteration in inhibition pattern has probably its root elsewhere. The crystal structure of Zol with T201A supports this hypothesis (Figure 5.9).

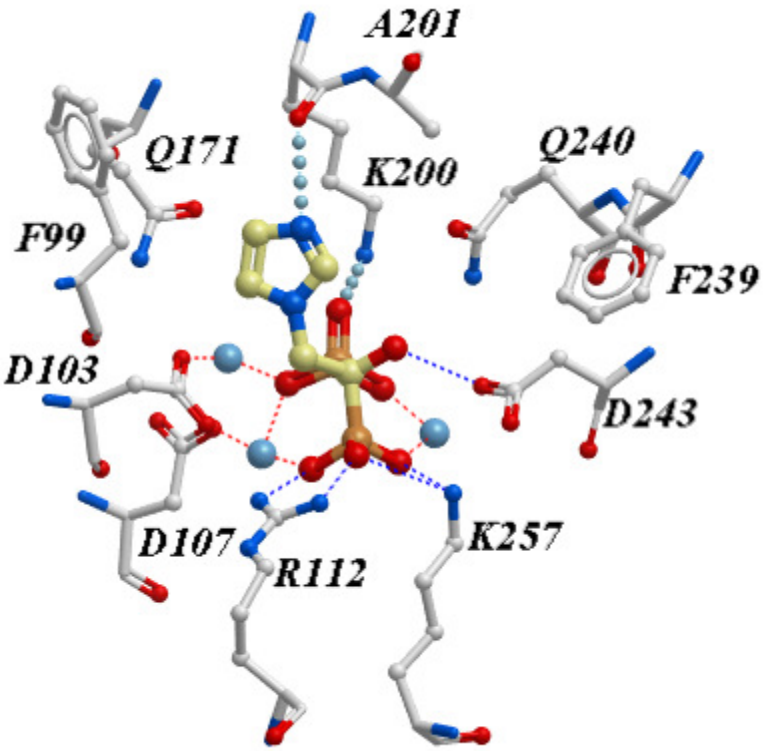


Figure 5.9: Maintenance of Lys200: FPPS hydrogen bond in T201A mutant is sufficient to properly position the imidazole ring of Zol in the allylic binding pocket. In T201A mutant, abolition of the Thr201 hydrogen bond with Zol does not alter the position of imidazole ring, as electrostatic interactions of surrounding residues with pyrophosphate moiety (blue dashed lines) and salt bridge interactions (orange dashed lines) with Mg ions (blue spheres) properly orientate Zol to the binding pocket.

Final inhibition by Zol is equally suppressed in K200L and K200E FPPS mutants but is increased in K200G mutant (Table 5.3), leading to deviation from the Morrison's 1:1 binding model, as was observed in Tyr204 mutants (Section 4.5.2). Again, the decrease in Ki* in K200L/K200E can be attributed to the high IPP concentration and disrupted enzyme isomerization, as described above for Ris. The increase in the binding pocket size in K200G mutant, might allow proximity of Zol to the hydrophobic binding pocket, thus re-enforcing the existing hydrogen bond/electrostatic interactions between the imidazole ring and surrounding residues and promoting Zol fixation to the binding pocket.

5.4.2 Inhibition by the amino-alkyl bisphosphonates reveals the importance of Lys200 for enzyme isomerization

Inhibition patterns were examined for all amino-alkyl N-BPs and relevant comparisons were drawn regarding the effect of mutation in Ki, Ki* and K_{isom} (Table 5.4).

Table 5.4: Comparison between WT and Lys200 mutants Ki and Ki* rates by Iba, Ale and Pam. Data were analyzed for significance with one way ANOVA and Tukey post – hoc test as grouped below.

Group of comparison	Construct no 1	Construct no 2	1 vs 2 Iba	1 vs 2 Ale	1 vs 2 Pam
K200G Ki & Ki*	K200G Ki	K200G Ki*	unaltered	> (p <0.001)	> (p <0.05)
K200L Ki & Ki*	K200L Ki	K200L Ki*	unaltered	< (p <0.05)	> (p <0.001)
K200E Ki & Ki*	K200E Ki	K200E Ki*	unaltered	unaltered	> (p <0.001)
All constructs Ki	K200G Ki	WT Ki	< (p <0.001)	unaltered	unaltered
	K200G Ki	K200L Ki	< (p <0.001)	unaltered	< (p <0.001)
	K200G Ki	K200E Ki	< (p <0.001)	< (p <0.001)	< (p <0.001)
	K200L Ki	WT Ki	< (p <0.01)	unaltered	> (p <0.001)
	K200L Ki	K200E Ki	unaltered	< (p <0.001)	< (p <0.001)
	K200E Ki	WT Ki	< (p <0.05)	> (p<0.001)	> (p <0.001)
All constructs Ki*	K200G Ki*	WT Ki*	unaltered	unaltered	unaltered
	K200G Ki*	K200L Ki*	< (p <0.001)	unaltered	unaltered
	K200G Ki*	K200E Ki*	< (p <0.05)	< (p<0.001)	< (p <0.001)
	K200L Ki*	WT Ki*	> (p <0.001)	unaltered	unaltered
	K200L Ki*	K200E Ki*	unaltered	< (p <0.001)	< (p <0.001)
	K200E Ki*	WT Ki*	> (p <0.01)	> (p <0.001)	> (p <0.001)

In case of Iba, competitive inhibition was increased in all mutants, indicating that displacement of GPP is favoured in Lys substitutions. Considering the positioning of the n-pentyl group of Iba in the FPPS interface, where normally the growing isoprenoid chain binds, any product disruption in FPPS catalysis would result in decreased affinity of the binding pocket for the isoprenoid

products, thus favouring their displacement by the long hydrophobic side-chain of Iba. In K200G, the enlargement of the isoprenoid binding pocket allows better accommodation of the long Iba side-chain which displaces GPP from the binding site. In K200L, the decreased affinity for IPP compromises the rate of GPP synthesis, reducing its availability for competition with Iba. Finally in K200E, a combination of the high K_m for GPP and IPP disrupts GPP formation and liberation, favouring Iba binding. Since the methyl group of Iba confers rigidity and prevents rotation of the side-chain, any adopted conformation once bound to the pocket would be securely preserved in Lys200 FPPS mutants.The significant increase in Ki* for K200L and K200E but not in K200G can be attributed to decreased IPP binding and thus shifting of the reaction towards the non-isomerized state, favouring reversibility. Furthermore, the increased Ki* for K200G, despite not being statistically different from that of the WT, indicates that disruption of existing van der Waals interactions upon Lys200 substitution might also contribute in decreased final inhibition of all K200G constructs.

Having established that hydrophobicity of the binding pocket is far more important than hydrogen bonding between N-BP and Lys200 in the maintenance of inhibition by heterocyclic bisphosphonates, the absence of such hydrogen bond between Ale

or Pam and Lys200 cannot account for any decreased inhibition observed. With Ale, Ki and Ki* was significantly increased for K200E but remained statistically unchanged for K200G and K200L mutants, albeit somewhat decreased in K200L. However the most impressive results were obtained with quantification of Pam inhibition, as Ki and Ki* were both unaltered in K200G, suppressed in K200L and inhibition was effectively abolished in the K200E mutant. A similar pattern of inhibition was expected for Ale and Pam, however the remarkably high Ki and Ki* values of K200E with Pam are difficult to explain. In the absence of a crystal structure of any mutant with Ale or Pam we can only speculate about the structural alterations that could account for the remarkable difference in inhibition pattern. Glycine is an apolar aminoacid whereas Leu maintains the residue hydrophobicity but neither substitution has the potential of altering the interaction between the enzyme and the hydrophilic ionizable amino-group of either Ale or Pam, thus inhibition remains virtually unaffected. The reversal in polarity resulting from K200E substitution alters the inhibition profile for both Ale and Pam, as Ale is a more flexible molecule than Pam due to presence of the additional carbon-carbon bond that allows greater rotation of the side-chain amino group, its inhibition is less suppressed in K200E.

As a consequence of an increased Ki or Ki*, K_{isom} was decreased in all mutants, indicating the importance of Lys200 for enzyme isomerization.

5.5 CONCLUSIONS

The Lys200 mutant studies have proven to be very useful in further elucidating the complicated ionization-condensation-elimination FPPS catalytic mechanism as well as the main interactions of the N-BPs with the allylic binding pocket. All Lys200 substitutions confirmed that maintenance of hydrophobicity of the binding pocket is essential for substrate binding and FPP generation. Any alteration in the polarity of the amino-acid in this position has a negative effect on DMAPP orientation and binding. This effect is more severe when polarity is reversed, as binding of the IPP molecule is also compromised with a concomitant effect on GPP liberation and accommodation in the isoprenoid lipid binding pocket. Defective GPP or IPP binding is a result of individual alterations or a combination in the following: allylic binding pocket size, breakage of hydrogen bond between DMAPP and Lys200, IPP misplacement in the homoallylic binding pocket, C-terminal shifting. In the case of K200E mutant, GPP

defective binding may lead to reversibility of reaction with a possible alteration of catalytic product.

The Lys200 substitution alters the inhibition pattern of N-BPs in different ways. The weakening of the hydrogen bond between the carbonyl oxygen of Lys200 and amino-group in Ris and Zol does not seem to cause any alteration in the orientation of heterocyclic rings nor does it negatively affect enzyme inhibition. Furthermore, the disruption of the direct interaction between the side-chain amino-group of Lys200 and the phosphonate moiety of Ris and Zol does not affect the N-BP binding, perhaps because the remaining salt-bridge interactions between phosphonates and adjacent residues can still aid N-BP binding and orientation to the allylic pocket. It is rather the poor IPP binding and thus the defective enzyme: inhibitor isomerisation that compromises overall inhibition. Substitution of Lys200 favours Iba competitive inhibition, possibly due to increase in binding pocket size that allows accommodation of the long isoprenoid tail of Iba and does not favour binding of isoprenoid products. Finally the major decrease of Ale and abolition of Pam inhibition in K200E but not in K200G or K200L demonstrates the importance of the hydrophobic character for N-BP binding which is also dependent on structural flexibility of the individual BPs. The unexpected suppression of all calculated K_{isom} indicates the vital role of Lys200 in the slow-

binding FPPS mechanism, indicating a reversible and competitive inhibition. Further structural studies are essential to fully establish the role of Lys200 in N-BP binding whereas product analysis would identify alterations in the ratio of GPP and FPP synthesis between mutants.

6. FPPS MUTATIONS IN HIGHLY CONSERVED RESIDUES THAT SEVERELY COMPROMISE THE CATALYTIC ACTIVITY AND N- BP BINDING

6.1 INTRODUCTION

Structural alignment of various prenyltransferases including FPPS and GGPP reveals the presence of four highly conserved residues, all of which have been previously implicated in substrate binding and catalysis: Phe239, Arg112, Asp103 and Asp107 (Ashby and Edwards, 1990, Koyama *et al.*, 1996).

The Phe239 maps to the highly conserved VI region, identified by Koyama et al. (1996) and due to its high hydrophobicity it was implicated in binding the alkyl moieties of the substrate. Mutation studies on the conserved Phe239-Glu240 motif in *B. stearothermophilus* indicated a possible role for Phe239 to hold the DMAPP or GPP molecule in the correct position for subsequent condensation with IPP (Koyama *et al.*, 1995) whereas the hydrogen bonding between Glu240 and the oxygen at C_1 of the substrate increases the binding affinity of DMAPP to region VI. Despite of the fact that an interaction between Phe239-Gly240 is necessary to

keep the allylic substrate in a productive form, the role of Phe239 role in catalysis is supposedly far more important, as this residue controls the enzyme's affinity for DMAPP and maintains hydrophobicity for the binding of the long hydrocarbon GPP tail. Furthermore Phe239 is responsible for recognition and correct location of the 3-methyl group of isoprenoid substrate, properly orienting the allylic substrate for catalysis (Koyama *et al.*, 1995). The role of Phe239 in substrate positioning was confirmed by early structural studies on *E.coli* FPPS, where, the hydrophobic tail of DMAPP was positioned in close proximity to Phe239 and at hydrogen bond distance to Glu240. This study additionally revealed that, not only DMAPP or GPP binding, but also the reactive conformation of IPP was strongly related to the hydrophobicity of the environment, whose maintenance was also dependent on the presence of aromatic Phe239 (Hosfield *et al.*, 2004). Structural studies on human FPPS revealed the close proximity of the long hydrocarbon chain of IPP to Phe239 (Figure 1.7), supporting the direct involvement of Phe239 in IPP interactions and binding site which is fully formed in partially closed conformation (Rondeau *et al.*, 2006). Indeed, the position of Phe239 is strongly affected by the conformational changes taking place after IPP binding which result in a dramatic shifting of the basic C-terminal tail and stabilization of the closed conformation

(Rondeau *et al.*, 2006).Therefore, Phe239 together with other residues, seems to be involved in ordering the substrate binding in partially closed conformation, orienting IPP and DMAPP for catalysis in closed conformation and stabilizing the generated carbocation intermediate by providing a hydrophobic environment that would exclude water from the active site (Rondeau *et al.*, 2006).

The pivotal role of Arg residues mainly associated with the active site in catalysis was first demonstrated by studies on FPPS isolated from pig liver where, inactivation of adjacent arginines rendered the enzyme inert (Baba and Allen, 1984, Barnard and Popjak, 1980). It was therefore suggested that the conserved Arg112 may play a role in substrate binding and enzyme activation (Joly and Edwards, 1993). Mutagenesis studies with the rat enzyme yielded contradictory results, as they confirmed the importance of Arg112 for catalysis and formation of enzyme: PPi :FPP complex, but failed to associate this residue with participation in substrate affinity or binding (Joly and Edwards, 1993). Similar studies with *S. cerevisiae* FPPS confirmed a pivotal role of Arg112 in catalysis, as its substitution severely suppressed the k_{cat} (Song and Poulter, 1994) but did not shed any light on the role of this residue in substrate binding. Structural studies on *E. coli* FPPS, indicated that Arg112, along with Lys257 shield the non-metal

ligated pyrophosphate oxygen of DMAPP from the bulk solvent, aiding in the formation of the catalytic base for proton abstraction from the C_2 carbon of IPP in the condensed carbocation intermediate and liberation of the isoprenoid product (Figure 1.7) (Hosfield *et al.*, 2004). This theory suggests a possible role of Arg112 in K_m^{IPP} affinity and binding. A direct interaction of Arg112 and Arg113 with the pyrophosphate moiety of IPP contributes in fixation of homoallylic substrate (Rondeau *et al.*, 2006).

Finally, Asp103 and Asp107 belong to the highly conserved aspartate-rich motifs and were implicated in allylic and homoallylic substrate binding (Ashby and Edwards, 1990). Mutagenesis of either Asp103 or Asp107 in rat and yeast enzymes had a severe effect on catalysis, but the studies failed to show any relationship of either residue in substrate affinity (Joly and Edwards, 1993, Song and Poulter, 1994). Structural studies on avian prenyltransferase indicated a possible role of Asp107 in IPP binding (Tarshis *et al.*, 1994) which was confirmed by later studies in human FPPS, indicating that electrostatic interactions between Asp107/Asp174 and Lys266 contribute to stabilization of the partially closed conformation triggered upon IPP binding (Figure 1.9)(Rondeau *et al.*, 2006).

Studies on human FPPS indicated Phe239 as one of the major hydrophobic amino-acids that surround the heterocyclic ring of Ris

(Figure 5.4)(Kavanagh *et al.*, 2006b), however a direct role of this residue in N-BP binding was never proposed. In *T. cruzi* FPPS crystal structure, Arg112 was shown to directly interact with the phosphonate moieties of Ris (Gabelli *et al.*, 2006), whereas in human, Arg112 along with Lys200 and Lys257 make direct salt-bridge interactions with the phosphonate moiety of all clinically relevant N-BPs examined in this study (Kavanagh *et al.*, 2006b, Rondeau *et al.*, 2006). Finally, both Asp103 and Asp107 form salt bridge interactions with Mg^{2+} ions and pyrophosphate moieties of N-BP, aiding the orientation and stabilization of the bound N-BP (Kavanagh *et al.*, 2006b, Rondeau *et al.*, 2006).

The role of the residues described above in catalysis and N-BP binding was investigated via the following mutations: i) The aromatic Phe239 was mutated to the aliphatic Ala (F239A), to abolish hydrophobic interactions between FPPS: substrates or FPPS: N-BPs (Figure 6.1 A) ii) The positively charged Arg112 was mutated to the hydrophobic Leu (R112L), to abolish the proposed phosphonate-enzyme interactions and disrupt the catalytic binding site (Figure 6.1 B) and iii) The negatively charged Asp103-Asp107 were both mutated to Ala (DADA), to investigate their importance in FPPS substrate and N-BP binding (Figure 6.1C).

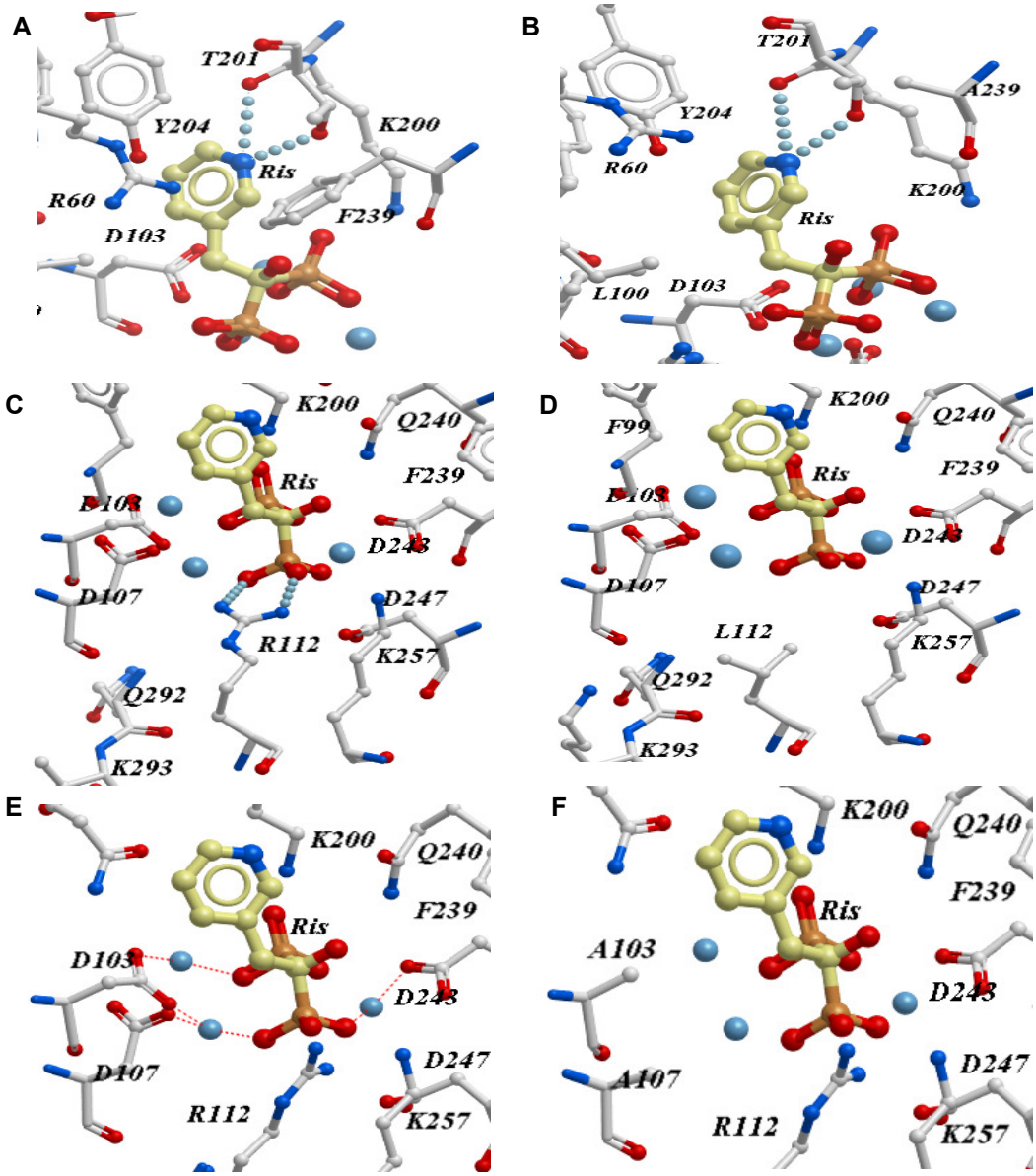


Figure 6.1: Proposed mutation effects on highly conserved prenyltransferase residues that alter the strength of N-BP binding. Interactions of the aromatic Phe239 with the phosphonate groups of N-BPs (A) are abolished in F239A substitution (B). Electrostatic interactions (blue dotted lines) between the negatively charged phosphonate groups of N-BPs and Arg112 (C) are abolished in R112L substitution (D) and Asp103/Asp107 residues are implicated metal coordination (orange lines) in N-BP binding (E) which should be severely compromised in DADA mutation (F). Mg ions shown as light blue spheres.

6.2 KINETIC CHARACTERIZATION OF F239A, R112L AND DADA MUTANTS

Determination of kinetic parameters was carried out for the purified F239A and R112L FPPS mutants (Table 6.1). No activity was detected in the DADA mutant.

Table 6.1: Kinetic parameters for FPPS WT, F239A and R112L mutants. Results for K_m and k_{cat} are expressed as means +/- SEM, $n \geq 6$, $R^2 \geq 0.9$

	WT	F239A	R112L
K_m^{GPP} (μM^{-1})	2.07 ± 0.2	2.51 ± 0.4	4.5 ± 1.2
K_m^{IPP} (μM^{-1})	1.8 ± 0.3	40 ± 10.8	48.32 ± 11.7
k_{cat} (s^{-1})	0.385 ± 0.015	0.0011 ± 0.0003	0.00043 ± 0.000006
k_{cat}/K_m^{IPP} ($\mu M^{-1}/s^{-1}$)	0.6	0.000028	0.000009

Comparison of substrate saturation between WT and F239A mutant indicated a statistically unaltered K_m^{GPP} but a 20 –fold increase for the K_m^{IPP}. The maintenance of K_m^{GPP} to physiological levels was also observed in *B. stearothermophilus* studies of F239A mutants, but that study did not confirm any active involvement of this residue in GPP binding (Koyama *et al.*, 1995). It can therefore be suggested that maintenance of hydrophobicity of this residue for catalysis is more important for DMAPP rather than GPP as

substrates, as the presence of Phe239 was previously shown to determine DMAPP but not GPP binding (Koyama *et al.*, 1995). The nature of DMAPP and GPP binding to the allylic FPPS site is strongly determined by the length of their isoprenoid chain, with the longer hydrocarbon GPP chain protruding deeper than DMAPP into the allylic binding pocket and therefore capable of forming interactions with several hydrophobic residues that keep GPP in a reactive conformation, despite the absence of Phe239. Indeed, Phe239 is not implicated in stabilization of the FPPS open conformation which is responsible for the GPP release and its translocation to the allylic binding site for subsequent interaction with IPP (Rondeau *et al.*, 2006).

The increase in the K_m^{IPP} value for F239A FPPS might be attributed to the low affinity for DMAPP that compromises subsequent enzyme interaction with the first molecule of IPP and thus formation of a carbocation intermediate. However, the presence of Gln240 may still preserve some DMAPP binding to the enzyme, as the formation of hydrogen bond between the negatively charged oxygen of DMAPP and hydrogen of the NH_2 group of Gln240 persists. If this is the case, catalysis can still proceed albeit with a slower rate, with GPP formation somewhat suppressed but its subsequent affinity for binding to the allylic site unaffected. However, as Phe239 is directly involved in stabilization of the fully

closed conformation and placement of the IPP into the binding pocket, the absence of the aromatic ring contributes to the mislocalization of IPP and inability of the C-terminal tail to form a lid over the IPP binding pocket, compromising FPP synthesis. It is therefore the second IPP binding event that would be severely compromised, shifting the equilibrium of the reaction to the left hand site and perhaps leading to GPP accumulation, as observed in the K200E FPPS mutant (Section 5.2). In this case, GPP production could counteract the defective synthesis caused by the incorrect orientation of DMAPP, resulting in an unaltered K_m^{GPP}. This would explain the low k_{cat} and k_{cat}/K_m values, as the reaction mechanism is disrupted at two points; Ala239 cannot orientate the DMAPP for FPPS binding and closure of the IPP binding pocket is obstructed, leading to impaired FPP but not GPP synthesis.

A very similar kinetic profile was observed with the R112L mutation, raising the K_m^{GPP} by 2-fold but severely compromising the enzyme's ability to bind IPP, as shown by the 20-fold increased K_m^{IPP}. As previously mentioned, no change in the substrate affinity upon Arg112 substitution has been experimentally shown in other organisms, despite of the fact that it was suspected to participate in substrate binding and affinity (Barnard and Popjak, 1980, Joly and Edwards, 1993, Song and Poulter, 1994). However the findings in the current study support the catalytic model proposed by

Hosfield et al. (2004) that suggests a direct involvement of Arg112 in the de-protonation of the C_2 hydrogen of the IPP molecule bound to the carbocation intermediate, which leads to GPP product release. In addition, Arg112 has been implicated in the stabilization of the leaving pyrophosphate group prior to release of FPP in the second round of catalysis (Joly and Edwards, 1993). Therefore a mutation of Arg112 severely disrupts catalysis, as shown by the k_{cat} and k_{cat}/K_m values (Table 6.1), because it compromises IPP proton abstraction, GPP liberation and subsequent binding to the allylic site (thus raising the K_m^{GPP}) and eventually FPP product formation and liberation.

In the case of the DADA mutant, no activity was observed, whereas individual D103A and D107A mutations in *E.coli* FPPS severely lowered the k_{cat} (Song and Poulter, 1994) and D103E and D107Q mutations in rat enzyme (Joly and Edwards, 1993) had a similar effect. From the present study, it is clear that disruption of both highly conserved Asp residues completely abolishes catalysis, highlighting their essential role.

6.3 CRYSTAL STRUCTURES OF F239A AND R112L CONFIRM KINETIC DATA

In the F239A and R112L constructs the dramatic increase of K_m^{IPP} compared to WT was attributed to disruption of different stages of catalytic mechanism. The F239A mutation was considered to alter the hydrophobic environment surrounding the bound IPP molecule and thus could have a negative impact on the stabilization of partially- and fully-closed conformations of FPPS, C-terminal switch and eventually product release. Any disruption of the homoallylic binding pocket formation would account for impaired binding of IPP. In the R112L mutant, formation of a carbocation intermediate should proceed without any anticipated problems; however inability of the Leu112 to aid abstraction of the C_2 hydrogen of the IPP from the non-metal ligated pyrophosphate would lead to impaired GPP release and defective binding of the second IPP molecule. Structural studies were employed in order to confirm any possible alteration in the formation of the homoallylic binding site and IPP position that could account for the increased K_m^{IPP} and thus be of support of the proposed residue roles in catalysis.

6.3.1 The crystal structures of F239A FPPS reveals a shift in the C-terminal tail

Superposition of the WT crystal structure in complex with Zol and IPP with F239A FPPS crystal structure with Ris and IPP revealed no alteration in either IPP binding or N-BP positions (Figure 6.2). Similarly, the position of important amino-acids playing a part in the formation of allylic binding pocket such as Lys200, Thr201, Tyr204, Arg112, Asp103 and Asp107 were not affected by the mutation, confirming that Phe239 does not play a role in GPP synthesis or binding. However, in the F239A FPPS structure the basic C-terminal tail was shifted away from the IPP binding site with a calculated RMSD of 1.45 Å compared to WT position, confirming the importance of this residue in stabilizing the closed conformation which in turn would compromise IPP fixation to the binding pocket and FPP liberation. A similar profile was observed by superposition of the WT crystal structure in complex with Zol and IPP with the F239A crystal structure in complex with Pam and IPP with a calculated RMSD for C-terminal shifting of 1.41 Å (Figure 6.3). Unfortunately, the ^{351}RRK^{353} residues are not visible in either mutant structure which would allow a more accurate calculation of the C-terminal shifting.

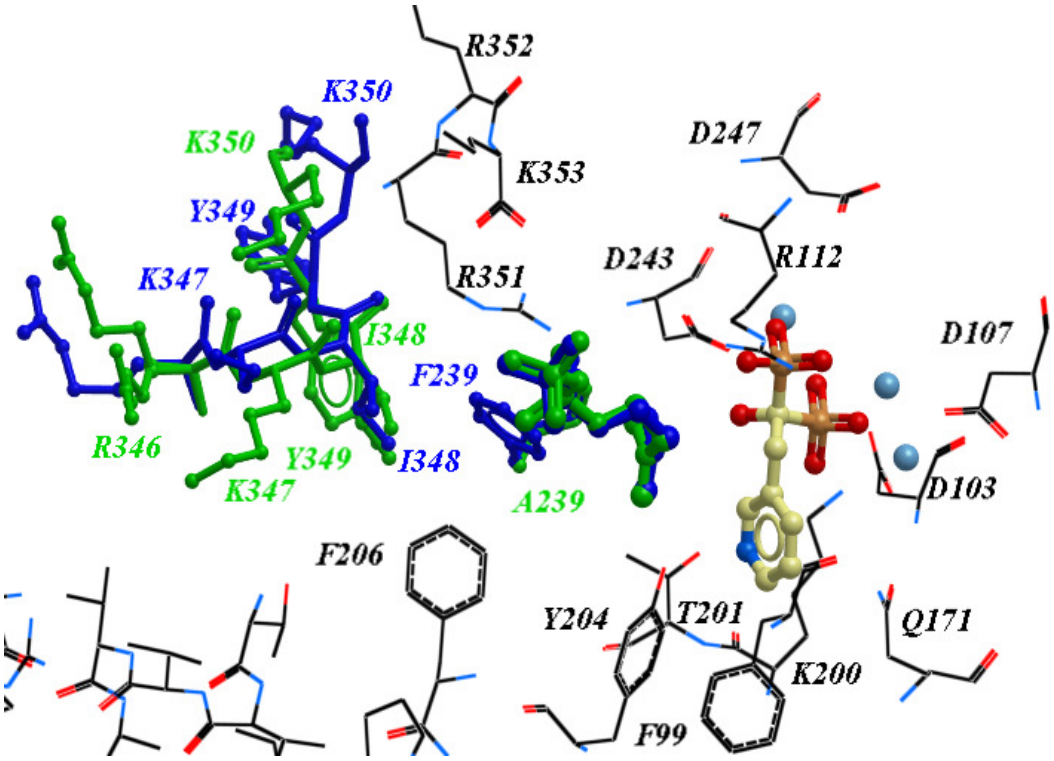


Figure 6.2: Superposition of WT FPPS and F239A mutant crystal structures in complex with Zol and IPP or Ris and IPP respectively reveals changes in the positions of the C-terminal tail. Upon IPP binding to the homoallylic pocket of WT FPPS, the C-terminal basic tail of the FPPS forms a lid over the IPP binding site and stabilization of the fully closed conformation occurs. The Phe239, along with other amino-acids, contributes to the maintenance of hydrophobicity of the binding pocket and is affected by the conformational switch triggered upon IPP binding. In the crystal structure of F239A FPPS with IPP and Ris, the IPP binding is unaffected and the Ris position unaltered. However, the position of the C-terminal lid is shifted away from the IPP as indicated by the calculated RMSD which is 1.45 Å, indicating inability of the mutant to switch to the fully closed conformation and thus to stabilize the IPP binding. In WT FPPS, IPP and residues are labeled in blue, in F239A FPPS, IPP and residues are labeled in green, Mg in light blue spheres. WT adapted from pdb: 1ZW5 (Rondeau *et al*. 2006)

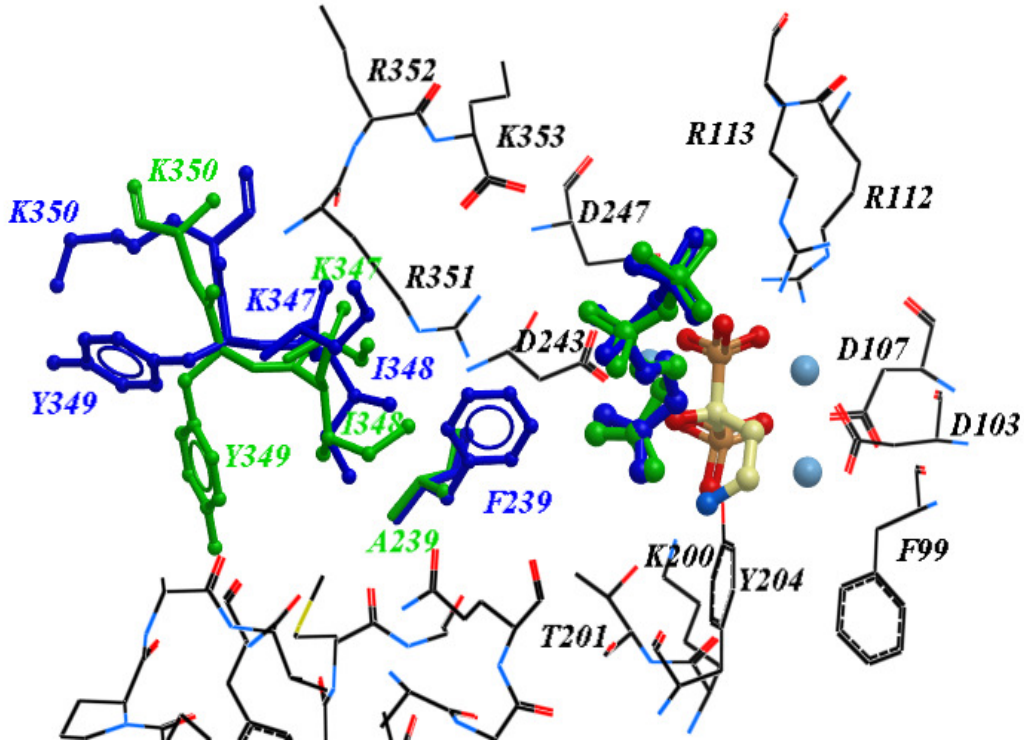


Figure 6.3: The superposition of WT: IPP: Zol and F239A: IPP: Pam crystal structures reveals changes in the C-terminal tail. A similar profile to Figure 6.3 is observed in F239A FPPS crystal structure with IPP and Pam, where the calculated RMSD of the C-terminal ^{347}KIYK^{350} residue is 1.41 Å. In WT FPPS, IPP and residues are labeled in blue, in F239A FPPS IPP and residues are labeled in green, Mg in light blue spheres. WT adapted from pdb: 1ZW5 (Rondeau *et al*. 2006).

6.3.2 The crystal structure of R112L reveals disruption of the catalytic base for proton abstraction from the carbocation intermediate

Superposition of the WT crystal structure in complex with Zol and IPP with R112L FPPS mutant with IPP revealed no shifting of

the C-terminal tail or of the IPP binding site, indicating proper formation of the IPP binding pocket (Figure 6.4).

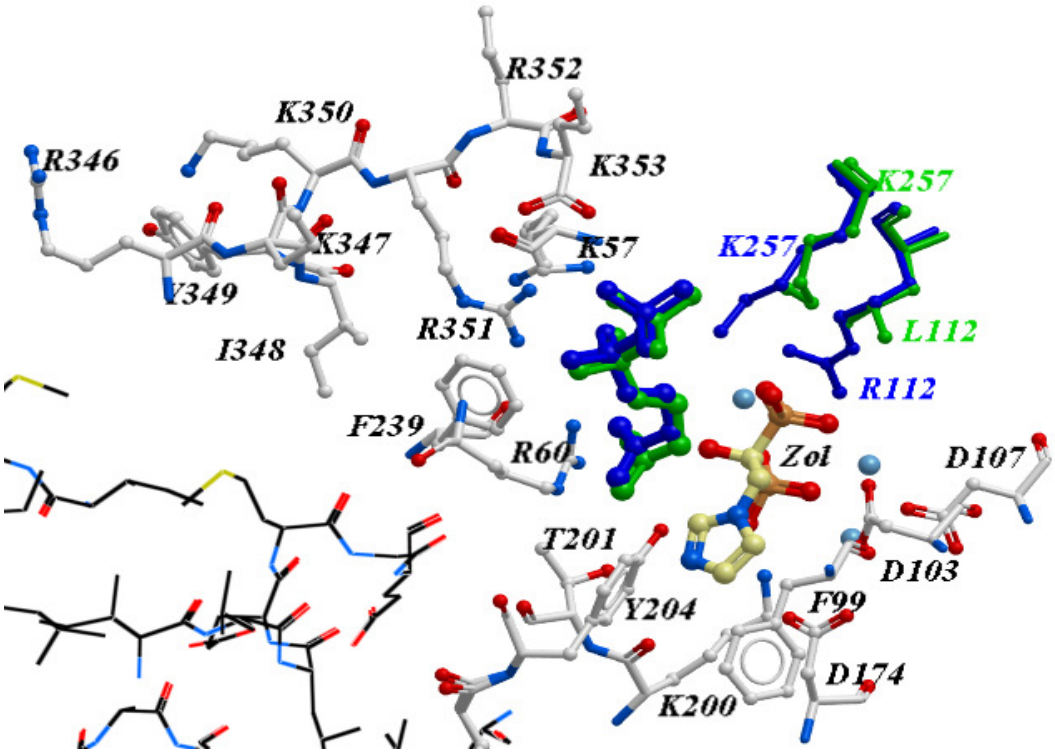


Figure 6.4: Superposition of WT: IPP: Zol and R112L: IPP crystal structures reveals inability of the enzyme to form the catalytic base for IPP proton abstraction by the carbocation intermediate. The apolar Leu112 and the consequent shift of Lys257 residue disrupt the proposed catalytic base for DMAPP binding. The position of: IPP binding and C-terminal tail ^{346}RKIYKRRK^{353} remains unaltered. Similarly the positions of amino-acids that contribute to the fully closed conformation (Lys57, Arg60), partially closed conformation (Arg103, Arg107, Arg174) and allylic binding (Lys200, Thr201, Tyr204) are unaffected. Inability of the Zol to co-crystalize with R112L: IPP indicated the importance of the Leu112 for N-BP binding.

However, the replacement of the positively charged Arg112 by the apolar Leu results in a change in position of Lys257 which is

mainly responsible for the formation of the catalytic base for DMAPP binding and which is essential for proton abstraction from the C_2 carbon of IPP and FPP liberation (Hosfield *et al.*, 2004). Similarly, the phosphonate moieties of Zol cannot form any electrostatic interactions with the Leu112, due to the increased residue distance and change in polarity, failing to secure Zol in the allylic binding pocket. Indeed, our repeated failure to co-crystalize R112L FPPS with N-BP indicates that abolition of the phosphonate-enzyme interactions due to the mutated Arg112 severely compromises N-BP binding and fixation in the allylic pocket.

6.4 INVESTIGATION OF THE INHIBITION MODE OF F239A FPPS MUTANT BY N-BPs

The mode of competitive and mixed inhibition of F239A by the five clinical N-BPs was assessed at time points chosen based on its individual kinetic behaviour (Table 6.2). More specifically, Ki was calculated from data obtained after a 7 min incubation, as 3 and 5 min incubation yielded statistically inaccurate values due to the low catalytic turnover of the enzyme. Ki* was calculated after 10 min pre-incubation period, as in all previous mutants.

Table 6.2: Estimation of Ki, Ki* and Kisom of WT and F239A FPPS mutant derived from inhibition assays with N-BPs. Initial inhibition constant (Ki) values were obtained when inhibition assays were initiated by the addition of enzyme and 3 min, 5 min or 7 min incubation whereas final Ki (Ki*) was calculated when enzyme was pre-incubated with BP for 10 minutes and the reaction started by the addition of substrate. The constants obtained were then corrected for the affinity for GPP as described in section 2.25. K_{isom} was calculated from Ki and Ki* as described in section 2.25. Results are expressed as means $^{+/-}$SEM, $R^2 > 0.95$ and $n \geq 6$. Negative values are denoted in red.

BP	Construct	Ki (nM)	Ki* (nM)	K_{isom} (GPP)	K_{isom} (IPP)
Ris	WT	56.6 ± 3.1	0.8 ± 0.06	69.3	82
	F239A	65.1 ± 13.5	45.6± 8.5	0.4	6.1
Zol	WT	62.9 ± 5.1	0.06 ± 0.03	1076.9	1271
	F239A	0.57 ± 1.9	0.38 ± 1.1	0.5	6.4
Iba	WT	207.7 ± 13.4	4.6 ± 0.4	44.1	52.3
	F239A	64.67 ± 16.4	12.63 ± 4.3	4.1	24.6
Ale	WT	388.3 ± 31.3	56.5 ± 4.9	5.9	7.1
	F239A	28.02 ± 9.84	73.22 ± 9.8	-0.6	0.9
Pam	WT	181.5 ± 6	51.9 ± 3.3	2.5	3.1
	F239A	894.5± 96	794.29 ± 74.1	0.1	4.6

No inhibition data were obtained for R112L as the enzyme activity was extremely low and did not allow significant incorporation of radioactivity into the product in the presence of N-BP. Similarly, no data could be produced for the DADA mutant. Despite several crystallization attempts, no crystals were obtained

for either R112L or DADA with inhibitor, therefore structural studies could not be conducted.

6.4.1 Inhibition by heterocyclic N-BPs reveals the importance of the hydrophobic C-terminal tail switch for the stabilization of the enzyme: inhibitor isomerization state

Different patterns were observed for Ris and Zol inhibition with a calculated Ki slightly elevated for Ris but strongly reduced for Zol, whereas Ki* produced by both inhibitors was increased. It was previously demonstrated that the imidazole ring of Zol is highly orientated by the Lys200 and Thr201 bifurcated hydrogen bond (Rondeau *et al.*, 2006) and that it can still be properly fixed to the allylic binding pocket even upon disruption of one of the two hydrogen bonds (Section 5.3). Furthermore, the F239A mutation does not affect stabilization of the open conformation, as indicated for the unaltered K_m^{GPP} value, which favours occupation of the allylic binding site. The proposed alterations of the homoallylic binding site cannot have any impact on the strength of initial Zol binding, which can easily compete with GPP and finally occupy the allylic binding pocket. This event may be reinforced by the incorrect orientation of the DMAPP substrate for proper catalysis as a result of the mutated Phe239, which may favour the well-

orientated Zol rather than GPP binding to the allylic pocket, increasing the strength of inhibition. However, Phe239 seems to significantly contribute to the maintenance of the hydrophobic character of the Ris binding pocket (Kavanagh *et al.*, 2006b), therefore its mutation strongly compromises the ability of Ris to compete with GPP, possibly due to disruption of electrostatic interaction, despite no change in the size of the DMAPP/GPP binding pocket (Figure 6.5).

The decreased final inhibition of F239A mutant with both heterocyclic N-BPs can be attributed to the altered interactions supporting the position of IPP in the homoallylic binding pocket, leading to a defective switching of the highly basic hydrophobic tail and inability of the FPPS enzyme to maintain the isomerized state (Figure 6.2). Indeed, the reduced K_{isom} values confirm the reversibility of inhibition and support the proposed role of Phe239 in conformational changes leading to stabilization of the fully closed conformation and enzyme: inhibitor isomerization state.

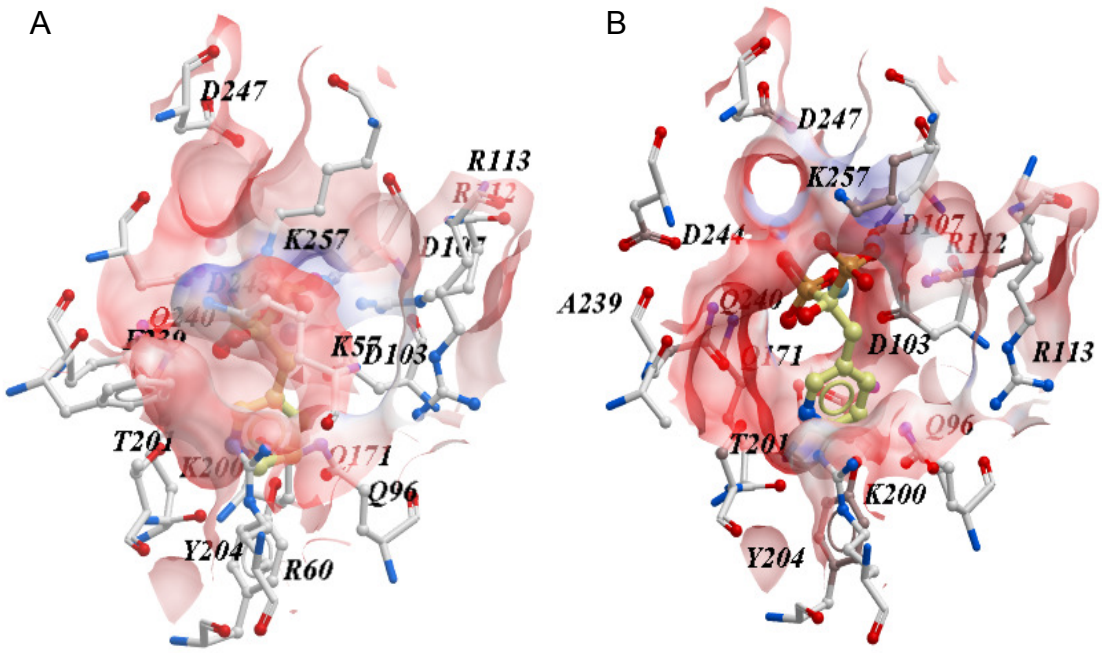


Figure 6.5: Crystal structure of F239A FPPS: Ris reveals disruption of electrostatic interactions in the allylic binding pocket that contribute to the decreased Ris binding. A) In WT FPPS in complex with Ris, electrostatic interactions between phosphonates and selected FPPS residues and Mg ions contribute to the fixation of Ris in the allylic binding pocket. B) Disrupted electrostatic interactions between phosphonate and surrounding residues due to alteration in hydrophobicity contribute to the decreased Ris inhibition in F239A FPPS mutant. Surface charge distribution: negatively charged residues is coloured red and positively charged is coloured blue.

6.4.2 Inhibition by the amino-alkyl bisphosphonates is strongly suppressed in the F239A mutant

Kinetic studies performed on F239A FPPS indicated a similar inhibition profile for both Iba and Ale, with Ki values dramatically suppressed and Ki* slightly elevated. The increased competitive inhibition cannot be attributed to the incorrect orientation of DMAPP and its reduced availability for reacting with IPP, because

the K_m^{GPP} value indicates GPP availability for competition with the N-BP for the allylic site. However the decreased hydrophobicity of the allylic pocket may favour binding of the highly charged hydrophilic Iba and Ale over the long hydrocarbon tail of GPP, with the more hydrophilic and flexible Ale which is the strongest competitive inhibitor after Zol. Another contributing factor to the remarkable increase in competitive inhibition by Ale may be the conservation of the hydrogen bond between the hydroxyl oxygen of Thr201 and the amino-group which can orientate the side-chain in the binding pocket.

Finally both Ki and Ki* for F239A were remarkably increased with the structurally more rigid Pam, indicating loss of both competitive and mixed inhibition. Superposition of the WT with F239A FPPS crystal structures in complex with Pam reveals a shifting in the position of key amino-acids playing part in stabilization of the closed conformation such as Arg57 and Arg60 with the most dramatic alteration on the structural rearrangement of Thr201, where the methyl group and the hydroxyl moiety exchange orientations, leading to the disruption of van der Waals contacts and electrostatic interactions between Thr201 and Pam (Figure 6.6), essential to stabilize the substrate/inhibitor binding and delimit the formation of allylic binding pocket. Abnormal shifting of C-terminal tail was also observed, leading to the

complete destabilization of the closed conformation and thus loss of inhibition by Pam (Figure 6.6).

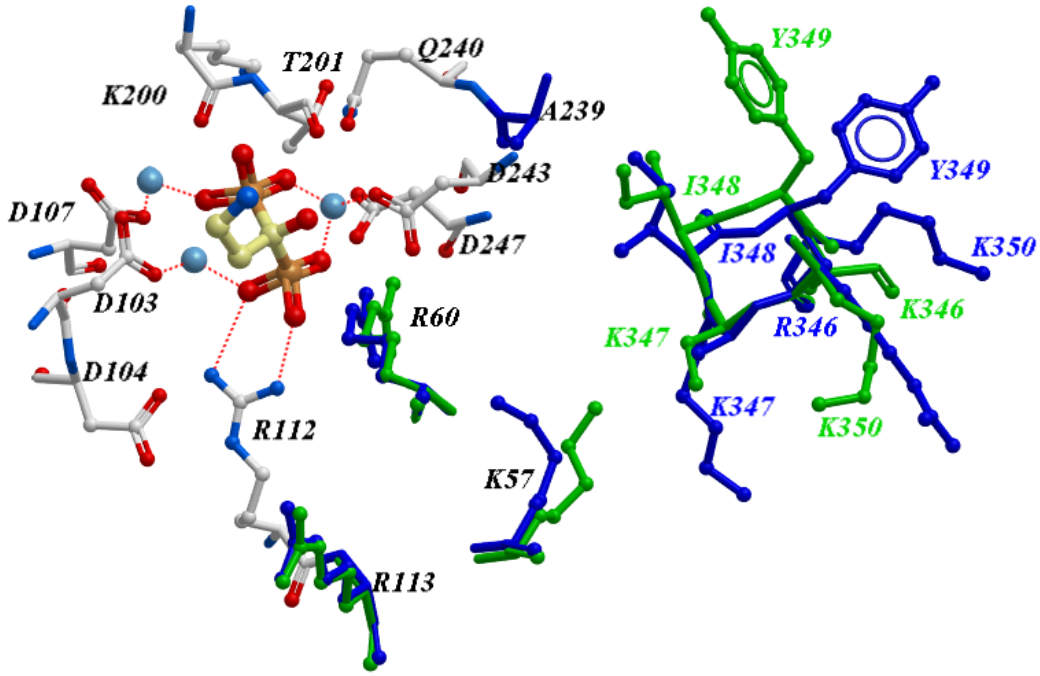


Figure 6.6: Shifting in amino-acid positions in F239A FPPS in complex with Pam destabilizes the closed conformation and the enzyme: inhibitor isomerization step. Structural rearrangement of Thr201 which aids in the formation of the allylic binding pocket and binding of Pam, leads in disorientation of Pam and loss of initial and final inhibition. Structural rearrangement of the C-terminal tail is also inhibited in F239A FPPS. In WT FPPS, IPP and residues are labeled in blue, in F239A FPPS residues are labeled in green, Mg in light blue spheres. WT adapted from pdb: 2F89 (Rondeau *et al.* 2006).

It is well known that aromatic ring interactions with cations can reinforce the ligand affinities of certain substrates (Dougherty, 1996). The increased Ki* as well as K_{isom} observed with all aminoalkyl N-BPs can be therefore attributed to the loss of

electrostatic attraction between the positively charged amino-group of N-BP with the aromatic ring of Phe239. Finally, the decreased affinity for IPP binding confirmed by structural data, leads to a defective closure of the IPP binding pocket and thus destabilization of the enzyme: inhibitor isomerisation state which accounts for the reversibility of inhibition.

6.5 CONCLUSIONS

The present study represents the first major attempt to evaluate the proposed role of highly conserved FPPS residues in substrate binding, catalysis and stabilization of interactions with individual N-BPs. The findings underline the important aspects of subtle differences between clinical N-BPs and elucidate important aspects in the complex nature of FPPS catalysis.

Structural and kinetic studies indicated an active involvement of Phe239 in the maintenance of hydrophobicity of allylic binding pocket, the formation of the homoallylic binding pocket, the C-terminal basic shifting and the stabilization of the closed conformation in FPPS. Disruption of electrostatic interactions supporting IPP binding and positioning to the homoallylic pocket was responsible for the elevated K_m^{IPP}. The unaltered K_m^{GPP} indicates no alteration in GPP availability, but cannot provide any

information towards the involvement of Phe239 in individual steps of GPP synthesis. Indeed, maintenance of [GPP] at physiological levels might be a result of an impaired FPP synthesis due to the decreased FPPS affinity for the IPP, which shifts the reaction equilibrium to the left hand site. The inability of the GPP to react with IPP may counteract the limited GPP production as a result of DMAPP disorientation in the allylic pocket and account for the low catalytic turnover.

The differences in the impact of F239A mutation in the inhibition mode by the five clinical N-BPs reflect the heterogeneity in the nature of interactions of individual N-BPs which dictate their strength of binding. The decreased hydrophobicity of the allylic pocket favours the binding of the highly charged hydrophilic Iba and Ale over the long hydrocarbon tail of GPP, but reduces the affinity for the heterocyclic ring of Ris. On the contrary, the competitive inhibition produced by Zol is strongly increased, perhaps as a result of the DMAPP disorientation which impairs GPP synthesis, favouring Zol binding to the pocket. The altered conformation of Thr201 disrupts previous electrostatic interactions between this residue and Pam and the concomitant destabilization of the FPPS closed conformation contributes to its inability to compete for and occupy the allylic binding pocket. Finally, the decreased time-dependent inhibition of F239A mutant with all

examined N-BPs was mainly attributed to the reduced affinity of the enzyme for IPP, the defective switching to the closed conformation and prevalence of the transition state over the enzyme: inhibitor isomerized state. The role of DMAPP in F239A FPPS catalysis and crystal structure will be confirmed by future kinetic and crystallographic assays.

Kinetic and structural studies indicated that Arg112 substitution led to a structural rearrangement of Lys257 which severely obstructed the formation of the proposed catalytic base, essential for proton abstraction by the condensed carbocation intermediate. The impaired GPP synthesis and decreased availability for binding to the allylic pocket in combination to the disorientation of the Lys257 has a negative impact on the binding of the second IPP molecule and thus on the FPP formation. The elevated K_m^{GPP} and K_m^{IPP} values confirm the Arg112 involvement in substrate binding and disprove previous reports which failed to associate this residue with substrate regulation. Furthermore, the inability of the apolar Leu112 to interact with the leaving pyrophosphate group prior to the FPP release strongly compromises the FPP synthesis and thus reduces the enzyme catalytic turnover. The abolition of electrostatic interactions between Arg112 and phosphonate groups of N-BPs severely

compromised the N-BP binding to the allylic pocket, demonstrating for the first time the pivotal role of Arg112 in the N-BP fixation.

Finally, disruption of two highly conserved Asp103 and Asp107 was the only mutation that abolished catalysis, confirming the importance of aspartate-rich motif in the mechanism of action of FPPS.

7. INSIGHTS INTO THE ASSEMBLY AND STRUCTURE OF RGGT CATALYTIC COMPONENTS

7.1 INTRODUCTION

Despite of the fact that intracellular processing of protein has been a hot topic of investigation since 1950s (Palade, 1975), the importance of post-translational modification of proteins by prenyltransferases for the proper function of cellular mechanisms was underestimated and therefore not thoroughly investigated until the early 1990s (Casey, 1995, Seabra *et al.*, 1991). The complexity of RGGT catalysis as the result of the dependence of the interactions between its specific protein components, did not allow elucidation of the reaction mechanism until 1996 (Shen and Seabra, 1996). RABGGT subunits were first co-purified from rat brain (Seabra *et al.*, 1992a, Seabra *et al.*, 1992b) and it was observed that prenylation of Rab substrates was not feasible unless another component, REP, was also present. Furthermore, the requirement of $MgCl_2$ for catalysis was confirmed and the participation of $ZnCl_2$ and NaCl was also proved to be important, albeit inhibitory at elevated concentrations (Seabra *et al.*, 1992a). Individual cloning of *S. cereviciae* RABGGT components in *E. coli*

has been attempted, but it was only possible to successfully express and purify RABGGTB and not RABGGTA (Dursina *et al.*, 2002), and its purification from yeast finally succeeded with positive results. Large scale purification of mammalian RGGT components in *E.coli* was attempted by several groups, all leading to poor protein yield regarding RABGGTA, REP1 or REP2 (Armstrong *et al.*, 1993), whereas the homologous yeast proteins were successfully produced (Witter and Poulter, 1996). Because of these difficulties, the first enzyme assays using mammalian proteins were performed with RABGGT and REP components directly purified from bovine brain or rat liver by traditional methods, limiting the availability of the various proteins (Alexandrov *et al.*, 1994, Andres *et al.*, 1993, Cremers *et al.*, 1994). Co-expression of both subunits in *E. coli* via a cleavable glutathione S transferase tag (GST) appended to truncated RABGGTA led to a high protein yield and the purified enzyme was capable of performing geranylgeranylation (Kalinin *et al.*, 2001). The GST tag is more specific than hexahistidine tag and optimizes selective elution and iterative folding of the target protein (Hutchinson and Chase, 2006) however it may also lead to oxidative aggregation or target degradation (De Marco *et al.*, 2004, Kaplan *et al.*, 1997) and is not recommended when the target

enzyme is dependent on metal ions for catalysis, in this case zinc, as it is known to interfere with catalytic processes.

Recombinant rat RABGGT was successfully purified from Sf9 insect cells to apparent homogeneity (Smeland *et al.*, 1994). Co-infection of Sf9 cells with recombinant baculovirus containing truncated versions of both subunits was also performed (Alexandrov *et al.*, 1999, Armstrong *et al.*, 1995) and it was preferable, as presence of both subunits is essential for catalysis.

Cloning of mammalian REP1 was first attempted in yeast and Sf9 cells with encouraging results (Andres *et al.*, 1993, Seabra, 1996, Sidorovitch *et al.*, 2002). In addition, partially purified fractions containing REP activity were used for RGGT assays (Overmeyer *et al.*, 2001), but these are not suitable for protein crystallization and proper enzyme assay or investigation of function. Expression of the yeast homologue of CHM was also successfully performed in *E.Coli* (Bauer *et al.*, 1996, Miaczynska *et al.*, 1997) while CHML expression was only feasible in baculoviral system (Armstrong *et al.*, 1995, Cremers *et al.*, 1994).

Currently, the most broadly used expression method for all RGGT components is the baculoviral system (Alexandrov *et al.*, 1999, Baron and Seabra, 2008). Insertion of the gene of interest into the baculovirus genome is based on successful cloning of the target cDNA into the chosen baculovirus shuttle vector (bacmid)

placed downstream of the polyhedrin promoter and flanked by the viral sequence (Armstrong *et al.*, 1995, Shrestha *et al.*, 2008). The resulting recombinant virus is subsequently used for infection of lepidopteran Sf9 cells where the polyhedrin promoter drives the expression of the target protein. The crucial advantage of insect cell hosts is the similarity of the posttranslational protein modification processes to that of higher eukaryotes, rendering the environment more suitable to the expression of human genes (Jarvis *et al.*, 1996). However, while production of a glycerol stock from recombinant *E.coli* leads to the expression and purification of up to 12 L of protein in TB media from bacterial expression after *lac* operon induction via IPTG, maintenance of a high titre viral stock for subsequent infections of Sf9 cells is vital in baculoviral system. This problem, in combination with the fact that target expression level by the polyhedrin promoter is only achieved when the viral replication cycle is complete (Passarelli *et al.*, 1994), maximizes the risk of bacterial or yeast infection of the Sf9 cultures while still in the incubation period (for most constructs at least 48 hr) that would compromise the protein purity. Furthermore, apart from being time consuming, baculoviral expression is a costly procedure and thus, if bacterial expression is possible albeit minimal, it should be attempted to be optimized before switching to baculovirus system.

The extensive availability of vectors and protein tags for *E.coli* cloning in SGC (Savitsky *et al.*, 2010) as well as the codon optimization in host cells that can optimize co-expression (Burgess-Brown *et al.*, 2008), prompted investigation in the present study of the expression of all the individual components, as well as co-expression in the bacterial system. The baculoviral system was subsequently employed in order to optimize the protein yield, solubility, stability and purity, where the *E.coli* purification failed to produce functional constructs. Therefore, the main aim of the experiments described below was the cloning, expression and purification of each individual component of the ternary catalytic complex formed from: RABGGTA and RABGGTB full length subunits, CHM or CHML and finally the two selected Rab substrates, RAB6B and RAB7 as a starting point for further kinetic and structural analysis.

7.2 EXPRESSION AND PURIFICATION STRATEGIES OF RGGT IN *E. COLI*

The RABGGT subunits are reported to be unstable when expressed individually (Armstrong *et al.*, 1995) and their tight association is essential for proper catalysis (Seabra *et al.*, 1992b). Individual expression of subunits was the easiest option and was

therefore attempted first, because this approach aims for the *in vitro* reconstitution of the complex from individual components. However, the method does not guarantee a successful assembly of both subunits as a functional entity when subsequently put together in the assay. Co-expression of both subunits is more desirable but also laborious as its successful outcome is dependent on multiple factors such as choice of a suitable tag and vector, optimization of elution conditions (preferably low salt to avoid complex dissociation) and limitation of purification methods available in order to maintain interaction of both subunits. Furthermore, co-expression may offer the advantage of maintaining protein-protein interactions *in vivo* but decreases the protein yield as a result of the increased number of induced genes in the culture (Johnston *et al.*, 2000, Romier *et al.*, 2006).

7.2.1 Single expression of RABGGTA and RABGGTB

For single test expressions, RABGGTA and RABGGTB were individually cloned in LIC enabled vectors (Section 2.3 and Appendix B) and subsequently tested for the presence of soluble protein (Table 7.1). Expression of promising constructs was scaled up and subsequent purification was attempted. As a default a low temperature (18°C) was chosen for expression of protein constructs as it favours the native state of a protein and prevents self-

association and misfolding by decelerating *lac* operon induction (Georgiou and Valax, 1996). However expression of some constructs is favoured at higher temperatures but the best results were obtained at 18 °C with no expression at 25 °C or 37 °C (data not shown). To optimize the expression and yield of both subunits, three different concentrations of IPTG (0.2, 0.5 and 1 mM) in either LB or TB were also tested, without alteration in protein yield.

Table 7.1 Results from 50 ml test expressions of RABGGTA and RABGGTB.

Vector	Subunit	Expression level	Attachment to resin
pNIC28_Bsa4	RABGGTA RABGGTB	none low	n/a some
pNIC_CTHF	RABGGTA RABGGTB	low high	some some
pBEN1	RABGGTA RABGGTB	none high	n/a yes
pNH_TrxT	RABGGTA RABGGTB	none low	some some

Failure to properly express RABGGTA probably arises from formation of inclusion bodies that force improper folding or protein aggregation (Dursina *et al.*, 2002). This was apparent when RABGGTA obtained from whole cells after low speed centrifugation was tested on SDS-PAGE gel and compared with the homogenized lysate collected after high speed centrifugation (Figure 7.1). The observed accumulation of RABGGTA in the non-lysed protein

sample and the minimal recovery in the lysed protein clearly demonstrates the deposition of protein aggregates into inclusion bodies, rendering the purification procedure time-consuming.

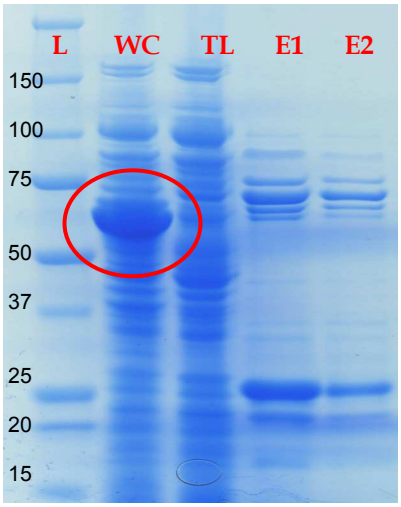


Figure 7.1: Recombinant RABGGTA accumulates in inclusion bodies in *E.coli* cells. An aliquot of the protein extract obtained from whole cells (WC) of recombinant RABGGTA cloned in pNIC28_CTHF *E.coli* was loaded on SDS-PAGE gel and compared to an aliquot of total lysate (TL) obtained from the same purification procedure. The aggregated protein (in red circle) is visible in WC sample whereas RABGGTA in TL and eluted samples after Ni-NTA purification (E1, E2) is scarce.

The only construct that was found to yield soluble RABGGTA incorporated a C-terminal 6His tag in the expression pNIC_CTHF vector. Purification of RABGGTA was achieved by IMAC and subsequent gel filtration (Figure 7.2) or anion exchange (Section 2.17.6). In both cases the yield did not exceed 2 mg/L which was sufficient for kinetic studies but not for crystal trials. Production of up to 12 L of lysate was essential in order to obtain a high protein yield, however practical problems arose due to limitations in cell

lysate loading on Ni-sepharose resin, as it can lead to unspecific protein binding, due to Ni^{2+} stripping by lysate components (Magnusdottir *et al.*, 2009).

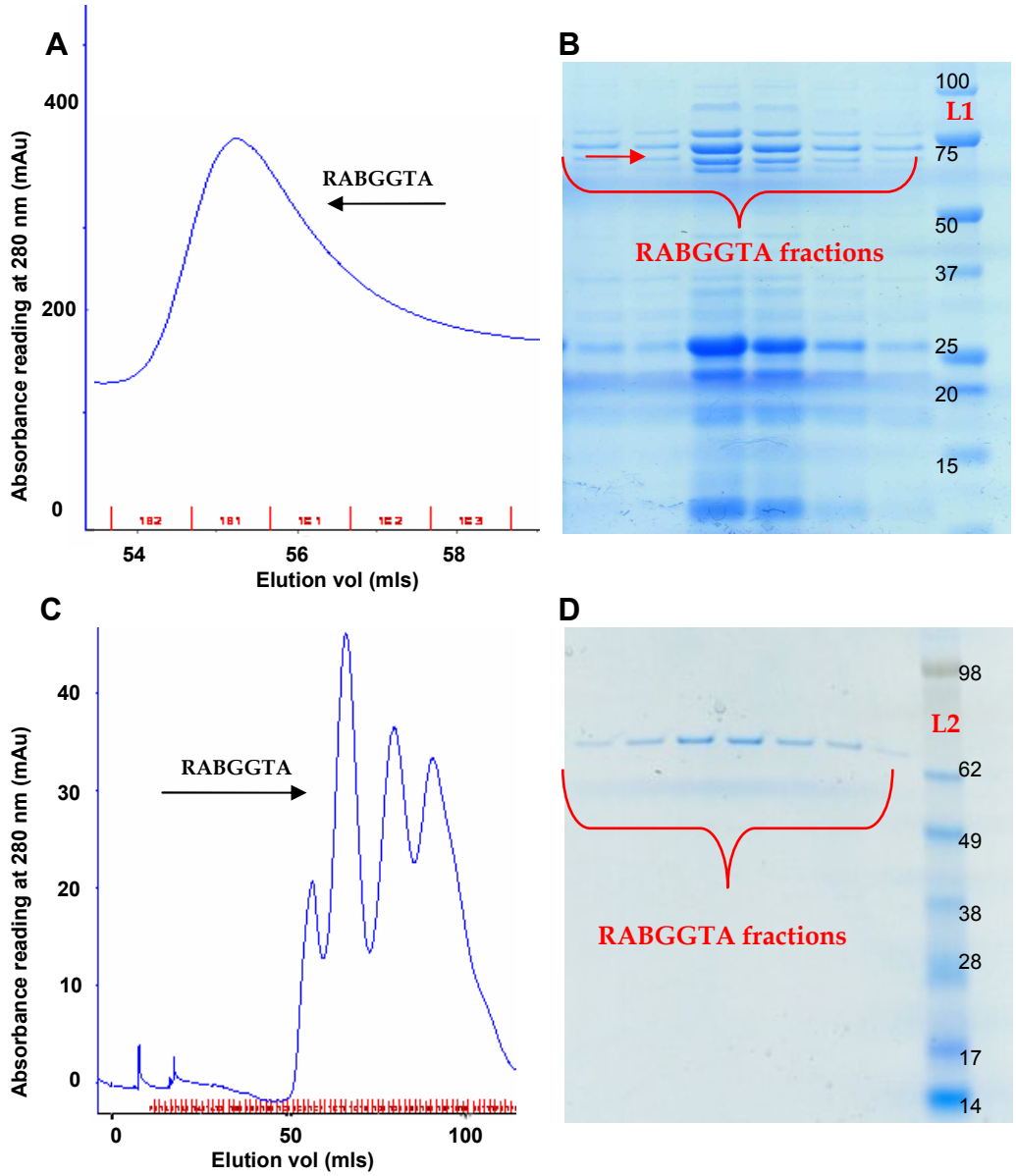


Figure 7.2: Elution profiles of RABGGTA. RABGGTA was cloned in pNIC_CTHF that allowed fusion of C-terminal 6-His protein tag and purification of the construct by A) IMAC (Section 2.17.3) and C) GF (Section 2.17.4) with a final yield of 2 mg/L of culture. B) Protein fractions eluted at 54-58 mls were tested for the presence of 77 kDa band on SDS-PAGE and D) Protein fractions approximately eluted at 60-70 mls (peak no 2) were

tested for the presence of 77 kDa band on SDS-PAGE L1: Biorad All Blue precision plus prestained protein ladder L2: Seeblueplus2 Prestained standard ladder (Invitrogen).

On the contrary, RABGGTB was abundantly expressed from vectors that enabled protein expression with a C-terminal 6-His tag or Streptavidin Binding Peptide/ Solubility Enhancement Tag (SBP/SET). The best results were achieved with the SBP/SET tag fusion protein system (construct cloned in pBEN1 vector) that allowed successful purification of RABGGTB with a single manual elution from streptavidin/agarose resin (Figure 7.3).

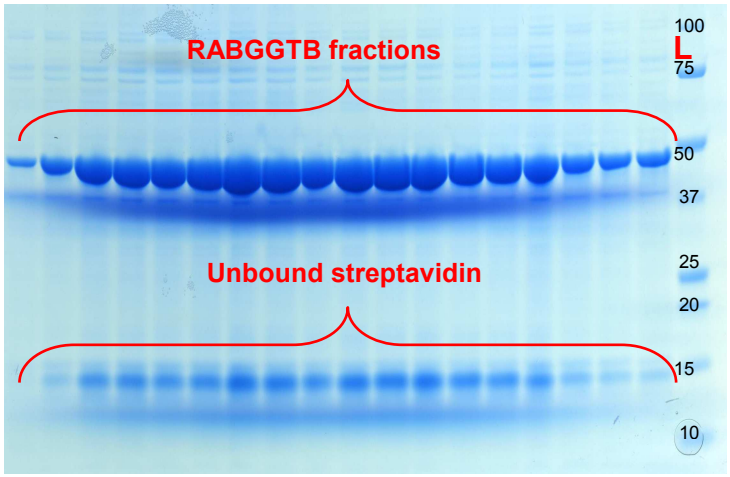


Figure 7.3: Successful purification of RABGGTB is detected by SDS-PAGE analysis. RABGGTB was cloned in pBEN1 vector that allowed fusion of N-terminal SBP/SET protein tag and one-step manual purification of the construct from streptavidin/agarose resin with a final yield of 40 mg/L of culture. L: Biorad All blue Precision Plus Protein pre-stained ladder

Verification of RABGGTA and RABGGTB identity and stability was performed by trypsin digestion, ESI-TOF and western blotting using the anti-FLAG antibody (Figure 7.4). Removal of either the hexahistidine or streptavidin protein tag resulted in proteolysis and thus TEV cleavage was not a selected purification method in this case. Furthermore, RABGGTA was prone to proteolysis and therefore purification steps were minimized to avoid protein degradation.

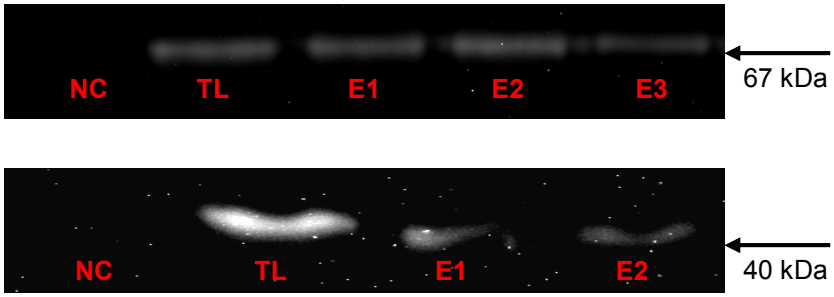


Figure 7.4: Successful isolation of RABGGTA and RABGGTB is detected by Western blotting analysis. Pre-cleared cell extracts from RABGGTA (top panel) and RABGGTB recombinant proteins (bottom panel) obtained from IMAC (2.17.3) and GF (2.17.4) purification steps were subjected to western blotting and the protein of interest was detected with FLAG antibody visualized with IgG HPR. TL: Total Lysate, NC: negative control, E1-E2-E3: Elution samples

The detection of a successful complex formation of purified proteins was tested by mixing the RABGGTA: RABGGTB in 1:1 molar ratio, allowing their interaction for 20 min at 37 °C and subsequently analysing the product by gel filtration using a pre-

calibrated column. In order to separately determine the retention volume of each protein, RABGGTA and RABGGTB were first individually eluted from the column, then the reaction mixture was applied. A single peak corresponding to a molecular weight of around 105 kDa on the pre-equilibrated Superdex 200 column indicated interaction of RABGGTA and RABGGTB and not elution of the individual subunits, confirming the formation of RABGGTA complex and thus protein integrity (Figure 7.5). Subsequent SDS-PAGE analysis of peak fractions confirmed the identity of the individual subunits in this peak.

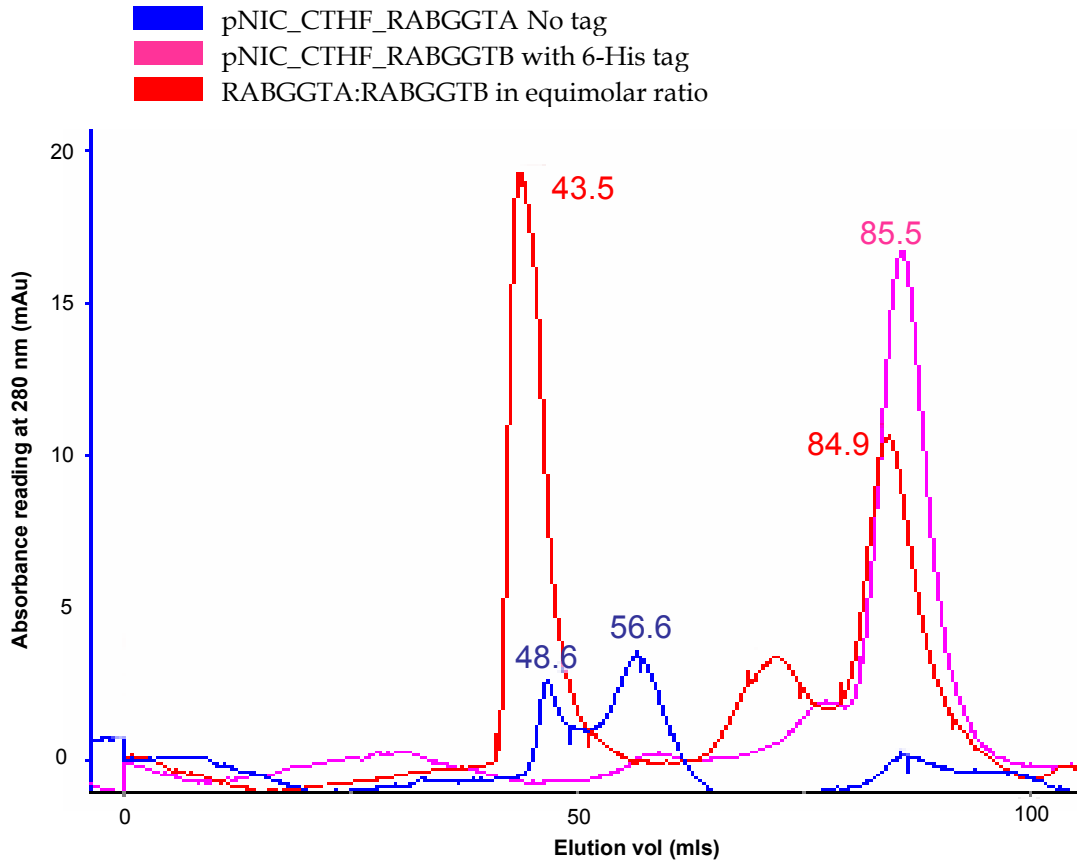


Figure 7.5: Confirmation of RABGGTA and RABGGTB complex identity by gel filtration on a pre-calibrated Superdex 200 GF column. The column was calibrated with the following molecular mass standards (Sigma): blue dextran (2000 kDa), aprotinin (651.2 kDa), albumin (66.7 kDa), cytochrome C (12 kDa). The pure RABGGTA is eluted at 56.6 ml however when it is untagged and in absence of RABGGTB it is prone to aggregation. For this reason, two peaks are visible, one at 48.6 ml corresponding to aggregated RABGGTA and a second one at 56.6 ml, corresponding to the 74 kDa RABGGTA subunit. RABGGTB is only stable when tagged and is eluted as a single peak at 85.5 ml corresponding to the 40 kDa subunit**.** When the two subunits are combined in the presence of $MgCl_2$ and allowed to react for 20 min at 37 ^{o}C, then RABGGT complex can be formed and elutes at 43.5 ml corresponding to a molecular weight of 114 kDa while excess RABGGTB elutes at 84.9 ml. All eluted samples were tested on SDS-PAGE to confirm protein identity.

7.2.2 Co-expression strategies for RABGGTA and RABGGTB

In vivo preparation of the RABGGT complex was attempted by plasmid-mediated co-expression of RABGGTA and RABGGTB subunits in order to confer optimized yield and activity as opposed to the *in vitro* complex reconstitution of individual components described above. Co-expression aimed to prevent RABGGTA proteolysis and misfolding and to increase complex activity. The main strategies of co-expression enable expression of individual subunits with unique fusion tags, so as to ensure proper complex formation and co-elution is a result of concurrent expression.

7.2.2.1 Cloning both subunits in different multiple cloning sites (MCS) of the same plasmid

For co-expression of subunits, the bicistronic pET-DUET and pCOLA vectors were used. The pET expression system, developed by Novagen, includes hybrid promoters and multiple cloning sites and requires a host bacterial strain lysogenized by a DE3 phase fragment that promotes induction of the *lac* operon by IPTG which in turn initiates T7 polymerase transcription and thus target gene expression (Sorensen and Mortensen, 2005). The pCOLA expression vector is SGC designed, based on the original pET-DUET, but uses kanamycin as plasmid resistant marker which has

the advantage of stability in the medium, whereas ampicillin is susceptible to degradation in high density cultures (Sorensen and Mortensen, 2005). Furthermore pCOLA vector incorporates a TEV cleavage site for subsequent elimination of hexahistidine protein tag, if necessary. Both vectors are low-copy plasmids therefore expression of cloned proteins was also expected to be low. However, the advantage of bicistronic vectors is the equimolar expression of the cloned subunits, as expression is driven from a single promoter.

In all constructs and combinations examined, expression of both subunits was achieved; however attachment of the protein to either Ni-NTA or streptavidin column was poor, limiting the already scarce purification strategies available for co-expressed constructs (Table 7.2, no 1-5), (Figure 7.6 A).

7.2.2.2 Subcloning of either alpha or beta subunit previously cloned in a high copy plasmid to a bicistronic vector

In this case one cloned subunit in a high copy plasmid which incorporated either the specific SBP/SET or C-6His terminal tag was subcloned to the MCS2 of pET-DUET vector, whereas the second subunit was simply cloned to the bicistronic vector (Table 7.2, no 6-9). This strategy allowed incorporation of multiple tags

that aimed to increase construct solubility (S and SET), specific binding (SBP) or promote selection from Ni-NTA column and thus facilitate purification. This method should overcome possible obstacles in complex formation that could arise from the nature of specific purification tags (Fribourg *et al.*, 2001) by allowing testing of multiple constructs. Dual tagging can also allow separation of proteins in individual components if required (Tolia and Joshua-Tor, 2006). Furthermore, expression level should still remain equivalent for both subunits, as it should be driven by the promoter of the bicistronic vector and not of the high copy number vector.

Test expressions with cloned constructs allowed production of both subunits in similar quantity and the SBP tag seemed to enhance solubility of the RABGGTA subunit, however the protein failed to bind to Ni-NTA or even to the more specific streptavidin resin (Figure 7.6 B).

7.2.2.3 Cloning of each subunit in individual plasmids and co-expression by a high copy vector

This strategy aimed to raise expression level of both subunits as they would be cloned in a high copy plasmid, however does not guarantee balanced production of both subunits. The main

difficulty in this strategy is the maintenance of two unique plasmids in *E. coli*, as they should have two different origin and replicons and should be compatible (Sorensen and Mortensen, 2005). This is a laborious procedure and therefore the last to be attempted using the *E.coli*, when expression was observed in bicistronic vectors. The subunit of interest (in this case RABGGTA) was first cloned in pNIC_CTHF vector, that allowed incorporation of a 6His terminal tag as well as a FLAG tag for immunoprecipitation or western blotting analysis. Subsequently, pNIC_CTHF_RABGGTA was subcloned in the co-expression pCOEX vector that allowed incorporation of an N-terminal 6His tag. The constructs were first cloned in MachI cells, but then transformed in BL21 cells that would allow lac operon activation via IPTG. Then, competent BL21 cells containing the pCOEX_RABGGTA strain were prepared. Finally, RABGGTB cloned in pBEN-1 vector, was successfully incorporated in pCOEX vector with a simple transformation. It was essential to ensure that both pCOEX and pBEN1 plasmids used had different origin of replication and different antibiotic resistance to prevent plasmid segregation and also bacterial cell strains were carefully selected for the same reason (Ho *et al.*, 2002, Romier *et al.*, 2006, Tolia and Joshua-Tor, 2006). The resulting construct (Table 7.2, no 10) gave the highest expression levels of RABGGTA subunit observed in co-expression and attached to Ni-

NTA column, but unfortunately with the lowest purity (Figure 7.6 C).

Table 7.2: Co-expression strategies in *E.coli* led to successful co-purification of RABGGTA/RABGGTB subunits. 1-5: Co-expression by cloning subunits in individual MCS of bi-cistronic vectors; 6-9: Co- expression by sub-cloning a high copy plasmid in MCS2 of a bicistronic vector and 10: co-expression by incorporation of pBEN1_RABGGTB plasmid into pCOEX_RABGGTA vector. MCS: multiple cloning site

No	Vector	MCS1	MCS2	Expression	Attachment to resin
1	pET-DUET	RABGGTA N-6His tag	RABGGTB No tag	yes	some
2	pET-DUET	RABGGTB N-6His tag	RABGGTA No tag	yes	none
3	pET-DUET	RABGGTA N-6His tag	RABGGTB S tag	yes	some
4	pET-DUET	RABGGTB N-6His tag	RABGGTA No tag	yes	none
5	pCOLA	RABGGTB N-6His tag	RABGGTA No tag	yes	none
6	pET-DUET	RABGGTA N-6His /C-6His	RABGGTB S tag	yes	some
7	pET-DUET	RABGGTB N-6His /C-6His	RABGGTA S /SBP/SET tag	yes	some
8	pET-DUET	RABGGTA N-6His tag	RABGGTB S /SBP/SET tag	yes	some
9	pET-DUET	RABGGTB N-6His tag	RABGGTA S /SBP/SET tag	yes	none
10	pCOEX	RABGGTA N-6His /C-6His	RABGGTB S /SBP/SET tag	yes	some

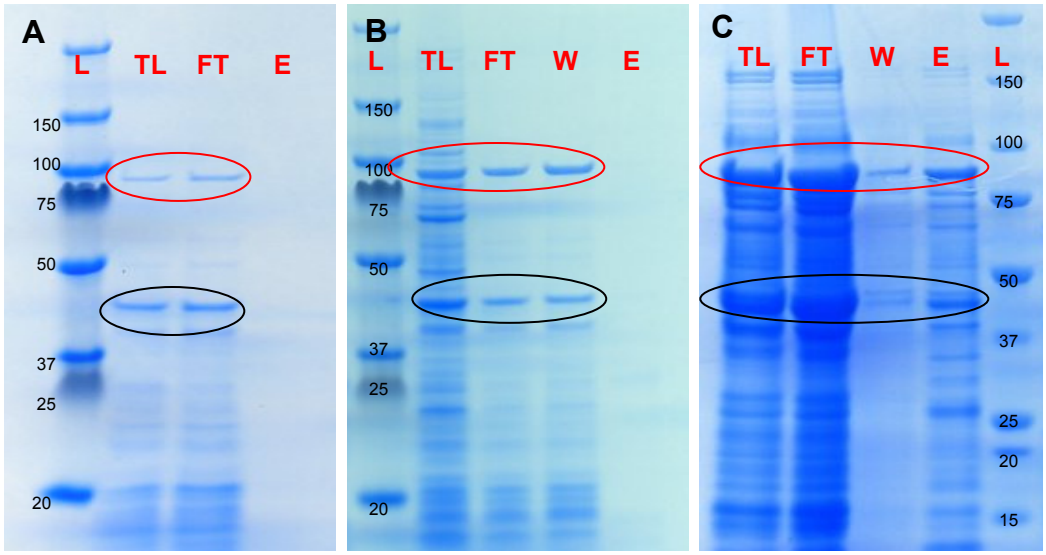


Figure 7.6: Co-expression strategies of RABGGT lead to successful production of both subunits, albeit with low yield. Representative examples from each co-expression strategy include A) construct no 1 with equivalent expression of RABGGT subunits but failure to attach to Ni-NTA B) construct no 9 with similar profile to no 1 and C) construct no 10 with high expression level of both subunits but partial attachment to NiNTA. L: Biorad protein ladder, TL: total lysate, FT: flow through, E: elution W: wash with washing buffer. RABGGTA in red circle, RABGGTB in black circle

7.3 EXPRESSION OF CHML AND CHM IN *E.COLI* LEADS TO SEVERE PROTEOLYSIS

Purification of CHML and CHM from bacterial vectors proved to be a very difficult process. Generally, in all purification schemes attempted for CHML, the 6x-His-tag failed to attach to Ni-NTA column. Similar results were observed when either N-terminal or C-terminal 6-His tags were used, indicating that the position of the tag did not influence the result (Table 7.3). Poor attachment of a protein target to Ni-NTA could be attributed to a hindered

interaction of a 6x-His tag with Ni^{2+}, even under denaturing conditions. To overcome this problem, CHML was also cloned in pBEN1 vector, allowing incorporation of the more specific SBP tag and subsequent purification from streptavidin/agarose resin. However attempts to elute CHML from streptavidin were also not very successful, although the eluted protein was purer in comparison to the hexahistidine tagged constructs. Therefore a more plausible explanation for the failure of CHML to bind to the resin of choice might be the presence of a buried tag, resulting from improper protein folding attributed to the expression of the protein in a bacterial environment.

Table 7.3: Purification trials of CHML expressed in *E.coli* and their outcome

Construct	Step 1	Step 2	Step 3	Yield (mg/L)
pNIC_CTHF_CHML	IMAC	TEV cleavage	GF	0.7
pNIC28_Bsa4_CHML	Manual elution Ni-NTA	IMAC	GF	0.4
pNIC28_Bsa4_CHML	IMAC	TEV cleavage	GF	0.4
pNIC28_Bsa4_CHML	Ammonium sulphate fract.	IMAC	TEV cleavage	1
pNIC28_Bsa4_CHML	IMAC	TEV cleavage	Anion exchange	1
pBEN1_CHML	Manual elution strept.	GF	-	1
pNH-TrxT_CHML	Manual elution Ni-NTA	-	-	< 0.1

The poor expression of CHML observed in each case was a result of low solubility and rapid degradation of the product. To overcome such problems, several strategies were employed. As the presence of hexahistidine tag does not seem to promote protein solubility or attachment to Ni column, purification via Ni-NTA was not suitable and more traditional purification methods were explored. Ammonium sulphate fractionation was used as first purification step, aiming to reduce hydrophilic interactions and successfully precipitate CHML. Furthermore, as the 6x-His tag cannot dramatically alter protein properties normally, TEV cleavage was employed to allow successful binding of contaminated proteins to the Ni column and elution of the desired protein.

The presence of SET1 tag in pBEN cloned construct should enhance solubility of REP constructs and decrease the possibility of improper folding (Waugh, 2005) whereas the longest and more specific SBP tag should minimize the possibility of burial in the secondary protein structure, hindering it from the solvent. Also the fusion of the protein with a thioredoxin tag was aimed at increasing solubility and additionally to prevent protein precipitation or inclusion body formation (LaVallie *et al.*, 2003). In all steps described above, the protein was rapidly processed and fresh protease inhibitors were added between each purification step to limit degradation possibly attributed to the action of serine

proteases (Sidorovitch *et al.*, 2002) but in each case there was a rapid protein degradation and instability. An assay for complex formation by analytical gel filtration chromatography, as described in Alexandrov *et al.* (1999) using purified RAB6B:CHML, RAB7:CHML and RAB7:CHM demonstrated inability of either REP to recognize the substrate (Figure 7.7). The absence of complex formation between unprenylated REP1 and Rab substrate can be sometimes attributed to the low concentration of REP and not to the fact that it cannot bind the substrate (Baron and Seabra, 2008), but elevated concentrations of CHM or CHML did not affect Rab binding and displayed similar profiles as in Figure 7.7 (data not shown).

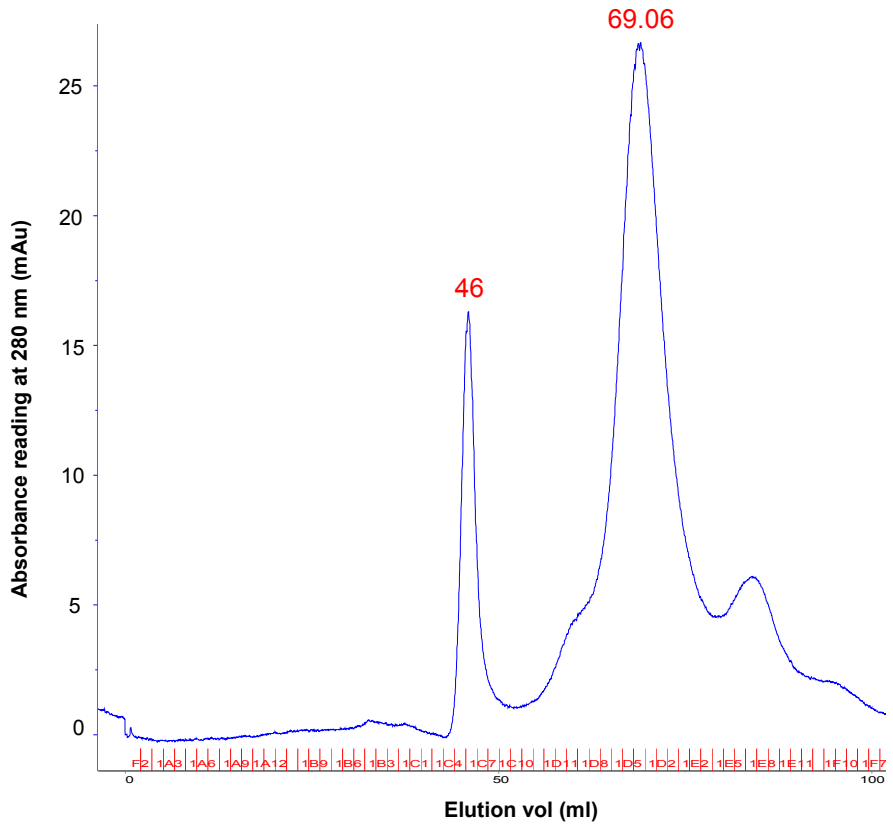


Figure 7.7: Analytical gel filtration on a Superdex 200 column shows that CHML fails to recognize and bind RAB6B substrate When injected individually, the retention time for CHML and RAB6B corresponded to 46 ml and 69 ml respectively. 10 µM of CHML were mixed with 50 µM of tagged RAB6B in presence of 2 mM $MgCl_2$ and incubated at RT for 20 min and then at 37 ºC for 15 min to allow possible complex formation prior injected to the column. There was no evidence of the formation of a 120 kDa complex which should peak at 38 ml and the retention time of substrates remained as described above as they both eluted from GF in their monomeric state and their identity was confirmed via SDS-PAGE.

CHM test expression trials gave similar results to CHML, including poor attachment of the protein to the resin of choice, increased proteolysis and low yield (Table 7.4). Furthermore, taking into account the extensive homology of the proteins, the

difficulties encountered in purification process of CHM can be attributed to the same reasons as described for CHML in Section 4.3, concluding that another expression system was required for the appropriate expression of both CHML and CHM.

Table 7.4: Purification trials of CHM constructs and their outcome

Construct	Step 1	Step 2	Purity	Yield (mg/L)
pNIC28_Bsa4_CHM	IMAC	GF	medium	1.4
pBEN1_CHM	Manual elution strept/agarose	-	low	< 0.1
pNH_TrxT	Manual elution Ni-NTA	-	low	1

Summarizing the above observations, the following conclusion can be drawn for CHM/CHML constructs i) their solubility is reduced in the bacterial system and cannot be enhanced with traditional purification methods or using a variety of tags ii) protein degradation occurs which can only be attributed to bacterial proteases and iii) there is a need for an alternative expression system to overcome these difficulties.

7.4 PURIFICATION OF RAB SUBSTRATES FROM RECOMBINANT *E.COLI* VECTORS RESULTS IN HIGH YIELD

Rab proteins are dependent on REP interaction in order to complete successful prenylation when forming a complex with RGGT, however, in contrast with CHM, CHML is unable to support prenylation of all Rabs (Goody *et al.*, 2005) or binds with a considerably lower affinity to certain Rabs (Rak *et al.*, 2004). In these particular experiments, RAB6B and RAB7 were the substrates of choice, as their prenylation rate is roughly equivalent for both CHM and CHML (Cremers *et al.*, 1994, Seabra, 1996) and can be used as substrate for either protein, without alteration of the rate of GG transfer by RGGT.

7.4.1 RAB6B is highly expressed in recombinant *E.coli*

Human RAB6B was expressed from pLIC-GST vector (Appendix B) with an N-terminal GST fusion tag followed by a 6His tag with a thrombin cleavage site. The soluble fraction was subjected to IMAC (2.17.3) (Figure 7.8). Fractions containing RAB6B were pooled and elution buffer was exchanged with thrombin cleavage buffer (2.17.7). Both tags were removed by incubation with thrombin protease (2.17.5) and were successfully separated from the protein by IMAC. Finally thrombin was

separated from RAB6B by anion exchange chromatography (2.17.6) (Figure 7.8). A typical yield was 3 mg/L of protein.

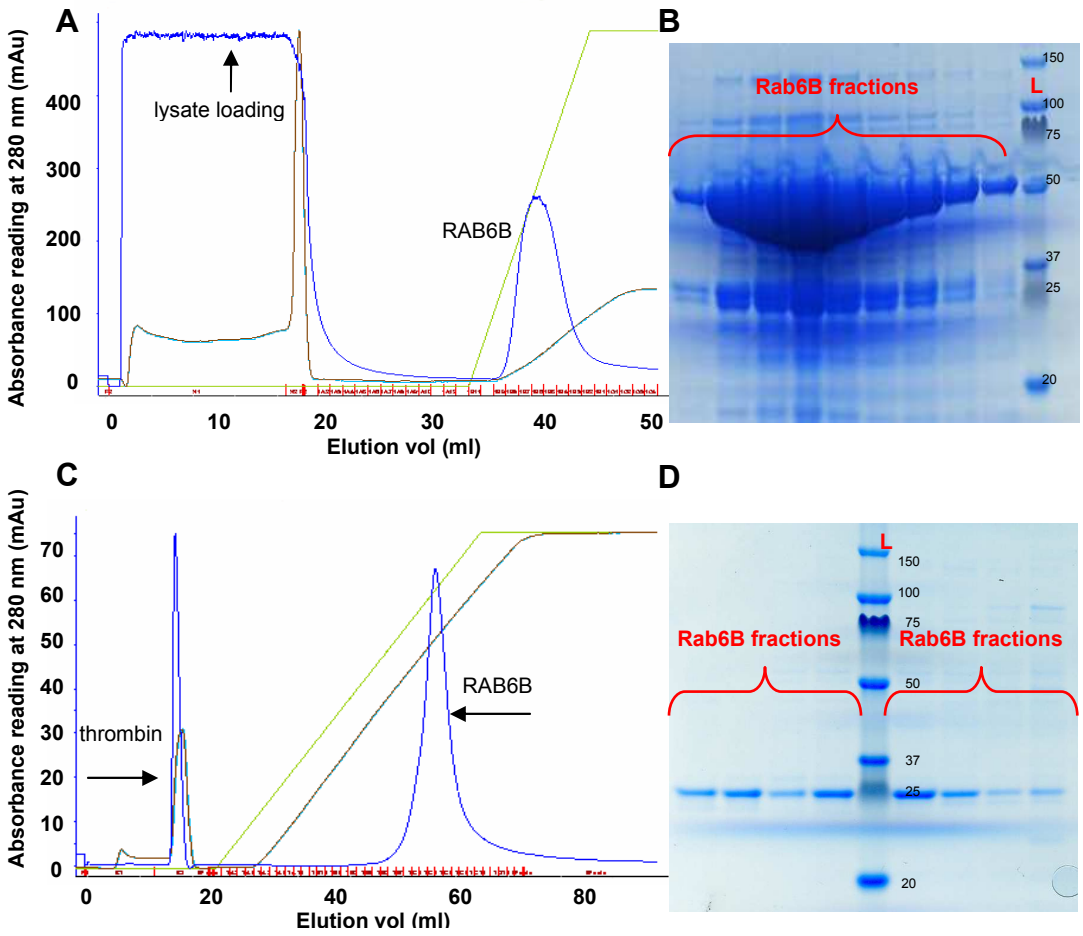


Figure 7.8: Successful purification RAB6B from *E.coli*. Elution profiles of Rab6B obtained from the various purification stages performed on Akta Express system (left hand site). The absorbance at 280 nm (blue line), the salt gradient (green line) and the conductance of the eluent (brown line) were monitored continuously. All purified fraction were subjected to SDS-PAGE analysis to confirm integrity of protein (right hand site). A) Affinity chromatography followed by B) SDS-PAGE analysis was performed as described in section 2.15.4. The eluted protein was approximately 51 kDa. C) Anion exchange chromatography and D) SDS-PAGE of RAB6B performed as described in section 2.17.6 and 2.19.1 respectively. The successfully purified and cleaved protein was determined to be around 23.4 kDa. L: Biorad dual color protein ladder.

7.4.2 Purification of RAB7 from *E. coli* is only feasible at low salt concentration

The RAB7 expression and purification method followed the RAB6B one with the only difference being that TEV cleavage was employed instead of the thrombin cleavage tag. In most purifications, the hexahistidine protein tag was not removed, as high yield of pure protein was obtained in only two steps and as tag was not very large like the GST or bound to alter protein properties (Figure 7.9). It was however observed that RAB7 precipitated out of solution when purified at 500 mM NaCl and thus reduction of the salt concentration at 100 mM was essential to maintain the integrity and function of RAB7.

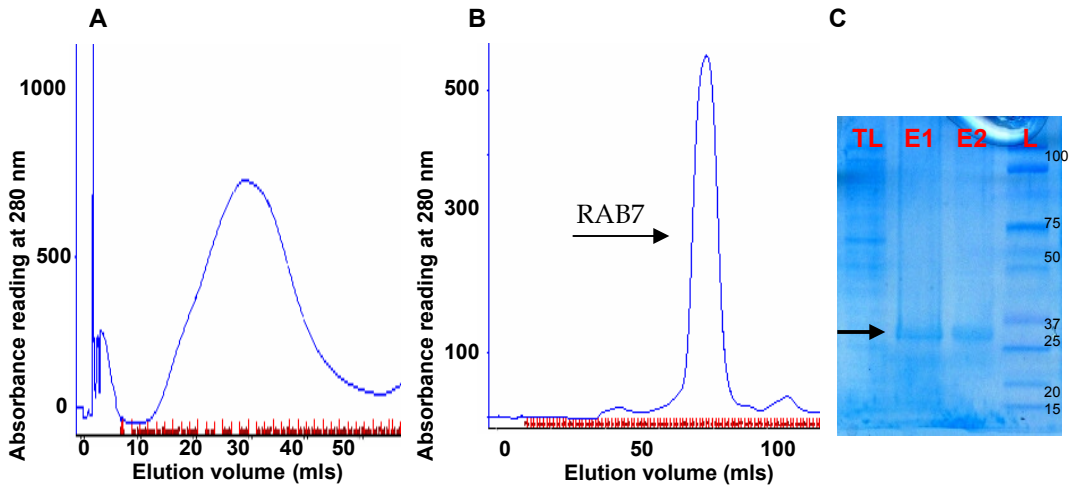


Figure 7.9: RAB7 was successfully purified by IMAC and gel filtration from *E.coli*. Elution profiles of Rab7 obtained from the various purification stages performed on Akta Express system. A) IMAC of RAB7 was performed as described in section 2.17.3. Successfully eluted protein was approximately 25 kDa. B) Gel filtration of RAB7 performed as described in section 2.17.4. C) SDS-PAGE gel showing the purified protein (arrow) at 25 kDa TL: total lysate E1-E2: Eluted fractions from gel filtration column and L: Biorad dual color protein ladder.

7.5 RGGT ASSAYS REVEAL GERANYLGERANYLATION WITH DUAL EXPRESSION CONSTRUCTS

Following successful expression and purification of RGGT components, a series of activity assays were performed in order to test the functional status of RABGGT and assembly of individual components to an active complex. The preferred assay method was based on Baron et al. 2008, except that GDP was also added to the reaction mixture, as there was no indication of the endogenous level of GDP synthesis in *E.coli*. In order to test whether activity

observed is a result of product formation and not an artifact, four different incubation time points were selected (15, 30, 45, 60 min) where the radiolabelled Rab product should increase with incubation time, until perhaps reaching a plateau. Moreover, different negative controls were used to exclude false positive results: i) absence of RGGT enzyme ii) absence of RAB6B or RAB7 and iii) absence of CHML or CHM in REP presence. In cases i) and ii) no radioactive incorporation should be observed, as there is no enzyme to carry out the transfer or no substrate to bind respectively. In case iii) some activity might still be observed, as absence of chaperone protein should decrease binding of RGGT to Rab substrate but not completely abolish it. Furthermore as different constructs are stably expressed in high (CHM and CHML) or low salt concentrations (RAB7, RGGT complex) a compromise for the assay buffer and protein storage buffer was necessary for maintenance of all components in solution.

Assay performed for RABGGT obtained from dual expression construct no 1 indicated successful geranylgeranylation with a calculated rate of 0.0034 nmol/min/nmol and a k_{cat} of 0.00056 sec^{-1}. This rate is lower when compared to the published values for RABGGT (Thoma *et al.*, 2000). As expected, absence of RAB7 or RGGT in the assays did not result in detectable activity whereas

the absence of CHML seemed to significantly reduce, but not completely abolish GG transfer (Figure 7.10).

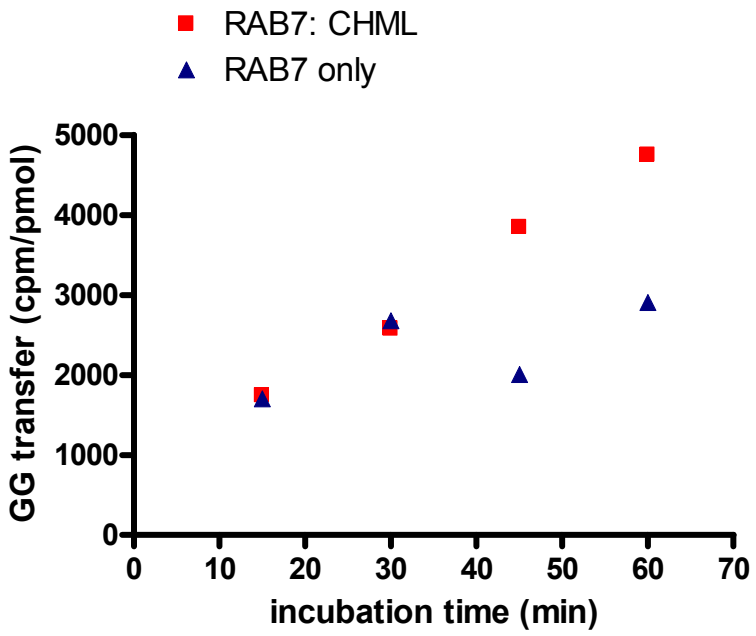


Figure 7.10: Time-course of RAB7 geranylgeranylation catalyzed by the dual expressed RABGGT.

No activity was observed with RAB6B: CHML or RAB6B CHM substrates for either single or dual expression constructs. In agreement to this outcome, no complex formation was observed in assays of analytical gel filtration, where RGGT components were incubated at 37 °C for 30 min in presence of GGPP. As RAB6B is recorded to be the slowest Rab recognized by CHM or CHML, absence of activity might be a combination to low REP availability as well as slow rate of association. Furthermore no activity was obtained for single expressed constructs with RAB7 substrate. A

possible explanation for the latter could be inability of REP substrate to alter protein folding in individually expressed RABGGT that leaves association and recognition of alpha and beta subunits unaffected, but alters its functional status and compromises its ability to recognize and bind to its chaperone protein.

Crystallization trials using single expression constructs with coarse screens were not successful whereas trials with dual expression constructs were not performed due to time limitations.

7.6 BACULOVIRAL EXPRESSION OF RGGT COMPLEX

All purification attempts of RGGT from *E. coli* resulted in low protein yield or insoluble protein, indicating that the bacterial expression environment is probably not ideal for correct protein folding. It was therefore decided to switch the expression of RGGT complex to another system, enhancing protein solubility. The baculoviral system was the obvious choice as it has been successfully used to generate all soluble RGGT components, albeit with truncated version of RABGGTA (Armstrong *et al.*, 1995).

Cloning all four RGGT components into the transfer vector pFastBac_CTHF was performed as described in Section 2.3; the vector of choice has a hexahistidine tag that allows target

purification from Ni-NTA and a FLAG tag, that permits protein identification via Western blotting. Prepared bacmid DNA was successfully transfected into Sf9 cells and after the end of 72 hr incubation period, enlarged, elongated infected cells were visible for all constructs whereas control, uninfected cells were confluent and abundant (Figure 7.11 A). Cells obtained from subsequent infections of Sf9 cells for production of P1/P2 viral stocks as described in 2.31 indicated similar profile, but unfortunately it was not possible to scale up expression and successfully produce P3 viral stock, as infected cells examined under inverted microscope gave a picture similar to 7.11 B (results not shown).

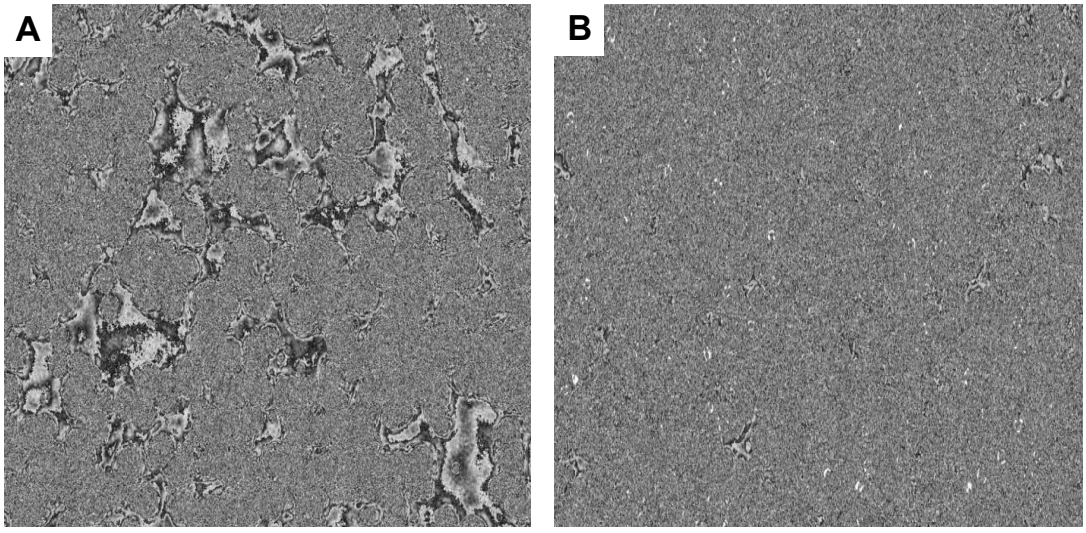


Figure 7.11: Photomicrograph of insect cells transduced with a bacmid virus as described in 2.31. The Sf9 cells were transduced with 100 plaque-forming units of virus per cell and photographed 72 hrs after the addition of the virus. Clear areas with infected, enlarged cells were visible in all samples (panel A) whereas control cells remain small and abundant (panel B). X40 magnification.

The most abundantly expressed protein was RABGGTB, as it was present in cell lysate obtained from P0 and P1 viral stock, whereas no other construct was expressed at such high viral titre (Figure 7.12).

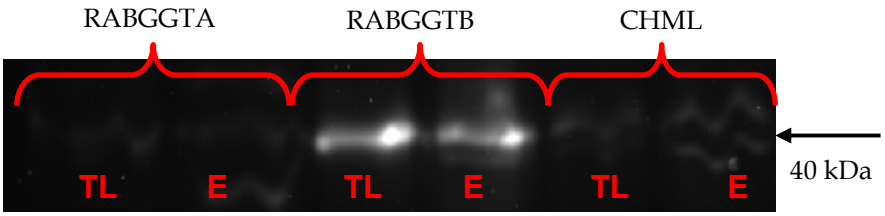


Figure 7.12: Presence of a 40 kDa band in RABGGTB but not in RABGGTA and CHML lysate obtained from P0 viral stock indicates successful expression of Beta subunit. Pre-cleared cell extracts infected with P1 baculoviral stock of RABGGTA, RABGGTB and CHML constructs were obtained from IMAC (2.17.3) purification steps and subjected to Western blotting, along with total lysate and the protein of interest was detected with FLAG antibody visualized with IgG HPR. TL: Total Lysate, E: Elution samples

A band corresponding to approximately 70 kDa was visible in RABGGTA total lysate, flow through and eluted sample of Sf9 cell lysates infected with P2 stock but not in the RABGGTB eluted sample used as negative control, indicating expression of RABGGTA subunit (Figure 7.13 A). A band of approximately 80 kDa was detected by western blotting CHM samples of Sf9 infected cells with P2 stock (Figure 7.13 B). Similarly, a 80 kDa band was

present in total lysate and flow through by western blot of CHML samples of both P1 and P2 stock but not in the eluted ones, indicating possible expression of CHML but inability to attach to Ni-NTA (Figure 7.13 C).

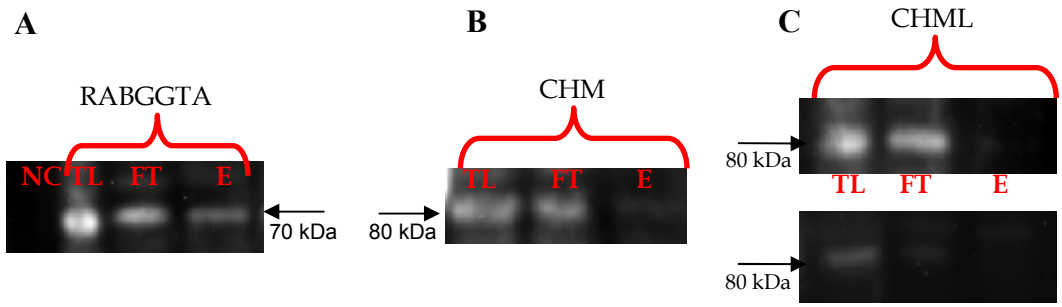


Figure 7.13: The presence of a 70 kDa band in RABGGTA but not in RABGGTB indicates successful elution of alpha subunit. B) Presence of a 80 kDa band in CHM and C) CHML sample indicates possible expression of REP. Pre-cleared cell extracts of Sf9 cells infected with P2 viral stock from A) RABGGTA B) CHM and C) CHML constructs were obtained from IMAC (2.17.3) purification steps and subjected to Western blotting, along with total lysate and the protein of interest was detected with FLAG antibody visualized with IgG HPR. TL: Total Lysate, FT: flow through, E: Elution samples

Despite successful infection and possible detection of RGGT proteins in Sf9 cell lysates, subsequent infection and scaling up of expression in 100 ml cultures from produced P3 viral stock was not successful, as observed cells showed no sign of viral infection on examination with an inverted microscope. The reasons for the unsuccessful scale up of baculoviral expression are not clear. The

stock of Sf9 cells was properly split every two days and maintained at 27 ºC at 180 rpm with proper aeration. This, in combination to the presence of a proper control sample in each viral stock, ensured proper infection in every step of viral amplification, as it is possible to incorrectly attribute the morphology of old cells with limited nutrients to a successful infection (Shrestha *et al.*, 2008). The presence of 2 % FBS in high density cultures helped to maintain cell viability and inhibit clumping whereas no viral stock was kept in culture for more than 72 hr as virus produced at a very late phase decrease the efficiency of infection and protein production. Prolonged cultures are also known to increase Sf9 cell lysis and thus proteolytic activity that disrupts target protein expression (Kost *et al.*, 2005). As RGGT constructs appear to be successfully expressed in the baculoviral system, optimization of the protein yield by testing multiple truncated constructs should be attempted next.

7.7 CONCLUSIONS

The protein production of all RGGT components proved a very challenging task with some surprising results. For individual expression or co-expression, all described strategies were employed to enable protein expression and yield optimization including: IPTG

and medium selection, temperature of induction, tag purification, antibiotic resistance, protease inhibition, combination of traditional/novel purification schemes, host selection. This study is the first one to confirm successful expression and purification of the full length human RABGGTA construct in *E.coli*, where all other groups failed to obtain expression (Dursina *et al.*, 2002). Successful co-expression of RABGGT subunits in *E.coli* was also achieved, despite of the failure of this strategy to minimize protein degradation, advance proper folding and optimize activity (Li *et al.*, 1997). Indication for a functional full length RABGGT co-expressed in *E.coli* is also provided in this report and it is a novel finding, encouraging further crystallographic studies that will, for the first time, succeed in revealing structure of full length RABGGTA subunit in human.

Given the indication for the low activity observed with CHML/RAB7 substrates for the dual expression construct, scaling up of the protein for further crystallization trials should be attempted. Absence of CHML: RAB6B formation complex in analytical gel filtration chromatography supports the activity assay data whereas CHML: RAB7 binding remains to be tested. Given the fact that as complex formation was demonstrated for RABGGTA: RABGGTB single expression constructs and that enzyme activity with CHML: RAB7 was recorded for dual expression constructs,

absence of RGGT activity in simple expression constructs might be attributed to the inability of CHM / CHML to recognize and bind RGGT, due to an alteration in protein folding and not mainly due to REP proteolysis. Successful crystallographic studies can clarify this point.

Production of P0/P1/P2 viral titre for all constructs was achieved in a baculoviral system but scaling up the expression failed. There was indication of a significant expression level in total extracts as well as in 1 and 3 ml preparations but not in 100 ml cultures. It is possible that the viral titre is low and thus not sufficient to infect large amounts of Sf9 cells and enable sufficient protein preparation. Also, protein might be lost in centrifugation, and is therefore not visible in eluted fractions in Western blots or SDS-PAGE gels. Thus, effective recovery and crystallization of RGGT proteins from the baculovirus system would require additional creation and testing of truncated constructs, optimization of scaling up of protein yield for successful infection of 1L cell cultures. Co-expression of RGGT subunits with the chaperone protein REP might promote the production of properly folded protein and result in increased yield (Higgins *et al.*, 2003).

8. IN VITRO EFFECTS OF N-BPs ON OSTEOCLASTOGENESIS

8.1 INTRODUCTION

The N-BPs are thought to mainly exert their pharmacophore effects on inhibition of bone resorption by targeting OCs (Boonekamp *et al.*, 1986, Flanagan and Chambers, 1989, Hughes *et al.*, 1989). N-BPs are proposed to drive OC apoptosis or compromise their ability to resorb bone by either directly targeting FPPS and thereby inhibiting prenylation of small regulatory proteins, essential for OC survival and function (Dunford *et al.*, 2001), or indirectly by inducing γ-δ T cell activation and OC lysis, through cytoplasmic accumulation of DMAPP and IPP, mainly after chronic administration of the drugs (Roelofs *et al.*, 2009, Thompson *et al.*, 2006b). The observation that cleavage of the mammalian sterile 20-like kinase which is considered responsible for OC apoptosis, was blocked by addition of geranylgeraniol but not farnesol to N-BP treated OCs (Fisher *et al.*, 1999, Reszka *et al.*, 1999), indicating that specific blockage of RGGT and thus loss of GGPP might be the main cause of OC apoptosis (Coxon *et al.*, 2000).

Although the cytotoxic effect of BPs on the differentiation and viability of cells of osteocytic/macrophage lineage was documented

(Cecchini *et al.*, 1987, Cecchini and Fleisch, 1990, Stevenson and Stevenson, 1986), there are still controversies regarding their effect on osteogenic cells located earlier in the differentiation line such as OC precursors and monocytes, which may also be involved in the action of BPs on bone resorption.

Many questions have been posed regarding the exact localization of BP within bone, as well as the ability of cells other than OC to take up N-BPs *in vivo.* Early studies have indicated that BPs may act not only by inhibiting the activity of mature OC but also by decreasing osteoclastogenesis (Lowik *et al.*, 1988). It was observed that BPs decreased the proportion of multinucleated cells expressing markers of the osteoclastic lineage (calcitonin, TRAcP) in human long-term bone marrow cultures (Hughes *et al.*, 1989). A defective osteoclastic resorption observed with 15-day mouse metatarsal explants treated with BPs was attributed to suppression of early OC precursors without however altering the osteoclastogenic capacity of the mature osteogenic cells (Van Beek *et al.*, 2002). Investigation of the localization and cellular uptake of BP *in vivo* using the FAM-RIS analogue that was shown to inhibit protein prenylation in cells (Kashemirov *et al.*, 2008) indicated Ris uptake not only by OC but also the bone surface in osteocytic lacunae close to vascular channels, monocytes and macrophages in the bone marrow (Roelofs *et al.*, 2010).

Circulating OC precursors in peripheral blood can be mobilized by chemotaxis and recruited as a source of replenishment in selected sites in bone marrow, especially during bone remodeling or fracture repair (Malone *et al.*, 1982, Udagawa *et al.*, 1990). It was shown that circulating mononuclear OC precursors obtained from PBMCs can differentiate *in vitro* in cultures enriched with M-CSF and RANKL and finally mature into functional OCs (Fujikawa *et al.*, 1996, Hofbauer *et al.*, 1999, Matayoshi *et al.*, 1996, Quinn *et al.*, 1998). Treatment of isolated monocytes from PBMCs with RANKL and M-CSF leads to the generation of mature OCs after 14 days. On day 0, the isolated monocytes are small, spherical and mononuclear and supported in tissue culture only by M-CSF. On day 7, the precursor cells are still mononuclear but have an enlarged cytoplasm and start expressing the surface receptors for RANKL. On day 14 and upon the influence of RANKL present in the culture media, larger multinucleate cells of OC-like appearance are visible. These cells express all the known markers of mature OCs but are not capable of bone resorption until day 21 of culture (Figure 8.1).

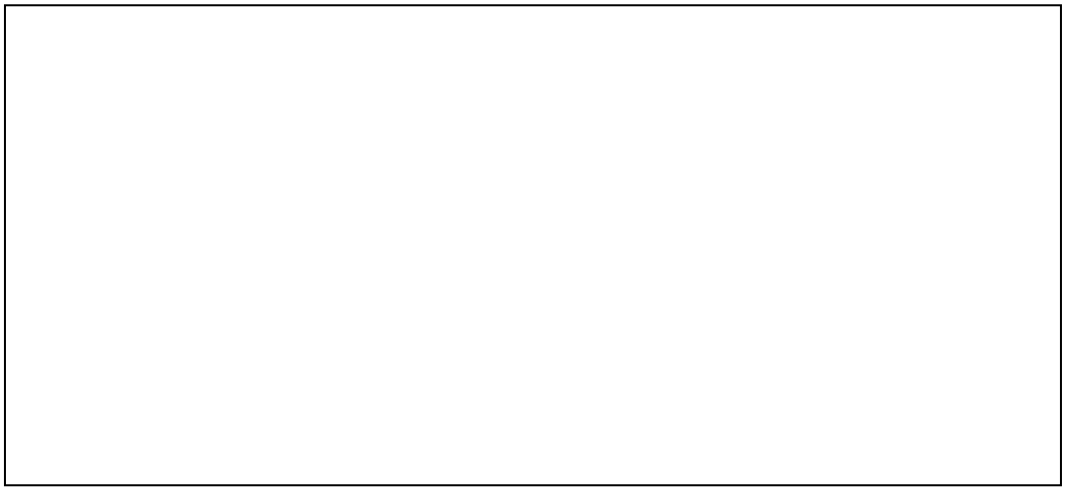


Figure 8.1: Stages of OC development from BPMCs in tissue culture. **Figure has been removed due to Copyright restrictions**

In the current study a novel method was designed for the *in vitro* evaluation of the effects of N-BP administration on distinct stages of osteoclastogenesis, in order to assess the drug efficacy on formation and morphology of mature OC. The effects of Ris, Zol, Iba and Ale on the *in vitro* osteoclastogenesis were examined in PBMC cultures where the relevant N-BP was added between i) days 0-14 to determine the overall effect of the drug on the suppression of osteoclastogenesis ii) days 0-7 to assess the effect of the drug on OC precursor viability and differentiation while simultaneously assessing any alteration towards their commitment to the OC lineage upon drug withdrawal at day 7 and iii) days 7-14 to investigate suppression of differentiation of OC mononucleate precursor cells to mature OC, without affecting the number of monocytic precursors. This study also aims to link the observed

FPPS inhibition kinetics to the physical alterations in OC formation and morphology and to confirm that the observed potency of individual BPs in kinetic studies has an impact on defects observed in osteoclastogenesis.

8.2 MAIN EXPERIMENTAL DESIGN AND LIMITATIONS OF THE CURRENT STUDY

The concentrations of N-BP used in tissue culture experiments were initially based on the kinetic data arising from inhibition curves of WT FPPS with individual N-BPs. The selected concentrations were adapted for individual N-BPs after performing preliminary experiments where the viability of PBMCs was tested (data not shown), leading to the use of a range of concentrations between 0-500 nM. Identification and characterization of the multinucleated cells was also confirmed by Western blot analysis of the three major markers of mature OCs (calcitonin, OSCAR, cathepsin K) performed on cell lysates obtained from cultures maintained in N-BP concentrations close to the IC_{50} values of individual BPs (10 nM for Ris and Zol, 100 nM for Iba and Ale). Human PBMCs were used as a source of OC precursors and were cultured on 24 well plates for 15 days as described in Section 2.30.1. At the end of the culture period, the number of generated

multinucleated cells exhibiting OC characteristics, their area and the number of nuclei per cell were determined. Relevant comparisons between treated and untreated cultures indicated a significant ($p>0.001$) and dose-dependent reduction in OC formation whereas comparisons between the different N-BPs determined their *in vitro* efficacy.

This designed *in vitro* assay with the absence of a mineralized matrix cannot distinguish between the formation of active (bone resorbing) or inactive (inert) OCs and may perhaps unintentionally include multinucleate cells such as macrophages in the statistical analysis and thus obscure the results obtained. Cultures of isolated hPBMCs in presence and absence of clinical BPs were performed in parallel and used as internal standard to validate the alterations of the bone resorbing effect of mature OCs (data not shown). However, it was not possible to quantify the amount of BPs that was ultimately absorbed by the dentine slices used due to the different molecular status of BP and matrix (soluble and solid form) and thus it is difficult to correlate the dose-response effect of individual BP on OC suppression and bone resorption.

It should be stated that due to the length of individual experiments, the high cost of maintenance of the OC in tissue culture and the difficulty of obtaining blood samples in sufficient quantity to perform a complete experimental set, only three sets of

data per treatment were obtained. There are four different factors-treatments to be taken under consideration: (i) the incubation profile (0 – 7 days, 7 – 14 days and 0 – 14 days), (ii) the N-BP selected (Ris, Zol, Iba, and Ale), (iii) the N-BP concentration (0, 1, 10, 100, 250, and 500 nM), and (iv) the origin of the blood (7 different individuals). For simplicity, initial *post hoc* pairwise comparisons, each one at fixed drug concentration and incubation time, were performed which confirmed the parametric nature of results. However these comparisons disproved the initial assumption in the experimental design which excluded the influence of origin of the blood on the relative cell count. Therefore in any parameter explored (OC number, size or nuclei number) there have been two variances: the blood origin (BO) and the N-BP used (BP). In cases where an equal amount of data was available for comparison, a two-way ANOVA test was used. However, in cases where the experimental design was unbalanced (for example, fewer viable cells were available for determination of OC size at 500 nM in Zol treatment than for the weaker inhibitor Iba), results could not be analysed with a two–way ANOVA and were analysed with a General Linear Model (Grafen and Hails, 2002). This model assumes that the variance (with respect to a grand mean) of all the experimental results is partitioned into the influence (i) of blood origin (BO) and (ii) of BP, and that which doesn't fit these two is

assigned to random error. The significance of the two factors is then assessed from the BO-error and BP-error ratios. In most cases, the influence of the BO dominated the results, obscuring the influence of BP, thus only preliminary observations regarding the nature of inhibition can be made at this stage. However the outcome of the present laboratory findings can serve as a pilot study in order to evaluate the physiological impact of the FPPS inhibition and to gain some insights on the morphological and physiological alterations observed in the *in vitro* osteoclastogenesis.

8.3 INHIBITION OF OSTEOCLASTOGENESIS BY N-BPs IS MAINLY ATTRIBUTED TO THE DECREASED PRECURSOR AVAILABILITY AND NOT TO A DEFECTIVE COMMITMENT TO THE OSTEOCLASTIC LINEAGE

Assessment of newly formed OC obtained following individual N-BP treatments indicated a dose-dependent reduction in OC numbers compared to the control, with threshold effects apparent at >10 nM drug concentrations. For both day 0-14 and day 7-14 treatments, the blood origin influenced the results and therefore the statistical analysis could not be performed. The trend of OC formation in 0-14 group indicated the following order of potency: Ris = Zol >> Ale = Iba with Ris showing similar potency to Zol (IC_{50}

10.3 ± 3 nM and 14.9 ± 6.5 nM respectively) followed by Ale and Iba (IC_{50} 15.8 ± 13 nM and 37.4 ± 28 nM respectively). An identical order of potency was obtained with the N-BP treatment at days 7-14 with similar IC_{50} values for the pairs Ris-Zol (IC_{50} 76.6 ± 30.8 nM versus 43.8 ±18.7 nM) and Ale-Iba (IC_{50} 275.4 ± 46.8 nM versus 232.3 ± 123 nM).

The results obtained after the day 0-7 treatment for selected drug concentrations of 100, 250 and 500 nM indicate that the influence of the N-BP is significant ($p = 0.016$) and not dominated by the blood origin ($p = 0.757$) (General Linear Model) (Figure 8.2). The *post hoc* comparisons indicated that the order of N-BP efficacy is: Zol> Ris >> Iba> Ale which is also in agreement with the kinetic studies on WT FPPS. Therefore Zol appeared to be the most potent N-BP in the inhibition of OC formation from the isolated monocytes, followed by Ris, Iba and Ale with respective IC_{50} of 7.4 ± 3 nM, 9 ± 4.9 nM, 20.9 ± 9.5 nM and 51.3 ± 28 nM.

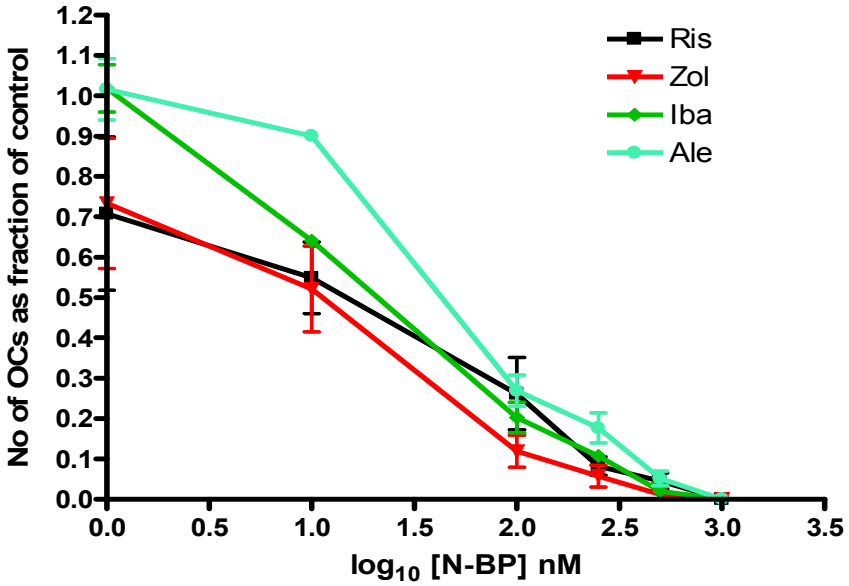


Figure 8.2: Effect on N-BP treatment of OC cells for day 0- 7. OC numbers shown as percentage of the control (untreated) cells. Results shown as means of SEM (6 replicates) and represent three individual experiments.

Studies on the effect of the individual N-BP treatment in the various stages of osteoclastogenesis indicated that suppression of OC numbers was more dramatic when drug was administered from the day zero of PBMC culture, with no recovery in OC formation upon drug withdrawal at day 7 (Figure 8.3). On the contrary, osteoclastogenesis was less affected by individual N-BPs when OC precursors were allowed to form (day 0-7) and drug was added from day 7 onwards. The OC precursor apoptosis upon drug administration at day 7-14 could be a result of a decrease in a cytokine, such as OPG, essential for OC formation and survival

(D'Amelio *et al.*, 2010) whereas a decreased OC number at treatments 0-14 and 0-7 days can mainly reflect a reduction on monocyte numbers in the culture. Furthermore, apoptosis studies following drug administration at day 0-2 indicated a prevalence of dead cells over living cells in the tissue culture, confirming the rapid action of N-BP on OC survival (data not shown). Taken together, the results indicate that the reduced number of OC can be attributed to the increased apoptosis of monocytes at days 0-7, leading to a reduced availability of OC precursors rather than to a reduced commitment of the formed precursors to the OC lineage.

The data obtained here are not in accord with previous clinical studies with Ale, which indicated an increase in OC number by a factor of 2.6 in post-menopausal women receiving 10 mg of Ale per day for 3 years as compared to the placebo group (Weinstein *et al.*, 2009). Such an increase in OC numbers was also observed upon treatment with Iba and Ris but not with the non-nitrogen BPs and was attributed to an increased bone surface (Bikle *et al.*, 1994) or recruitment to resorption sites mainly observed after the first 48 hr of administration (Fisher *et al.*, 2000). On the contrary, a decreased number of both OC and their precursors were noted in Zol administered stroke patients (Poole *et al.*, 2009) whereas increased OC numbers were not found upon treatment with Zol.

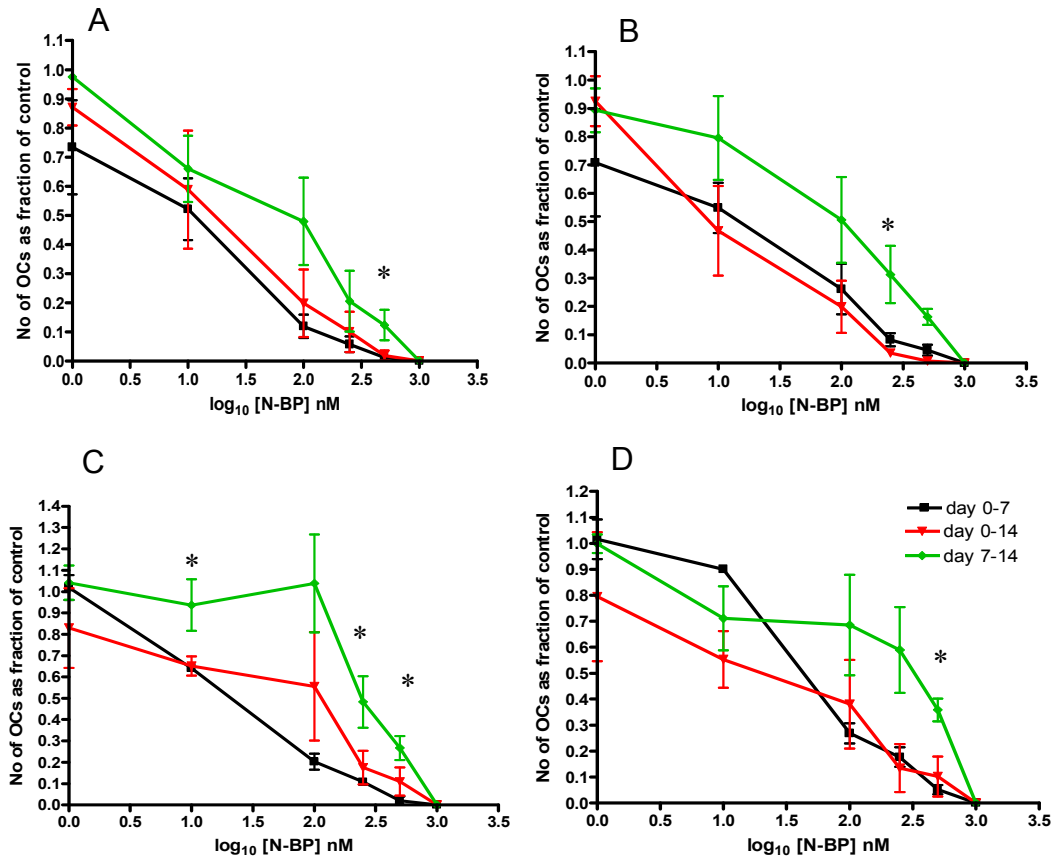


Figure 8.3: Comparison of the effects of A)Ris B)Zol C)Iba and D)Ale on distinct stages of osteoclastogenesis. Administration of N-BP at day 7-14 has a less adverse effect on osteoclastogenesis with all examined drugs compared to day 0-14 and day 0-7. OC numbers are shown as percentage of the control (untreated) cells. Results shown as means of SEM (6 replicates) and represent three individual experiments. * denotes $p<0.05$ between day 7-14 and other two groups (One-way ANOVA with Tukey post-hoc test).

8.4 ALTERATIONS IN MORPHOLOGY OF IBA- AND ALE-TREATED OCs INDICATE INCREASED FUSION OF OC PRECURSORS

Subtle changes in OC morphology such as altered cytoskeleton, abnormal formation of resorption pits and decreased

ruffle border have been observed following BP administration and were reported to be connected to their reduced capacity of resorbing bone (Sato and Grasser, 1990, Sato *et al.*, 1991, Selander *et al.*, 1994).

In the present study it was generally very difficult to draw any conclusions regarding OC size and number of nuclei per cell, as analysis with the general linear model proved that results were all BO dependent, with use of fresh blood in the cultures resulting in formation of larger and multinucleated OCs and use of stored blood yielding smaller and less abundant OCs. However comparison of N-BP treatments obtained from stored blood indicated that at chosen concentrations of 10 nM and 100 nM, an increase of OC size was observed in Ale and Iba cultures for the 7-14 day group only (Figure 8.4 and 8.5). Similarly, the number of nuclei per OC, was increased in Ale- but not in Iba-treated OC for the 7-14 day group, indicating increased fusion of OC precursors (data not shown). In contrast, Zol and Ris did not modify either the size or the number of nuclei per OC in any treatment (Figure 8.6).

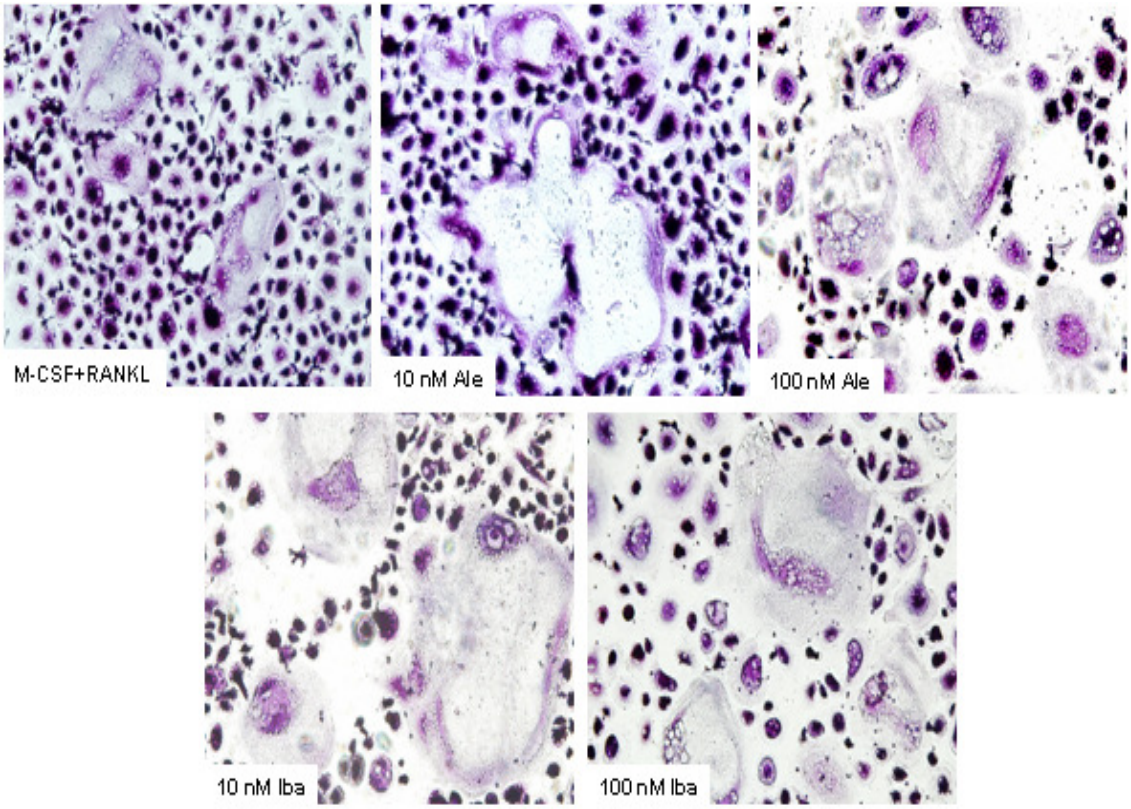


Figure 8.4: An augmentation in the area of Ale- and Iba- treated OCs for day 7-14 is observed at drug concentrations of 10 nM and 100 nM. Representative images of OC were obtained after treatment with M-CSF and RANKL for 14 consecutive days and with either Ris or Zol for the days 7-14 as described in Section 30.1 and stained for TRAcP as described in Section 30.3. Magnification x10.

The distinctive effect of Ale on OC precursors compared to other N-BPs is in agreement with reports of patients treated with Ale, where a number of giant non-resorbing OC was correlated to the cumulative administered dose in post-menopausal women (Weinstein *et al.*, 2009). Indeed, some studies indicated that inhibition of bone resorption by Ale was mainly a result of their

disrupted cell organelle morphology and cytoskeletal alterations and was independent of apoptosis (Alakangas *et al.*, 2002, Halasy-Nagy *et al.*, 2001). The mechanism by which Ale and Iba increase the size of OC precursor is currently not known and requires further investigation.

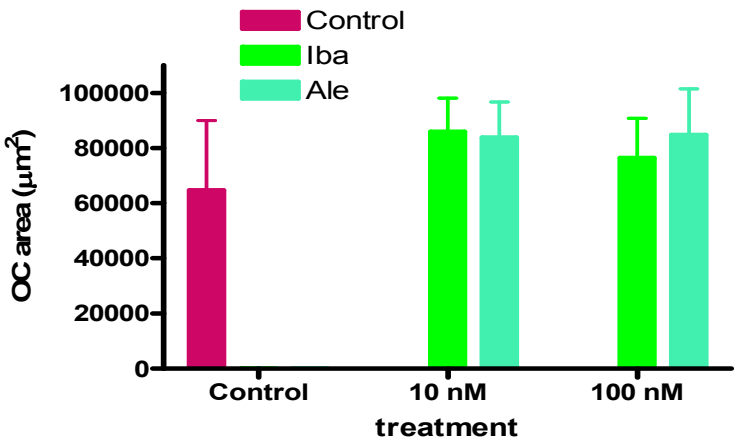


Figure 8.5: Increased size of OC area following treatment between day 7-14 with 10 and 100 nM Iba or Ale. Results shown as means of SEM and represent three individual experiments with blood obtained from Bristol blood bank.

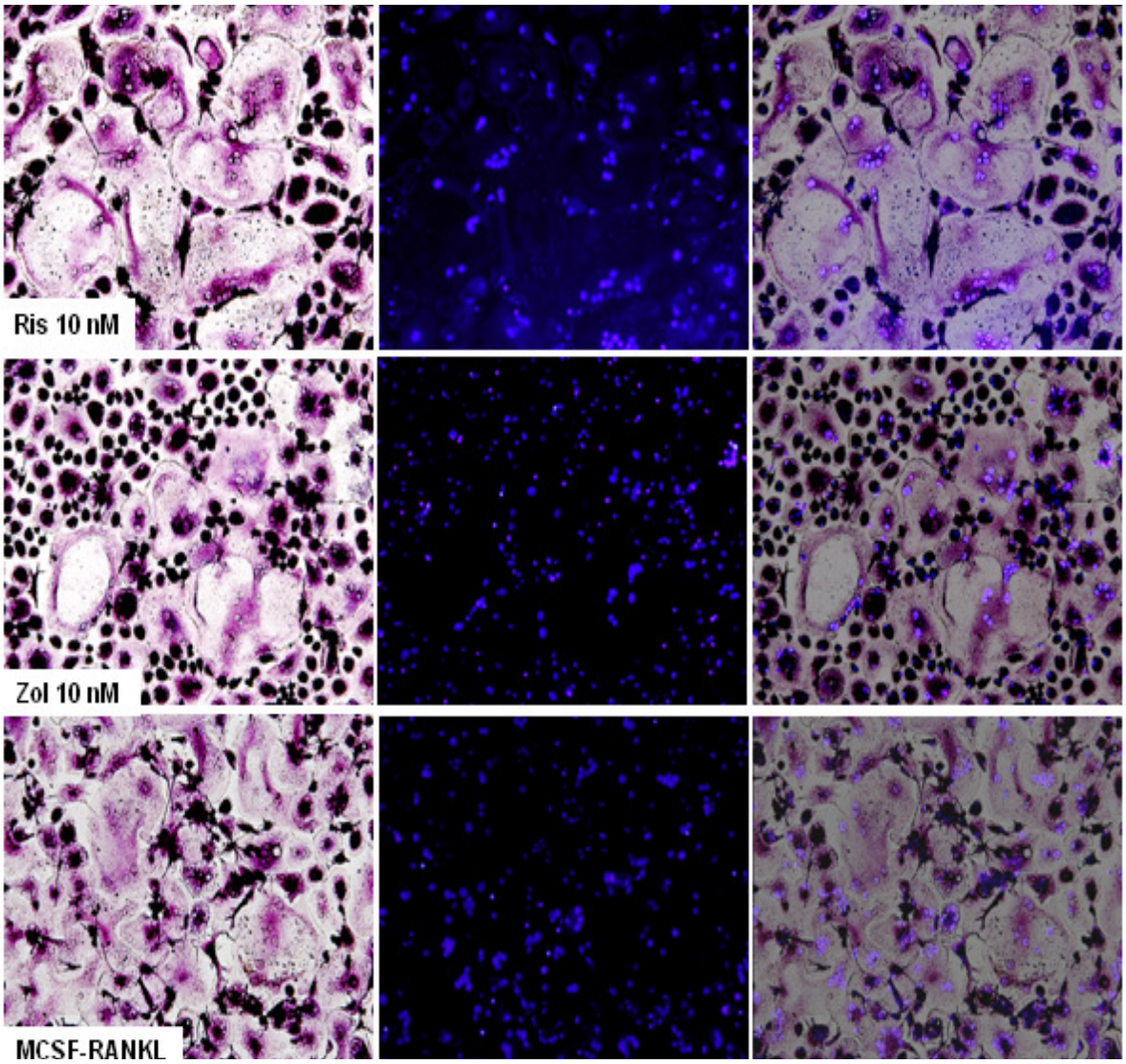


Figure 8.6: Ris and Zol treatment does not modify the size of OC. Representative images from an individual experiment with fresh blood for the treatment day 7-14. Representative images of OC were obtained after incubation with M-CSF and RANKL for 15 consecutive days and with either Ris or Zol for the days 7-14 as described in Section 30.1 and stained for TRAcP and DAPI as described in Section 30.3. TRAcP staining (left) DAPI (middle), merged (right), Magnification x10.

8.5 CONCLUSIONS

The current OC culture system proved to be a good model to study the *in vitro* effects of N-BPs on osteoclastogenesis. All experiments clearly demonstrated that all the N-BPs examined significantly and dose-dependently suppress osteoclastogenesis. The impact of N-BP seems to be more severe on the monocytic rather than the OC precursor cell line, as osteoclastogenesis is irreversibly inhibited following drug administration at day 0 without much influence on the commitment of the formed precursor cells to the OC lineage, in the presence of M-CSF and RANKL. The N-BP application between day 0-7 confirmed Zol as the most potent suppressor of osteoclastogenesis, mainly exerting its effect by inducing apoptosis of the cultured monocytes, while Ris, Iba and Ale were progressively less potent. With the exception of Ale, there is general agreement between the WT FPPS inhibition data and the observed apoptotic effect on individual N-BPs on OCs, which may be attributed to decreased prenylation. However the results with Ale shows a decreased IC_{50} value for all incubation intervals studied compared to the IC_{50} obtained for FPPS activity. This suggests that Ale may promote monocytic apoptosis by a mechanism independent of its effect on FPPS. However detection and quantification of unprenylated GTPases in OC cultures treated

with N-BPs is necessary to investigate the effect of Ale compared to the other N-BPs.

Investigations of individual OCs indicated an increase in size of Ale- and Iba- treated cells but only with 10 nM and 100 nM N-BPs and for day 7-14. The effect was more profound with Ale, where an increased number of nuclei per individual OC indicated increased fusion of OC precursors. This observation confirms the different effects of individual N-BPs upon OC, as Ale-treated cells were the least affected by apoptosis. However formation of large OCs might also result in an altered cytoskeleton leading to their inability to resorb bone. Future resorption assays on dentine slices saturated with an effective concentration of N-BP might answer this question.

It should be noted that the results described in this chapter are only preliminary as there were only three groups of experimental data and variances arising from the blood origin were responsible for statistically inaccurate results. In retrospect, a better experimental design could have been attempted if the blood had been obtained from matched sources (e.g. ethnic origin, gender, freshly isolated or from blood bank, blood group) or if a greater number of experimental datasets had been incorporated into the study.

9. GENERAL DISCUSSION

9.1 THE IMPORTANCE OF KEY FPPS RESIDUES IN CATALYSIS AND N-BP BINDING: PRESENT AND FUTURE STUDIES

The main focus of this thesis was the exploration of biochemical and structural alterations of human FPPS occurring upon N-BP binding and was investigated via site-chain directed mutagenesis of key residues proposed to interfere with drug or substrate binding. The interpretation of the experimental findings aids in prioritizing the importance of the individual FPPS conformational changes occurring during catalysis or N-BP binding and either confirms, disproves or adds to our knowledge of the existing catalytic and inhibition mechanisms. More specifically, the degree of involvement of the selected amino-acids in FPPS catalysis and N-BP binding was correlated to the structural changes that accompany the mutations and alterations of the proposed kinetic model, as described below.

9.1.1 The impact of FPPS mutations on enzyme catalysis and substrate binding

The following subsections (9.1.1.1 to 9.1.1.7) aim to classify the studied amino-acids studied according to their importance and involvement in distinct aspects of the FPPS enzymatic reaction. A summary of the current findings in combination with proposed future studies, confirmation or rejection of existing theories or introduction of new schemes can be found in Table 9.1.

9.1.1.1 Catalytic mechanism

Among the residues examined, the highly conserved aspartate motif including Asp103 and Asp107 was proved to be pivotal for catalysis, as the DADA FPPS mutation completely abolished FPPS activity, indicating the importance of the maintenance of the negatively charged Asp in stabilization of the partially closed enzyme conformation. As the closure of the allylic binding site entrance is strictly dependent on the movement of two highly conserved aspartate motifs triggered upon occupation of the binding pocket by the substrate or inhibitor (Rondeau *et al.*, 2006) it seems that any disruption of this step leads to abolition of catalysis. The experimental data are in agreement with studies performed

with rat FPPS (Joly and Edwards, 1993) and yeast FPPS (Song and Poulter, 1994), where, any individual mutation (conserved or not conserved) of Asp103 or Asp107, severely compromised catalysis, but failed to indicate any possible involvement of either residue to substrate binding, as originally proposed (Ashby and Edwards, 1990). However, the individual effect of Asp103 or Asp107 mutations were not assessed here and absence of either enzymatic activity or crystal structure of the DADA mutant means that there is no information regarding product formation or the accompanying conformational alterations.

Assessment of the catalytic efficiency of the remainder of mutants examined was accomplished by comparison of the K_{cat}/K_m^{IPP} resulting ratio, which takes into account the variation of IPP specificity in individual mutants. It was therefore shown that removal of the catalytic base for proton abstraction from IPP in the condensed carbocation intermediate in the R112L mutation strongly suppressed catalysis. Catalysis was also severely reduced (21000 fold) when formation of the IPP binding pocket was obstructed in F239A mutant but less so when the affinity for both GPP and IPP was altered (in Lys200 mutations 5500- 1900 fold decrease) whereas when only the IPP binding was

compromised (Tyr204 mutations) the enzyme preserved up to 80% of its catalytic activity. Summarizing the above results, Asp103 and Asp107 are the most pivotal residues taking part in catalysis, followed by Arg112, Phe239, Lys200 and Tyr204.

9.1.1.2 GPP product formation and liberation

Among the residues examined, Lys200 was shown to be the most strongly implicated in GPP binding, as K200E and K200G substitutions alter the hydrophobic character and size of the allylic binding pocket and thus reduce the enzyme specificity for GPP binding. The unaltered K_m^{GPP} in K200L FPPS confirms that maintenance of the hydrophobic character of the residue is essential for allylic binding. The two-fold increase in K_m^{GPP} observed in the R112L mutant possibly arises from impaired GPP liberation due to disruption of the catalytic mechanism upon carbocation formation but not from a conformational alteration of the GPP binding site. Removal of the aromatic Phe239 in F239A FPPS does not affect GPP binding despite of the decreased hydrophobicity and thus the minor increase in K_m^{GPP} probably originates from low DMAPP affinity which in turn slightly compromises GPP binding. Finally Tyr204 substitutions had no effect on GPP/FPP product formation.

9.1.1.3 DMAPP binding

Kinetic and crystallographic data show a potential involvement of Lys200 and Phe239 residues in DMAPP binding. More specifically, misalignment of DMAPP in K200G possibly reflects the inability of the enzyme to recognize and bind the first IPP molecule. Abolition of the Lys200 positive charge in the K200L mutant results in the loss of electrostatic attraction between DMAPP and FPPS and finally, dislocation of the DMAPP in K200E due to the repulsion generated by the negatively charged Glu accounts for impaired GPP binding and catalysis. The F239A FPPS data confirm the proposed role of Phe239 in orientation of DMAPP for catalysis (Koyama *et al.*, 1995), as the decreased GPP affinity cannot be attributed to either de-stabilization of the partially closed conformation or alteration of the allylic binding pocket. It has to be stated that the conclusions drawn regarding DMAPP orientation are only based on existing FPPS catalytic models whereas explanations of the present data can account for but not actively demonstrate any alteration occurring in DMAPP level. Kinetic studies where DMAPP will be used as substrate followed by thin layer chromatographic analysis of the products as well as co-crystallization of the above mutants with DMAPP and IPP

will be employed in future studies to confirm the above theories.

9.1.1.4 IPP saturation

All the examined constructs showed a negative effect on affinity for IPP, arising from: i) obstruction of IPP binding to the homoallylic pocket and formation of carbocation intermediate, ii) impaired IPP reaction with the GPP and formation of FPP, iii) lack of orientation of the bound IPP in the pocket and iv) a combination (i) and (ii). More specifically, the most profound alteration was observed in K200E FPPS where, dislocation of DMAPP causes impaired IPP binding (case i) and FPP formation (case ii) and a remarkably increased K_m^{IPP}. A similar situation occurs in K200L and K200G FPPS, however the unaltered affinity for GPP somehow compensates for the reduced Leu200 or Gly200- assisted binding to the diphosphate moieties of IPP, allowing progression of catalysis. Obstruction of IPP reaction with GPP (case ii) was observed in F239A. Inability of Leu112 to aid abstraction of the C_2 hydrogen of the IPP from the non-metal ligated pyrophosphate in R112L FPPS leads to defective reaction of IPP with the GPP (case ii) but not with DMAPP. Finally, lack of orientation of the IPP (case iii) towards the

carbocation site might account for the misplacement of IPP in the binding pocket.

9.1.1.5 Impaired FPP synthesis and GPP accumulation

Two residues were considered important for product specificity in FPPS: Lys200 and Phe239. In K200E, the concomitant increase in K_m^{GPP} and K_m^{IPP} may accelerate GPP synthesis and compromise FPP synthesis, altering the end product of reaction as previously observed in bacteria (Koyama *et al.*, 1995) and yeast (Blanchard and Karst, 1993). In F239A, IPP binding is severely compromised, shifting the equilibrium of the reaction to the left hand side and perhaps leading to GPP accumulation. Future experimental work by mass spectrometric analysis of the reaction products will confirm or disprove the above theories.

9.1.1.6 C-terminal lid formation and thus E:I complex isomerization

Destabilization of the fully closed conformation and impaired IPP binding pocket formation has a negative impact on IPP affinity and mainly on the enzyme: inhibitor isomerization step which accounts for the strength of inhibition by N-BPs (Kavanagh *et al.*, 2006b). Shifting of the C-terminal tail away from the IPP binding pocket was observed in K200G and F239A, with concomitant reduction of IPP

affinity and favouring the non-isomerized enzyme:inhibitor state which probably accounts for reversibility of inhibition. The remainder of the mutations (R112L, K200L, Y204F, Y204A) reveal no disruption of C-terminal lid formation and thus enzyme: inhibitor isomerization effects whereas the lack of crystal structures for either K200E or DADA FPPS constructs does not permit us to draw any conclusions regarding the role of these aminoacids in the positioning of the C-terminal basic tail.

9.1.1.7 GPP binding pocket formation

A dramatic enlargement of the allylic binding site due to the replacement of Leu with Gly was observed in K200G mutation which may have resulted in decreased specificity of the allylic binding pocket for DMAPP or GPP, permitting accommodation of IPP instead.

Table 9.1: Summary of suggested role of individual FPPS mutations (next page**):** in I) catalysis, II) GPP product formation and liberation III) DMAPP orientation, IV) IPP saturation, V) Impaired FPP synthesis and GPP accumulation, VI) C-terminal lid formation and thus E:I isomerization and VII) GPP binding pocket formation proves, disproves or introduces new theories and is a subject of future studies.

Mutation	I	II	III	IV	V	VI	VII	Theories proved	Theories disproved	Theories introduced	Future work
Y204F	√	—	?	√√	—	—	—	n.a.	n.a.	involvement in catalysis/IPP binding	Co-crystallization with DMAPP-IPP
Y204A	√	—	—	√√	—	—	—	n.a.	n.a.	involvement in catalysis/IPP binding	Co-crystallization with DMAPP-IPP
K200G	√√	√	√?	√	—	√√	√√√	Poulter, 1976 Koyama et al. 1996 Tarshis et al. 1996	none	alteration of allylic binding site reduced specificity for FPPS destabilization of closed conformation	thin layer chromatography mass spectrometry of products Co-crystallization with DMAPP-IPP
K200L	√√	—	√?	√√	—	—	—	Plochocka et al. 2000 Rondeau et al. 2006; Kavanagh et al. 2006	Brems et.al. 1981; Blanchard et al. 1993	maintenance of hydrophobicity is essential for formation of allylic binding pocket	thin layer chromatography mass spectrometry of products Co-crystallization with DMAPP-IPP
K200E	√√	√√	√?	√√√	√?	?	—	Sanchez et al. 2006	none	alteration of catalytic product	as in K200G and K200L
R112L	√√√	√	?	√√	—	—	—	Song et al. 1994 Hosfield et al. 2004 Rondeau et al. 2006	Joly et al. 1993	defective 2nd IPP binding	None needed
F239A	√√	—	√?	√√	√?	√√	—	Koyama et al. 1995 Hosfield et al. 2004 Rondeau et al. 2006	none	alteration of catalytic product shifting of C-terminal tail defective 2nd IPP binding	mass spectrometry of products
DADA	√√√	?	?	?	?	?	—	Ashby et al. 1990 Joly et al. 1993 Song et al. 1994 Tarshis et al. 1994 Rondeau et al. 2006	none	complete abolition of catalysis	kinetic and structural studies on individual D103A & D107A FPPS

√√√	very important	—	not involved
√√	important	?	unknown
√	involved	n.a.	not applicable
√?	possibly involved		

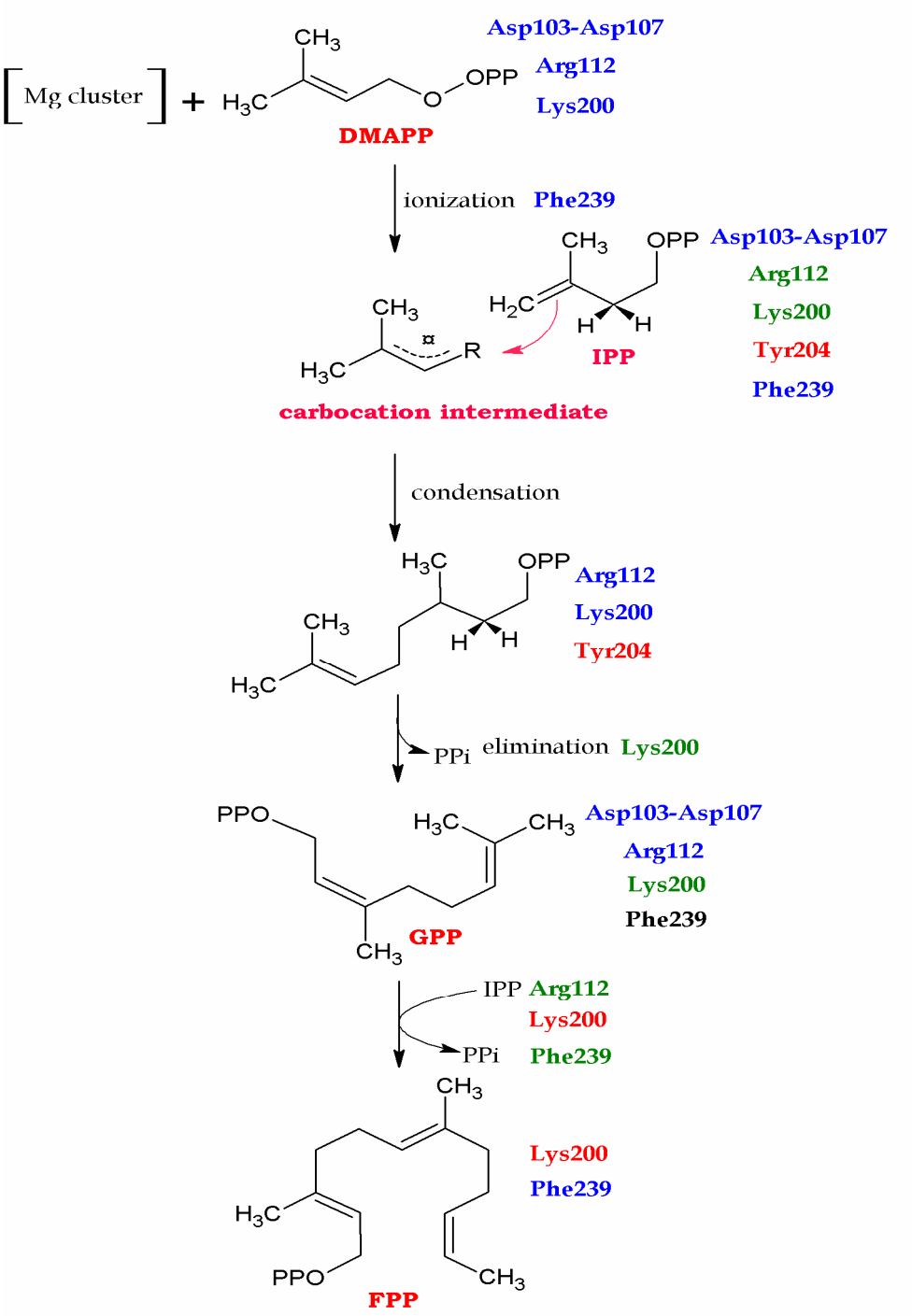


Figure 9.1: Major amino-acids that play pivotal role in FPPS catalytic mechanism as identified in the current study. This scheme comprises an update of the existing mechanism as denoted in Figure 1.26. The present study either confirms (in green), rejects (in black) or introduces (in red) the involvement of FPPS side-chain residues in catalytic mechanism. In blue: role not examined.

9.1.2 The impact of FPPS mutations on N-BP binding and inhibition

The following sections (9.1.2.1 to 9.1.2.4) highlight the major molecular mechanisms that arise from interactions between individual amino-acids and govern the FPPS inhibition by the major clinical N-BPs. A summary of the current findings along with the proposed future work can be found in Tables 9.2 and 9.3 and in Figure 10.2.

9.1.2.1 Ris

All constructs studied exhibited a higher or unaltered Ki and Ki* for Ris compared to WT enzyme, indicating the importance of examined residues in Ris binding. The weakest inhibition was observed with Lys200 FPPS mutants and collectively the data disproved the importance of the hydrogen-bond between the carbonyl oxygen of Lys200 and Ris for drug binding or change in isomerization state (Kavanagh *et al.*, 2006b). It is rather the alteration of the hydrophobic character of the allylic binding pocket which accounts for the reduced Ris binding. Two more factors contribute to the reduction of the binding of Ris to the FPPS in the allylic binding site which accentuate the effect in K200E FPPS: i) the abundance of GPP in the active site due to the

increased K_m^{GPP} and K_m^{IPP} which favours its accumulation and ii) the impaired IPP binding which reduces fixation of Ris and sequestration of the site from bulk solvent and accounts for the impaired enzyme: inhibitor isomerization step.

In F239A FPPS, the decreased initial and final inhibition by Ris is a combination of: i) disrupted electrostatic interactions between phosphonate and surrounding residues due to alteration in hydrophobicity and ii) defective switching of the highly basic hydrophobic tail which compromises maintenance of the isomerized state. Finally, the Tyr mutations confirmed the role of aromatic ring but not of the hydroxyl moiety of Tyr204 in Ris binding. Furthermore, a typical aromatic interaction between the phenyl ring of Tyr204 and Ris may result in expulsion of water of the active site and thus account for a large entropic change that strengthens Ris inhibition.

9.1.2.2 Zol

The interpretation of the kinetic and crystallographic data that aimed to assess the inhibition mode of FPPS produced by Zol proved to be the most challenging one and revealed the different nature of Zol inhibition compared to the heterocyclic Ris, but also a deviation from the standard 1:1 enzyme: inhibitor binding ratio

observed in WT and most mutants. The unexpectedly increased inhibition observed in Tyr204 mutants was attributed to: i) lengthening of the Lys200 and Thr201 bifurcated hydrogen bond with the nitrogen atom of the imidazole ring which is positioned deeper in the allylic binding pocket and ii) allosteric regulation occurring upon binding of one Zol molecule which prevents flexing of the second FPPS monomer, which is otherwise catalytically active. Conservation of the Thr201 hydrogen bond with Ris following disruption of the Lys200 with Ris in all Lys200 mutated FPPS constructs rescues the orientation of the imidazole ring whereas reinforcement of electrostatic interactions secures Zol in the binding pocket (in K200G). The increased initial inhibition observed in F239A is possibly an effect of the defective orientation of the DMAPP, which impairs GPP synthesis and concomitantly favours the binding of the well-orientated Zol to the allylic pocket. Finally the reduced overall inhibition observed in K200L, K200E and F239A mainly originates from the disrupted enzyme: isomerization step due to defective IPP binding or switching of the highly basic hydrophobic tail.

9.1.2.3 Iba

All designed mutations with the exception of Y204F FPPS reinforced the strength of competitive inhibition produced by Iba, and accounts for the different mechanisms. The decreased Ki in all Lys200 mutated FPPS constructs observed with Iba is a combination of: i) the rigidity of Iba molecule due to the presence of the methyl group which secures the maintenance of any adopted conformation once bound to the pocket and ii) the decreased affinity of the binding pocket for the isoprenoid products which favours allylic displacement by the long hydrophobic side chain of Iba. The Tyr204 mutations confirm the importance of hydrophobic and electrostatic interactions of the Iba pentyl side chain for FPPS inhibition which are reinforced in the absence of the bulky phenyl ring in Y204A. Finally, the increased binding of the highly hydrophobic Iba in F239A might be attributed to the decreased hydrophobicity of the allylic pocket which favours the long hydrocarbon tail of Iba over GPP binding.

9.1.2.4 Ale and Pam

Kinetic and crystallographic studies revealed that the mode of FPPS inhibition by Ale and Pam is governed by identical mechanisms, with subtle differences mainly arising from their

structural flexibility. More specifically, all point mutations indicated that: i) the hydrophobicity of the binding pocket is important for maintenance of Ale and Pam inhibition ii) the rupture of hydrogen bond between Ale or Pam and Lys200 or Tyr204 does not compromise competitive inhibition iii) the more hydrophobic and flexible Ale which is a stronger competitive inhibitor and iv) the phenyl ring of Tyr204 is important in the development of van der Waals/ electrostatic interactions.

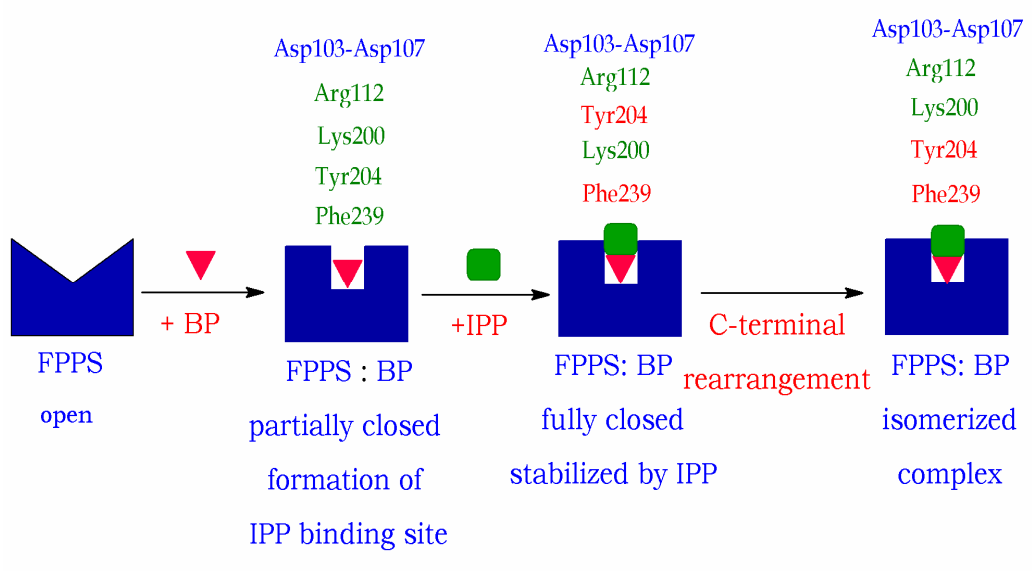


Figure 9.2: Updated schematic representation of the mode of inhibition of FPPS by N-BPs. The major amino-acids that are confirmed (in green), or identified (in red) to play a pivotal role in the binding and successful FPPS inhibition by the N-BPs in accordance to the findings of the present research.

Table 9.2: Observed effects of the studied FPPS mutations in N-BP binding

Mutation			Ki*						Ki		
	Ris	Zol	Iba	Ale	Pam		Ris	Zol	Iba	Ale	Pam
Y204F	—	++	—	- - -	- -		—	—	—	—	—
Y204A	+	++	—	- - -	+		+++	- - -	-	-	—
K200G	+++	- - -	—	—	—		—	—	- - -	—	—
K200L	+++	++	+++	—	—		—	—	- -	—	+++
K200E	+++	+++	++	+++	+++		+++	—	-	+++	+++
F239A	+++	—	++	++	+++		++	- - -	- - -	- - -	+++

+++	greatly increased (p <0.001)
++	increased (p<0.01)
+	slightly increased (p<0.05)
—	unaltered
-	slightly decreased (p<0.05)
- -	decreased (p<0.01)
- - -	greatly decreased (p <0.001)

Table 9.3: Current studies on the interaction of individual point mutations with the major clinical N-BPs prove, disprove or introduce new theories and are a subject of future studies

Construct	Theories confirmed	Theories introduced	Future work
Tyr204	Burley et al. 1986 Kavanagh et al. 2006 Yin et al. 2006 Dunford et al. 2008	van der Waals- electrostatic interactions between phenyl ring and N-BP aromatic ring of Tyr204 essential for N-BP inhibition allosteric regulation of FPPS by Zol OH moiety does not favour competitive inhibition protonated form of Ris by FPPS does not play important role in N-BP inhibition	pH studies
Lys200	Martin et al. 1999 Rondeau et al. 2006 Kavanagh et al. 2006 Dunford et al. 2008	rupture of the hydrogen bond of Lys200 with the imidazole ring does not affect drug binding hydrophobicity of the allylic binding pocket is essential for N-BP binding structural flexibility of the individual BPs important for binding increase in binding pocket size favours Iba binding	Xtal structure of K200E with N-BPs
Phe239	Kavanagh et al. 2006 Gabelli et al. 2006 Rondeau et al. 2006	DMAPP disorientation which impairs GPP synthesis and favours Zol binding decreased hydrophobicity of the allylic pocket favours the binding of Iba & Ale Ris binding is reduced due to decreased hydrophobicity	Xtal structure with Pam

9.2 UNRAVELLING THE ASSEMBLY OF RGGT CATALYTIC COMPONENTS: PRESENT AND FUTURE STUDIES

This project constitutes the first major attempt to fully characterize the interaction and assembly of human RGGT catalytic components. Individual subunit expression in bacteria led to purification of full length RABGGTA and RABGGTB that were capable of recognizing and binding to each other and forming a stable complex, which however was apparently unable to associate with REP and perform geranylgeranylation of Rab. Dual expression of RABGGT was also successful, leading to functional protein and allowing a calculation of a geranylgeranylation rate, albeit low due to REP2 instability. This is the first report to provide indication for a functional full length expression of all RGGT components in *E.coli*. These novel findings encourage more extensive kinetic and crystallographic studies of RGGT components purified from bacterial system that will i) fully characterize the RABGGT complex with different Rabs and REP1 or REP2 and ii) reveal the structure of full length RABGGTA subunit in human.

Successful infection and detection of full length RGGT components in Sf9 cell lysates was also achieved, but failure to scale up protein production hindered the performance of kinetic

and crystallographic studies. Future work with the baculoviral system will aim to: i) scale up individual expression of all RGGT components ii) test various truncated constructs to achieve optimization of protein yield iii) co-express RGGT with the chaperone protein REP to promote the production of properly folded protein.

Crystallization of PC: RGGT and PC: REP: RGGT: Rab complexes should reveal the putative binding site of PC binding and confirm the existence of reaction transition states during the complex double geranylgeranylation reaction suggested by Baron et al. 2008. Confirmation of the interaction of PCs with RGGT is essential for structural optimization and improved selectivity of PCs, as these inhibitors may represent useful novel therapeutic agents in anti-tumour and Rab- associated diseases.

9.3 EFFECTS OF MAJOR CLINICAL N-BPs ON OSTEOCLASTOGENESIS: PRESENT AND FUTURE STUDIES

This report confirms the adverse effects of Ris, Zol, Iba and Ale on OC precursors and monocytes, which are possibly responsible for the anti-resorptive action of N-BPs *in vivo*. The N-BPs were found to mainly exert their anti-resoptive effect by promoting apoptosis of monocytes at days 0-7 with no recovery of

osteoclastogenesis after drug withdrawal on day 7. Suppression of differentiation of OC mononucleate precursor cells and promotion of their apoptosis was also observed, albeit with a less dramatic rate compared to the adverse drug effects on monocytes. The calculated IC_{50} values for all incubation intervals studied and for Ris, Zol and Iba were in general agreement with the WT FPPS inhibition data obtained from kinetic studies and confirm the link between the observed apoptotic effect and decreased protein prenylation. However the combination of i) a decreased IC_{50} value for Ale and for all three incubation intervals studied compared to the IC_{50} obtained for FPPS activity ii) an increased fusion of OC precursors, resulting in increased number of nuclei per individual OC, suggest an alternative mechanism of action for Ale. Future studies will focus on the elucidation of the Ale inhibitory action in *in vitro* osteoclastogenesis mainly by: i) investigation of prenylation effect in OC cultures ii) assessment of possible accumulation of IPP in OC and iii) evidence of possible association of OC precursors with T-cell IPP receptors.

9.4 THE RELEVANCE OF THE ENZYMATIC/MODELING STUDIES WITH REGARD TO THE IN VIVO POTENCY OF N-BPs: PRESENT AND FUTURE STUDIES

The *in vivo* antiresorptive potency of BPs is ultimately related to their *in vitro* ability to inhibit protein prenylation in OCs, as confirmed by the enzymatic/modeling studies. The rank order of inhibitory potency of N-BPs on FPPS in enzymatic assays coincided with their rank order of *in vivo* efficacy and thus their antiresorptive potency in animal models, as previously described by Dunford *et al* (2001). In all the mutants studied, the calculated K_{isom} for the clinically relevant N-BPs indicated that Zol exerted the strongest inhibitory effect, closely followed by Ris. Iba, with its more highly substituted nitrogen moiety remained more potent than Ale and Pam. Surprisingly Ale and Pam, which have similar structures with a basic primary nitrogen atom in an alkyl chain, exhibited different kinetic behaviour, with Ale always a stronger inhibitor than Pam, with the latter more susceptible to reversibility upon amino-acid substitutions and structural alterations.

Modeling studies on mutated FPPS confirmed the ability of Zol to strongly and irreversibly bind to the allylic site, mimicking

the carbocation intermediate and suppressing FPPS catalysis. As predicted from structure-activity relationship studies which associated the nitrogen atom of the heterocyclic ring with the irreversible binding to the allylic pocket, Ris and Zol remained the most potent FPPS inhibitors, particularly with inhibition by Zol being unaffected by the disruption of hydrogen bond interactions between its heterocyclic ring and mutated side-chain residues of FPPS. This stabilization of allylic binding site was not as firm for the aminoalkyl binding N-BPs Ale, Iba and Pam, and mixed/final inhibition was prone to reversibility upon substitution of individual side-chain residues that disrupted the proposed electrostatic interactions-hydrogen bonding. Indeed, the associated conformational changes that led to the switching of the C-terminal tail, kinetically quantified by K_{isom}, were significantly suppressed in the case of Iba, Ale and Pam, with the latter completely losing its inhibitory potency in Lys200 substitutions. On the contrary, Zol and Ris, displayed irreversible binding characteristics with most mutated FPPS constructs and any observed suppression of K_{isom} was mainly attributed to the inability to saturate FPPS with IPP or to a weak competitive inhibition between N-BP and GPP which indirectly compromised the reversibility of inhibition, without however abolishing it. Furthemore, both Ris and Zol are the stronger suppressors of *in*

vitro osteoclastogenesis, inducing apoptosis of either OC precursors or mature multinucleate cells, supporting the theory that OC apoptosis may be a major mechanism whereby BPs reduce OC numbers and activity (Hughes *et al.*, 1995).

In certain cases the *in vitro* studies on OC targets in combination with the enzymatic assays have failed to reproduce the relative *in vivo* potencies of clinical BPs. As a characteristic example the lack of efficacy of Ris which remains a strong inhibitor of FPPS and osteoclastogenesis *in vitro*, but reduces bone turnover to a lesser extent than all the other clinical N-BPs examined and has a lower mineral affinity that Ale *in vivo* (Russell *et al.*, 2007). Similarly Iba remains a potent inhibitor in vertebral but not in non-vertebral fractures, indicating that pharmacokinetics, in particular drug distribution might play a more important role than the mineral affinity binding or the potency to inhibit FPPS. The observation that concurrent treatment of parathyroid hormone with Ale may interfere with the anabolic response to parathyroid hormone indicates a different mechanism of action for this BP (Finkelstein *et al.*, 2006). In the experiments described here, Ale remains a potent inhibitor of FPPS but its antiresorptive potency seems to be associated with an alteration of the OC precursor fusion rather than a suppression of protein prenylation due to malfunction of FPPS.

Furthermore should be stated that the unique profiles of pharmacological potency of BPs and thus their ranked potency of resorption inhibition is not so profound in humans, where eventually the lower effective doses of all clinical BPs produce similar effects (Russell *et al.*, 2008). It may be that alternative metabolic pathways other than mevalonate pathway are involved in regulation of osteoclastogenesis and are responsible for the anti-resorptive potency of BPs which can uncouple their effects from those on protein prenylation but this theory remains to be experimentally tested.

10. LIST OF REFERENCES

Abrahamsen, B. 2010. Bisphosphonate adverse effects, lessons from large databases. *Curr Opin Rheumatol* **22**:404-409.

Adami, S., A. K. Bhalla, R. Dorizzi, F. Montesanti, S. Rosini, G. Salvagno, and V. Lo Cascio. 1987. The acute-phase response after bisphosphonate administration. *Calcif Tissue Int* **41**:326-331.

Alakangas, A., K. Selander, M. Mulari, J. Halleen, P. Lehenkari, J. Monkkonen, J. Salo, and K. Vaananen. 2002. Alendronate disturbs vesicular trafficking in osteoclasts. *Calcif Tissue Int* **70**:40-47.

Alexandrov, K., H. Horiuchi, O. Steele-Mortimer, M. C. Seabra, and M. Zerial. 1994. Rab escort protein-1 is a multifunctional protein that accompanies newly prenylated rab proteins to their target membranes. *EMBO J* **13**:5262-5273.

Alexandrov, K., I. Simon, V. Yurchenko, A. Iakovenko, E. Rostkova, A. J. Scheidig, and R. S. Goody. 1999. Characterization of the ternary complex between Rab7, REP-1 and Rab geranylgeranyl transferase. *Eur J Biochem* **265**:160-170.

Allen, M. R. 2009. Bisphosphonates and osteonecrosis of the jaw: moving from the bedside to the bench. *Cells Tissues Organs* **189**:289-294.

Alory, C., and W. E. Balch. 2001. Organization of the Rab-GDI/CHM superfamily: the functional basis for choroideremia disease. *Traffic* **2**:532-543.

Amin, D., S. A. Cornell, S. K. Gustafson, S. J. Needle, J. W. Ullrich, G. E. Bilder, and M. H. Perrone. 1992. Bisphosphonates used for the treatment of bone disorders inhibit squalene synthase and cholesterol biosynthesis. *J Lipid Res* **33**:1657-1663.

Anant, J. S., L. Desnoyers, M. Machius, B. Demeler, J. C. Hansen, K. D. Westover, J. Deisenhofer, and M. C. Seabra. 1998. Mechanism of Rab geranylgeranylation: formation of the catalytic ternary complex. *Biochemistry* **37**:12559-12568.

Anant, J. S., O. C. Ong, H. Y. Xie, S. Clarke, P. J. O'Brien, and B. K. Fung. 1992. In vivo differential prenylation of retinal cyclic GMP phosphodiesterase catalytic subunits. *J Biol Chem* **267**:687-690.

Andres, D. A., M. C. Seabra, M. S. Brown, S. A. Armstrong, T. E. Smeland, F. P. Cremers, and J. L. Goldstein. 1993. cDNA cloning of component A of Rab geranylgeranyl transferase and demonstration of its role as a Rab escort protein. *Cell* **73**:1091-1099.

Arai, F., T. Miyamoto, O. Ohneda, T. Inada, T. Sudo, K. Brasel, T. Miyata, D. M. Anderson, and T. Suda. 1999. Commitment and differentiation of osteoclast precursor cells by the sequential expression of c-Fms and receptor activator of nuclear factor kappaB (RANK) receptors. *J Exp Med* **190**:1741-1754.

Armstrong, S. A., M. S. Brown, J. L. Goldstein, and M. C. Seabra. 1995. Preparation of recombinant Rab geranylgeranyltransferase and Rab escort proteins. *Methods Enzymol* **257**:30-41.

Armstrong, S. A., M. C. Seabra, T. C. Sudhof, J. L. Goldstein, and M. S. Brown. 1993. cDNA cloning and expression of the alpha and beta subunits of rat Rab geranylgeranyl transferase. *J Biol Chem* **268**:12221-12229.

Artz, J. D., J. E. Dunford, M. J. Arrowood, A. Dong, M. Chruszcz, K. L. Kavanagh, W. Minor, R. G. Russell, F. H. Ebetino, U. Oppermann, and R. Hui. 2008. Targeting a uniquely nonspecific prenyl synthase with bisphosphonates to combat cryptosporidiosis. *Chem Biol* **15**:1296-1306.

Artz, J. D., A. K. Wernimont, J. E. Dunford, M. Schapira, A. Dong, Y. Zhao, J. Lew, R. G. Russell, F. H. Ebetino, U. Oppermann, and R. Hui. 2010. Molecular characterization of a novel geranylgeranyl pyrophosphate synthase from Plasmodium parasites. *J Biol Chem* **286**:3315-3322.

Ash, P., J. F. Loutit, and K. M. Townsend. 1980. Osteoclasts derived from haematopoietic stem cells. *Nature* **283**:669-670.

Ashby, M. N., and P. A. Edwards. 1990. Elucidation of the deficiency in two yeast coenzyme Q mutants. Characterization of the structural gene encoding hexaprenyl pyrophosphate synthetase. *J Biol Chem* **265**:13157-13164.

Aslanidis, C., and P. J. de Jong. 1990. Ligation-independent cloning of PCR products (LIC-PCR). *Nucleic Acids Res* **18**:6069-6074.

Axen, R., and P. Vretblad. 1971. Binding of proteins to polysaccharides by means of cyanogen halides. Studies on cyanogen bromide treated Sephadex. *Acta Chem Scand* **25**:2711-2716.

Baba, T., and C. M. Allen. 1984. Inactivation of undecaprenyl pyrophosphate synthetase with a photolabile analog of farnesyl pyrophosphate. *Biochemistry* **23**:1312-1322.

Barnard, G. F., and G. Popjak. 1980. Characterization of liver prenyl transferase and its inactivation by phenylglyoxal. *Biochim Biophys Acta* **617**:169-182.

Barnard, G. F., and G. Popjak. 1981. Human liver prenyltransferase and its characterization. *Biochim Biophys Acta* **661**:87-99.

Baron, R. A., and M. C. Seabra. 2008. Rab geranylgeranylation occurs preferentially via the pre-formed REP-RGGT complex and is regulated by geranylgeranyl pyrophosphate. *Biochem J* **415**:67-75.

Baron, R. A., R. Tavare, A. C. Figueiredo, K. M. Blazewska, B. A. Kashemirov, C. E. McKenna, F. H. Ebetino, A. Taylor, M. J. Rogers, F. P. Coxon, and M. C. Seabra. 2009. Phosphonocarboxylates inhibit the second geranylgeranyl addition by Rab geranylgeranyl transferase. *J Biol Chem* **284**:6861-6868.

Bauer, B. E., S. Lorenzetti, M. Miaczynska, D. M. Bui, R. J. Schweyen, and A. Ragnini. 1996. Amino- and carboxy-terminal domains of the yeast Rab escort protein are both required for binding of Ypt small G proteins. *Mol Biol Cell* **7**:1521-1533.

Benford, H. L., J. C. Frith, S. Auriola, J. Monkkonen, and M. J. Rogers. 1999. Farnesol and geranylgeraniol prevent activation of caspases by aminobisphosphonates: biochemical evidence for two distinct pharmacological classes of bisphosphonate drugs. *Mol Pharmacol* **56**:131-140.

Berenson, J. R., L. S. Rosen, A. Howell, L. Porter, R. E. Coleman, W. Morley, R. Dreicer, S. A. Kuross, A. Lipton, and J. J. Seaman. 2001. Zoledronic acid reduces skeletal-related events in patients with osteolytic metastases. *Cancer* **91**:1191-1200.

Bergo, M. O., G. K. Leung, P. Ambroziak, J. C. Otto, P. J. Casey, A. Q. Gomes, M. C. Seabra, and S. G. Young. 2001. Isoprenylcysteine carboxyl methyltransferase deficiency in mice. *J Biol Chem* **276**:5841-5845.

Bikle, D. D., E. R. Morey-Holton, S. B. Doty, P. A. Currier, S. J. Tanner, and B. P. Halloran. 1994. Alendronate increases skeletal mass of growing rats during unloading by inhibiting resorption of calcified cartilage. *J Bone Miner Res* **9**:1777-1787.

Blair, H. C., S. L. Teitelbaum, R. Ghiselli, and S. Gluck. 1989. Osteoclastic bone resorption by a polarized vacuolar proton pump. *Science* **245**:855-857.

Blanchard, L., and F. Karst. 1993. Characterization of a lysine-to-glutamic acid mutation in a conservative sequence of farnesyl diphosphate synthase from Saccharomyces cerevisiae. *Gene* **125**:185-189.

Bloch, K. 1965. The biological synthesis of cholesterol. *Science* **150**:19-28.

Bloch, K., and D. Rittenberg. 1942. On the utilization of acetic acid for cholesterol formation. *Journal of Biological Chemistry* **145**:625-636.

Body, J. J., I. J. Diel, R. Bell, M. Pecherstorfer, M. R. Lichinitser, A. F. Lazarev, D. Tripathy, and B. Bergstrom. 2004. Oral ibandronate improves bone pain and preserves quality of life in patients with skeletal metastases due to breast cancer. *Pain* **111**:306-312.

Bohren, K. M., C. E. Grimshaw, C. J. Lai, D. H. Harrison, D. Ringe, G. A. Petsko, and K. H. Gabbay. 1994. Tyrosine-48 is the proton donor and histidine-110 directs substrate stereochemical selectivity in the reduction reaction of human aldose reductase: enzyme kinetics and crystal structure of the Y48H mutant enzyme. *Biochemistry* **33**:2021-2032.

Boissier, S., M. Ferreras, O. Peyruchaud, S. Magnetto, F. H. Ebetino, M. Colombel, P. Delmas, J. M. Delaisse, and P. Clezardin. 2000. Bisphosphonates inhibit breast and prostate carcinoma cell invasion, an early event in the formation of bone metastases. *Cancer Res* **60**:2949-2954.

Boissier, S., S. Magnetto, L. Frappart, B. Cuzin, F. H. Ebetino, P. D. Delmas, and P. Clezardin. 1997. Bisphosphonates inhibit prostate and breast carcinoma cell adhesion to unmineralized and mineralized bone extracellular matrices. *Cancer Res* **57**:3890-3894.

Boonekamp, P. M., L. J. van der Wee-Pals, M. M. van Wijk-van Lennep, C. W. Thesing, and O. L. Bijvoet. 1986. Two modes of action of bisphosphonates on osteoclastic resorption of mineralized matrix. *Bone Miner* **1**:27-39.

Bossard, M. J., T. A. Tomaszek, S. K. Thompson, B. Y. Amegadzie, C. R. Hanning, C. Jones, J. T. Kurdyla, D. E. McNulty, F. H. Drake, M. Gowen, and M. A. Levy. 1996. Proteolytic activity of human osteoclast cathepsin K. Expression, purification, activation, and substrate identification. *J Biol Chem* **271**:12517-12524.

Boyce, B. F., and L. Xing. 2007. Biology of RANK, RANKL, and osteoprotegerin. *Arthritis Res Ther* **9 Suppl 1**:S1.

Boyle, W. J., W. S. Simonet, and D. L. Lacey. 2003. Osteoclast differentiation and activation. *Nature* **423**:337-342.

Bramucci, M. G., and V. Nagarajan. 1996. Direct selection of cloned DNA in Bacillus subtilis based on sucrose-induced lethality. *Appl Environ Microbiol* **62**:3948-3953.

Brems, D. N., E. Bruenger, and H. C. Rilling. 1981. Isolation and characterization of a photoaffinity-labeled peptide from the catalytic site of prenyltransferase. *Biochemistry* **20**:3711-3718.

Brocklehurst, K. 1994. A sound basis for pH-dependent kinetic studies on enzymes. *Protein Eng* **7**:291-299.

Brooks, B., and W. F. Benisek. 1992. Specific activation of a tyrosine----glycine mutant of delta 5-3-ketosteroid isomerase by phenols. *Biochem Biophys Res Commun* **184**:1386-1392.

Brooks, B., R. S. Phillips, and W. F. Benisek. 1998. High-efficiency incorporation in vivo of tyrosine analogues with altered hydroxyl acidity in place of the catalytic tyrosine-14 of Delta 5-3-ketosteroid isomerase of Comamonas (Pseudomonas) testosteroni: effects of the modifications on isomerase kinetics. *Biochemistry* **37**:9738-9742.

Brown, M. S., and J. L. Goldstein. 1979a. Familial hypercholesterolemia: model for genetic receptor disease. *Harvey Lect* **73**:163-201.

Brown, M. S., and J. L. Goldstein. 1979b. Receptor-mediated endocytosis: insights from the lipoprotein receptor system. *Proc Natl Acad Sci U S A* **76**:3330-3337.

Brown, M. S., and J. L. Goldstein. 1980. Multivalent feedback regulation of HMG CoA reductase, a control mechanism coordinating isoprenoid synthesis and cell growth. *J Lipid Res* **21**:505-517.

Brown, M. S., and J. L. Goldstein. 1985. The LDL receptor and HMG-CoA reductase--two membrane molecules that regulate cholesterol homeostasis. *Curr Top Cell Regul* **26**:3-15.

Buhaescu, I., and H. Izzedine. 2007. Mevalonate pathway: a review of clinical and therapeutical implications. *Clin Biochem* **40**:575-584.

Burger, E. H., J. W. Van der Meer, J. S. van de Gevel, J. C. Gribnau, G. W. Thesingh, and R. van Furth. 1982. In vitro formation of osteoclasts from long-term cultures of bone marrow mononuclear phagocytes. *J Exp Med* **156**:1604-1614.

Burgess-Brown, N. A., S. Sharma, F. Sobott, C. Loenarz, U. Oppermann, and O. Gileadi. 2008. Codon optimization can improve expression of human genes in Escherichia coli: A multi-gene study. *Protein Expr Purif* **59**:94-102.

Burgess, T. L., Y. Qian, S. Kaufman, B. D. Ring, G. Van, C. Capparelli, M. Kelley, H. Hsu, W. J. Boyle, C. R. Dunstan, S. Hu, and D. L. Lacey. 1999. The ligand for osteoprotegerin (OPGL) directly activates mature osteoclasts. *J Cell Biol* **145**:527-538.

Burley, S. K., and G. A. Petsko. 1986. Amino-aromatic interactions in proteins. *FEBS Lett* **203**:139-143.

Burstone, M. S. 1958. Histochemical demonstration of acid phosphatases with naphthol AS-phosphates. *J Natl Cancer Inst* **21**:523-539.

Calero, M., C. Z. Chen, W. Zhu, N. Winand, K. A. Havas, P. M. Gilbert, C. G. Burd, and R. N. Collins. 2003. Dual prenylation is required for Rab protein localization and function. *Mol Biol Cell* **14**:1852-1867.

Cane, D. E., C. Abell, P. H. Harrison, B. R. Hubbard, C. T. Kane, R. Lattman, J. S. Oliver, and S. W. Weiner. 1991. Terpenoid biosynthesis and the stereochemistry of enzyme-catalysed allylic addition-elimination reactions. *Philos Trans R Soc Lond B Biol Sci* **332**:123-129.

Casey, P. J. 1995. Protein lipidation in cell signaling. *Science* **268**:221-225.

Casey, P. J., and M. C. Seabra. 1996. Protein prenyltransferases. *J Biol Chem* **271**:5289-5292.

Cecchini, M. G., R. Felix, H. Fleisch, and P. H. Cooper. 1987. Effect of bisphosphonates on proliferation and viability of mouse bone marrow-derived macrophages. *J Bone Miner Res* **2**:135-142.

Cecchini, M. G., and H. Fleisch. 1990. Bisphosphonates in vitro specifically inhibit, among the hematopoietic series, the development of the mouse mononuclear phagocyte lineage. *J Bone Miner Res* **5**:1019-1027.

Clark, S. A., W. W. Ambrose, T. R. Anderson, R. S. Terrell, and S. U. Toverud. 1989. Ultrastructural localization of tartrate-resistant, purple acid phosphatase in rat osteoclasts by histochemistry and immunocytochemistry. *J Bone Miner Res* **4**:399-405.

Clarke, S. 1992. Protein isoprenylation and methylation at carboxyl-terminal cysteine residues. *Annu Rev Biochem* **61**:355-386.

Clarke, S., J. P. Vogel, R. J. Deschenes, and J. Stock. 1988. Posttranslational modification of the Ha-ras oncogene protein: evidence for a third class of protein carboxyl methyltransferases. *Proc Natl Acad Sci U S A* **85**:4643-4647.

Clezardin, P., F. H. Ebetino, and P. G. Fournier. 2005. Bisphosphonates and cancer-induced bone disease: beyond their antiresorptive activity. *Cancer Res* **65**:4971-4974.

Cole, P. A., A. D. Courtney, K. Shen, Z. Zhang, Y. Qiao, W. Lu, and D. M. Williams. 2003. Chemical approaches to reversible protein phosphorylation. *Acc Chem Res* **36**:444-452.

Copeland, R. A. 1996. *Enzymes : a practical introduction to structure, mechanism and data analysis*. Viley-VCH, New York ; Chichester.

Cornforth, J. W., R. H. Cornforth, G. Popjak, and I. Y. Gore. 1958. Studies on the biosynthesis of cholesterol. 5. Biosynthesis of squalene from DL-3-hydroxy-3-methyl [2-14C] pentano-5-lactone. *Biochem J* **69**:146-155.

Cornforth, J. W., R. H. Cornforth, G. Popjak, and L. Yengoyan. 1966. Studies on the biosynthesis of cholesterol. XX. Steric course of decarboxylation of 5-pyrophosphomevalonate and of the carbon to carbon bond formation in the biosynthesis of farnesyl pyrophosphate. *J Biol Chem* **241**:3970-3987.

Cornforth, J. W., and G. Popjak. 1959. Mechanism of biosynthesis of squalene from sesquiterpenoids. *Tetrahedron Letters* **1**:29-35.

Couture, J. F., E. Collazo, J. S. Brunzelle, and R. C. Trievel. 2005. Structural and functional analysis of SET8, a histone H4 Lys-20 methyltransferase. *Genes Dev* **19**:1455-1465.

Coxon, F. P., M. H. Helfrich, B. Larijani, M. Muzylak, J. E. Dunford, D. Marshall, A. D. McKinnon, S. A. Nesbitt, M. A. Horton, M. C. Seabra, F. H. Ebetino, and M. J. Rogers. 2001. Identification of a novel phosphonocarboxylate inhibitor of Rab geranylgeranyl transferase that specifically prevents Rab prenylation in osteoclasts and macrophages. *J Biol Chem* **276**:48213-48222.

Coxon, F. P., M. H. Helfrich, R. Van't Hof, S. Sebti, S. H. Ralston, A. Hamilton, and M. J. Rogers. 2000. Protein geranylgeranylation is required for osteoclast formation, function, and survival: inhibition by bisphosphonates and GGTI-298. *J Bone Miner Res* **15**:1467-1476.

Cremers, F. P., S. A. Armstrong, M. C. Seabra, M. S. Brown, and J. L. Goldstein. 1994. REP-2, a Rab escort protein encoded by the choroideremia-like gene. *J Biol Chem* **269**:2111-2117.

Crepin, S., M. L. Laroche, B. Sarry, and L. Merle. 2010. Osteonecrosis of the jaw induced by clodronate, an alkylbiphosphonate: case report and literature review. *Eur J Clin Pharmacol* **66**:547-554.

Cresson, E. L., K. Folkers, C. H. Hoffman, G. D. Macrae, H. R. Skeggs, D. E. Wolf, and L. D. Wright. 1956. Discovery of a new acetate-replacing factor. *J Bacteriol* **72**:519-524.

D'Amelio, P., A. Grimaldi, M. A. Cristofaro, M. Ravazzoli, P. A. Molinatti, G. P. Pescarmona, and G. C. Isaia. 2010. Alendronate reduces osteoclast precursors in osteoporosis. *Osteoporos Int* **21**:1741-1750.

De Marco, V., G. Stier, S. Blandin, and A. de Marco. 2004. The solubility and stability of recombinant proteins are increased by their fusion to NusA. *Biochem Biophys Res Commun* **322**:766-771.

De Waard, A., A. H. Phillips, and K. Bloch. 1959. Mechanism of formation of isopentenyl pyrophosphate [13]. *Journal of the American Chemical Society* **81**:2913-2914.

Deneris, E. S., R. A. Stein, and J. F. Mead. 1984. In vitro biosynthesis of isoprene from mevalonate utilizing a rat liver cytosolic fraction. *Biochem Biophys Res Commun* **123**:691-696.

Derenne, S., M. Amiot, S. Barille, M. Collette, N. Robillard, P. Berthaud, J. L. Harousseau, and R. Bataille. 1999. Zoledronate is a potent inhibitor of myeloma cell growth and secretion of IL-6 and MMP-1 by the tumoral environment. *J Bone Miner Res* **14**:2048-2056.

Desnoyers, L., and M. C. Seabra. 1998. Single prenyl-binding site on protein prenyl transferases. *Proc Natl Acad Sci U S A* **95**:12266-12270.

Donninger, C., and G. Popjak. 1966. Studies on the biosynthesis of cholesterol. 18. The stereospecificity of mevaldate reductase and the biosynthesis of asymmetrically labelled farnesyl pyrophosphate. *Proc R Soc Lond B Biol Sci* **163**:465-491.

Dorsey, J. K., and J. W. Porter. 1968. The inhibition of mevalonic kinase by geranyl and farnesyl pyrophosphates. *J Biol Chem* **243**:4667-4670.

Dougherty, D. A. 1996. Cation-pi interactions in chemistry and biology: a new view of benzene, Phe, Tyr, and Trp. *Science* **271**:163-168.

Drake, F. H., R. A. Dodds, I. E. James, J. R. Connor, C. Debouck, S. Richardson, E. Lee-Rykaczewski, L. Coleman, D. Rieman, R. Barthlow, G. Hastings, and M. Gowen. 1996. Cathepsin K, but not cathepsins B, L, or S, is abundantly expressed in human osteoclasts. *J Biol Chem* **271**:12511-12516.

Dunford, J. E., A. A. Kwaasi, M. J. Rogers, B. L. Barnett, F. H. Ebetino, R. G. Russell, U. Oppermann, and K. L. Kavanagh. 2008. Structure-activity relationships among the nitrogen containing bisphosphonates in clinical use and other analogues: time-dependent inhibition of human farnesyl pyrophosphate synthase. *J Med Chem* **51**:2187-2195.

Dunford, J. E., M. J. Rogers, F. H. Ebetino, R. J. Phipps, and F. P. Coxon. 2006. Inhibition of protein prenylation by bisphosphonates causes sustained activation of Rac, Cdc42, and Rho GTPases. *J Bone Miner Res* **21**:684-694.

Dunford, J. E., K. Thompson, F. P. Coxon, S. P. Luckman, F. M. Hahn, C. D. Poulter, F. H. Ebetino, and M. J. Rogers. 2001. Structure-activity relationships for inhibition of farnesyl diphosphate synthase in vitro and inhibition of bone resorption in vivo by nitrogen-containing bisphosphonates. *J Pharmacol Exp Ther* **296**:235-242.

Dursina, B., N. H. Thoma, V. Sidorovitch, A. Niculae, A. Iakovenko, A. Rak, S. Albert, A. C. Ceacareanu, R. Kolling, C. Herrmann, R. S. Goody, and K. Alexandrov. 2002. Interaction of yeast Rab geranylgeranyl transferase with its protein and lipid substrates. *Biochemistry* **41**:6805-6816.

Emsley, P., and K. Cowtan. 2004. Coot: model-building tools for molecular graphics. *Acta Crystallogr D Biol Crystallogr* **60**:2126-2132.

Evans, P. 2006. Scaling and assessment of data quality. *Acta Crystallogr D Biol Crystallogr* **62**:72-82.

Faccio, R., D. V. Novack, A. Zallone, F. P. Ross, and S. L. Teitelbaum. 2003. Dynamic changes in the osteoclast cytoskeleton in response to growth factors and cell attachment are controlled by beta3 integrin. *J Cell Biol* **162**:499-509.

Farnsworth, C. C., M. C. Seabra, L. H. Ericsson, M. H. Gelb, and J. A. Glomset. 1994. Rab geranylgeranyl transferase catalyzes the geranylgeranylation of adjacent cysteines in the small GTPases Rab1A, Rab3A, and Rab5A. *Proc Natl Acad Sci U S A* **91**:11963-11967.

Farnsworth, C. C., S. L. Wolda, M. H. Gelb, and J. A. Glomset. 1989. Human lamin B contains a farnesylated cysteine residue. *J Biol Chem* **264**:20422-20429.

Ferretti, G., A. Fabi, P. Carlini, P. Papaldo, P. Cordiali Fei, S. Di Cosimo, N. Salesi, D. Giannarelli, A. Alimonti, B. Di Cocco, G. D'Agosto, V. Bordignon, E. Trento, and F. Cognetti. 2005. Zoledronic-acid-induced circulating level modifications of angiogenic factors, metalloproteinases and proinflammatory cytokines in metastatic breast cancer patients. *Oncology* **69**:35-43.

Fersht, A. 1998. *Structure and mechanism in protein science : a guide to enzyme catalysis and protein folding*. W.H. Freeman ;Macmillan, New York Basingstoke.

Finkelstein, J. S., B. Z. Leder, S. M. Burnett, J. J. Wyland, H. Lee, A. V. de la Paz, K. Gibson, and R. M. Neer. 2006. Effects of teriparatide, alendronate, or both on bone turnover in osteoporotic men. *J Clin Endocrinol Metab* **91**:2882-2887.

Fisher, J. E., G. A. Rodan, and A. A. Reszka. 2000. In vivo effects of bisphosphonates on the osteoclast mevalonate pathway. *Endocrinology* **141**:4793-4796.

Fisher, J. E., M. J. Rogers, J. M. Halasy, S. P. Luckman, D. E. Hughes, P. J. Masarachia, G. Wesolowski, R. G. Russell, G. A. Rodan, and A. A. Reszka. 1999. Alendronate mechanism of action: geranylgeraniol, an intermediate in the mevalonate pathway, prevents inhibition of osteoclast formation, bone resorption, and kinase activation in vitro. *Proc Natl Acad Sci U S A* **96**:133-138.

Flanagan, A. M., and T. J. Chambers. 1989. Dichloromethylenebisphosphonate (Cl2MBP) inhibits bone resorption through injury to osteoclasts that resorb Cl2MBP-coated bone. *Bone Miner* **6**:33-43.

Flanagan, A. M., and T. J. Chambers. 1991. Inhibition of bone resorption by bisphosphonates: interactions between bisphosphonates, osteoclasts, and bone. *Calcif Tissue Int* **49**:407-415.

Fleisch, H., R. G. Russell, and M. D. Francis. 1969. Diphosphonates inhibit hydroxyapatite dissolution in vitro and bone resorption in tissue culture and in vivo. *Science* **165**:1262-1264.

Fleisch, H., R. G. Russell, and F. Straumann. 1966. Effect of pyrophosphate on hydroxyapatite and its implications in calcium homeostasis. *Nature* **212**:901-903.

Fleisch, H. A., R. G. Russell, S. Bisaz, R. C. Muhlbauer, and D. A. Williams. 1970. The inhibitory effect of phosphonates on the formation of calcium phosphate crystals in vitro and on aortic and kidney calcification in vivo. *Eur J Clin Invest* **1**:12-18.

Fournier, P. G., F. Daubine, M. W. Lundy, M. J. Rogers, F. H. Ebetino, and P. Clezardin. 2008. Lowering bone mineral affinity of bisphosphonates as a therapeutic strategy to optimize skeletal tumor growth inhibition in vivo. *Cancer Res* **68**:8945-8953.

Fournier, P. G., V. Stresing, F. H. Ebetino, and P. Clezardin. 2010. How do bisphosphonates inhibit bone metastasis in vivo? *Neoplasia* **12**:571-578.

Francis, M. D., R. G. Russell, and H. Fleisch. 1969. Diphosphonates inhibit formation of calcium phosphate crystals in vitro and pathological calcification in vivo. *Science* **165**:1264-1266.

Fribourg, S., C. Romier, S. Werten, Y. G. Gangloff, A. Poterszman, and D. Moras. 2001. Dissecting the interaction network of multiprotein complexes by pairwise coexpression of subunits in E. coli. *J Mol Biol* **306**:363-373.

Frith, J. C., J. Monkkonen, S. Auriola, H. Monkkonen, and M. J. Rogers. 2001. The molecular mechanism of action of the antiresorptive and antiinflammatory drug clodronate: evidence for the formation in vivo of a metabolite that inhibits bone resorption and causes osteoclast and macrophage apoptosis. *Arthritis Rheum* **44**:2201-2210.

Frith, J. C., J. Monkkonen, G. M. Blackburn, R. G. Russell, and M. J. Rogers. 1997. Clodronate and liposome-encapsulated clodronate are metabolized to a toxic ATP analog, adenosine 5'-(beta, gamma-dichloromethylene) triphosphate, by mammalian cells in vitro. *J Bone Miner Res* **12**:1358-1367.

Fujikawa, Y., J. M. Quinn, A. Sabokbar, J. O. McGee, and N. A. Athanasou. 1996. The human osteoclast precursor circulates in the monocyte fraction. *Endocrinology* **137**:4058-4060.

Fukuda, A., A. Hikita, H. Wakeyama, T. Akiyama, H. Oda, K. Nakamura, and S. Tanaka. 2005. Regulation of osteoclast apoptosis and motility by small GTPase binding protein Rac1. *J Bone Miner Res* **20**:2245-2253.

Gabelli, S. B., J. S. McLellan, A. Montalvetti, E. Oldfield, R. Docampo, and L. M. Amzel. 2006. Structure and mechanism of the farnesyl diphosphate synthase from Trypanosoma cruzi: implications for drug design. *Proteins* **62**:80-88.

Gallizia, A., C. de Lalla, E. Nardone, P. Santambrogio, A. Brandazza, A. Sidoli, and P. Arosio. 1998. Production of a soluble and functional recombinant streptavidin in Escherichia coli. *Protein Expr Purif* **14**:192-196.

Garzoni, L. R., A. Caldera, N. Meirelles Mde, S. L. de Castro, R. Docampo, G. A. Meints, E. Oldfield, and J. A. Urbina. 2004. Selective in vitro effects of the farnesyl pyrophosphate synthase inhibitor risedronate on Trypanosoma cruzi. *Int J Antimicrob Agents* **23**:273-285.

Gaylor, J. L. 2002. Membrane-bound enzymes of cholesterol synthesis from lanosterol. *Biochem Biophys Res Commun* **292**:1139-1146.

Georgiou, G., and P. Valax. 1996. Expression of correctly folded proteins in Escherichia coli. *Curr Opin Biotechnol* **7**:190-197.

Ghosh, S., J. M. Chan, C. R. Lea, G. A. Meints, J. C. Lewis, Z. S. Tovian, R. M. Flessner, T. C. Loftus, I. Bruchhaus, H. Kendrick, S. L. Croft, R. G. Kemp, S. Kobayashi, T. Nozaki, and E. Oldfield. 2004. Effects of bisphosphonates on the growth of Entamoeba histolytica and Plasmodium species in vitro and in vivo. *J Med Chem* **47**:175-187.

Glickman, J. F., and A. Schmid. 2007. Farnesyl pyrophosphate synthase: real-time kinetics and inhibition by nitrogen-containing bisphosphonates in a scintillation assay. *Assay Drug Dev Technol* **5**:205-214.

Gober, H. J., M. Kistowska, L. Angman, P. Jeno, L. Mori, and G. De Libero. 2003. Human T cell receptor gammadelta cells recognize endogenous mevalonate metabolites in tumor cells. *J Exp Med* **197**:163-168.

Goldstein, J. L., and M. S. Brown. 1984. Progress in understanding the LDL receptor and HMG-CoA reductase, two membrane proteins that regulate the plasma cholesterol. *J Lipid Res* **25**:1450-1461.

Goldstein, J. L., and M. S. Brown. 1990. Regulation of the mevalonate pathway. *Nature* **343**:425-430.

Goldstein, J. L., Y. K. Ho, M. S. Brown, T. L. Innerarity, and R. W. Mahley. 1980. Cholesteryl ester accumulation in macrophages resulting from receptor-mediated uptake and degradation of hypercholesterolemic canine beta-very low density lipoproteins. *J Biol Chem* **255**:1839-1848.

Goodman, D. S., and G. Popjak. 1960. Studies on the biosynthesis of cholesterol. XII. Synthesis of allyl pyrophosphates from mevalonate and their conversion into squalene with liver enzymes. *J Lipid Res* **1**:286-300.

Goody, R. S., T. Durek, H. Waldmann, L. Brunsveld, and K. Alexandrov. 2005. Application of protein semisynthesis for the construction of functionalized posttranslationally modified rab GTPases. *Methods Enzymol* **403**:29-42.

Gordon, J. A. 1991. Use of vanadate as protein-phosphotyrosine phosphatase inhibitor. *Methods Enzymol* **201**:477-482.

Gotoh, T., T. Koyama, and K. Ogura. 1992. Farnesyl diphosphate synthase and solanesyl diphosphate synthase reactions of diphosphate-modified allylic analogs: the significance of the diphosphate linkage involved in the allylic substrates for prenyltransferase. *J Biochem* **112**:20-27.

Grafen, A., and R. Hails. 2002. *Modern statistics for the life sciences*. Oxford University Press, Oxford.

Green, J. R. 2003. Antitumor effects of bisphosphonates. *Cancer* **97**:840-847.

Green, J. R. 2005. Skeletal complications of prostate cancer: pathophysiology and therapeutic potential of bisphosphonates. *Acta Oncol* **44**:282-292.

Guo, Z., Y. W. Wu, D. Das, C. Delon, J. Cramer, S. Yu, S. Thuns, N. Lupilova, H. Waldmann, L. Brunsveld, R. S. Goody, K. Alexandrov, and W. Blankenfeldt. 2008a. Structures of RabGGTase-substrate/product complexes provide insights into the evolution of protein prenylation. *EMBO J* **27**:2444-2456.

Guo, Z., Y. W. Wu, K. T. Tan, R. S. Bon, E. Guiu-Rozas, C. Delon, T. U. Nguyen, S. Wetzel, S. Arndt, R. S. Goody, W. Blankenfeldt, K. Alexandrov, and H. Waldmann. 2008b. Development of selective RabGGTase inhibitors and crystal structure of a RabGGTase-inhibitor complex. *Angew Chem Int Ed Engl* **47**:3747-3750.

Halasy-Nagy, J. M., G. A. Rodan, and A. A. Reszka. 2001. Inhibition of bone resorption by alendronate and risedronate does not require osteoclast apoptosis. *Bone* **29**:553-559.

Hamm, H. E., and A. Gilchrist. 1996. Heterotrimeric G proteins. *Curr Opin Cell Biol* **8**:189-196.

Hancock, J. F., A. I. Magee, J. E. Childs, and C. J. Marshall. 1989. All ras proteins are polyisoprenylated but only some are palmitoylated. *Cell* **57**:1167-1177.

Hattersley, G., J. Owens, A. M. Flanagan, and T. J. Chambers. 1991. Macrophage colony stimulating factor (M-CSF) is essential for osteoclast formation in vitro. *Biochem Biophys Res Commun* **177**:526-531.

Henning, U., E. M. Moslein, and F. Lynen. 1959. Biosynthesis of terpenes. V. Formation of 5-pyrophosphomevalonic acid by phosphomevalonic kinase. *Arch Biochem Biophys* **83**:259-267.

Henry, D. H., L. Costa, F. Goldwasser, V. Hirsh, V. Hungria, J. Prausova, G. V. Scagliotti, H. Sleeboom, A. Spencer, S. Vadhan-Raj, R. von Moos, W. Willenbacher, P. J. Woll, J. Wang, Q. Jiang, S. Jun, R. Dansey, and H. Yeh. 2011. Randomized, double-blind study of denosumab versus zoledronic acid in the treatment of bone metastases in patients with advanced cancer (excluding breast and prostate cancer) or multiple myeloma. *J Clin Oncol* **29**:1125-1132.

Hewitt, R. E., A. Lissina, A. E. Green, E. S. Slay, D. A. Price, and A. K. Sewell. 2005. The bisphosphonate acute phase response: rapid and copious production of proinflammatory cytokines by peripheral blood gd T cells in response to aminobisphosphonates is inhibited by statins. *Clin Exp Immunol* **139**:101-111.

Higgins, M. K., M. Demir, and C. G. Tate. 2003. Calnexin co-expression and the use of weaker promoters increase the expression of correctly assembled Shaker potassium channel in insect cells. *Biochim Biophys Acta* **1610**:124-132.

Hinson, D. D., K. L. Chambliss, M. J. Toth, R. D. Tanaka, and K. M. Gibson. 1997. Post-translational regulation of mevalonate kinase by intermediates of the cholesterol and nonsterol isoprene biosynthetic pathways. *J Lipid Res* **38**:2216-2223.

Ho, T. Q., Z. Zhong, S. Aung, and J. Pogliano. 2002. Compatible bacterial plasmids are targeted to independent cellular locations in Escherichia coli. *EMBO J* **21**:1864-1872.

Hofbauer, L. C., F. Gori, B. L. Riggs, D. L. Lacey, C. R. Dunstan, T. C. Spelsberg, and S. Khosla. 1999. Stimulation of osteoprotegerin ligand and inhibition of osteoprotegerin production by glucocorticoids in human osteoblastic lineage cells: potential paracrine mechanisms of glucocorticoid-induced osteoporosis. *Endocrinology* **140**:4382-4389.

Holen, I., and C. M. Shipman. 2006. Role of osteoprotegerin (OPG) in cancer. *Clin Sci (Lond)* **110**:279-291.

Hortobagyi, G. N., R. L. Theriault, L. Porter, D. Blayney, A. Lipton, C. Sinoff, H. Wheeler, J. F. Simeone, J. Seaman, and R. D. Knight. 1996. Efficacy of pamidronate in reducing skeletal complications in patients with breast cancer and lytic bone metastases. Protocol 19 Aredia Breast Cancer Study Group. *N Engl J Med* **335**:1785-1791.

Hosfield, D. J., Y. Zhang, D. R. Dougan, A. Broun, L. W. Tari, R. V. Swanson, and J. Finn. 2004. Structural basis for bisphosphonate-mediated inhibition of isoprenoid biosynthesis. *J Biol Chem* **279**:8526-8529.

Hudock, M. P., C. E. Sanz-Rodriguez, Y. Song, J. M. Chan, Y. Zhang, S. Odeh, T. Kosztowski, A. Leon-Rossell, J. L. Concepcion, V. Yardley, S. L. Croft, J. A. Urbina, and E. Oldfield. 2006. Inhibition of Trypanosoma cruzi hexokinase by bisphosphonates. *J Med Chem* **49**:215-223.

Hughes, D. E., B. R. MacDonald, R. G. Russell, and M. Gowen. 1989. Inhibition of osteoclast-like cell formation by bisphosphonates in long-term cultures of human bone marrow. *J Clin Invest* **83**:1930-1935.

Hughes, D. E., K. R. Wright, H. L. Uy, A. Sasaki, T. Yoneda, G. D. Roodman, G. R. Mundy, and B. F. Boyce. 1995. Bisphosphonates promote apoptosis in murine osteoclasts in vitro and in vivo. *J Bone Miner Res* **10**:1478-1487.

Hutchinson, M. H., and H. A. Chase. 2006. Adsorptive refolding of histidine-tagged glutathione S-transferase using metal affinity chromatography. *J Chromatogr A* **1128**:125-132.

Jager, W., A. Schafer, J. Kalinowski, and A. Puhler. 1995. Isolation of insertion elements from gram-positive Brevibacterium, Corynebacterium and Rhodococcus strains using the Bacillus subtilis sacB gene as a positive selection marker. *FEMS Microbiol Lett* **126**:1-6.

Jahnke, W., J.-M. Rondeau, S. Cotesta, A. Marzinzik, X. PellÃ©, M. Geiser, A. Strauss, M. GÃ¶tte, F. Bitsch, R. Hemmig, C. l. Henry, S. Lehmann, J. F. Glickman, T. P. Roddy, S. J. Stout, and J. R. Green. 2010. Allosteric non-bisphosphonate FPPS inhibitors identified by fragment-based discovery. *Nat Chem Biol* **6**:660-666.

Jarvis, D. L., C. Weinkauf, and L. A. Guarino. 1996. Immediate-early baculovirus vectors for foreign gene expression in transformed or infected insect cells. *Protein Expr Purif* **8**:191-203.

Johnston, K., A. Clements, R. N. Venkataramani, R. C. Trievel, and R. Marmorstein. 2000. Coexpression of proteins in bacteria using T7-based expression plasmids: expression of heteromeric cell-cycle and transcriptional regulatory complexes. *Protein Expr Purif* **20**:435-443.

Joly, A., and P. A. Edwards. 1993. Effect of site-directed mutagenesis of conserved aspartate and arginine residues upon farnesyl diphosphate synthase activity. *J Biol Chem* **268**:26983-26989.

Kalinin, A., N. H. Thoma, A. Iakovenko, I. Heinemann, E. Rostkova, A. T. Constantinescu, and K. Alexandrov. 2001. Expression of mammalian geranylgeranyltransferase type-II in Escherichia coli and its application for in vitro prenylation of Rab proteins. *Protein Expr Purif* **22**:84-91.

Kaplan, W., P. Husler, H. Klump, J. Erhardt, N. Sluis-Cremer, and H. Dirr. 1997. Conformational stability of pGEX-expressed Schistosoma japonicum glutathione S-transferase: a detoxification enzyme and fusion-protein affinity tag. *Protein Sci* **6**:399-406.

Kashemirov, B. A., J. L. Bala, X. Chen, F. H. Ebetino, Z. Xia, R. G. Russell, F. P. Coxon, A. J. Roelofs, M. J. Rogers, and C. E. McKenna. 2008. Fluorescently labeled risedronate and related analogues: "magic linker" synthesis. *Bioconjug Chem* **19**:2308-2310.

Kavanagh, K. L., J. E. Dunford, G. Bunkoczi, R. G. Russell, and U. Oppermann. 2006a. The crystal structure of human geranylgeranyl pyrophosphate synthase reveals a novel hexameric arrangement and inhibitory product binding. *J Biol Chem* **281**:22004-22012.

Kavanagh, K. L., K. Guo, J. E. Dunford, X. Wu, S. Knapp, F. H. Ebetino, M. J. Rogers, R. G. Russell, and U. Oppermann. 2006b. The molecular mechanism of nitrogen-containing bisphosphonates as antiosteoporosis drugs. *Proc Natl Acad Sci U S A* **103**:7829-7834.

Kellogg, B. A., and C. D. Poulter. 1997. Chain elongation in the isoprenoid biosynthetic pathway. *Curr Opin Chem Biol* **1**:570-578.

Khosla, S. 2001. Minireview: the OPG/RANKL/RANK system. *Endocrinology* **142**:5050-5055.

Khosla, S., D. Burr, J. Cauley, D. W. Dempster, P. R. Ebeling, D. Felsenberg, R. F. Gagel, V. Gilsanz, T. Guise, S. Koka, L. K. McCauley, J. McGowan, M. D. McKee, S. Mohla, D. G. Pendrys, L. G. Raisz, S. L. Ruggiero, D. M. Shafer, L. Shum, S. L. Silverman, C. H. Van Poznak, N. Watts, S. B. Woo, and E. Shane. 2007. Bisphosphonate-associated osteonecrosis of the jaw: report of a task force of the American Society for Bone and Mineral Research. *J Bone Miner Res* **22**:1479-1491.

Kim, N., M. Takami, J. Rho, R. Josien, and Y. Choi. 2002. A novel member of the leukocyte receptor complex regulates osteoclast differentiation. *J Exp Med* **195**:201-209.

Ko, J. S., and G. W. Bernard. 1981. Osteoclast formation in vitro from bone marrow mononuclear cells in osteoclast-free bone. *Am J Anat* **161**:415-425.

Kodama, H., M. Nose, S. Niida, and A. Yamasaki. 1991. Essential role of macrophage colony-stimulating factor in the osteoclast differentiation supported by stromal cells. *J Exp Med* **173**:1291-1294.

Kondo, M., A. J. Wagers, M. G. Manz, S. S. Prohaska, D. C. Scherer, G. F. Beilhack, J. A. Shizuru, and I. L. Weissman. 2003. Biology of hematopoietic stem cells and progenitors: implications for clinical application. *Annu Rev Immunol* **21**:759-806.

Konstantinopoulos, P. A., M. V. Karamouzis, and A. G. Papavassiliou. 2007. Post-translational modifications and regulation of the RAS superfamily of GTPases as anticancer targets. *Nat Rev Drug Discov* **6**:541-555.

Koshland, D. E. 2002. The Application and Usefulness of the Ratio kcat/KM. *Bioorganic Chemistry* **30**:211-213.

Kost, T. A., J. P. Condreay, and D. L. Jarvis. 2005. Baculovirus as versatile vectors for protein expression in insect and mammalian cells. *Nat Biotechnol* **23**:567-575.

Koyama, T., S. Obata, M. Osabe, A. Takeshita, K. Yokoyama, M. Uchida, T. Nishino, and K. Ogura. 1993. Thermostable farnesyl diphosphate synthase of Bacillus stearothermophilus: molecular cloning, sequence determination, overproduction, and purification. *J Biochem* **113**:355-363.

Koyama, T., M. Tajima, T. Nishino, and K. Ogura. 1995. Significance of Phe-220 and Gln-221 in the catalytic mechanism of farnesyl diphosphate synthase of Bacillus stearothermophilus. *Biochem Biophys Res Commun* **212**:681-686.

Koyama, T., M. Tajima, H. Sano, T. Doi, A. Koike-Takeshita, S. Obata, T. Nishino, and K. Ogura. 1996. Identification of significant residues in the substrate binding site of Bacillus stearothermophilus farnesyl diphosphate synthase. *Biochemistry* **35**:9533-9538.

Kunzmann, V., E. Bauer, J. Feurle, F. Weissinger, H. P. Tony, and M. Wilhelm. 2000. Stimulation of gammadelta T cells by aminobisphosphonates and induction of antiplasma cell activity in multiple myeloma. *Blood* **96**:384-392.

Kurihara, N., C. Chenu, M. Miller, C. Civin, and G. D. Roodman. 1990. Identification of committed mononuclear precursors for osteoclast-like cells formed in long term human marrow cultures. *Endocrinology* **126**:2733-2741.

Lacal, J. C. 1997. Regulation of proliferation and apoptosis by Ras and Rho GTPases through specific phospholipid-dependent signaling. *FEBS Lett* **410**:73-77.

Lacey, D. L., E. Timms, H. L. Tan, M. J. Kelley, C. R. Dunstan, T. Burgess, R. Elliott, A. Colombero, G. Elliott, S. Scully, H. Hsu, J. Sullivan, N. Hawkins, E. Davy, C. Capparelli, A. Eli, Y. X. Qian, S. Kaufman, I. Sarosi, V. Shalhoub, G. Senaldi, J. Guo, J. Delaney, and W. J. Boyle. 1998. Osteoprotegerin ligand is a cytokine that regulates osteoclast differentiation and activation. *Cell* **93**:165-176.

Lane, K. T., and L. S. Beese. 2006. Thematic review series: lipid posttranslational modifications. Structural biology of protein farnesyltransferase and geranylgeranyltransferase type I. *J Lipid Res* **47**:681-699.

Langston, A. L., M. K. Campbell, W. D. Fraser, G. S. MacLennan, P. L. Selby, and S. H. Ralston. 2010. Randomized trial of intensive bisphosphonate treatment versus symptomatic management in Paget's disease of bone. *J Bone Miner Res* **25**:20-31.

Laskovics, F. M., and C. D. Poulter. 1981. Prenyltransferase; determination of the binding mechanism and individual kinetic constants for farnesylpyrophosphate synthetase by rapid quench and isotope partitioning experiments. *Biochemistry* **20**:1893-1901.

LaVallie, E. R., E. A. DiBlasio-Smith, L. A. Collins-Racie, Z. Lu, and J. M. McCoy. 2003. Thioredoxin and related proteins as multifunctional fusion tags for soluble expression in E. coli. *Methods Mol Biol* **205**:119-140.

Lehenkari, P. P., M. Kellinsalmi, J. P. Napankangas, K. V. Ylitalo, J. Monkkonen, M. J. Rogers, A. Azhayev, H. K. Vaananen, and I. E. Hassinen. 2002. Further insight into mechanism of action of clodronate: inhibition of mitochondrial ADP/ATP translocase by a nonhydrolyzable, adenine-containing metabolite. *Mol Pharmacol* **61**:1255-1262.

Lehninger, A. L. 1982. *Principles of biochemistry*. Worth Publishers, New York, N.Y.

Leung, K. F., R. Baron, B. R. Ali, A. I. Magee, and M. C. Seabra. 2007. Rab GTPases containing a CAAX motif are processed post-geranylgeranylation by proteolysis and methylation. *J Biol Chem* **282**:1487-1497.

Leung, K. F., R. Baron, and M. C. Seabra. 2006. Thematic review series: lipid posttranslational modifications. geranylgeranylation of Rab GTPases. *J Lipid Res* **47**:467-475.

Lewis, M. J., I. M. Prosser, A. Mohib, and L. M. Field. 2008. Cloning and characterisation of a prenyltransferase from the aphid Myzus persicae with potential involvement in alarm pheromone biosynthesis. *Insect Mol Biol* **17**:437-443.

Leyes, A. E., J. A. Baker, and C. D. Poulter. 1999. Biosynthesis of isoprenoids in Escherichia coli: stereochemistry of the reaction catalyzed by farnesyl diphosphate synthase. *Org Lett* **1**:1071-1073.

Li, C., J. W. Schwabe, E. Banayo, and R. M. Evans. 1997. Coexpression of nuclear receptor partners increases their solubility and biological activities. *Proc Natl Acad Sci U S A* **94**:2278-2283.

Liang, P. H., T. P. Ko, and A. H. Wang. 2002. Structure, mechanism and function of prenyltransferases. *Eur J Biochem* **269**:3339-3354.

Lindberg, M., C. Yuan, A. Dewaard, and K. Bloch. 1962. On the mechanism of formation of isopentenylpyrophosphate. *Biochemistry* **1**:182-188.

Ling, Y., G. Sahota, S. Odeh, J. M. Chan, F. G. Araujo, S. N. Moreno, and E. Oldfield. 2005. Bisphosphonate inhibitors of Toxoplasma gondi growth: in vitro, QSAR, and in vivo investigations. *J Med Chem* **48**:3130-3140.

Lovell, S. C., I. W. Davis, W. B. Arendall, 3rd, P. I. de Bakker, J. M. Word, M. G. Prisant, J. S. Richardson, and D. C. Richardson. 2003. Structure validation by Calpha geometry: phi,psi and Cbeta deviation. *Proteins* **50**:437-450.

Lowik, C. W., G. van der Pluijm, L. J. van der Wee-Pals, H. B. van Treslong-De Groot, and O. L. Bijvoet. 1988. Migration and phenotypic transformation of osteoclast precursors into mature osteoclasts: the effect of a bisphosphonate. *J Bone Miner Res* **3**:185-192.

Luckman, S. P., F. P. Coxon, F. H. Ebetino, R. G. Russell, and M. J. Rogers. 1998a. Heterocycle-containing bisphosphonates cause apoptosis and inhibit bone resorption by preventing protein prenylation: evidence from structure-activity relationships in J774 macrophages. *J Bone Miner Res* **13**:1668-1678.

Luckman, S. P., D. E. Hughes, F. P. Coxon, R. Graham, G. Russell, and M. J. Rogers. 1998b. Nitrogen-containing bisphosphonates inhibit the mevalonate pathway and prevent post-translational prenylation of GTP-binding proteins, including Ras. *J Bone Miner Res* **13**:581-589.

Lynen, F. 1967. Biosynthetic pathways from acetate to natural products. *Pure Appl Chem* **14**:137-167.

Lynen, F., U. Henning, C. Bublitz, B. Sorbo, and L. Kroplin-Rueff. 1958. [The chemical mechanism of acetic acid formation in the liver.]. *Biochem Z* **330**:269-295.

Magnusdottir, A., I. Johansson, L. G. Dahlgren, P. Nordlund, and H. Berglund. 2009. Enabling IMAC purification of low abundance recombinant proteins from E. coli lysates. *Nat Methods* **6**:477-478.

Malone, J. D., S. L. Teitelbaum, G. L. Griffin, R. M. Senior, and A. J. Kahn. 1982. Recruitment of osteoclast precursors by purified bone matrix constituents. *J Cell Biol* **92**:227-230.

Marma, M. S., Z. Xia, C. Stewart, F. Coxon, J. E. Dunford, R. Baron, B. A. Kashemirov, F. H. Ebetino, J. T. Triffitt, R. G. Russell, and C. E. McKenna. 2007. Synthesis and biological evaluation of alpha-halogenated bisphosphonate and phosphonocarboxylate analogues of risedronate. *J Med Chem* **50**:5967-5975.

Marshall, C. J. 1993. Protein prenylation: A mediator of protein-protein interactions. *Science* **259**:1865-1866.

Martin, M. B., W. Arnold, H. T. Heath, 3rd, J. A. Urbina, and E. Oldfield. 1999. Nitrogen-containing bisphosphonates as carbocation transition state analogs for isoprenoid biosynthesis. *Biochem Biophys Res Commun* **263**:754-758.

Martin, M. B., J. S. Grimley, J. C. Lewis, H. T. Heath, 3rd, B. N. Bailey, H. Kendrick, V. Yardley, A. Caldera, R. Lira, J. A. Urbina, S. N. Moreno, R. Docampo, S. L. Croft, and E. Oldfield. 2001. Bisphosphonates inhibit the growth of Trypanosoma brucei, Trypanosoma cruzi, Leishmania donovani, Toxoplasma gondii, and Plasmodium falciparum: a potential route to chemotherapy. *J Med Chem* **44**:909-916.

Martin, M. B., J. M. Sanders, H. Kendrick, K. de Luca-Fradley, J. C. Lewis, J. S. Grimley, E. M. Van Brussel, J. R. Olsen, G. A. Meints, A. Burzynska, P. Kafarski, S. L. Croft, and E. Oldfield. 2002. Activity of bisphosphonates against Trypanosoma brucei rhodesiense. *J Med Chem* **45**:2904-2914.

Marx, R. E. 2003. Pamidronate (Aredia) and zoledronate (Zometa) induced avascular necrosis of the jaws: a growing epidemic. *J Oral Maxillofac Surg* **61**:1115-1117.

Matayoshi, A., C. Brown, J. F. DiPersio, J. Haug, Y. Abu-Amer, H. Liapis, R. Kuestner, and R. Pacifici. 1996. Human blood-mobilized hematopoietic precursors differentiate into osteoclasts in the absence of stromal cells. *Proc Natl Acad Sci U S A* **93**:10785-10790.

Matsuoka, S., H. Sagami, A. Kurisaki, and K. Ogura. 1991. Variable product specificity of microsomal dehydrodolichyl diphosphate synthase from rat liver. *J Biol Chem* **266**:3464-3468.

Maurer-Stroh, S., S. Washietl, and F. Eisenhaber. 2003. Protein prenyltransferases. *Genome Biol* **4**:212.

McCoy, A. J., R. W. Grosse-Kunstleve, P. D. Adams, M. D. Winn, L. C. Storoni, and R. J. Read. 2007. Phaser crystallographic software. *J Appl Crystallogr* **40**:658-674.

McCoy, A. J., R. W. Grosse-Kunstleve, L. C. Storoni, and R. J. Read. 2005. Likelihood-enhanced fast translation functions. *Acta Crystallogr D Biol Crystallogr* **61**:458-464.

McKenna, C. E., B. A. Kashemirov, K. M. Blazewska, I. Mallard-Favier, C. A. Stewart, J. Rojas, M. W. Lundy, F. H. Ebetino, R. A. Baron, J. E. Dunford, M. L. Kirsten, M. C. Seabra, J. L. Bala, M. S. Marma, M. J. Rogers, and F. P. Coxon. 2010. Synthesis, chiral high performance liquid chromatographic resolution and enantiospecific activity of a potent new geranylgeranyl transferase inhibitor, 2-hydroxy-3-imidazo[1,2-a]pyridin-3-yl-2-phosphonopropionic acid. *J Med Chem* **53**:3454-3464.

McTaggart, S. J. 2006. Isoprenylated proteins. *Cell Mol Life Sci* **63**:255-267.

Mekkriengkrai, D., T. Sando, K. Hirooka, J. Sakdapipanich, Y. Tanaka, E. Fukusaki, and A. Kobayashi. 2004. Cloning and characterization of farnesyl diphosphate synthase from the rubber-producing mushroom Lactarius chrysorrheus. *Biosci Biotechnol Biochem* **68**:2360-2368.

Menaa, C., N. Kurihara, and G. D. Roodman. 2000. CFU-GM-derived cells form osteoclasts at a very high efficiency. *Biochem Biophys Res Commun* **267**:943-946.

Miaczynska, M., S. Lorenzetti, U. Bialek, R. M. Benito-Moreno, R. J. Schweyen, and A. Ragnini. 1997. The yeast Rab escort protein binds intracellular membranes in vivo and in vitro. *J Biol Chem* **272**:16972-16977.

Michaelson, D., W. Ali, V. K. Chiu, M. Bergo, J. Silletti, L. Wright, S. G. Young, and M. Philips. 2005. Postprenylation CAAX processing is required for proper localization of Ras but not Rho GTPases. *Mol Biol Cell* **16**:1606-1616.

Minkin, C. 1982. Bone acid phosphatase: tartrate-resistant acid phosphatase as a marker of osteoclast function. *Calcif Tissue Int* **34**:285-290.

Miyamoto, T., O. Ohneda, F. Arai, K. Iwamoto, S. Okada, K. Takagi, D. M. Anderson, and T. Suda. 2001. Bifurcation of osteoclasts and dendritic cells from common progenitors. *Blood* **98**:2544-2554.

Miyamoto, T., and T. Suda. 2003. Differentiation and function of osteoclasts. *Keio J Med* **52**:1-7.

Molendijk, W. J., A. van Oudenaren, H. van Dijk, M. R. Daha, and R. Benner. 1986. Complement split product C5a mediates the lipopolysaccharide-induced mobilization of CFU-s and haemopoietic progenitor cells, but not the mobilization induced by proteolytic enzymes. *Cell Tissue Kinet* **19**:407-417.

Monkkonen, H., S. Auriola, P. Lehenkari, M. Kellinsalmi, I. E. Hassinen, J. Vepsalainen, and J. Monkkonen. 2006. A new endogenous ATP analog (ApppI) inhibits the mitochondrial adenine nucleotide translocase (ANT) and is responsible for the apoptosis induced by nitrogen-containing bisphosphonates. *Br J Pharmacol* **147**:437-445.

Moores, S. L., M. D. Schaber, S. D. Mosser, E. Rands, M. B. O'Hara, V. M. Garsky, M. S. Marshall, D. L. Pompliano, and J. B. Gibbs. 1991. Sequence dependence of protein isoprenylation. *J Biol Chem* **266**:14603-14610.

Morag, Y., M. Morag-Hezroni, D. A. Jamadar, B. B. Ward, J. A. Jacobson, S. R. Zwetchkenbaum, and J. Helman. 2009. Bisphosphonate-related osteonecrosis of the jaw: a pictorial review. *Radiographics* **29**:1971-1984.

Morgan, G. J., F. E. Davies, W. M. Gregory, K. Cocks, S. E. Bell, A. J. Szubert, N. Navarro-Coy, M. T. Drayson, R. G. Owen, S. Feyler, A. J. Ashcroft, F. Ross, J. Byrne, H. Roddie, C. Rudin, G. Cook, G. H. Jackson, and J. A. Child. 2010. First-line treatment with zoledronic acid as compared with clodronic acid in multiple myeloma (MRC Myeloma IX): a randomised controlled trial. *Lancet* **376**:1989-1999.

Morrison, J. F. 1969. Kinetics of the reversible inhibition of enzyme-catalysed reactions by tight-binding inhibitors. *Biochim Biophys Acta* **185**:269-286.

Morrison, J. F., and C. T. Walsh. 1988. The behavior and significance of slow-binding enzyme inhibitors. *Adv Enzymol Relat Areas Mol Biol* **61**:201-301.

Morton, A. R., and A. Howell. 1988. Bisphosphonates and bone metastases. *Br J Cancer* **58**:556-557.

Nakagawa, N., M. Kinosaki, K. Yamaguchi, N. Shima, H. Yasuda, K. Yano, T. Morinaga, and K. Higashio. 1998. RANK is the essential signaling receptor for osteoclast differentiation factor in osteoclastogenesis. *Biochem Biophys Res Commun* **253**:395-400.

Nakashima, T., Y. Kobayashi, S. Yamasaki, A. Kawakami, K. Eguchi, H. Sasaki, and H. Sakai. 2000. Protein expression and functional difference of membrane-bound and soluble receptor activator of NF-kappaB ligand: modulation of the expression by osteotropic factors and cytokines. *Biochem Biophys Res Commun* **275**:768-775.

Nancollas, G. H., R. Tang, R. J. Phipps, Z. Henneman, S. Gulde, W. Wu, A. Mangood, R. G. Russell, and F. H. Ebetino. 2006. Novel insights into actions of bisphosphonates on bone: differences in interactions with hydroxyapatite. *Bone* **38**:617-627.

Neville-Webbe, H. L., M. Gnant, and R. E. Coleman. 2010. Potential anticancer properties of bisphosphonates. *Semin Oncol* **37 Suppl 1**:S53-65.

Nicholson, G. C., J. M. Moseley, P. M. Sexton, F. A. Mendelsohn, and T. J. Martin. 1986. Abundant calcitonin receptors in isolated rat osteoclasts. Biochemical and autoradiographic characterization. *J Clin Invest* **78**:355-360.

Nijweide, P. J., E. H. Burger, and J. H. Feyen. 1986. Cells of bone: proliferation, differentiation, and hormonal regulation. *Physiol Rev* **66**:855-886.

Olkkonen, V. M., and E. Ikonen. 2000. Genetic defects of intracellular-membrane transport. *N Engl J Med* **343**:1095-1104.

Otto, J. C., E. Kim, S. G. Young, and P. J. Casey. 1999. Cloning and characterization of a mammalian prenyl protein-specific protease. *J Biol Chem* **274**:8379-8382.

Overmeyer, J. H., A. L. Wilson, and W. A. Maltese. 2001. Membrane targeting of a Rab GTPase that fails to associate with Rab escort protein (REP) or guanine nucleotide dissociation inhibitor (GDI). *J Biol Chem* **276**:20379-20386.

Painter, J., and E. A. Merritt. 2006. Optimal description of a protein structure in terms of multiple groups undergoing TLS motion. *Acta Crystallogr D Biol Crystallogr* **62**:439-450.

Palade, G. 1975. Intracellular aspects of the process of protein synthesis. *Science* **189**:347-358.

Papapoulos, S. E. 2010. Use of bisphosphonates in the management of postmenopausal osteoporosis. *Ann N Y Acad Sci*.

Passarelli, A. L., J. W. Todd, and L. K. Miller. 1994. A baculovirus gene involved in late gene expression predicts a large polypeptide with a conserved motif of RNA polymerases. *J Virol* **68**:4673-4678.

Pazianas, M., C. Cooper, F. H. Ebetino, and R. G. Russell. 2010. Long-term treatment with bisphosphonates and their safety in postmenopausal osteoporosis. *Ther Clin Risk Manag* **6**:325-343.

Pereira-Leal, J. B., M. Strom, R. F. Godfrey, and M. C. Seabra. 2003. Structural determinants of Rab and Rab Escort Protein interaction: Rab family motifs define a conserved binding surface. *Biochem Biophys Res Commun* **301**:92-97.

Pfeffer, S. R., A. B. Dirac-Svejstrup, and T. Soldati. 1995. Rab GDP dissociation inhibitor: putting rab GTPases in the right place. *J Biol Chem* **270**:17057-17059.

Pfeilschifter, J., C. Chenu, A. Bird, G. R. Mundy, and G. D. Roodman. 1989. Interleukin-1 and tumor necrosis factor stimulate the formation of human osteoclastlike cells in vitro. *J Bone Miner Res* **4**:113-118.

Phan, R. M., and C. D. Poulter. 2000. Synthesis of geranyl S-thiolodiphosphate. A new alternative substrate/inhibitor for prenyltransferases. *Org Lett* **2**:2287-2289.

Pival, S. L., M. Klimacek, R. Kratzer, and B. Nidetzky. 2008. Tyr-51 is the proton donor-acceptor for NAD(H)-dependent interconversion of xylose and xylitol by Candida tenuis xylose reductase (AKR2B5). *FEBS Lett* **582**:4095-4099.

Plasmans, C. M., P. H. Jap, W. Kuijpers, and T. J. Slooff. 1980. Influence of a diphosphonate on the cellular aspect of young bone tissue. *Calcif Tissue Int* **32**:247-266.

Plochocka, D., F. Karst, E. Swiezewska, and A. Szkopinska. 2000. The role of ERG20 gene (encoding yeast farnesyl diphosphate synthase) mutation in long dolichol formation. Molecular modeling of FPP synthase. *Biochimie* **82**:733-738.

Poole, K. E., S. Vedi, I. Debiram, C. Rose, J. Power, N. Loveridge, E. A. Warburton, J. Reeve, and J. Compston. 2009. Bone structure and remodelling in stroke patients: early effects of zoledronate. *Bone* **44**:629-633.

Popjak, G., and J. W. Cornforth. 1966. Substrate stereochemistry in squalene biosynthesis: The first Ciba medal lecture. *Biochem J* **101**:553 b554-568.

Popjak, G., D. S. Goodman, J. W. Cornforth, R. H. Cornforth, and R. Ryhage. 1961. Mechanism of squalene biosynthesis from mevalonate and farnesyl pyrophosphate. *Biochem Biophys Res Commun* **4**:138-142.

Popjak, G., L. Gosselin, I. Y. Gore, and R. G. Gould. 1958. Studies on the biosynthesis of cholesterol. 6. Coenzyme requirements of liver enzymes for synthesis of squalene and of sterol from DL-3-hydroxy-3-methyl-[2-14C] pentano-5-lactone. *Biochem J* **69**:238-248.

Porter, J. W., and S. L. Spurgeon. 1981. *Biosynthesis of isoprenoid compounds*. Wiley, New York.

Poulter, C. D., J. C. Argyle, and E. A. Mash. 1978. Farnesyl pyrophosphate synthetase. Mechanistic studies of the 1'-4 coupling reaction with 2-fluorogeranyl pyrophosphate. *J Biol Chem* **253**:7227-7233.

Poulter, C. D., and H. C. Rilling. 1976. Prenyltransferase: the mechanism of the reaction. *Biochemistry* **15**:1079-1083.

Powell, H. R. 1999. The Rossmann Fourier autoindexing algorithm in MOSFLM. *Acta Crystallogr D Biol Crystallogr* **55**:1690-1695.

Pylypenko, O., A. Rak, R. Reents, A. Niculae, V. Sidorovitch, M. D. Cioaca, E. Bessolitsyna, N. H. Thoma, H. Waldmann, I. Schlichting, R. S. Goody, and K. Alexandrov. 2003. Structure of Rab escort protein-1 in complex with Rab geranylgeranyltransferase. *Mol Cell* **11**:483-494.

Quinn, J. M., J. Elliott, M. T. Gillespie, and T. J. Martin. 1998. A combination of osteoclast differentiation factor and macrophage-colony stimulating factor is sufficient for both human and mouse osteoclast formation in vitro. *Endocrinology* **139**:4424-4427.

Raikkonen, J., J. C. Crockett, M. J. Rogers, H. Monkkonen, S. Auriola, and J. Monkkonen. 2009. Zoledronic acid induces formation of a pro-apoptotic ATP analogue and isopentenyl pyrophosphate in osteoclasts in vivo and in MCF-7 cells in vitro. *Br J Pharmacol* **157**:427-435.

Rak, A., O. Pylypenko, A. Niculae, R. S. Goody, and K. Alexandrov. 2003. Crystallization and preliminary X-ray diffraction analysis of monoprenylated Rab7 GTPase in complex with Rab escort protein 1. *J Struct Biol* **141**:93-95.

Rak, A., O. Pylypenko, A. Niculae, K. Pyatkov, R. S. Goody, and K. Alexandrov. 2004. Structure of the Rab7:REP-1 complex: insights into the mechanism of Rab prenylation and choroideremia disease. *Cell* **117**:749-760.

Ralston, S., U. Patel, W. Fraser, S. Gallacher, F. Dryburgh, R. Cowan, and I. Boyle. 1989. Comparison of three intravenous bisphosphonates in cancer-associated hypercalcaemia. *The Lancet* **334**:1180-1182.

Ralston, S. H., A. L. Langston, and I. R. Reid. 2008. Pathogenesis and management of Paget's disease of bone. *Lancet* **372**:155-163.

Rasteiro, R., and J. B. Pereira-Leal. 2007. Multiple domain insertions and losses in the evolution of the Rab prenylation complex. *BMC Evol Biol* **7**:140.

Reed, B. C., and H. C. Rilling. 1976. Substrate Binding of avian liver prenyltransferase. *Biochemistry* **15**:3739-3745.

Reid, T. S., K. L. Terry, P. J. Casey, and L. S. Beese. 2004. Crystallographic analysis of CaaX prenyltransferases complexed with substrates defines rules of protein substrate selectivity. *J Mol Biol* **343**:417-433.

Reiss, Y., J. L. Goldstein, M. C. Seabra, P. J. Casey, and M. S. Brown. 1990. Inhibition of purified p21ras farnesyl:protein transferase by Cys-AAX tetrapeptides. *Cell* **62**:81-88.

Reszka, A. A., J. M. Halasy-Nagy, P. J. Masarachia, and G. A. Rodan. 1999. Bisphosphonates act directly on the osteoclast to induce caspase cleavage of mst1 kinase during apoptosis. A link between inhibition of the mevalonate pathway and regulation of an apoptosis-promoting kinase. *J Biol Chem* **274**:34967-34973.

Ridley, A. J. 2006. Rho GTPases and actin dynamics in membrane protrusions and vesicle trafficking. *Trends Cell Biol* **16**:522-529.

Ridley, A. J., and A. Hall. 1992. The small GTP-binding protein rho regulates the assembly of focal adhesions and actin stress fibers in response to growth factors. *Cell* **70**:389-399.

Ridley, A. J., H. F. Paterson, C. L. Johnston, D. Diekmann, and A. Hall. 1992. The small GTP-binding protein rac regulates growth factor-induced membrane ruffling. *Cell* **70**:401-410.

Rilling, H. C., and K. Bloch. 1959. On the mechanism of squaiene biogenesis from mevalonic acid. *J Biol Chem* **234**:1424-1432.

Risley, J. M. 2002. Cholesterol Biosynthesis: Lanosterol to Cholesterol. *Journal of Chemical Education* **79**:377-null.

Roberts, S. C. 2007. Production and engineering of terpenoids in plant cell culture. *Nat Chem Biol* **3**:387-395.

Rodriguez, N., B. N. Bailey, M. B. Martin, E. Oldfield, J. A. Urbina, and R. Docampo. 2002. Radical cure of experimental cutaneous leishmaniasis by the bisphosphonate pamidronate. *J Infect Dis* **186**:138-140.

Roelofs, A. J., F. P. Coxon, F. H. Ebetino, M. W. Lundy, Z. J. Henneman, G. H. Nancollas, S. Sun, K. M. Blazewska, J. L. Bala, B. A. Kashemirov, A. B. Khalid, C. E. McKenna, and M. J. Rogers. 2010. Fluorescent risedronate analogues reveal bisphosphonate uptake by bone marrow monocytes and localization around osteocytes in vivo. *J Bone Miner Res* **25**:606-616.

Roelofs, A. J., M. Jauhiainen, H. Monkkonen, M. J. Rogers, J. Monkkonen, and K. Thompson. 2009. Peripheral blood monocytes are responsible for gammadelta T cell activation induced by zoledronic acid through accumulation of IPP/DMAPP. *Br J Haematol* **144**:245-250.

Rogers, M. J., R. J. Brown, V. Hodkin, G. M. Blackburn, R. G. Russell, and D. J. Watts. 1996. Bisphosphonates are incorporated into adenine nucleotides by human aminoacyl-tRNA synthetase enzymes. *Biochem Biophys Res Commun* **224**:863-869.

Rogers, M. J., S. Gordon, H. L. Benford, F. P. Coxon, S. P. Luckman, J. Monkkonen, and J. C. Frith. 2000. Cellular and molecular mechanisms of action of bisphosphonates. *Cancer* **88**:2961-2978.

Rogers, M. J., R. G. Russell, G. M. Blackburn, M. P. Williamson, and D. J. Watts. 1992. Metabolism of halogenated bisphosphonates by the cellular slime mould Dictyostelium discoideum. *Biochem Biophys Res Commun* **189**:414-423.

Rogers, M. J., X. Xiong, R. J. Brown, D. J. Watts, R. G. Russell, A. V. Bayless, and F. H. Ebetino. 1995. Structure-activity relationships of new heterocycle-containing bisphosphonates as inhibitors of bone resorption and as inhibitors of growth of Dictyostelium discoideum amoebae. *Mol Pharmacol* **47**:398-402.

Romier, C., M. Ben Jelloul, S. Albeck, G. Buchwald, D. Busso, P. H. Celie, E. Christodoulou, V. De Marco, S. van Gerwen, P. Knipscheer, J. H. Lebbink, V. Notenboom, A. Poterszman, N. Rochel, S. X. Cohen, T. Unger, J. L. Sussman, D. Moras, T. K. Sixma, and A. Perrakis. 2006. Co-expression of protein complexes in prokaryotic and eukaryotic hosts: experimental procedures, database tracking and case studies. *Acta Crystallogr D Biol Crystallogr* **62**:1232-1242.

Rondeau, J. M., F. Bitsch, E. Bourgier, M. Geiser, R. Hemmig, M. Kroemer, S. Lehmann, P. Ramage, S. Rieffel, A. Strauss, J. R. Green, and W. Jahnke. 2006. Structural basis for the exceptional in vivo efficacy of bisphosphonate drugs. *ChemMedChem* **1**:267-273.

Roodman, G. D. 2006. Regulation of osteoclast differentiation. *Ann N Y Acad Sci* **1068**:100-109.

Rosen, L. S., D. Gordon, S. Tchekmedyian, R. Yanagihara, V. Hirsh, M. Krzakowski, M. Pawlicki, P. de Souza, M. Zheng, G. Urbanowitz, D. Reitsma, and J. J. Seaman. 2003. Zoledronic acid versus placebo in the treatment of skeletal metastases in patients with lung cancer and other solid tumors: a phase III, double-blind, randomized trial--the Zoledronic Acid Lung Cancer and Other Solid Tumors Study Group. *J Clin Oncol* **21**:3150-3157.

Roskoski, R., Jr., and P. Ritchie. 1998. Role of the carboxyterminal residue in peptide binding to protein farnesyltransferase and protein geranylgeranyltransferase. *Arch Biochem Biophys* **356**:167-176.

Rudney, H. 1957. The biosynthesis of beta-hydroxy-beta-methylglutaric acid. *J Biol Chem* **227**:363-377.

Russell, R. G. 2006. Bisphosphonates: from bench to bedside. *Ann N Y Acad Sci* **1068**:367-401.

Russell, R. G., N. B. Watts, F. H. Ebetino, and M. J. Rogers. 2008. Mechanisms of action of bisphosphonates: similarities and differences and their potential influence on clinical efficacy. *Osteoporos Int* **19**:733-759.

Russell, R. G., Z. Xia, J. E. Dunford, U. Oppermann, A. Kwaasi, P. A. Hulley, K. L. Kavanagh, J. T. Triffitt, M. W. Lundy, R. J. Phipps, B. L. Barnett, F. P. Coxon, M. J. Rogers, N. B. Watts, and F. H. Ebetino. 2007. Bisphosphonates: an update on mechanisms of action and how these relate to clinical efficacy. *Ann N Y Acad Sci* **1117**:209-257.

Ruzicka, L. 1959. History of the Isoprene Rule. *Proceedings of the Chemical Society*:341-376.

Saad, F., D. M. Gleason, R. Murray, S. Tchekmedyian, P. Venner, L. Lacombe, J. L. Chin, J. J. Vinholes, J. A. Goas, and M. Zheng. 2004. Long-term efficacy of zoledronic acid for the prevention of skeletal complications in patients with metastatic hormone-refractory prostate cancer. *J Natl Cancer Inst* **96**:879-882.

Sanchez, V. M., A. Crespo, J. S. Gutkind, and A. G. Turjanski. 2006. Investigation of the catalytic mechanism of farnesyl pyrophosphate synthase by computer simulation. *J Phys Chem B* **110**:18052-18057.

Santini, D., B. Vincenzi, G. Avvisati, G. Dicuonzo, F. Battistoni, M. Gavasci, A. Salerno, V. Denaro, and G. Tonini. 2002. Pamidronate induces modifications of circulating angiogenetic factors in cancer patients. *Clin Cancer Res* **8**:1080-1084.

Sanz-Rodriguez, C. E., J. L. Concepcion, S. Pekerar, E. Oldfield, and J. A. Urbina. 2007. Bisphosphonates as inhibitors of Trypanosoma cruzi hexokinase: kinetic and metabolic studies. *J Biol Chem* **282**:12377-12387.

Sato, M., and W. Grasser. 1990. Effects of bisphosphonates on isolated rat osteoclasts as examined by reflected light microscopy. *J Bone Miner Res* **5**:31-40.

Sato, M., W. Grasser, N. Endo, R. Akins, H. Simmons, D. D. Thompson, E. Golub, and G. A. Rodan. 1991. Bisphosphonate action. Alendronate localization in rat bone and effects on osteoclast ultrastructure. *J Clin Invest* **88**:2095-2105.

Saunders, Y., J. R. Ross, K. E. Broadley, P. M. Edmonds, and S. Patel. 2004. Systematic review of bisphosphonates for hypercalcaemia of malignancy. *Palliat Med* **18**:418-431.

Savitsky, P., J. Bray, C. D. Cooper, B. D. Marsden, P. Mahajan, N. A. Burgess-Brown, and O. Gileadi. 2010. High-throughput production of human proteins for crystallization: the SGC experience. *J Struct Biol* **172**:3-13.

Schafer, W. R., and J. Rine. 1992. Protein prenylation: genes, enzymes, targets, and functions. *Annu Rev Genet* **26**:209-237.

Scheven, B. A., A. M. Wassenaar, E. W. Kawilarang-de Haas, and P. J. Nijweide. 1987. Comparison of direct and indirect radiation effects on osteoclast formation from progenitor cells derived from different hemopoietic sources. *Radiat Res* **111**:107-118.

Schibler, D., R. G. Russell, and H. Fleisch. 1968. Inhibition by pyrophosphate and polyphosphate of aortic calcification induced by vitamin D3 in rats. *Clin Sci* **35**:363-372.

Seabra, M. C. 1996. Nucleotide dependence of Rab geranylgeranylation. Rab escort protein interacts preferentially with GDP-bound Rab. *J Biol Chem* **271**:14398-14404.

Seabra, M. C. 1998. Membrane association and targeting of prenylated Ras-like GTPases. *Cell Signal* **10**:167-172.

Seabra, M. C., M. S. Brown, C. A. Slaughter, T. C. Sudhof, and J. L. Goldstein. 1992a. Purification of component A of Rab geranylgeranyl transferase: possible identity with the choroideremia gene product. *Cell* **70**:1049-1057.

Seabra, M. C., J. L. Goldstein, T. C. Sudhof, and M. S. Brown. 1992b. Rab geranylgeranyl transferase. A multisubunit enzyme that prenylates GTP-binding proteins terminating in Cys-X-Cys or Cys-Cys. *J Biol Chem* **267**:14497-14503.

Seabra, M. C., Y. K. Ho, and J. S. Anant. 1995. Deficient geranylgeranylation of Ram/Rab27 in choroideremia. *J Biol Chem* **270**:24420-24427.

Seabra, M. C., Y. Reiss, P. J. Casey, M. S. Brown, and J. L. Goldstein. 1991. Protein farnesyltransferase and geranylgeranyltransferase share a common alpha subunit. *Cell* **65**:429-434.

Selander, K., P. Lehenkari, and H. K. Vaananen. 1994. The effects of bisphosphonates on the resorption cycle of isolated osteoclasts. *Calcif Tissue Int* **55**:368-375.

Selander, K. S., J. Monkkonen, E. K. Karhukorpi, P. Harkonen, R. Hannuniemi, and H. K. Vaananen. 1996. Characteristics of clodronate-induced apoptosis in osteoclasts and macrophages. *Mol Pharmacol* **50**:1127-1138.

Shen, F., and M. C. Seabra. 1996. Mechanism of digeranylgeranylation of Rab proteins. Formation of a complex between monogeranylgeranyl-Rab and Rab escort protein. *J Biol Chem* **271**:3692-3698.

Shipman, C. M., M. J. Rogers, J. F. Apperley, R. G. Russell, and P. I. Croucher. 1997. Bisphosphonates induce apoptosis in human myeloma cell lines: a novel anti-tumour activity. *Br J Haematol* **98**:665-672.

Shipman, C. M., K. Vanderkerken, M. J. Rogers, J. M. Lippitt, K. Asosingh, D. E. Hughes, B. Van Camp, R. G. Russell, and P. I. Croucher. 2000. The potent bisphosphonate ibandronate does not induce myeloma cell apoptosis in a murine model of established multiple myeloma. *Br J Haematol* **111**:283-286.

Shrestha, B., C. Smee, and O. Gileadi. 2008. Baculovirus expression vector system: an emerging host for high-throughput eukaryotic protein expression. *Methods Mol Biol* **439**:269-289.

Sidorovitch, V., A. Niculae, N. Kan, A. C. Ceacareanu, and K. Alexandrov. 2002. Expression of mammalian Rab Escort protein-1 and -2 in yeast Saccharomyces cerevisiae. *Protein Expr Purif* **26**:50-58.

Silverman, S. L. 2009. New therapies for osteoporosis: zoledronic acid, bazedoxifene, and denosumab. *Curr Osteoporos Rep* **7**:91-95.

Silvius, J. R., and F. l'Heureux. 1994. Fluorimetric evaluation of the affinities of isoprenylated peptides for lipid bilayers. *Biochemistry* **33**:3014-3022.

Simonet, W. S., D. L. Lacey, C. R. Dunstan, M. Kelley, M. S. Chang, R. Luthy, H. Q. Nguyen, S. Wooden, L. Bennett, T. Boone, G. Shimamoto, M. DeRose, R. Elliott, A. Colombero, H. L. Tan, G. Trail, J. Sullivan, E. Davy, N. Bucay, L. Renshaw-Gegg, T. M. Hughes, D. Hill, W. Pattison, P. Campbell, S. Sander, G. Van, J. Tarpley, P. Derby, R. Lee, and W. J. Boyle. 1997. Osteoprotegerin: a novel secreted protein involved in the regulation of bone density. *Cell* **89**:309-319.

Sinensky, M. 2000. Recent advances in the study of prenylated proteins. *Biochim Biophys Acta* **1484**:93-106.

Smeland, T. E., M. C. Seabra, J. L. Goldstein, and M. S. Brown. 1994. Geranylgeranylated Rab proteins terminating in Cys-Ala-Cys, but not Cys-Cys, are carboxyl-methylated by bovine brain membranes in vitro. *Proc Natl Acad Sci U S A* **91**:10712-10716.

Sohara, Y., H. Shimada, and Y. A. DeClerck. 2005. Mechanisms of bone invasion and metastasis in human neuroblastoma. *Cancer Lett* **228**:203-209.

Song, L., and C. D. Poulter. 1994. Yeast farnesyl-diphosphate synthase: site-directed mutagenesis of residues in highly conserved prenyltransferase domains I and II. *Proc Natl Acad Sci U S A* **91**:3044-3048.

Sorensen, H. P., and K. K. Mortensen. 2005. Soluble expression of recombinant proteins in the cytoplasm of Escherichia coli. *Microb Cell Fact* **4**:1.

Stevenson, P. H., and J. R. Stevenson. 1986. Cytotoxic and migration inhibitory effects of bisphosphonates on macrophages. *Calcif Tissue Int* **38**:227-233.

Street, I. P., and C. D. Poulter. 1990. Isopentenyldiphosphate:dimethylallyldiphosphate isomerase: construction of a high-level heterologous expression system for the gene from Saccharomyces cerevisiae and identification of an active-site nucleophile. *Biochemistry* **29**:7531-7538.

Stresing, V., P. G. Fournier, A. Bellahcene, I. Benzaid, H. Monkkonen, M. Colombel, F. H. Ebetino, V. Castronovo, and P. Clezardin. 2010. Nitrogen-containing bisphosphonates can inhibit angiogenesis in vivo without the involvement of farnesyl pyrophosphate synthase. *Bone*.

Suda, T., N. Takahashi, and T. J. Martin. 1992. Modulation of osteoclast differentiation. *Endocr Rev* **13**:66-80.

Symons, M., and N. Rusk. 2003. Control of vesicular trafficking by Rho GTPases. *Curr Biol* **13**:R409-418.

Takai, Y., T. Sasaki, and T. Matozaki. 2001. Small GTP-binding proteins. *Physiol Rev* **81**:153-208.

Tanaka, S., N. Takahashi, N. Udagawa, T. Tamura, T. Akatsu, E. R. Stanley, T. Kurokawa, and T. Suda. 1993. Macrophage colony-stimulating factor is indispensable for both proliferation and differentiation of osteoclast progenitors. *J Clin Invest* **91**:257-263.

Tarshis, L. C., P. J. Proteau, B. A. Kellogg, J. C. Sacchettini, and C. D. Poulter. 1996. Regulation of product chain length by isoprenyl diphosphate synthases. *Proc Natl Acad Sci U S A* **93**:15018-15023.

Tarshis, L. C., M. Yan, C. D. Poulter, and J. C. Sacchettini. 1994. Crystal structure of recombinant farnesyl diphosphate synthase at 2.6-A resolution. *Biochemistry* **33**:10871-10877.

Tassone, P., S. Forciniti, E. Galea, G. Morrone, M. C. Turco, V. Martinelli, P. Tagliaferri, and S. Venuta. 2000. Growth inhibition and synergistic induction of apoptosis by zoledronate and dexamethasone in human myeloma cell lines. *Leukemia* **14**:841-844.

Tassone, P., P. Tagliaferri, C. Viscomi, C. Palmieri, M. Caraglia, A. D'Alessandro, E. Galea, A. Goel, A. Abbruzzese, C. R. Boland, and S. Venuta. 2003. Zoledronic acid induces antiproliferative and apoptotic effects in human pancreatic cancer cells in vitro. *Br J Cancer* **88**:1971-1978.

Tavormina, P. A., M. H. Gibbs, and J. W. Huff. 1956. The utilization of Î²-hydroxy-Î²-methyl-Î´-valerolactone in cholesterol biosynthesis [7]. *Journal of the American Chemical Society* **78**:4498-4499.

Tchen, T. T., and K. Bloch. 1957a. On the conversion of squalene to lanosterol in vitro. *J Biol Chem* **226**:921-930.

Tchen, T. T., and K. Bloch. 1957b. On the mechanism of enzymatic cyclization of squalene. *J Biol Chem* **226**:931-939.

Teitelbaum, S. L. 2000. Bone resorption by osteoclasts. *Science* **289**:1504-1508.

Teitelbaum, S. L., and F. P. Ross. 2003. Genetic regulation of osteoclast development and function. *Nat Rev Genet* **4**:638-649.

Thiebaud, D., A. Sauty, P. Burckhardt, P. Leuenberger, L. Sitzler, J. R. Green, A. Kandra, J. Zieschang, and P. Ibarra de Palacios. 1997. An in vitro and in vivo study of cytokines in the acute-phase response associated with bisphosphonates. *Calcif Tissue Int* **61**:386-392.

Thoma, N. H., A. Iakovenko, R. S. Goody, and K. Alexandrov. 2001a. Phosphoisoprenoids modulate association of Rab geranylgeranyltransferase with REP-1. *J Biol Chem* **276**:48637-48643.

Thoma, N. H., A. Iakovenko, A. Kalinin, H. Waldmann, R. S. Goody, and K. Alexandrov. 2001b. Allosteric regulation of substrate binding and product release in geranylgeranyltransferase type II. *Biochemistry* **40**:268-274.

Thoma, N. H., A. Iakovenko, D. Owen, A. S. Scheidig, H. Waldmann, R. S. Goody, and K. Alexandrov. 2000. Phosphoisoprenoid binding specificity of geranylgeranyltransferase type II. *Biochemistry* **39**:12043-12052.

Thoma, N. H., A. Niculae, R. S. Goody, and K. Alexandrov. 2001c. Double prenylation by RabGGTase can proceed without dissociation of the mono-prenylated intermediate. *J Biol Chem* **276**:48631-48636.

Thompson, K., M. J. Rogers, F. P. Coxon, and J. C. Crockett. 2006a. Cytosolic entry of bisphosphonate drugs requires acidification of vesicles after fluid-phase endocytosis. *Mol Pharmacol* **69**:1624-1632.

Thompson, K., J. Rojas-Navea, and M. J. Rogers. 2006b. Alkylamines cause Vgamma9Vdelta2 T-cell activation and proliferation by inhibiting the mevalonate pathway. *Blood* **107**:651-654.

Tolia, N. H., and L. Joshua-Tor. 2006. Strategies for protein coexpression in Escherichia coli. *Nat Methods* **3**:55-64.

Tsuchiya, T., Y. Matsumoto, and S. Kurihara. 1995. The fluorescent simultaneous azo dye technique for demonstration of tartrate-resistant acid phosphatase (TRAP) activity in osteoclast-like multinucleate cells. *Journal of Bone and Mineral Metabolism* **13**:71-76.

Tsuda, E., M. Goto, S. Mochizuki, K. Yano, F. Kobayashi, T. Morinaga, and K. Higashio. 1997. Isolation of a novel cytokine from human fibroblasts that specifically inhibits osteoclastogenesis. *Biochem Biophys Res Commun* **234**:137-142.

Udagawa, N. 2002. Mechanisms involved in bone resorption. *Biogerontology* **3**:79-83.

Udagawa, N., N. Takahashi, T. Akatsu, H. Tanaka, T. Sasaki, T. Nishihara, T. Koga, T. J. Martin, and T. Suda. 1990. Origin of osteoclasts: mature monocytes and macrophages are capable of differentiating into osteoclasts under a suitable microenvironment prepared by bone marrow-derived stromal cells. *Proc Natl Acad Sci U S A* **87**:7260-7264.

Udagawa, N., N. Takahashi, E. Jimi, K. Matsuzaki, T. Tsurukai, K. Itoh, N. Nakagawa, H. Yasuda, M. Goto, E. Tsuda, K. Higashio, M. T. Gillespie, T. J. Martin, and T. Suda. 1999. Osteoblasts/stromal cells stimulate osteoclast activation through expression of osteoclast differentiation factor/RANKL but not macrophage colony-stimulating factor: receptor activator of NF-kappa B ligand. *Bone* **25**:517-523.

van Beek, E., E. Pieterman, L. Cohen, C. Lowik, and S. Papapoulos. 1999a. Farnesyl pyrophosphate synthase is the molecular target of nitrogen-containing bisphosphonates. *Biochem Biophys Res Commun* **264**:108-111.

van Beek, E., E. Pieterman, L. Cohen, C. Lowik, and S. Papapoulos. 1999b. Nitrogen-containing bisphosphonates inhibit isopentenyl pyrophosphate isomerase/farnesyl pyrophosphate synthase activity with relative potencies corresponding to their antiresorptive potencies in vitro and in vivo. *Biochem Biophys Res Commun* **255**:491-494.

van Beek, E. R., C. W. Lowik, F. H. Ebetino, and S. E. Papapoulos. 1998. Binding and antiresorptive properties of heterocycle-containing bisphosphonate analogs: structure-activity relationships. *Bone* **23**:437-442.

Van Beek, E. R., C. W. Lowik, and S. E. Papapoulos. 2002. Bisphosphonates suppress bone resorption by a direct effect on early osteoclast precursors without affecting the osteoclastogenic capacity of osteogenic cells: the role of protein geranylgeranylation in the action of nitrogen-containing bisphosphonates on osteoclast precursors. *Bone* **30**:64-70.

van der Pluijm, G., H. Vloedgraven, E. van Beek, L. van der Wee-Pals, C. Lowik, and S. Papapoulos. 1996. Bisphosphonates inhibit the adhesion of breast cancer cells to bone matrices in vitro. *J Clin Invest* **98**:698-705.

Voet, D., and J. G. Voet. 1995. *Biochemistry*. Wiley, New York ; Chichester.

Wada, T., T. Nakashima, N. Hiroshi, and J. M. Penninger. 2006. RANKL-RANK signaling in osteoclastogenesis and bone disease. *Trends Mol Med* **12**:17-25.

Watts, N. B., and D. L. Diab. 2010. Long-term use of bisphosphonates in osteoporosis. *J Clin Endocrinol Metab* **95**:1555-1565.

Waugh, D. S. 2005. Making the most of affinity tags. *Trends Biotechnol* **23**:316-320.

Wei, S., H. Kitaura, P. Zhou, F. P. Ross, and S. L. Teitelbaum. 2005. IL-1 mediates TNF-induced osteoclastogenesis. *J Clin Invest* **115**:282-290.

Weinstein, J. D., R. Branchaud, S. I. Beale, W. J. Bement, and P. R. Sinclair. 1986. Biosynthesis of the farnesyl moiety of heme a from exogenous mevalonic acid by cultured chick liver cells. *Arch Biochem Biophys* **245**:44-50.

Weinstein, R. S., P. K. Roberson, and S. C. Manolagas. 2009. Giant osteoclast formation and long-term oral bisphosphonate therapy. *N Engl J Med* **360**:53-62.

Wilson, A. L., R. A. Erdman, F. Castellano, and W. A. Maltese. 1998. Prenylation of Rab8 GTPase by type I and type II geranylgeranyl transferases. *Biochem J* **333 (Pt 3)**:497-504.

Witter, D. J., and C. D. Poulter. 1996. Yeast geranylgeranyltransferase type-II: steady state kinetic studies of the recombinant enzyme. *Biochemistry* **35**:10454-10463.

Wong, B. R., J. Rho, J. Arron, E. Robinson, J. Orlinick, M. Chao, S. Kalachikov, E. Cayani, F. S. Bartlett, 3rd, W. N. Frankel, S. Y. Lee, and Y. Choi. 1997. TRANCE is a novel ligand of the tumor necrosis factor receptor family that activates c-Jun N-terminal kinase in T cells. *J Biol Chem* **272**:25190-25194.

Woodward, R. B., and K. Bloch. 1953. The cyclization of squalene in cholesterol synthesis *Journal of the American Chemical Society* **75**:2023-2024.

Wouters, J., Y. Oudjama, S. Ghosh, V. Stalon, L. Droogmans, and E. Oldfield. 2003. Structure and mechanism of action of isopentenylpyrophosphate-dimethylallylpyrophosphate isomerase. *J Am Chem Soc* **125**:3198-3199.

Wuersch, J., R. L. Huang, and K. Bloch. 1952. The origin of the issoctyl side chain of cholesterol. *J Biol Chem* **195**:439-446.

Yano, S., H. Zhang, M. Hanibuchi, T. Miki, H. Goto, H. Uehara, and S. Sone. 2003. Combined therapy with a new bisphosphonate, minodronate (YM529), and chemotherapy for multiple organ metastases of small cell lung cancer cells in severe combined immunodeficient mice. *Clin Cancer Res* **9**:5380-5385.

Yardley, V., A. A. Khan, M. B. Martin, T. R. Slifer, F. G. Araujo, S. N. Moreno, R. Docampo, S. L. Croft, and E. Oldfield. 2002. In vivo activities of farnesyl pyrophosphate synthase inhibitors against Leishmania donovani and Toxoplasma gondii. *Antimicrob Agents Chemother* **46**:929-931.

Yin, F., R. Cao, A. Goddard, Y. Zhang, and E. Oldfield. 2006. Enthalpy versus entropy-driven binding of bisphosphonates to farnesyl diphosphate synthase. *J Am Chem Soc* **128**:3524-3525.

Yoshida, H., S. Hayashi, T. Kunisada, M. Ogawa, S. Nishikawa, H. Okamura, T. Sudo, and L. D. Shultz. 1990. The murine mutation osteopetrosis is in the coding region of the macrophage colony stimulating factor gene. *Nature* **345**:442-444.

Zerial, M., and H. Stenmark. 1993. Rab GTPases in vesicular transport. *Curr Opin Cell Biol* **5**:613-620.

Zhang, D., S. M. Jennings, G. W. Robinson, and C. D. Poulter. 1993. Yeast squalene synthase: expression, purification, and characterization of soluble recombinant enzyme. *Arch Biochem Biophys* **304**:133-143.

Zhang, D., N. Udagawa, I. Nakamura, H. Murakami, S. Saito, K. Yamasaki, Y. Shibasaki, N. Morii, S. Narumiya, N. Takahashi, and et al. 1995. The small GTP-binding protein, rho p21, is involved in bone resorption by regulating cytoskeletal organization in osteoclasts. *J Cell Sci* **108 (Pt 6)**:2285-2292.

Zhang, F. L., and P. J. Casey. 1996. Protein prenylation: molecular mechanisms and functional consequences. *Annu Rev Biochem* **65**:241-269.

Zhang, H. 2003. Binding Platforms for Rab Prenylation and Recycling: Rab Escort Protein, RabGGT, and RabGDI. *Structure (London, England : 1993)* **11**:237-239.

Zhang, H., M. C. Seabra, and J. Deisenhofer. 2000. Crystal structure of Rab geranylgeranyltransferase at 2.0 A resolution. *Structure* **8**:241-251.

Zographos, S. E., N. G. Oikonomakos, H. B. Dixon, W. G. Griffin, L. N. Johnson, and D. D. Leonidas. 1995. Sulphate-activated phosphorylase b: the pH-dependence of catalytic activity. *Biochem J* **310 (Pt 2)**:565-570.

Zou, W., I. Hakim, K. Tschoep, S. Endres, and Z. Bar-Shavit. 2001. Tumor necrosis factor-alpha mediates RANK ligand stimulation of osteoclast differentiation by an autocrine mechanism. *J Cell Biochem* **83**:70-83.

Zou, W., and S. L. Teitelbaum. 2010. Integrins, growth factors, and the osteoclast cytoskeleton. *Ann N Y Acad Sci* **1192**:27-31.

APPENDIX A: PRIMERS USED IN PCR REACTIONS

PRIMERS FOR LIC CLONING

(fw: forward, rv: reverse, 000: N terminal cloning, 100: C terminal cloning)

RABGGTA-fw000	TAC TTC CAA TCC ATG CAC GGA CGC CTG AAG
RABGGTA-rv000	TAT CCA CCT TTA CTG TTA GGT GAG GAC GCT GCT AAC
RABGGTA-fw100	TTA AGA AGG AGA TAT ACT ATG CAC GGA CGC CTG AAG GTG
RABGGTA-rv100	GAT TGG AAG TAG AGG TTC TCT GC GGT GAG GAC GCT GCT AAC
RABGGTB-fw000	TAC TTC CAA TCC ATG GGC ACT CCA CAG AAG GAT
RABGGTB-rv000	TAT CCA CCT TTA CTG CTA GCT CAC TAG CTC AGG CTG
RABGGTB-fw100	TTA AGA AGG AGA TAT ACT ATG GGC ACT CCA CAG AAG GAT G
RABGGTB-rv100	GAT TGG AAG TAG AGG TTC TCT GC GCT CAC TAG CTC AGG CTG
CHM-fw000	TAC TTC CAA TCC ATG GCG GAT ACT CTC CC
CHM-rv000	TAT CCA CCT TTA CTG TTA TTC AGA GGA CTC CTC TAG G
CHM-fw100	TTA AGA AGG AGA TAT ACT ATG GCG GAT ACT CTC CCT TCG G
CHM-rv100	GAT TGG AAG TAG AGG TTC TCT GCT TCA GAG GAC TCC TCT AGG
CHML-fw000	TAC TTC CAA TCC ATG GCG GAC AAT CTT CCC ACA G
CHML-rv000	TAT CCA CCT TTA CTG CTA ATT TTG AAG GTG CTT CTC
CHML-fw100	TTA AGA AGG AGA TAT ACT ATG GCG GAC AAT CTT CCC ACA G
CHML-rv100	GAT TGG AAG TAG AGG TTC TCT GCA TTT TGA AGG TGC TTC TCT G

PRIMERS FOR pET-DUET CLONING

RABGGTA_EcoRI_fw	CCG GAA TTC G ATG CAC GGA CGC CTG AAG GTG
RABGGTA_SalI_rv	GAC GCG TCG AC TTA GGT GAG GAC GCT GC
RABGGTA_NdeI_fw	GGA ATT CCA TAT G ATG CAC GGA CGC CTG AAG GTG
RABGGTA_XhoI_rv	CCG CTC GAG TTA GGT GAG GAC GCT GC
RABGGTB_NdeI_fw	GGA ATT CCA TAT G ATG GGC ACT CCA CAG AAG GAT G
RABGGTB_XhoI_rv	CCG CTC GAG CTA GCT CAC TAG CTC AGG CTG
RABGGTB_EcoRI_fw	CCG GAA TTC G ATG GGC ACT CCA CAG AAG GAT G
RABGGTB_SalI_rv	GAC GCG TCG AC CTA GCT CAC TAG CTC AGG CTG

PRIMERS FOR RABGGTA and RABGGTB SUBCLONING

RABGGTA_GST_fw	GGA ATT C CAT ATG TCC CCT ATA CTA GGT TAT TGG
RABGGTA_XhoI_Stag_rv	CCG CTC GAG GGT GAG GAC GCT GCT AAC
RABGGTB_SET1_fw	GGA ATT C CAT ATG GAC CCC GAA GAG GCG AGT G
RABGGTB_XhoI_Stag_rv	CCG CTC GAG GCT CAC TAG CTC AGG CTG AAC
pNIC-CTHF_FLAG_rv	CCG CTC GAG TCA CTT ATC GTC GTC ATC CTT GTA ATC

APPENDIX B: MAIN FEATURES OF USED VECTORS

Name	Tag	Resistance	Cloning site	5 Seq primer	3 Seq primer
p11	(1)	Amp	NdeI BamHI	T7 –FW	pET- RV
pNIC28_Bsa4	(2)	Kan	5 Lic 3 Lic	pLIC –FW	pLIC-RV
pNIC-CTHF	(3)	Kan	5 Lic 3 Lic	pLIC –FW	pLIC -RV
pBEN1	(4)	Kan	5 Lic 3 Lic	pBEN –FW	pLIC –RV
pNH-TrxT	(5)	Kan	5 Lic 3 Lic	T7 –FW	T7 -RV
pCOEX1	(1)	Chlor	NdeI XhoI	T7 –FW	T7 -RV
pET-DUET	MCS1: (1) MCS2: (6)	Amp	MCS1: EcoRI-SalI MCS2: NdeI-XhoI	MCS1: pET-FW MCS2: DUETUP2	MCS1: DUETDOWN1 MCS2: T7 -RV
pCOLA	MCS1: (1) MCS2: (6)	Kan	MCS1: EcoRI-SalI MCS2: NdeI-XhoI	MCS1: pET-FW MCS2: DUET-UP2	MCS1: DUET-DOWN1 MCS2: T7-RV
pET28GST-LIC	(7)	Kan	5 Lic 3 Lic	pETGST-FW	T7 rev

TAGS
(1) MG**SSHHHHHH**SSGRENLYFQ*GH

Bold: N-terminal 6His tag, Underlined: TEV cleavage site

(2) MG**SSHHHHHH**SSGRENLYFQ*SM

Bold: N-terminal 6His tag, Underlined: TEV cleavage site

(3) AENLYFQ**SHHHHHH***DYKDDDDK*
Underlined: TEV cleavage site, **Bold:** C-terminal 6-His tag, *Italic:* FLAG tag

(4)MDPEEASVTSTEETLTPAQEAARTRAANKARKEAELAAAT*GWRGGHVVEGL AGELEQLRA***AEQ**TS*DEKTTRLEHHPQGQREPSGGCKLG*L GLGTENLYFQ*SM

Bold: SET1 tag**,** *italic*: SBP tag, underlined: TEV cleavage site

(5)M**HHHHHH**SSG*MSDKIIHLTDDSFDTDVLKADGAILVDFWAEWCGPCKMIAPIL DEIADEYQGKLTVAKLNIDQNPGTAPKYGIRGIPTLLLFKNGEVAATKVGALSKGQLK EFLDANLA*GTENLYFQ* SM

Bold: N-terminal 6His tag, *Italic:* Thioredoxin tag, Underlined: TEV cleavage site

(6) LETAAALFERQ HMDS*ST
S-tag

(7)MSPILGYWK*IKGLVQPTRLLLEYLEEKYEEHLYERDEGDKWRNKKFELGLEFPNLP YYIDGDVKLTQSMAIIRYIADKHNMLGGCPKERAEISMLEGAVLDIRYGVSRIAYSKD FETLKVDFLSKLPLKMFEDRLCHKTYLNGDHVTHPDFMLYDALDVVLYMDPMCLD AFPKLVCFKKRIEAIPQIDKYLKSSKYIAWPLQGWQATFGGGD*HPPKSDGSSMGSS**H HHHHH**SSGLVPRGS

Italic: GST tag **Bold:** 6His tag Underlined: thrombin cleavage site

SEQUENCING PRIMERS

T7 FW	TAATACGACTCACTATAGGG
T7 RV	GCTAGTTATTGCTCAGCGG
pET FW	ATGCGTCCGGCGTAGA
pET RV	ATGTTTGACAGCTTATCATCGA
pETGST FW	ATCGGATGGTTCATCCATGG
pBEN FW	ACCACCCTCAGGGCCAGCGG
pLIC FW	TGTGAGCGGATAACAATTCC
pLIC RV	AGCAGCCAACTCAGCTTCC
DUETUP2	TTGTACACGGCCGCATAATC
DUETDOWN1	GATTATGCGGCCGTGTACAA

Further details can be found on SGC website: http://www.sgc.ox.ac.uk/structures/MM/Vectors

APPENDIX C: PRIMER DESIGN FOR MUTAGENESIS

Point mutations were introduced to the target amino-acids (Table: C.1)

Table C.1: Point mutations designed

WT Codon	Mutant	Mutation Codon	Position
AAG	Ala	GCG	K57A
AAG	Gly	GGG	K200G
AAG	Glu	GAG	K200E
TTT	Ala	GCT	F239A
GAT	Ala	GCT	DADA
TAC	Phe	TTC	Y204F
TAC	Ala	GCC	Y204A
AAG	Leu	TTG	K200L
CGC	Leu	CTC	R112L

Both mutagenic primers must contain the desired mutation which should be surrounded by at least 10 bases and anneal to the same sequence on opposite strands of the plasmid (Table C.2).

Complementary forward (FW) and reverse (RV) mutagenesis primers had melting temperature higher than 78 ºC, length between 25 -45 bases, GC% content higher than 40 (Table C.3).

The melting temperature was calculated according to the formula:

$$T_{mel} = \frac{81.5 + 0.41(\%GC) - 675}{N - \%mismatch}$$

where N is the primer length and %GC and % mismatch are whole numbers.

Table C.2: Forward (FW) and Reverse (RV) primer sequence

name	Sequence
K57A_FW	CATT GGA GGC GCG TAT AAC CGG GGT TTG ACG
K57A_RV	CGT CAA ACC CCG GTT ATA CGC GCC TCC AAT G
K200G_FW	C AAA TCT ATT GTC AAG TAC GGG ACA GCT TTC TAC TCC TTC TAC C
K200G_RV	G GTA GAA GGA GTA GAA AGC TGT CCC GTA CTT GAC AAT AGA TTT G
K200E_FW	C AAA TCT ATT GTC AAG TAC GAG ACA GCT TTC TAC TCC TTC TAC C
K200E_RV	G GTA GAA GGA GTA GAA AGC TGT CTC GTA CTT GAC AAT AGA TTT G
F239A_FW	G GAG ATG GGG GAG TTC GCT CAG ATT CAG GAT GAT TAC C
F239A_RV	GGT A ATC ATC CTG AAT CTG AGC GAA CTC CCC CAT CTC C
DADA_FW	GCT TTC TTC CTG GTG GCA GCT GAC ATC ATG GAT TCA TCC
DADA_RV	GGA TGA ATC CAT GAT GTC AGC TGC CAC CAG GAA GAA AGC
Y204F_FW*	GTC AAG TAC AAG ACA GCT TTC TTC TCC TTC TAC CTT CC
Y204F_RV*	GG AAG GTA GAA GGA GAA GAA AGC TGT CTT GTA CTT GAC
Y204A_FW*	GTC AAG TAC AAG ACA GCT TTC GCC TCC TTC TAC CTT CC
Y204A_RV*	GG AAG GTA GAA GGA GGC GAA AGC TGT CTT GTA CTT GAC
K200L_FW*	C AAA TCT ATT GTC AAG TAC CTG ACA GCT TTC TAC TCC TTC TAC C
K200L_RV*	G GTA GAA GGA GTA GAA AGC TGT CAG GTA CTT GAC AAT AGA TTT G
R112L_FW*	G GAT TCA TCC CTT ACC CTC CGG GGA CAG ATC TGC
R112L_RV*	GCA GAT CTG TCC CCG GAG GGT AAG GGA TGA ATC C

Table C.3: Primer properties

Name	Length	# bp change	no Gs/Cs	GC %	Melting Tem (K)	% Mismatch
K57A	42	2	23	54.76	83.1	4.76
K200G	44	2	19	43.18	79.3	4.55
K200E	44	1	18	40.91	80.7	2.27
D103A	39	1	20	51.28	82.7	2.56
F239A	39	2	20	51.28	80.1	5.13
DADA	37	2	21	56.76	81.1	5.41
Y204F*	38	1	17	44.74	79.4	2.63
Y204A*	38	2	19	50	79	5.26
K200L*	44	2	18	40.91	78.4	4.55
R112L*	34	1	20	58.82	82.8	2.94

Primers designed by James Dunford

APPENDIX D: X-RAY DATA COLLECTION AND REFINEMENT STATISTICS

	T201A+Zol	**Y204F+Ris**	**Y204A+Ris**	**Y204A+Ris+ IPP**
Wavelength (Å)	0.9789	0.9796	0.9796	0.9796
Space group	$P4_12_12$	$P4_12_12$	$P4_12_12$	$P4_12_12$
Unit cell Dimensions (Å)	a=b=111.2 c= 67.09	a=b= 111.73 c=66.99	a=b= 111.62 c=66.71	a=b= 111.04 c=69.60
Resolution Range(Å)	37.07- 1.98 (2.09 - 1.98)	55.87 – 1.96 (2.07 - 1.96)	57.26 – 2.03 (2.14 - 2.03)	52.08 – 1.92 (2.02 - 1.92)
Redundancy	8.0 (8.0)	9.6 (9.4)	7.8 (5.4)	4.8 (4.6)
Completeness (%)	100.0 (100.0)	99.4 (98.0)	99.9 (100.0)	95.1 (94.6)
I/sigma (I)	10.7 (2.0)	11.4 (2.0)	10.0 (2.0)	9.3 (2.3)
R_{meas}	0.126 (1.137)	0.095 (0.906)	0.122 (0.784)	0.090 (0.553)
Resolution (Å)	1.98	1.96	2.03	1.92
R_{work}/R_{free}	0.183/0.205	0.199/0.234	0.187/0.218	0.190/0.188
Mean B factor (Å²)	43.53	56.50	41.42	40.46
Bond length (Å)	0.01	0.01	0.01	0.01
Bond angle (°)	0.91	0.94	0.92	0.88

	Y204A+Zol	**Y204A+Ale**	**Y204A+Pam**	**Y204A+Pam +IPP**
Wavelength (Å)	1.5418	0.9763	0.9796	0.9796
Space group	$P4_12_12$	$P4_12_12$	$P4_12_12$	$P4_12_12$
Unit cell Dimensions (Å)	a=b= 111.65 c=67.94	a=b= 111.50 c=66.53	a=b= 111.31 c=66.60	a=b= 111.40 c=70.36
Resolution Range(Å)	32.64 – 2.40 (2.53 - 2.40)	50.85 – 2.07 (2.22-2.07)	55.65 – 1.95 (2.06 - 1.95)	55.70 – 2.18 (2.30 - 2.18)
Redundancy	6.5 (6.1)	9.1 (9.4)	8.8 (8.3)	10.0 (9.7)
Completeness (%)	100.0 (99.9)	100.0 (100.0)	100.0 (100.0)	99.8 (100.0)
I/sigma (I)	10.2 (2.0)	10.3 (2.3)	10.4 (2.0)	8.6 (2.0)
R_{mean}	0.122 (0.708)	0.180 (1.064)	0.148 (1.079)	0.136 (1.045)
Resolution (Å)	2.4	2.07	1.95	2.18
R_{work}/R_{free}	0.197/0.250	0.187/0.211	0.178/0.212	0.223/0.278
Mean B factor (Å²)	55.26	33.97	34.29	72.95
Bond length (Å)	0.01	0.01	0.01	0.01
Bond angle (°)	0.98	0.91	0.89	1.03

	Y204A+ DMSPP +IPP	**K200G+Ris**	**K200L+Ris+ IPP**	**F239A+Ris**
Wavelength (Å)	0.9796	0.9796	1.5418	0.9796
Space group	$P4_12_12$	$P4_12_12$	$P4_12_12$	$P4_12_12$
Unit cell Dimensions (Å)	a=b= 112.07 c=67.32	a=b= 111.11 c=69.58	a=b= 111.74 c=66.60	a=b= 111.29 c=66.87
Resolution Range(Å)	51.31 – 2.96 (3.12 - 2.96)	52.09 – 2.11 (2.22 - 2.11)	35.33 – 2.35 (2.48 - 2.35)	42.77 – 1.43 (1.51 - 1.43)
Redundancy	7.0 (7.2)	10.6 (11.0)	8.6 (9.0)	10.8 (5.1)
Completeness (%)	100.0 (100.0)	99.8 (100.0)	99.3 (98.2)	99.9 (99.6)
I/sigma (I)	11.8 (1.8)	14.7 (2.9)	10.3 (2.0)	15.7 (2.0)
R_{mean}	0.091 (1.157)	0.096 (1.029)	0.171 (1.105)	0.089 (0.881)
Resolution (Å)	2.96	2.11	2.35	1.43
R_{work}/R_{free}	0.265/0.358	0.196/0.245	0.182/0.235	0.170/0.185
Mean B factor (Å²)	99.88	61.99	46.20	26.07
Bond length (Å)	0.01	0.01	0.01	0.01
Bond angle (°)	1.18	0.92	0.99	0.88

	F239A+Ris+ IPP	**F239A+Pam**	**F239A+Pam+ IPP**	**R112L+IPP**
Wavelength (Å)	0.9796	0.9796	0.9796	0.9796
Space group	$P4_12_12$	$P4_12_12$	$P4_12_12$	$P4_12_12$
Unit cell Dimensions (Å)	a=b= 111.26 c=66.51	a=b= 111.45 c=67.53	a=b= 111.21 c=67.27	a=b= 111.21 c=66.66
Resolution Range(Å)	37.09 – 1.46 (1.54 - 1.46)	42.98 -2.00 (2.11 – 2.0)	51.12- 2.10 (2.21 – 2.10)	37.07 – 1.70 (1.79 – 1.70)
Redundancy	9.5 (8.2)	10.6 (11.0)	10.6 (11.0)	12.8 (13.2)
Completeness (%)	99.3 (97.0)	99.8 (100.0)	99.9 (100.0)	99.9 (100.0)
I/sigma (I)	13.1 (2.1)	12.3 (2.7)	11.6 (2.7)	14.2 (2.7)
R_{mean}	0.125 (0.930)	0.117 (1.035)	0.120 (1.015)	0.106 (0.995)
Resolution (Å)	1.46	2	2.1	1.7
R_{work}/R_{free}	0.159/0.176	0.184/0.205	0.202/0.234	0.184/0.206
Mean B factor (Å²)	20.13	48.64	60.01	32.16
Bond length (Å)	0.01	0.01	0.01	0.01
Bond angle (°)	0.85	0.88	0.88	0.86